The Design of Novel DCB-3503 Analogues: Ligand-Based and Structure-Based Approaches

A Dissertation Presented for the

Doctor of Philosophy

Degree

The University of Tennessee, Knoxville

Yundi Gan

December 2015

DEDICATION

This dissertation is dedicated to

my father Qun Gan, my mother Yiping Liu

and all the other family members

who have always supported me.

ACKNOWLEDGEMENTS

Firstly, I would like to gratefully and sincerely thank my research advisor Dr. David Baker for his support, guidance and patience. I thank him for giving me such a wonderful opportunity to learn organic/medicinal chemistry. I would also like to thank Dr. Engin Serpersu and Dr. Jerome Baudry for giving me the opportunity to learn biochemistry and molecular modeling by working in their labs in the Department of Biochemistry and Cellular and Molecular Biology. I would like to thank Dr. Yung-Chi Cheng at Yale University School of Medicine for the collaboration. I am also grateful to Dr. John Bartmess, Dr. Brian Long and Dr. Jerome Baudry for being willing to serve in my committee.

Secondly, I would like to thank the past and present members of the Baker group: Dr. Costyl Njiojob and Dr. Brian LeCroix for teaching me organic chemistry and lab techniques, Dr. Samson Francis, Dr. Julio Gutierrez and Andy Hahn for their early developmental work, and Dr. Irene Abia, Bo Meng, Andrew Moss, Kevin Gayler and Nick Diloreto for their support and friendship.

I would also like to thank Dr. Ying Wang and Dr. Wing Lam from Dr. Yung-Chi Cheng's group for the biological studies of DCB-3503 analogues, and Sherin Raval from Dr. Engin Serpersu's group for teaching me the biochemistry lab techniques. I would also like to thank Dr. Carlos Steren for his assistance on the NMR spectroscopy, Dr. Liguo Song for his assistance on the mass spectrometry, and Dr. Zheng Lu for his assistance on the single-crystal X-ray crystallographic analysis.

Finally, I would like to thank the Department of Chemistry at the University of Tennessee, Knoxville and Science Alliance for their financial support.

ABSTRACT

This research centers around a tylophorine analogue, DCB-3503, a lead compound that possesses potent growth inhibitory activities against all 60 human-derived cell lines screened by the National Cancer Institute (NCI). In comparison with other known antitumor compounds using the NCI's COMPARE analysis, it is apparent that the compound is acting through a unique mechanism—one decidedly different from that of other known anticancer drugs. Additionally DCB-3503 has shown inhibitory activities against HepG2 (human hepatocellular cancer, HCC), PANC-1 (human pancreatic ductal carcinoma) and chemotherapeutic-resistant KB cell lines in the hands of our collaborator, Dr. Yung-Chi Cheng of Yale University School of Medicine. In order to predict structure–activity relationships, a Comparative Molecular Field Analysis (CoMFA) model was constructed, and several DCB-3503 analogues with higher projected antitumor activities were designed. These analogues included those with modifications at positions 3 and 7, with CoMFA indicating greatest tolerance at the 3-position. Results from biological studies suggested that a more complicated mechanism with different pathways for different analogues was operative. A biotinylated DCB-3503 analogue that was designed and synthesized previously in Dr. David Baker's lab was utilized by our Yale collaborators to snare a protein targeted by DCB-3503 type compounds. A cellular heat shock cognate protein 70 (Hsc70) was identified as one of the target proteins of DCB-3503 in an anti-hepatitis C virus (HCV) study. The target protein was then synthesized without and with ^{15}N [nitrogen-15] labeling in our lab, and the thermodynamic and NMR studies of its interactions with DCB-3503 were carried out. However, failure to elucidate the specific DCB-3503 and Hsc70 interactions by NMR studies prompted us to turn to computational simulations, where two docking models, including the one

based on DCB-3503 and the ATP-state Hsc70 nucleotide binding domain (NBD), and another based on DCB-3503 and the apo-state Hsc70 NBD, were constructed. The most reasonable docking pose of DCB-3503 was generated in the ATP-state protein based on the analysis of both the experimental observations and the docking scores. Design of more promising active candidates can likely be realized in the future through the study of the aforementioned docking pose.

TABLE OF CONTENTS

LIST OF FIGURES

LIST OF SCHEMES

INTRODUCTION

Tylophorine analogues are a group of phenanthroindolizidine alkaloids originally isolated from an Indian native plant, Tylophora indica.[5] Since their first isolation they have continued to be the targets of synthesis, modification and structure–activity relationship (SAR) studies.[6] In this research the modifications of a hydroxylated (+)-*S*-tylophorine analogue, DCB-3503, which is considered as a promising active anti-cancer drug candidate, was described. In the first part of this research, a ligand-based design was performed via Comparative Molecular Field Analysis (CoMFA) molecular modeling program. Several novel molecules designed based on DCB-3503 via CoMFA were synthesized and characterized, and their corresponding biological activities were tested. In the second part of this research, a structure-based approach was carried out using a biochemical probe molecule derived from DCB-3503. A protein involved in the development of hepatitis C virus (HCV) infection was identified as one of the target proteins for DCB-3503, and the overexpression and purification of this protein was carried out. The corresponding thermodynamic and NMR studies of the interactions between the ligand and the protein were performed. A docking model was then constructed with the aim of designing novel tylophorine analogues with improved efficacy against HCV.

PART ONE. THE LIGAND-BASED APPROACH

ABSTRACT

The ligand-based approach is centered around a tylophorine analogue, DCB-3503, a lead compound that possesses potent growth inhibitory activities against all 60 human-derived cell lines screened by the National Cancer Institute (NCI). Compared with other known antitumor compounds according to the NCI's COMPARE analysis, it is obvious that the compound is acting through a unique mechanism—one decidedly different from that of other known anticancer drugs. Additionally DCB-3503 has shown inhibitory activities against HepG2 (human hepatocellular cancer, HCC), PANC-1 (human pancreatic ductal carcinoma) and chemotherapeutic-resistant KB cell lines in the hands of our collaborator, Dr. Yung-Chi Cheng of Yale University School of Medicine. In order to aid in predicting structure–activity relationships, a Comparative Molecular Field Analysis (CoMFA) model was constructed, and several novel DCB-3503 analogues with higher projected antitumor activities were designed. These analogues included those with modifications at positions 3 and 7. CoMFA analysis suggested greatest tolerance for modifications at the 3-position. These novel DCB-3503 analogues were synthesized via a modification of a novel route, and the results from biological studies suggested that a more complicated mechanism with different pathways for different analogues was operative.

I. BACKGROUND

1. The Tylophorine Analogues and DCB-3503.

Tylophorine analogues are a group of phenanthroindolizidine alkaloids originally isolated from an Indian native plant, *Tylophora indica*.[5] Since their first isolation they have continued to be the targets of synthesis, modification and structure–activity relationship (SAR) studies because of their diverse pharmacological activities. DCB-3503, a hydroxylated (+)-*S*-tylophorine analogue, was recently derived and synthesized in Dr. Baker's lab and is considered as a promising active anti-cancer drug candidate.[6]

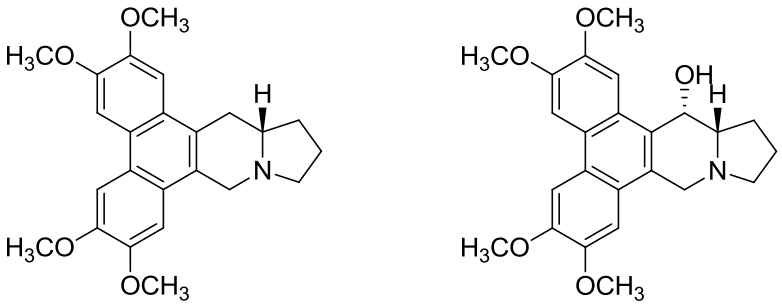

(+)-*S*-tylophorine **DCB-3503**

Figure 1. The structures of (+)-*S*-tylophorine and DCB-3503.

2. The Biological Evaluation of Tylophorine Analogues.

A great number of investigations have been carried out on these tylophorine analogues after their first isolation, and our studies were mainly focused on (+)-*S*-tylophorine and DCB-3503. In

the antitumor evaluation performed by National Cancer Institute (NCI), the two above-mentioned compounds showed a consistent and potent growth inhibitory activity ($GI_{50} \sim 10^{-8}$ M) against all 60 human-derived cell lines including some refractory cell lines such as lung cancer and melanoma cell lines. Furthermore, the COMPARE analysis of these two compounds conducted by the NCI showed a unique antitumor mechanism in comparison with other known antitumor compounds in clinical use.[7] In the most recent studies carried out in Dr. Yung-Chi Cheng's lab at the School of Medicine of Yale University, the above two compounds also showed a potent activity, both *in vitro* and *in vivo*, against the HepG2 (human hepatocellular cancer, HCC) cell line, which was not included in the 60 cell lines screened by NCI. However a discrepancy was discovered between the *in vitro* and *in vivo* activities against HepG2 cell line of these two compounds, as (+)-*S*-tylophorine was more active than DCB-3503 *in vitro*, while DCB-3503 was more active than (+)-*S*-tylophorine *in vivo*.[7] In addition, DCB-3503 was also able to suppress the activity of PANC-1 (human pancreatic ductal carcinoma) cell line and the chemotherapeutic resistant KB cell line with the overexpression of multidrug resistance and multidrug resistance-associated proteins.[7, 8] Further investigations on other biological activities were also carried out, as DCB-3503 was found to significantly suppress the development and progression of collagen-induced arthritis (CIA) and to abrogate the skin disease in systemic lupus erythematosus (SLE).[9, 10]

3. The Studies of the Mechanisms of Tylophorine Analogues.

It was believed the tylophorine analogues functioned through distinct mechanisms from the most current antitumor compounds, since they did not induce DNA damage, did not inhibit DNA

synthesis, and did not perturbate tubulin function according to the fact of failing to induce the protein p53 as the sensor of DNA damage after the treatment of DCB-3503.[7]

Further experiments revealed that the tylophorine analogues were able to inhibit nuclear factor-kappa B (NF-κB) pathway. NF-κB is a transcription factor that plays a vital role in inflammation and cell survival, and its overexpression is believed to be one mechanism of chemoresistance, as its activation will lead to the tumor cell survival, while its suppression will stimulate an apoptotic response.[11] The NF-κB transcription factor, which is usually constituted of proteins p65 and p50 as a heterodimer, is usually tightly regulated by interactions with inhibitory IκB proteins in the cytoplasm as an inactive complex. However, by activating the IκB kinase (IKK) via an upstream signal, the IκB proteins regulating the NF-κB heterodimer will be phosphorylated and further ubiquitinated and degraded, making the NF-κB heterodimer no longer regulated and free to enter the nucleus to activate specific target gene expression. In the meantime, the p65 is stimulated by phosphorylation as well, resulting in the transactivation of target genes in cooperation with other transcriptional regulators.[8, 12] It was found in Dr. Cheng's lab that after treatment with DCB-3503, the level of the phosphorylated p65 in cells decreased, suggesting a mechanism not through preventing NF-κB from binding to DNA, but, at least in part, through the degradation of the phosphorylated p65. Additionally DCB-3503 was able to down-regulate IKKa, which is a subunit of IKK, and ultimately deactivate the NF-κB heterodimer by preventing the phosphorylation of IκB proteins. Further study also indicated that IKK was responsible for the phosphorylation of p65, meaning the suppression of IKK by DCB-3503 can lead to the decreased level of phosphorylated p65, which eventually suppresses the activation of the NF-κB pathway.[8] The inhibitory effect of DCB-3503 on the NF-κB pathway

may also explain its activity against CIA and the skin disease in SLE, as both of them are generated partly by the inflammation caused via activation of the NF-κB pathway.[9, 10]

In a most recent study, it was found DCB-3503 was able to down-regulate a subset of proteins including cyclin D1 that play a key role during cell-cycle progress from the G_1 to the S phase. The overexpression of this group of proteins was found in many human tumor cells and was believed to be associated with chemoresistance in chemotherapy.[11] Further investigation showed the expression of cyclin D1 could be down-regulated in the first 15 min after the treatment of DCB-3503, and no cell type-specification was observed. Cheng's group then concluded that DCB-3503 was capable of inhibiting the synthesis of a protein with a short half-life, such as cyclin D1, via reducing the polypeptide chain elongation rate. Therefore, this mechanism of down-regulation of such proteins at the translational level truly makes DCB-3503 distinct from many current protein inhibitors and may serve to overcome chemoresistance in chemotherapy.[13]

Although the studies mentioned above presented several possible mechanisms, SAR studies on different tylophorine analogues with a variety of substituents and core groups showed the possible existence of other targets or mechanisms, and the unique mechanisms of a given tylophorine analogue might be far more complicated than what had been unveiled. The biologists were led to declare that structural similarity in these compounds may not be associated with similar modes of action—a perplexing situation for the medicinal chemists.[11, 14-18]

4. The Previous Synthesis of DCB-3503 and Its Analogues.

DCB-3503 was previously synthesized in Dr. Baker's lab utilizing a modified route from its first synthesis reported by Rapoport, and its anticancer activities were firstly tested by Baker

group in collaboration with NCI.[3, 6, 19, 20] The detailed modified synthesis is shown in Scheme 1. The key steps include a Perkin reaction, a $FeCl_3$-mediated ring closure reaction, and a stereoselective reduction of the ketone utilizing K-Selectride®.

Several DCB-3503 analogues were also synthesized, and the most important one was the propargyl group-modified DCB-3503 (DCB-3509), which provided the possibility to further synthesize the biotinylated DCB-3503 via copper-catalyzed azide–alkyne cycloaddition (CuAAC) click chemistry. The key modification involved the introduction of the propargyl group, not only as the moiety in the DCB-3509, but also as the protective group in the $FeCl_3$-mediated ring-closure step.[2]

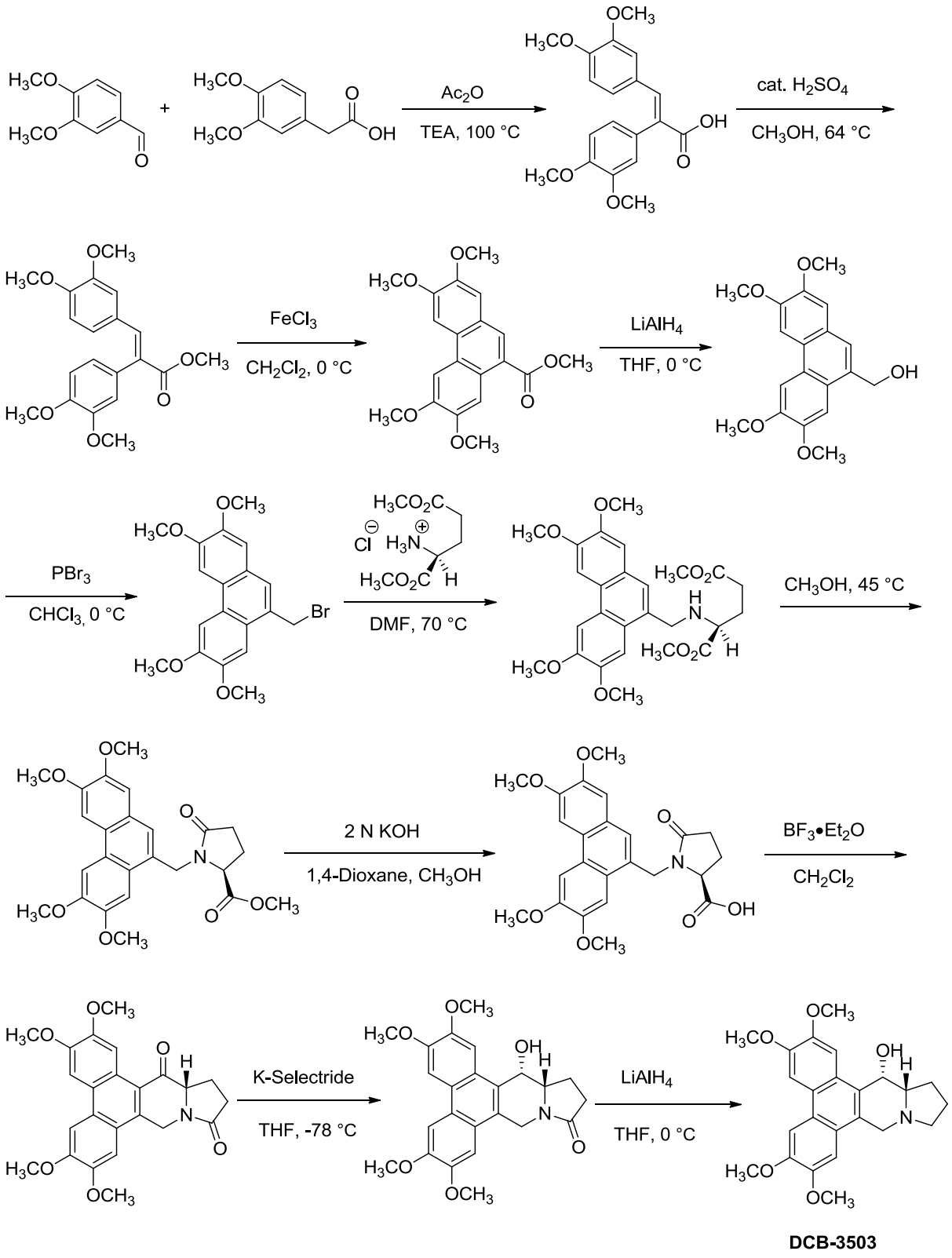

Scheme 1. The previous synthetic route of DCB-3503.[3]

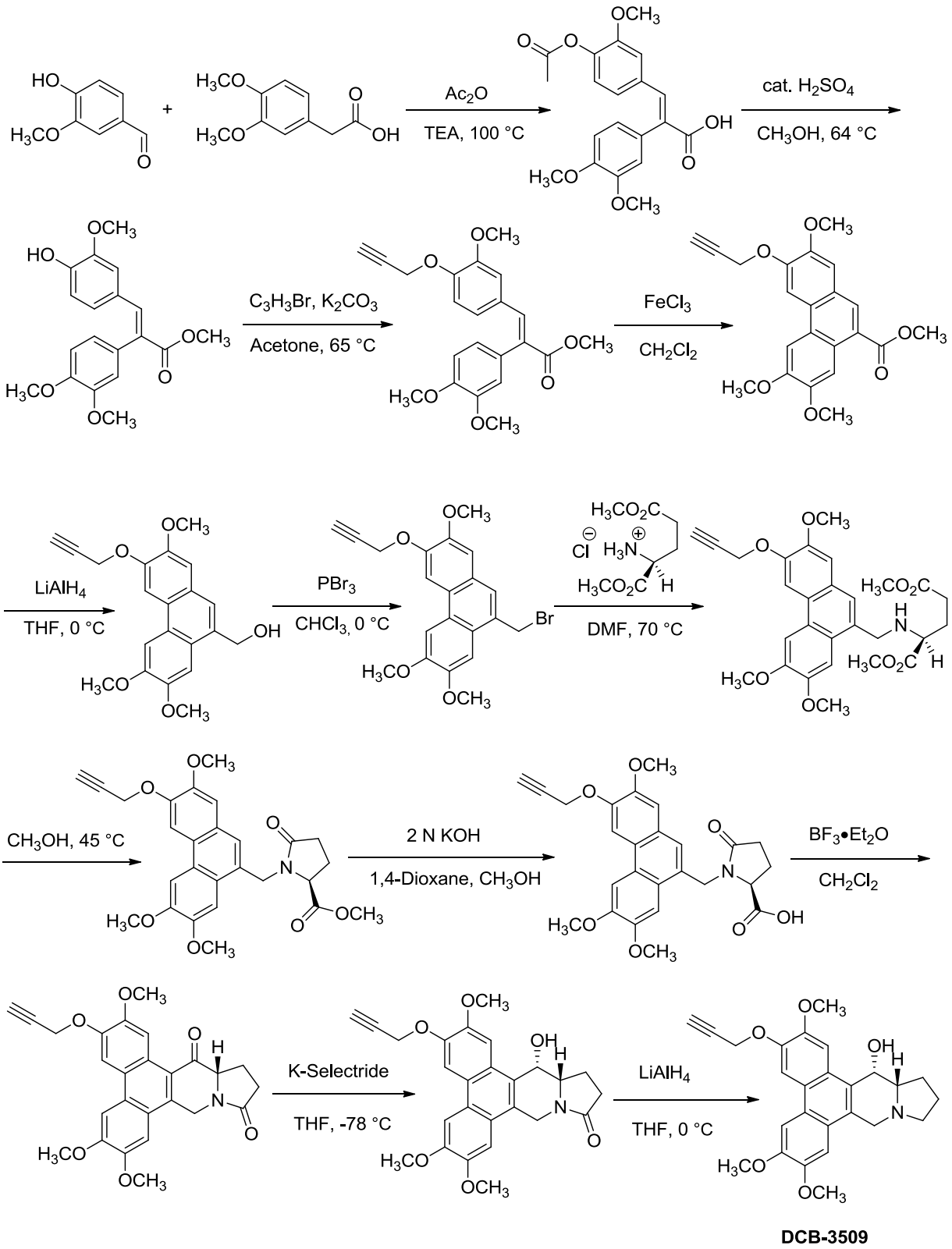

Scheme 2. The previous synthetic route to DCB-3509.[2]

II. STATEMENT OF THE PROBLEM

1. The Screening of Novel DCB-3503 Analogues.

In order to design molecules with higher biological activities, the screening of novel DCB-3503 analogues *in silico* was determined to be the first step in our approach. However due to the lack of specific targets of DCB-3503 according to the previous biological studies, a structure-based approach was not possible, so a ligand-based approach was selected. With a variety of tylophorine analogues possessing different structures and the corresponding biological activity data, the Comparative Molecular Field Analysis (CoMFA), which is a 3D quantitative structure–activity relationship (3D-QSAR) program, was selected as to derive potential candidate compounds. The CoMFA model would be constructed, and the newly designed DCB-3503 analogues would be tested in the model, and selection would be made based on the predicted activities.

2. The Synthesis of the Selected Novel DCB-3503 Analogues.

Several DCB-3503 analogues with more potential activities would be selected as the synthetic target molecules. A newly reported route to synthesize the indolizidine moiety of DCB-3503 shown in Scheme 3 would be attempted on the synthesis of the newly selected analogues.[1] The introduction of the novel route not only enabled one to reduce the overall steps of the synthesis, but also realized the possibility to modify the molecule with more sensitive groups due to the removal of the harsh reduction conditions at the last step in the previous synthetic route.

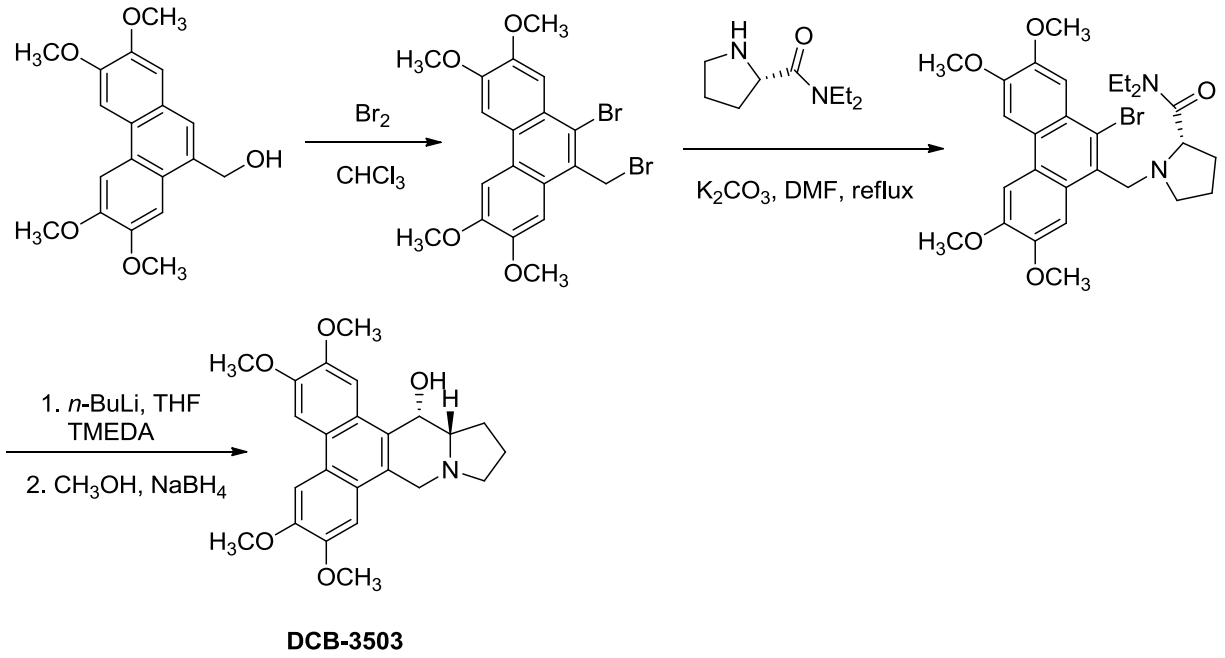

Scheme 3. The reported modifications of synthesis of DCB-3503.[1]

III. DISCUSSION

1. The Construction of Novel CoMFA Models of Tylophorine Analogues.

1.1. The Previous Ligand-Based Approach of Designing Novel Tylophorine Analogues.

Several groups including our own home carried out the syntheses and structure–activity relationship (SAR) studies on different structural analogues of tylophorine.[11, 14-18] In order to evaluate and screen novel DCB analogues in a better and faster approach, a CoMFA model was built in Dr. Baker's lab utilizing SYBYL 8.0 program.[3] CoMFA is a 3D quantitative structure–activity relationship (3D-QSAR) technique that is able to provide predictions of the behavior of newly designed compounds based on their analogues with known activities when the specific targets or mechanisms are unknown.[21, 22] In the CoMFA model previously established, a group of structural analogues of tylophorine with biological activities (GI_{50} against HepG2 cells) is shown in Figure 2.[3] These were selected as the training set for construction of the new model. A minimum of 10 molecules with a variety of different structures sharing a common structural core is necessary for building a reliable model in CoMFA. Each of the structures was superposed on the common core shown in Figure 3 to give an alignment, which was then embedded on a grid with a spacing of 2 Å. The steric and electrostatic fields of the alignment were calculated by a probe atom using Lennard–Jones potentials and coulombic potentials respectively, and were

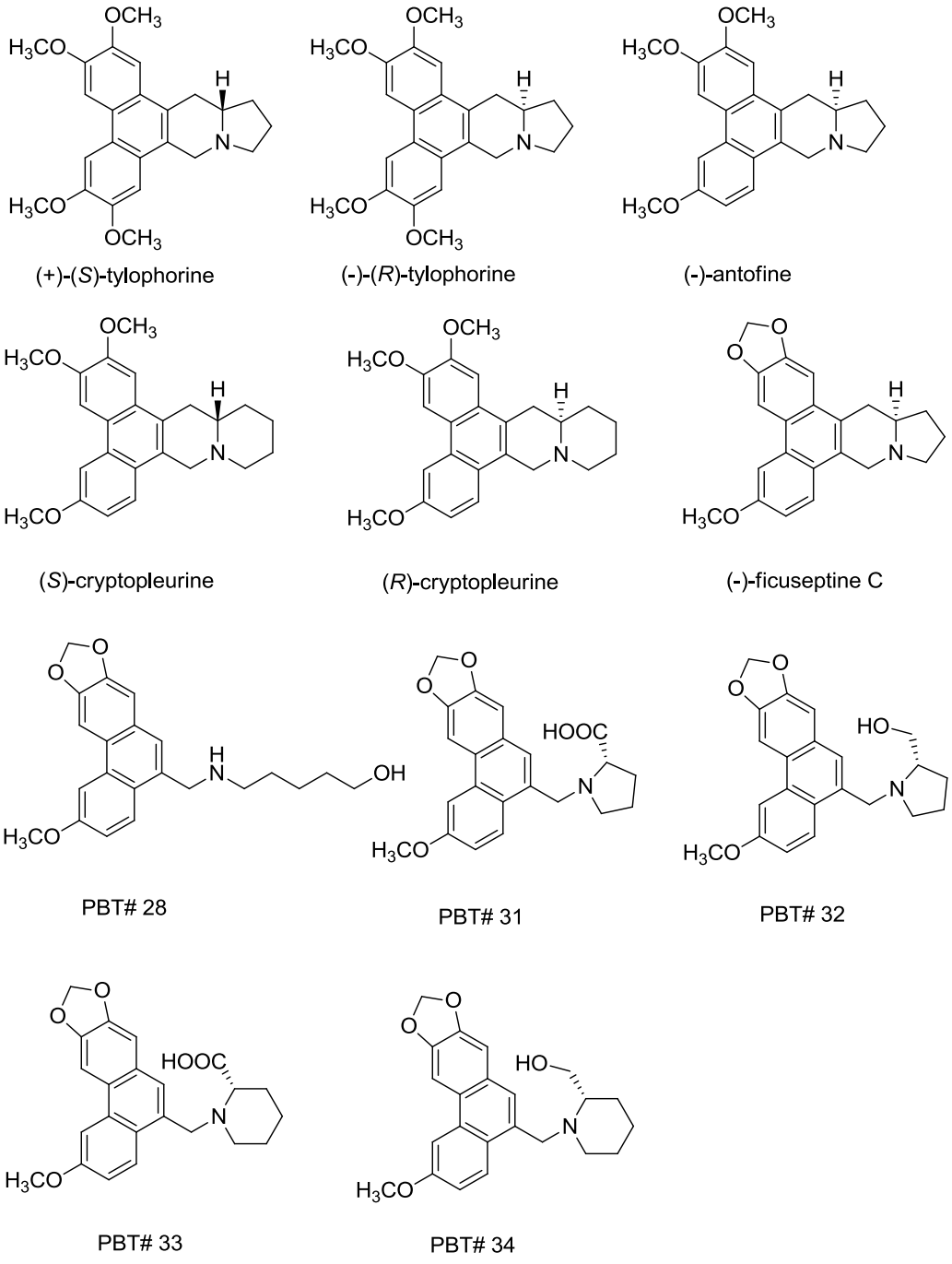

Figure 2. The group of molecules selected as the training set in the previous CoMFA model.

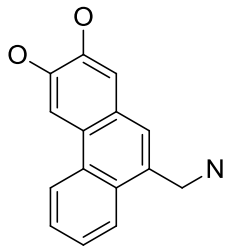

Figure 3. The common structural core of the alignment of the training set molecules.

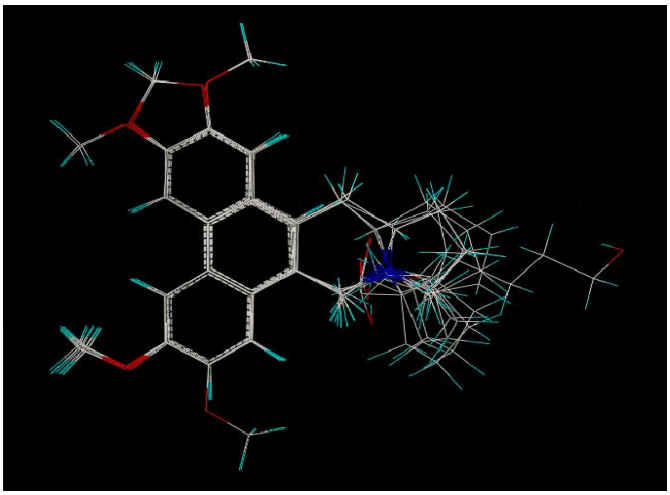

Figure 4. The alignment of the training set molecules.

afterwards correlated with the biological data shown in Table 1. After the validation of the model by Partial Least Squares (PLS) analysis, two contour maps were generated providing the future modification directions as shown in Figure 5 using (+)-(*S*)-tylophorine as a template, where a sterically bulky group was favored in the green area and disfavored in the yellow area, and negatively charged groups or H-bond acceptors would enhance the biological activity in the red area, whereas positively charged ones or H-bond donors were beneficial to the blue area. With the assistance from the contour maps the corresponding modifications could be made and the newly designed molecules were put into the CoMFA model for more accurate predictions on their biological activities. The synthetic targets could then be selected from the molecules with the highest predicted biological activities according to the CoMFA model.

Table 1. The biological data of the corresponding training set molecules.

	HepG2 GI_{50} (nM)	**HepG2 pGI_{50}**
(+)-(*S*)-tylophorine	11 ± 4	7.959
(-)-(*R*)-tylophorine	33 ± 2	7.481
(-)-antofine	4.9 ± 0.4	8.310
(*R*)-cryptopleurine	1.5 ± 0.2	8.824
(*S*)-cryptopleurine	1.5 ± 0.2	8.824
(-)-ficuseptine C	371 ± 27	6.431
	HepG2 GI_{50} (μM)	
PBT# 28	2.3 ± 0.3	5.638
PBT# 31	8.6 ± 3.6	5.066
PBT# 32	5.4 ± 1.4	5.268
PBT# 33	3 ± 0.7	5.523
PBT# 34	3.1 ± 1.0	5.509

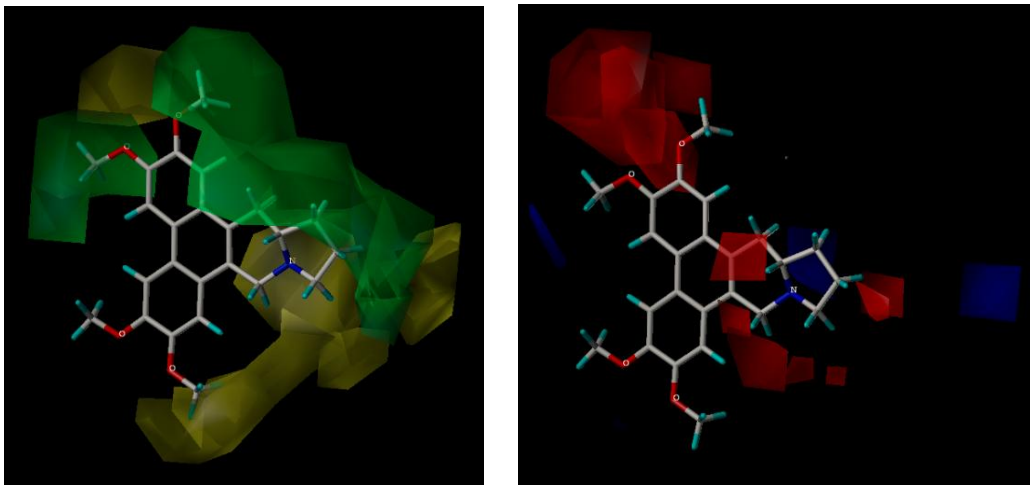

Figure 5. The contour maps of the CoMFA model. (Red area: negative charge and H-bond acceptors favored; Blue area: positive charge and H-bond donor favored; Green area: steric bulky groups favored; Yellow area: Steric bulky groups disfavored.)

1.2. The Construction of a Novel CoMFA Model.

In the most recent studies it was revealed that the molecules used in the training set in the previous CoMFA model, although they are structural analogues, may not be the functional analogues.[14, 15, 18] That is, their mechanisms of action may differ. According to the relative studies, the modifications on the A ring or E ring of (−)-antofine shown in Figure 6 resulted in compounds with two distinctive biological mechanisms compared with the original (−)-antofine one, and similar results were obtained on DCB-3503 and *rac*-cryptopleurine as well. Furthermore, either the expansion of the ring with different atoms or the modifications on the same ring with different functional groups or different chiralities would result in different mechanisms, indicating the possible existence of multi-mechanism and multi-targets of the tylophorine analogues.[14, 15] However, on the basis of the criteria of building a reliable CoMFA, the molecules selected as the training set, of which the specific mechanism or target may be unclear, should at least function through the same mechanism or on the same target.[22] Therefore, the previous CoMFA model built based on a group of different functional analogues with different targets in the HepG2 cells was considered as not quite satisfactory, and a new CoMFA model utilizing the molecules believed to target the same pathway (NF-κB pathway) as the training set was constructed.

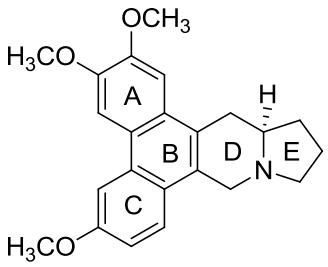

Figure 6. The structure of (−)-antofine.

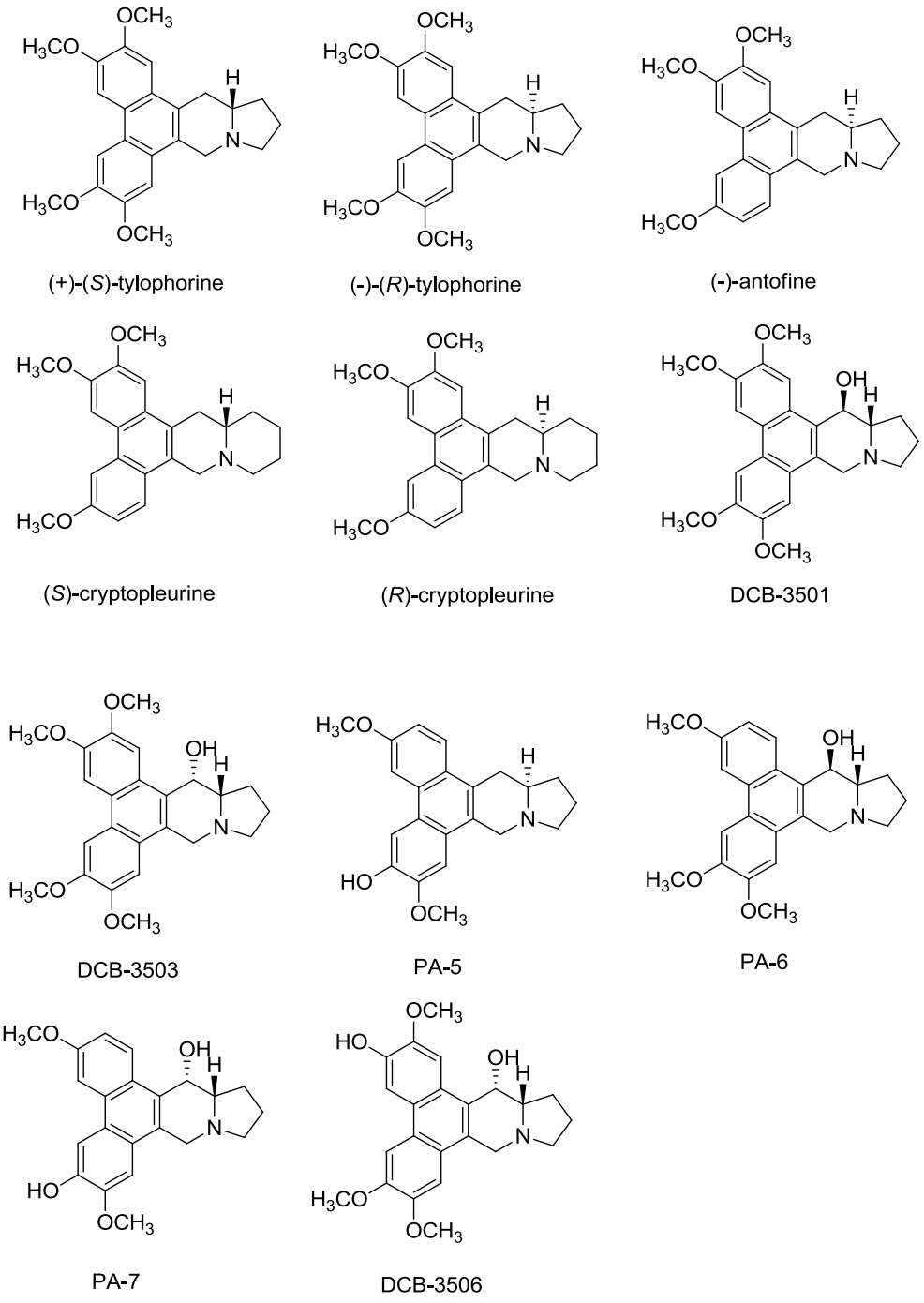

Figure 7. The molecules constituting of the training set in the novel CoMFA model.

As can be seem in Figure 7, 11 molecules screened in Dr. Cheng's lab that appeared via appropriate assays to target the NF-κB pathway were selected as the training set for the novel CoMFA model, and among them (*S*)-cryptopleurine and (*R*)-cryptopleurine were regarded separately with equal biological activity as they were tested as a racemic mixture.[11, 14]

The 11 molecules were firstly sketched in the SYBYL-X 2.1 program had MMFF94 charges assigned, and were energy minimized utilizing the MMFF94s force field. Then the alignment of all the molecules was carried out using a slightly different common core from the one used in the previous model due to the different positions of oxygens on the phenanthrene ring. Manual correction of the alignment on the methoxy groups was necessary if they were not in the same plane of the phenanthrene ring. Afterwards, the corresponding biological data, which are shown in Table 2 as IC_{50} vs. NF-κB pathway, were firstly converted to the corresponding −log units on an M^{-1} scale before application in the model. The steric and electrostatic fields of the alignment were then calculated using the Tripos Standard Force Field, and the biological data were correlated to these fields.

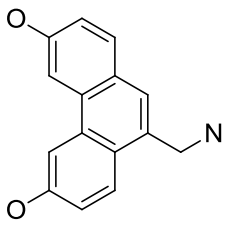

Figure 8. The common structural core of the alignment of the training set molecules in the novel CoMFA model.

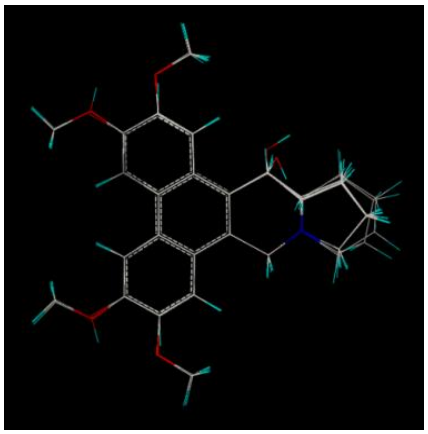

Figure 9. The alignment of the training set molecules in the novel CoMFA model.

Table 2. The corresponding biological data of the training set molecules in the novel CoMFA model.

	NF-κB IC_{50} (nM)	NF-κB pIC_{50}
(+)-(*S*)-tylophorine	41 ± 20	7.387
(-)-(*R*)-tylophorine	317 ± 51	6.499
(-)-antofine	7.3 ± 1.9	8.137
(*R*)-cryptopleurine	1.4 ± 0.6	8.854
(*S*)-cryptopleurine	1.4 ± 0.6	8.854
DCB-3501	315 ± 64	6.502
DCB-3506	322 ± 19	6.492
DCB-3503	87 ± 6	7.060
PA-5	11 ± 6	7.959
PA-6	12 ± 9	7.921
PA-7	10 ± 4	8.000

The validation of the model was carried out by running Partial Least Squares (PLS) analysis. A leave-one-out (LOO) cross-validation and a non-cross-validation were performed to give the correlated statistics. The q^2 resulted from the LOO cross-validation was an indication of the predictive abilities of the model and a value larger than 0.5 proves the robustness of the model.[23] The conventional correlation coefficient r^2, which was typically much larger than q^2, was obtained from the non-cross-validation providing the quality of the fit of the calculated data and observed data. The q^2, r^2 and the standard error of this newly built model were 0.570, 0.926 and 0.270, respectively, with an optimal number of components of 2, suggesting good predictive power.[24] The detailed CoMFA model calculation results are listed in Table 3.

1.3. The Screening and Designing of Novel DCB-3503 Analogues.

With the newly constructed model in hand, two contour maps were derived as shown in Figure 10 utilizing (+)-(*S*)-tylophorine as the template.

Based on the interpretation illustrated in the previous explanation of contour maps, several DCB-3503 analogues were designed aiming at decreasing the volume at the 7-position of the phenanthrene ring and increasing the volume at the 3-position as well as providing possible H-bond acceptors.

In order to decrease the volume of the substituent at the 7-position, hydrogen and halogens were considered as good candidates. Since similar hydrogen-substituted DCB-3503 at 6- and 7-positions has been synthesized and studied in Dr. Baker's lab, therefore only halogen substituted analogues were designed. However, in consideration of avoiding the addition of H-bond acceptors, only chlorine and bromine modified analogues were tested in the CoMFA model. Another reason to choose halogen is to study whether halogen bonding could play a role in the interaction of DCB-3503 analogues and their unknown receptors. Currently halogen bonding is becoming more and more significant in modern drug design due to its role to stabilize ligand–protein complexes.[25-28] Several triazole-modified analogues were also designed so as to increase the volume at 3-position. It is worth noting that some triazole analogues have been already synthesized in Dr. Baker's lab and have been successfully applied in the identification of one target protein of DCB-3503. The 3-propargyl-substituted analogue, which functions as the intermediate toward the synthesis of the triazole analogues, was also screened in the model. In addition, due to the increasing usage of fluorine in lead optimization in drug design and the already established synthetic steps of 3-propargyloxy substituted DCB-3503 analogue, a 3-

Table 3. The detailed results obtained from the novel CoMFA model.

	NF-κB pIC_{50} (experimental)	CoMFA Field	NF-κB pIC_{50} (predicted)	Residue
(+)-(*S*)-tylophorine	7.387	158	7.018	0.369
(-)-(*R*)-tylophorine	6.499	166	6.662	0.163
(-)-antofine	8.137	152	8.132	0.005
(*R*)-cryptopleurine	8.854	160	8.640	0.214
(*S*)-cryptopleurine	8.854	158	8.842	0.012
DCB-3501	6.502	160	6.813	0.311
DCB-3506	6.492	152	6.472	0.020
DCB-3503	7.060	160	7.010	0.050
PA-5	7.959	150	8.088	0.129
PA-6	7.921	148	7.597	0.324
PA-7	8.000	144	8.390	0.390

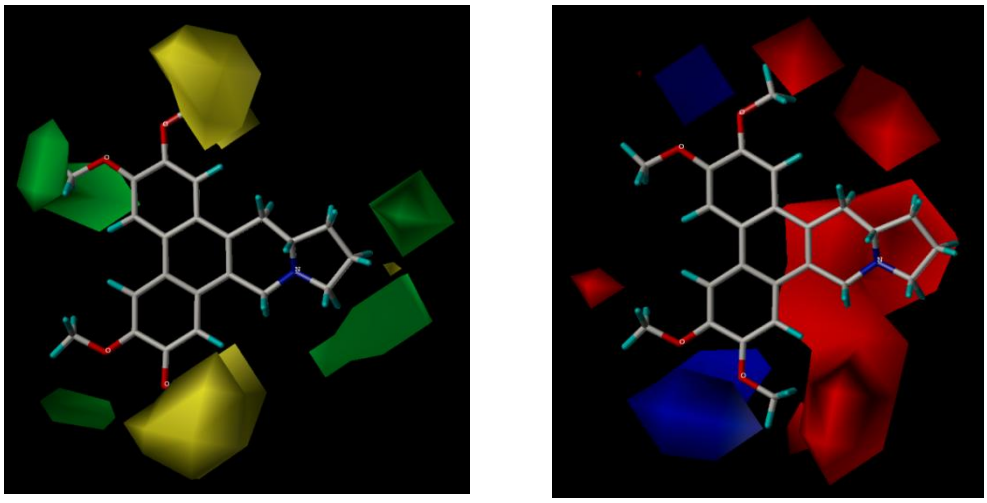

Figure 10. The contour maps of the CoMFA model. (Red area: negative charge and H-bond acceptors favored; Blue area: positive charge and H-bond donor favored; Green area: sterically bulky groups favored; Yellow area: Sterically bulky groups disfavored.)

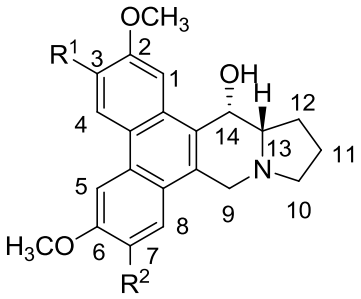

Figure 11. The basic structure and numbering system of DCB-3503 analogues.

difluorochloromethoxy substituted DCB-3503 analogue was designed and screened in the model as well. By substituting two hydrogens with two fluorines, it was expected to affect the conformation, hydrogen bonding and electrostatic interactions of the ligand with the proteins, together with its metabolic stability due to the well-known ability of fluorine to block the metabolic action of certain enzymes.[29]

The screening results are shown in Figure 12, and DCB-3503 was included in the screening placed in the testing set so as to validate the model. Additionally (−)-antofine was screened functioning as the template in the alignment of the testing set molecules to give a pIC_{50} of 8.132. According to the results, by replacing the 7-methoxy group of DCB-3503 with a chlorine or bromine, the pIC_{50} increased by around 0.8, and compound **1-1** was selected as the synthetic target due to its synthetic feasibility. However, on the basis of **1-1**, if the 3-methoxy group was modified to the propargyloxy, the activity was decreased by 0.030. It was decided to synthesize **1-3** in spite of its lower activity due to its role as the intermediate in the synthesis of the triazole analogues, which were screened to give significantly increased activities due to their corresponding volume increase at the 3-position from DCB-3503. In addition by substituting the 7-methoxy group with chlorine on **1-4**, although not as much as what was observed on DCB-

Compound No.	R	Predicted NF-κB pIC_{50}
DCB-3503	$R^1 = OCH_3$, $R^2 = OCH_3$	7.007
1-1 (DCB-3511)	$R^1 = OCH_3$, $R^2 = Cl$	7.832
1-2	$R^1 = OCH_3$, $R^2 = Br$	7.835
1-3 (DCB-3510)	$R^1 = HC{\equiv}C\text{-}CH_2\text{-}O$, $R^2 = Cl$	7.802
1-4	$R^1 = Triaz^1$, $R^2 = OCH_3$	7.108
1-5	$R^1 = Triaz^1$, $R^2 = Cl$	7.681
1-6	$R^1 = Triaz^2$, $R^2 = Cl$	7.734
1-7	$R^1 = Triaz^3$, $R^2 = Cl$	7.896
1-8	$R^1 = Triaz^4$, $R^2 = Cl$	7.871
1-9	$R^1 = Triaz^5$, $R^2 = Cl$	7.948
1-10	$R^1 = Triaz^6$, $R^2 = Cl$	7.982
1-11	$R^1 = Triaz^7$, $R^2 = Cl$	7.961
1-12	$R^1 = OCF_2H$, $R^2 = OCH_3$	6.908

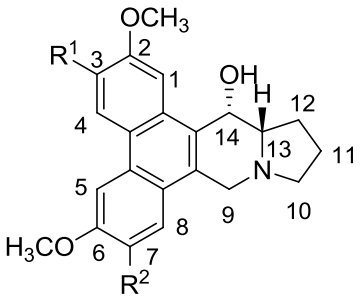

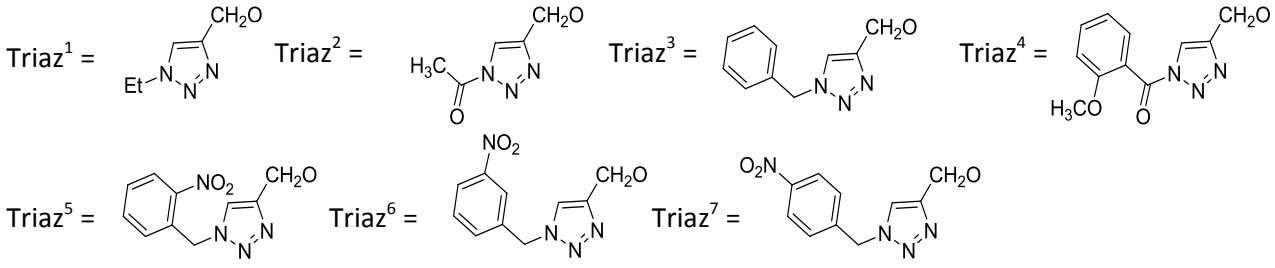

Figure 12. The designing and evaluation of the novel DCB-3503 analogues.

3503, the activity increased as well. Among all the triazole-modified candidates, **1-10** with the highest pIC_{50}, was selected as one synthetic target. The decision was made to synthesize compound **1-8**, although which was not as promising as **1-10**, the carbonyl group on the triazole occupies more volume than a methyl, which might contribute to the activities according to the contour maps. The last compound screened in the model was the difluoromethoxy modified compound, which showed an even lower predicted activity than DCB-3503 possibly due to the unwanted fluorine as the H-bonding acceptor rather than a donor at the 3-position. However, the purpose of adding fluorine as a hydrogen mimic was to study the possible electrostatic effects and metabolic stability that it might bring to the molecule; therefore, it was determined to keep **1-12** as a synthetic target.

2. The Synthesis of DCB-3511 (10)

The synthesis of DCB-3511 (**10**) was designed based on the already established route in Dr. Baker's lab and a recently reported synthetic route of phenanthroindolizidine alkaloids.[1, 3]

2.1. The Synthesis of Intermediate 1.

The synthesis of intermediate **1** was initiated by selecting anisic acid as the starting material. The method of adding sodium hydroxide solution, followed by sodium hypochlorite solution to an aqueous solution of anisic acid was firstly attempted, as was shown in Scheme 4.[30] However, after reaction for 1 h and work-up of the mixture, almost half of the starting material was detected on TLC plate, leaving the mixture as a sum of a small amount of the desired product with other impurities. To increase the yield, the reaction was allowed to stir for an extra 20 min,

but instead of increasing the yield, more impurities including the dichlorinated product were detected by mass spectrometry.

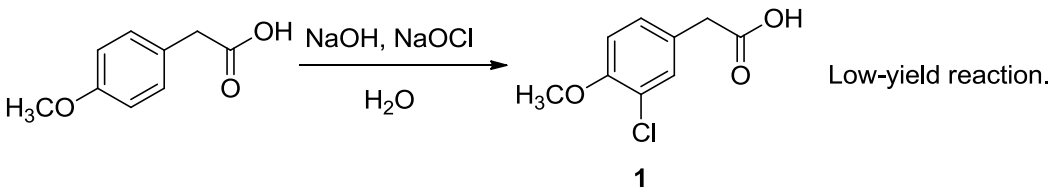

Scheme 4. The conditions utilized to synthesize intermediate 1 with a lower yield.

Due to the low yield and a large amount of impurities obtained from the above method, a second attempt, which is shown in Scheme 5, was carried out utilizing Oxone® as an oxidation agent and sodium chloride as the chlorine source.[31] The reaction was started with mixing Oxone® and a solution of anisic acid for 15 min, and the resulting mixture was then added sodium chloride and was allowed to stir for 6 h. Upon working up, only a trace amount of anisic acid and other impurities were indentified, making a yield of above 80% based on the integration of the ^{1}H NMR spectrum. The crude product was pure enough to be used in the next step without any further purification.

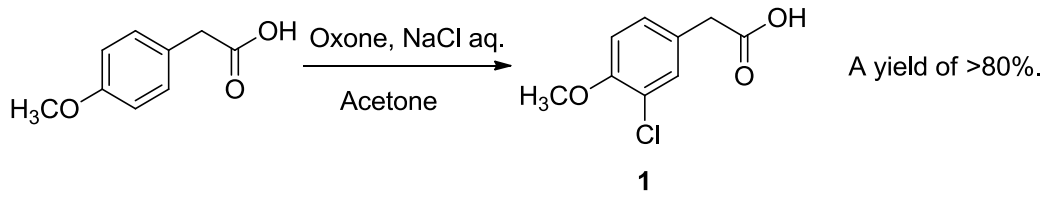

Scheme 5. The conditions utilized to synthesize intermediate 1 with a higher yield.

2.2. The Synthesis of Intermediates 2, 3 and 4.

The syntheses of intermediates **2**, **3** and **4** were carried out based on the similar steps that had been established in Dr. Baker's lab.[3]

In the preparation of intermediate **2** as shown in Scheme 5, the reaction mixture was successfully quenched by adding H_2O after cooling to room temperature. However, it was found difficult to dissolve the resulting slurry in the aqueous K_2CO_3 solution via refluxing by following the previously established procedures. The following extraction step utilizing ether was also attempted, and the resulting aqueous solution was further acidified with 2N HCl solution to give only a trace amount of white precipitate, which was later confirmed to be the product. Based on these observations, it was determined to use column chromatography (9:1 CH_2Cl_2:EtOAc) to isolate the desired product after the addition of H_2O. Instead of ether, dichloromethane was used to extract the mixture prior to running column chromatography, with the aim of increasing the yield (a yield of 46.0% was obtained).

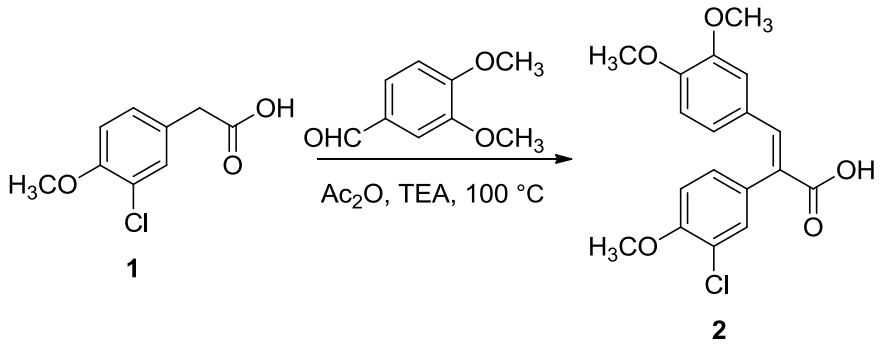

Scheme 6. The synthesis of intermediate 2.

Intermediate **3** was obtained in a yield of 92.5% by following the established step with no difficulty.[3] However, in the synthesis of intermediate **4**, due to the electron-withdrawing nature of the chlorine atom and the proposed mechanism of the $FeCl_3$-mediated ring closure reaction

shown in Scheme 8, longer reaction times and additional $FeCl_3$ were required.[32] It was determined that although stirring overnight with 8 equivalents of $FeCl_3$ was sufficient to convert most of the starting material, it was still necessary to check the reaction via TLC to assure whether another 8 equivalents of $FeCl_3$ were necessary after the overnight run. It was found that the majority of intermediate **3** could be converted completely to **4** with a yield of 90.2% within 3 h after the addition of the extra $FeCl_3$. However, it was surprising to observe that by adding the two batches of 8 equivalents of $FeCl_3$ all together at once and stirring overnight, there was still a large amount of starting material left in the reaction.

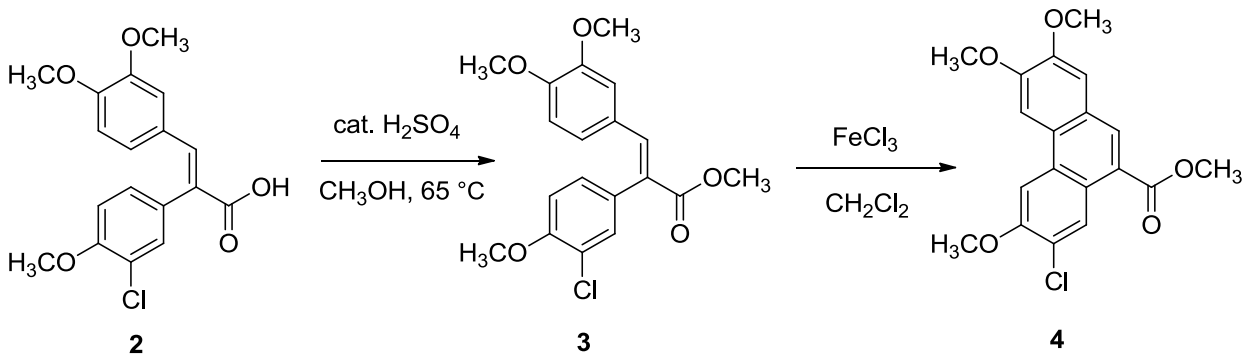

Scheme 7. The synthesis of intermediates 3 and 4.

2.3. The Synthesis of Intermediate 5.

The reported reduction conditions using $LiAlH_4$ was firstly attempted.[1] However, for most of the starting material, not only the ester moiety on **4** but also the chlorine attached to the aromatic system was reduced. A similar hydrogenolysis reaction has been reported on aryl bromides or aryl iodides, and on aryl chlorides if the reaction time is long enough.[33] Therefore, a milder reducing agent, $LiBH_4$, was then tested, which was shown to give a mixture of the desired

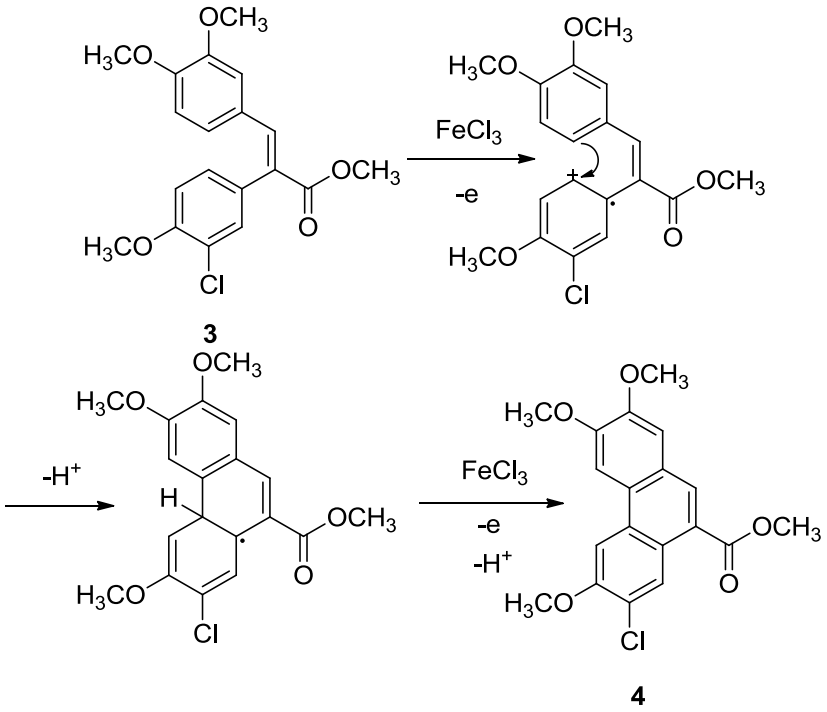

Scheme 8. The proposed mechanism of the ring-closure step.

product and a large amount the hydrogenolysis product. Thus a third reducing agent, DIBAL-H, was further evaluated, and upon quenching the reaction and filtering over Celite intermediate **5** was almost exclusively obtained with a yield of 87.8%. In addition the purity of the product in the residue resulted from the concentration of the filtrate was already high enough to be utilized directly in the next step reaction without further purification.

2.4. The Synthesis of Intermediate 6.

The brominated intermediate **6** was obtained by the addition of a bromine solution to a solution of compound **5** as shown in Scheme 10.[1] However, compared with the reported reaction on a related phenanthroindolizidine compound, the solid obtained after filtration was a mixture of two compounds. Therefore, further separation by column chromatography, followed by characterization by NMR spectroscopy and mass spectrometry were carried out. According to

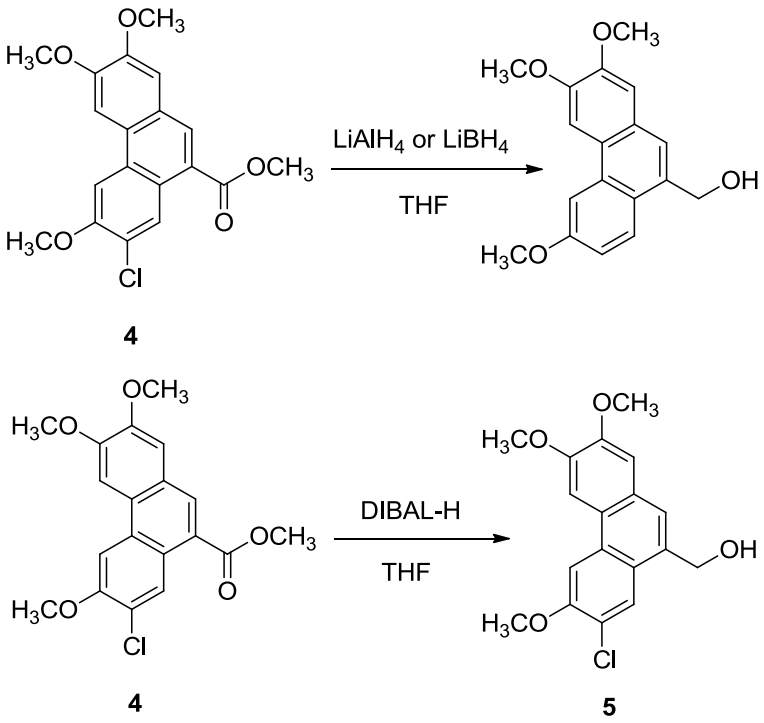

Scheme 9. The selection of the reducing agents in the synthesis of intermediate 5.

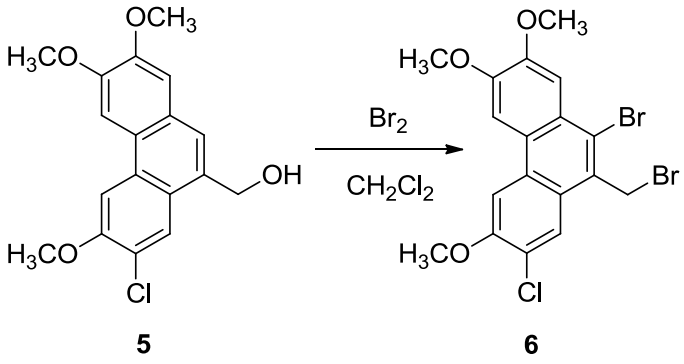

Scheme 10. The synthesis of intermediate 6.

the analysis results both of the two products were dibromo compounds, as they had identical mass values and similar NMR spectra. The major difference between the two compounds was determined to be the position of the bromine on the aromatic ring, and it has been observed previously that the bromine was capable of being attached at different positions on the aromatic system.[34] Fortunately, a crystal of the major product was produced via the diffusion crystallization method, and single-crystal X-ray crystallography confirmed the major compound in the mixture was the desired product **6**. However, the structure of the byproduct still remains unknown.

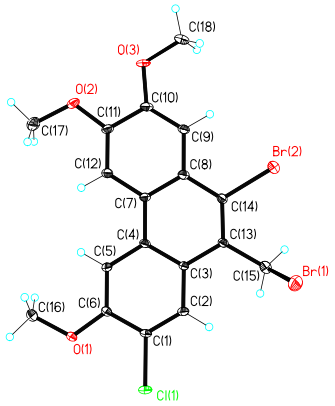

Figure 13. The single-crystal X-ray crystallographic analysis of the intermediate 6.

In order to increase the yield (38.7%), different reaction conditions were tested. The first attempt was to extend the reaction time up to 70 h. Unfortunately, by checking the reaction every hour after the addition of bromine, the byproduct was found to be formed almost simultaneously with the desired product. Meanwhile, the anticipated changes of the amount of the product were not obvious after 10 h reaction, suggesting a longer reaction time was ineffective. The reaction was also evaluated at lower temperature (-20 °C) during the addition of the bromine. Disappointedly a similar amount of the byproduct was also formed as when it was carried out at

0 °C. In addition, another bromination reagent, *N*-bromosuccinimide (NBS), was tested as well, disappointedly giving no product.[35]

By failing to increase the yield under a variety of conditions, speculations about the cause of the lower yield were made based on the proposed mechanism as shown in Scheme 11. According to the already reported bromination reactions, all the substituents on the aromatic ring system are electron-donating groups, which are beneficial to electrophilic attack based on the first step of the proposed mechanism. However, if one of the substituents is replaced with an electron-withdrawing group such as chlorine, the negative effect it generated could significantly lower the yield. In the meantime, the electron-withdrawing group at the 7-position might have an enormous effect on the electron density of the aromatic ring, leading to a byproduct with bromine on a different position.

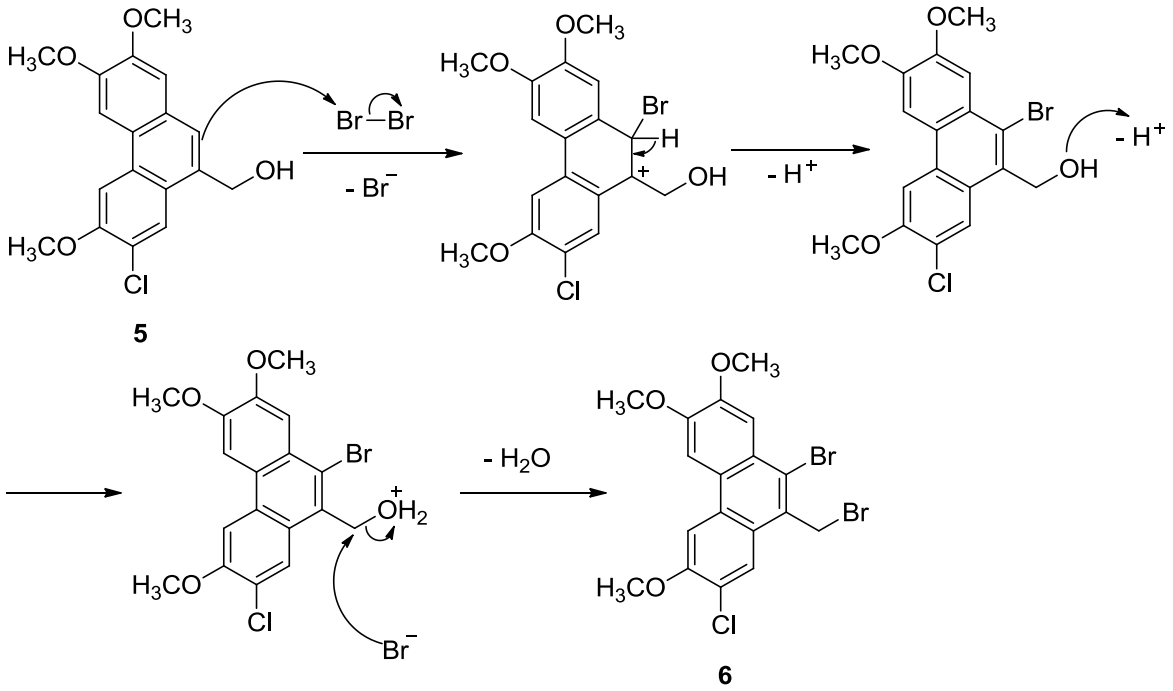

Scheme 11. The mechanism proposed for the bromination step.

2.5. The Synthesis of Intermediates 7 and 8.

For installation of the indolizidine ring system, intermediate **7** is required. The detailed synthesis of intermediate **7** was commenced with a reported route.[36] However, only a trace amount of product was discovered when the reaction conditions were strictly followed, which was to add *N,N'*-dicyclohexylcarbodiimide (DCC) after mixing diethylamine and *N*-Cbz-L-proline. A modified procedure was then tested by mixing DCC and *N*-Cbz-L-proline prior to adding diethylamine. The mixture was allowed to stir for 10 min at 0 °C until a white precipitate formed; afterwards, diethylamine was added, and the mixture was allowed to stir overnight at room temperature. The switch of the addition order allowed the formation of an adequate amount of *O*-acylisourea, which functions as a key intermediate in the coupling reaction. A moderate yield of 60.45% was achieved by using this modified procedure. In order to further increase the yield, it was attempted to heat the reaction in CH_3CN to 50 °C while stirring overnight, unfortunately, no dramatic improvement was observed. Further increasing the temperature to 80 °C and stirring overnight also resulted in no improvement in yield.

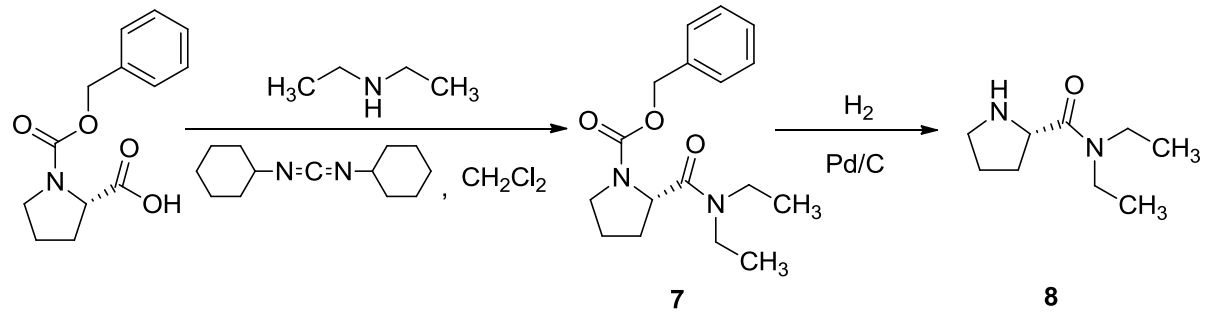

Scheme 12. The synthesis of intermediates 7 and 8.

With intermediate **7** in hands, the deprotection of the Cbz-group was carried out. Instead of using HBr in acetic acid as a deprotection reagent, a more convenient and cleaner hydrogenation method was introduced.[36, 37] In this method the intermediate **7** was mixed with Pd/C in ethanol, and the mixture was stirred under H_2 atmosphere (3 atm) for 4 h to obtain a clean product **8** with a 98.48% yield. Only simple filtration and concentration was necessary after the reaction and no further purification was needed. The measured specific rotation ($[\alpha]_D^{20}$ = -92.2 (*c* = 1.1, MeOH)) matches the reported value, indicating the no occurrence of possible racemization during the coupling reaction.[36]

2.6. The Synthesis of Intermediate 9 and DCB-3511 (10).

With intermediates **6** and **8** at hand, the coupling reaction with **8** was carried out with no major difficulties to give intermediate **9** with a yield of 68.2%. The specific rotation of **9** was measured (($[\alpha]_D^{20}$ = -57.9 (*c* = 2.7, CH_2Cl_2)) to assure that no racemization had taken place.

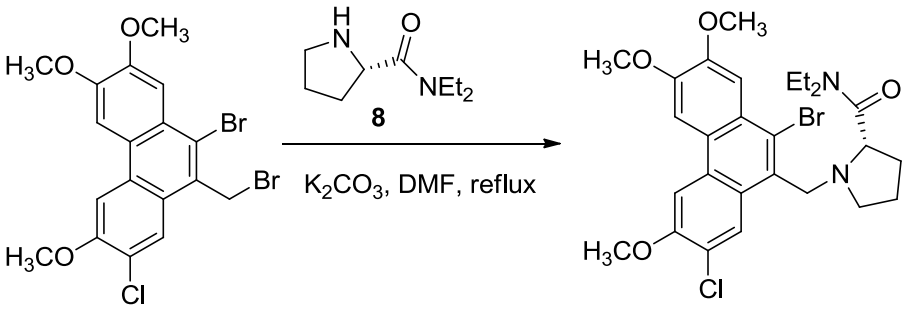

Scheme 13. The synthesis of intermediates 9.

To finish the synthesis, a ring closure-reaction was carried out under low temperature (-78 ℃), and $NaBH_4$ was utilized to give the stereoselective product DCB-3511 (**10**) in a

satisfactory yield of 89.6%, and the overall yield of the synthesis of DCB-3511 (**10**) is 6.77%. In order to confirm the purity and structure of this final product, an HPLC analysis and single-crystal X-ray analysis were performed. The stereoselectivity of $NaBH_4$ was confirmed by the correct X-ray crystal structure shown in Figure 14, and the single peak in the HPLC chromatogram shown in Figure 15 and the corresponding NMR spectra provided the information that no observable diastereomer was generated.

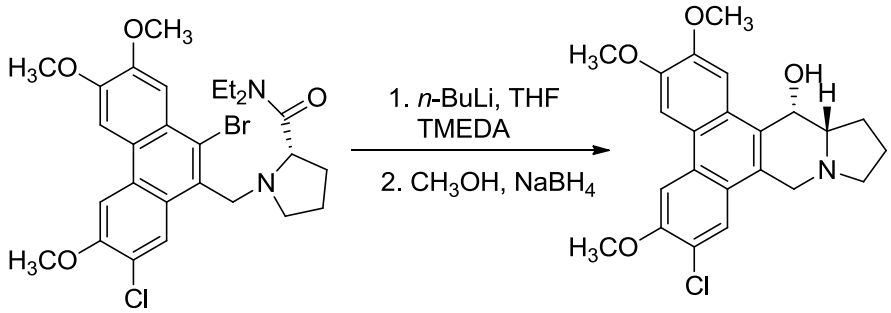

9 **10**

Scheme 14. The synthesis of DCB-3511 (10).

3. The Synthesis of DCB-3510 (18).

The synthesis of DCB-3510 was designed based on the synthesis of DCB-3511 and the established procedures in Dr. Baker's lab.[2, 3]

3.1. The Syntheses of Intermediates 11 to 15.

The syntheses of intermediates **11** and **12** was carried out based on the previously established procedures in Dr. Baker's lab.[3] Instead of veratraldehyde, intermediate **1** was condensed with vanillin under aldol conditions to give the intermediate **11** in a yield of 80.0%. Then an

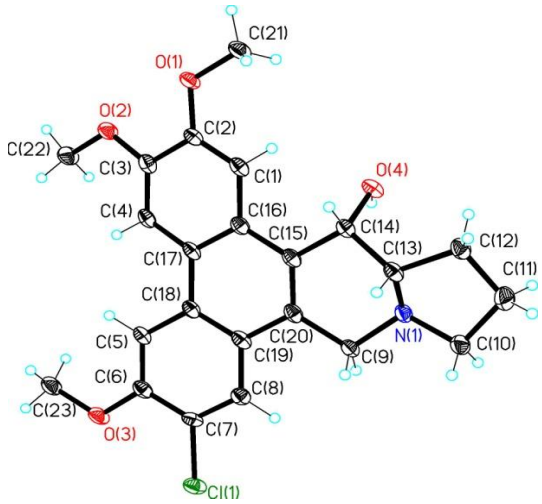

Figure 14. The single-crystal X-ray crystallographic analysis of DCB-3511 (10).

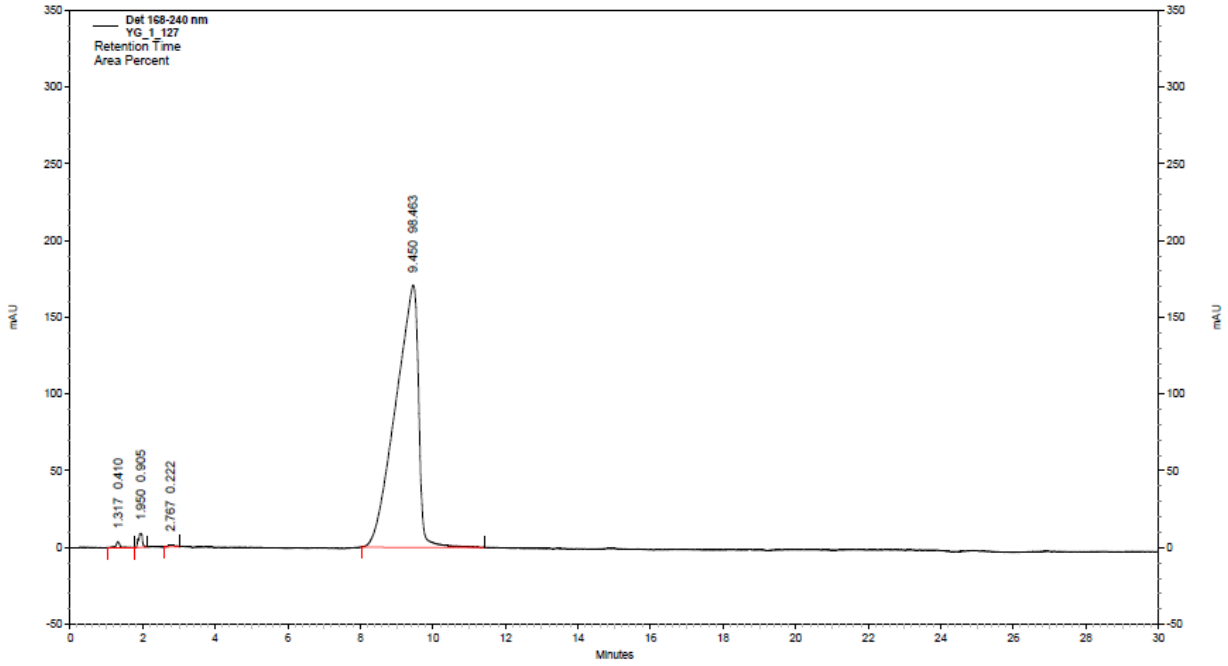

Figure 15. The HPLC analysis of DCB-3511 (10).

esterification was carried out to give **12** in a yield of 93.2% with no major difficulty. Afterwards intermediate **13** was synthesized with a yield of 93.3% by installing a propargyl group, which not only constituted an important moiety in the final product, but also functioned as an HO-protecting group during the ring-closure step.[2]

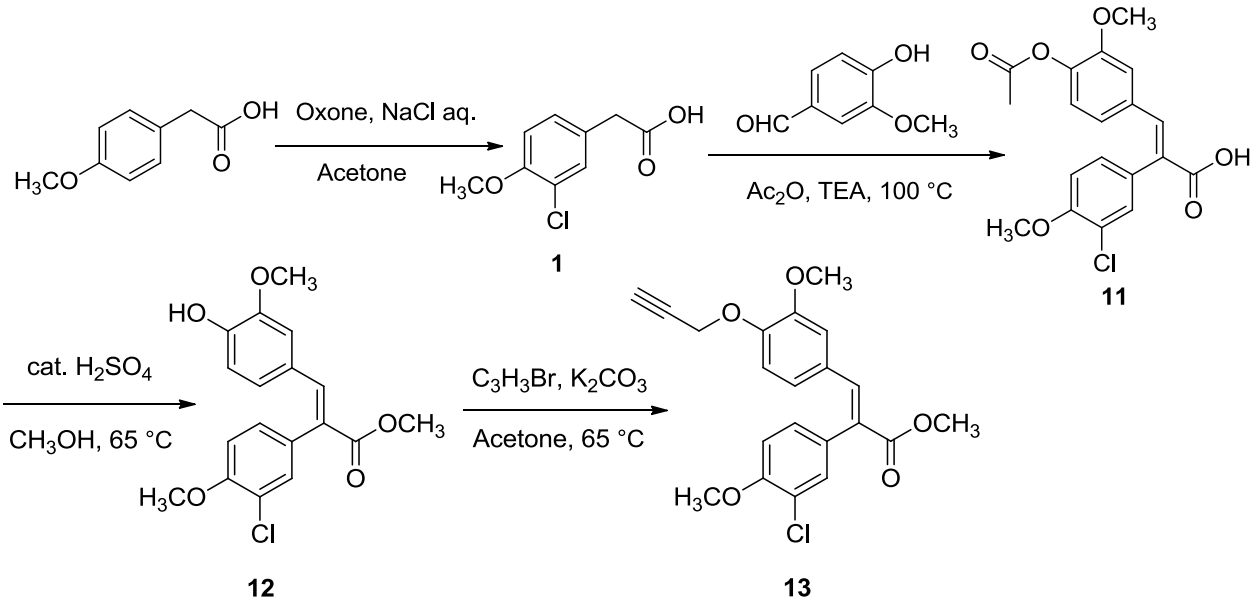

Scheme 15. The synthesis of intermediates of 11, 12 and 13.

The same conditions used to synthesize **4** were applied directly to making intermediate **14** without modifications, and a satisfactory yield of 80.3% was obtained. An additional 8 equivalents of $FeCl_3$ were necessary to convert all the starting material to product after 8 equivalents of $FeCl_3$ were used initially for the overnight reaction. However, a mixture in which a byproduct **14'** comprised up to 4.1% of the total weight was isolated and characterized by mass spectrometry and ^{1}H NMR spectroscopy. Interestingly, the byproduct has the same mass as the major product, and further study by ^{1}H NMR spectroscopy, which was shown in Figure 16, indicated the possibility of formation of a ring-closed product at a different aromatic carbon as indicated by the wide spin-spin splitting (9.0 Hz) at 8.90 ppm and 7.36 ppm, which suggests an

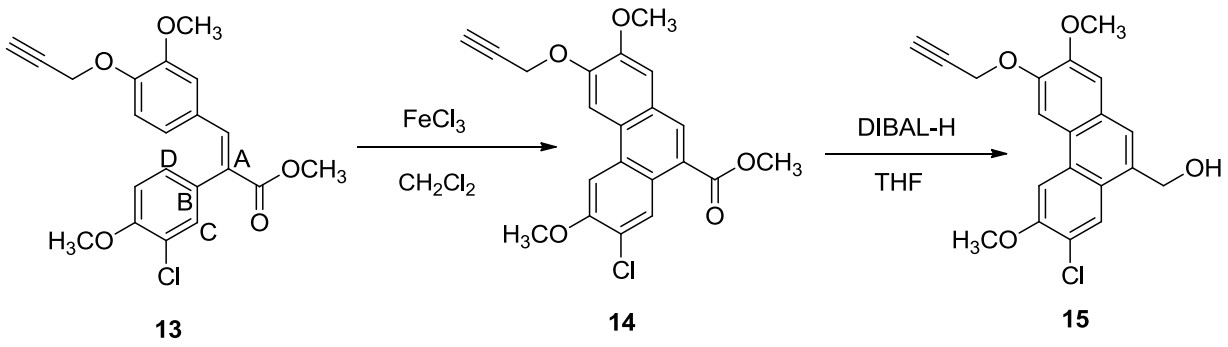

Scheme 16. The synthesis of intermediates of 14 and 15.

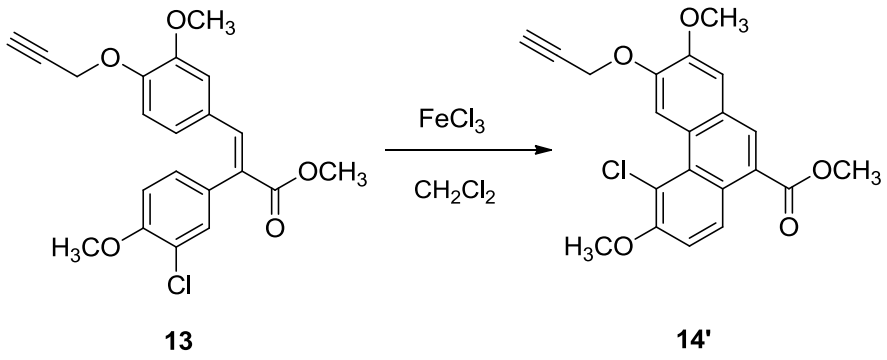

Scheme 17. The reaction generating byproduct 14'.

ortho arrangement of the two aromatic protons at H-7 and H-8. Speculation was made that since the southern ring could rotate along carbon A and carbon B bond, thus both carbon C and carbon D were able to be attacked by the northern ring according to the aforementioned mechanism, which resulted in different products. It was possible that the chlorine altered the electron density on the southern ring, which eventually made the carbon C capable of being oxidized for the ring closure.

Intermediate **15** could be obtained by the reduction of **14** utilizing DIBAL-H as well, and neither the propargyl group nor the chlorine was reduced during the reaction.

3.2. The Synthesis of Intermediate 16.

The initial plan of the synthesis of intermediate **16** was to install an alkyne protecting group before the bromination reaction due to the possibility of bromination of the alkyne. As shown in Scheme 18, dicobalt octacarbonyl was selected as the protective group in the proposed protecting route, and the desired product could be obtained by oxidative degradation using $Fe(NO_3)_3 \cdot 9H_2O$.[38] Unfortunately, no protected product was found after stirring for 36 h with 3 equivalents of dicobalt octacarbonyl; therefore, it was determined to test the direct bromination without protection as shown in Scheme 19.

To our delight the bromine added only to the aromatic ring to give a yield of 53.6% without interacting with the alkyne, and the attempted explanation was that the electron density of the aromatic ring is higher than that of the alkyne, which made it the preferred place to conduct the elctrophilic attack. A crystal of intermediate **16** was prepared, and the single-crystal X-ray crystallographic analysis was performed, providing the result seen in Figure 17.

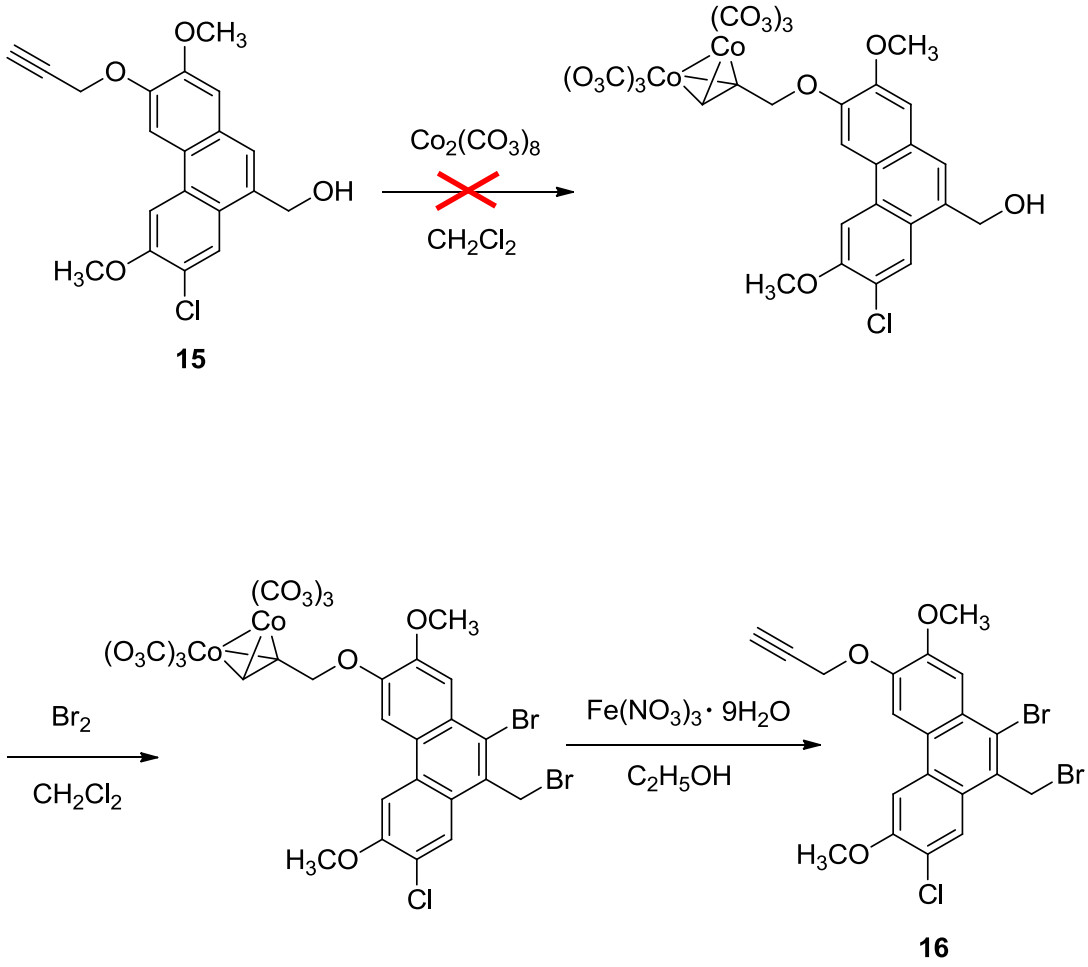

Scheme 18. The initial synthetic route to intermediate 16.

Figure 16. The ^{1}H NMR (300 MHz, $CDCl_3$) spectrum of the byproduct 14'. (First spectrum: Overall view; Second spectrum: Enlarged view of the aromatic protons).

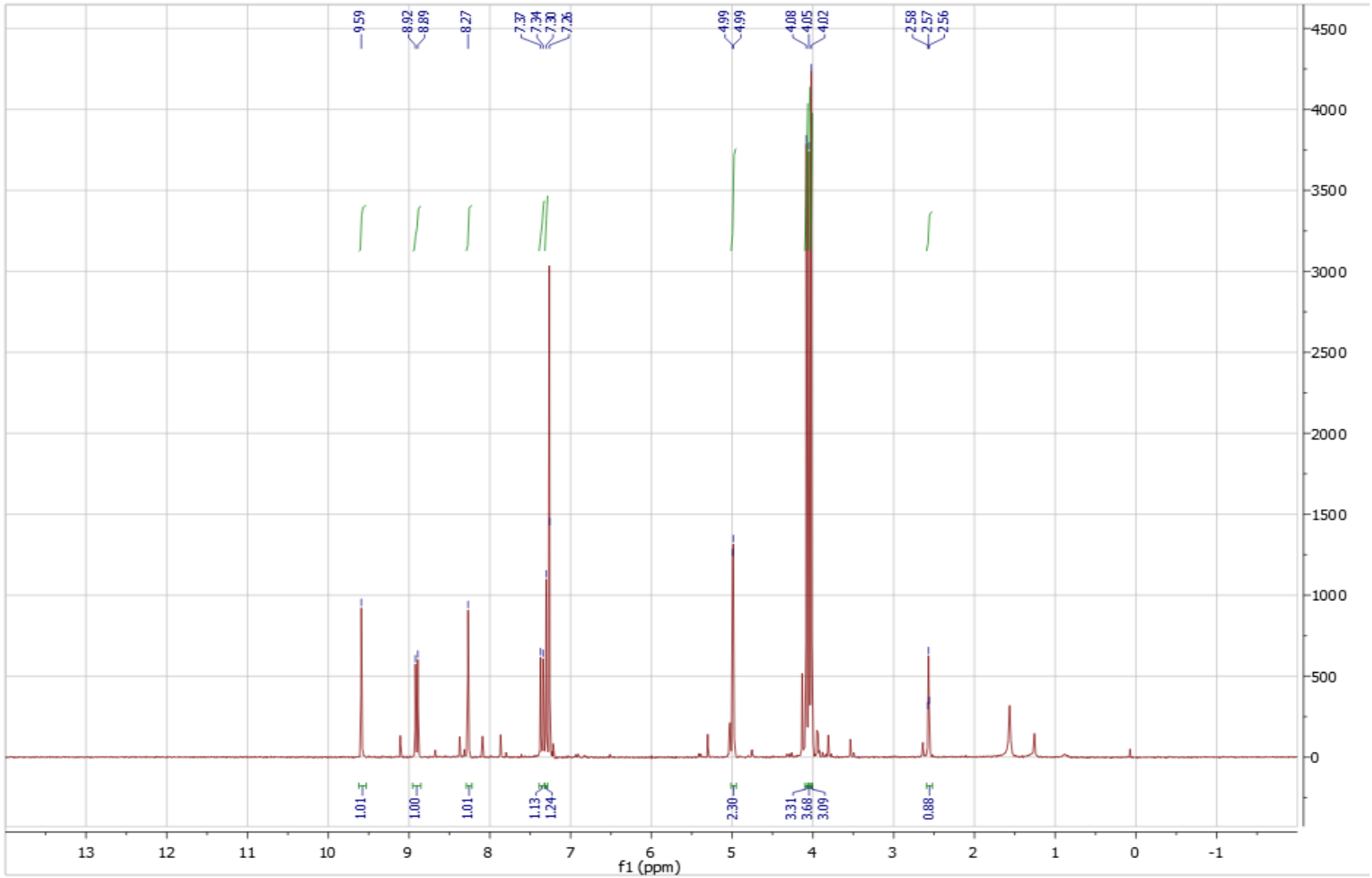

Figure 16. Cont'd.

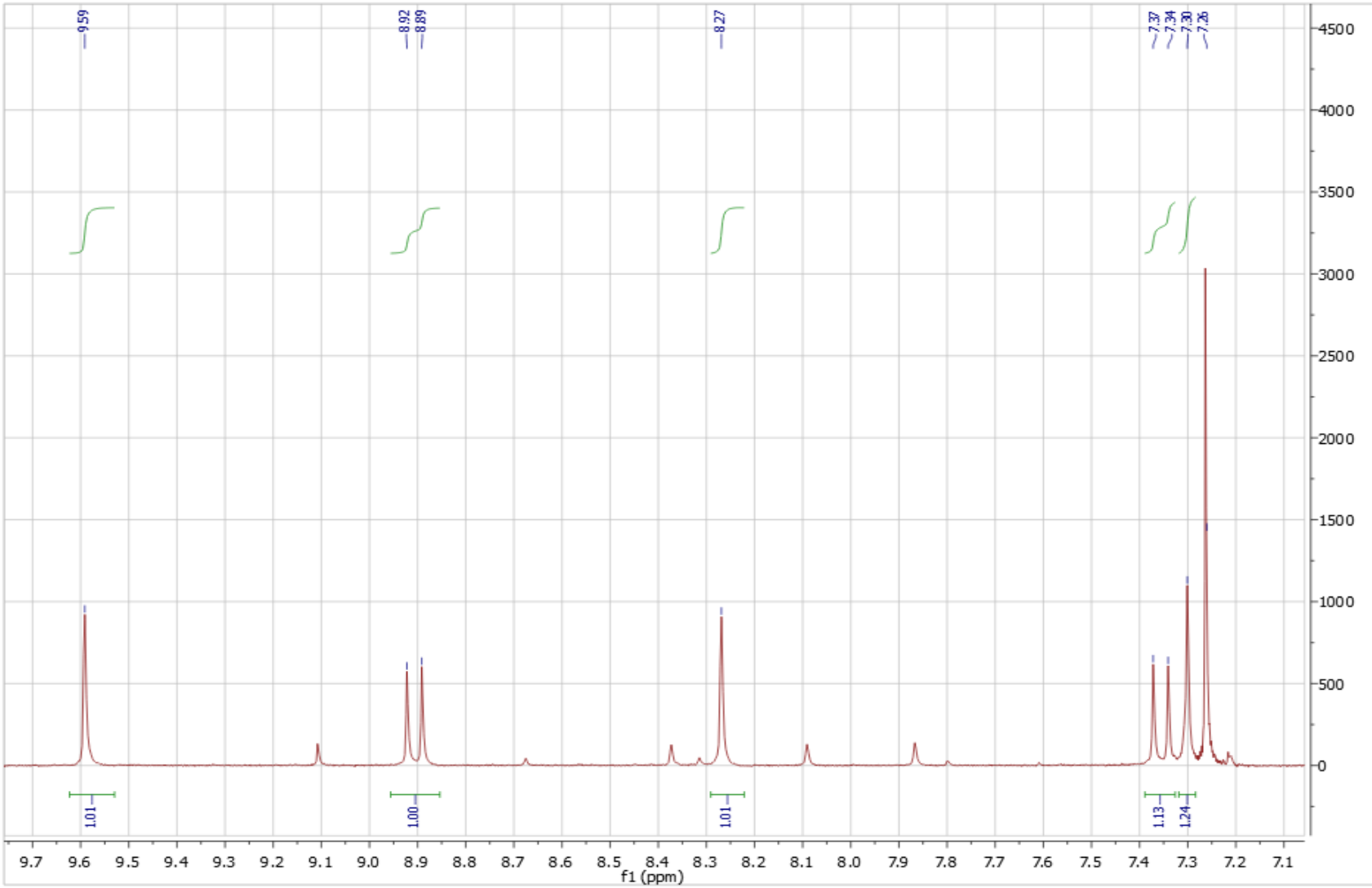

Figure 16. Cont'd.

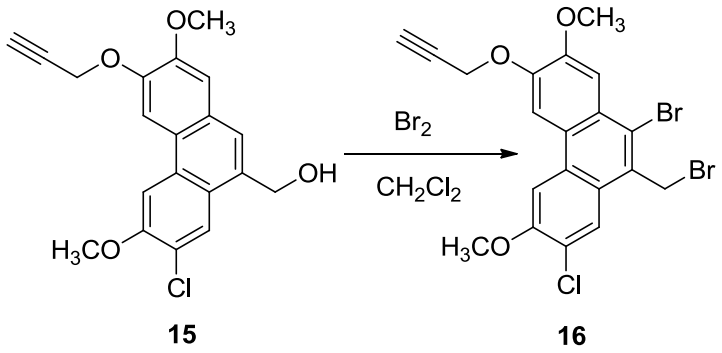

Scheme 19. The modified synthesis of intermediate 16.

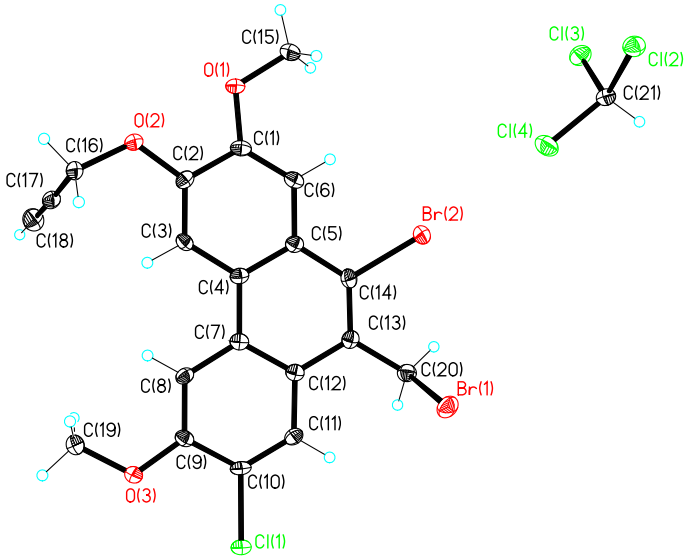

Figure 17. The single-crystal X-ray crystallographic analysis of intermediate 16.

3.3. The Synthesis of Intermediate 17.

With intermediate **16** in hand, the synthesis of **17** was carried out following the same procedure used in preparing intermediate **9**. However, in order to avoid the possible propargyl Claisen rearrangement which would yield the allene as shown in Scheme 20, the reaction temperature was lowered from reflux (153 °C) to 70 °C. These conditions were selected as all Claisen rearrangement reactions are said to happen above 100 °C if uncatalyzed.[39] Under these conditions the desired product was obtained with a yield of close to 90%. Additionally, a test of this reaction under reflux conditions was attempted, and several byproducts were obtained with no desired product detected. The ^{1}H NMR spectrum of the major byproducts was believed to be the rearranged product based on the disappearance of the terminal alkyne triplet peak in the high-field region and the appearance of a similar peak at 7.06 ppm representing the internal allene proton, as could be seen in Figure 18. In addition, the *m/z* of the $[M+H]^{+}$ peak of this byproduct was obtained as 587.13095 by mass spectrometry, which was almost identical as the one of **17** as 587.13118.

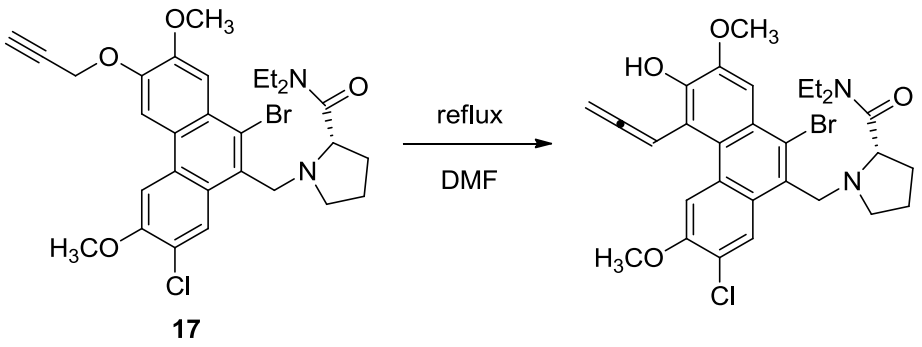

Scheme 20. The proposed formation of the unexpected product in the synthesis of intermediate 17.

Figure 18. The ^{1}H NMR (300 MHz, $CDCl_3$) spectrum of the unexpected product formed in the synthesis of intermediate 17. (First spectrum: Overall view; Last two spectra: Detailed view.)

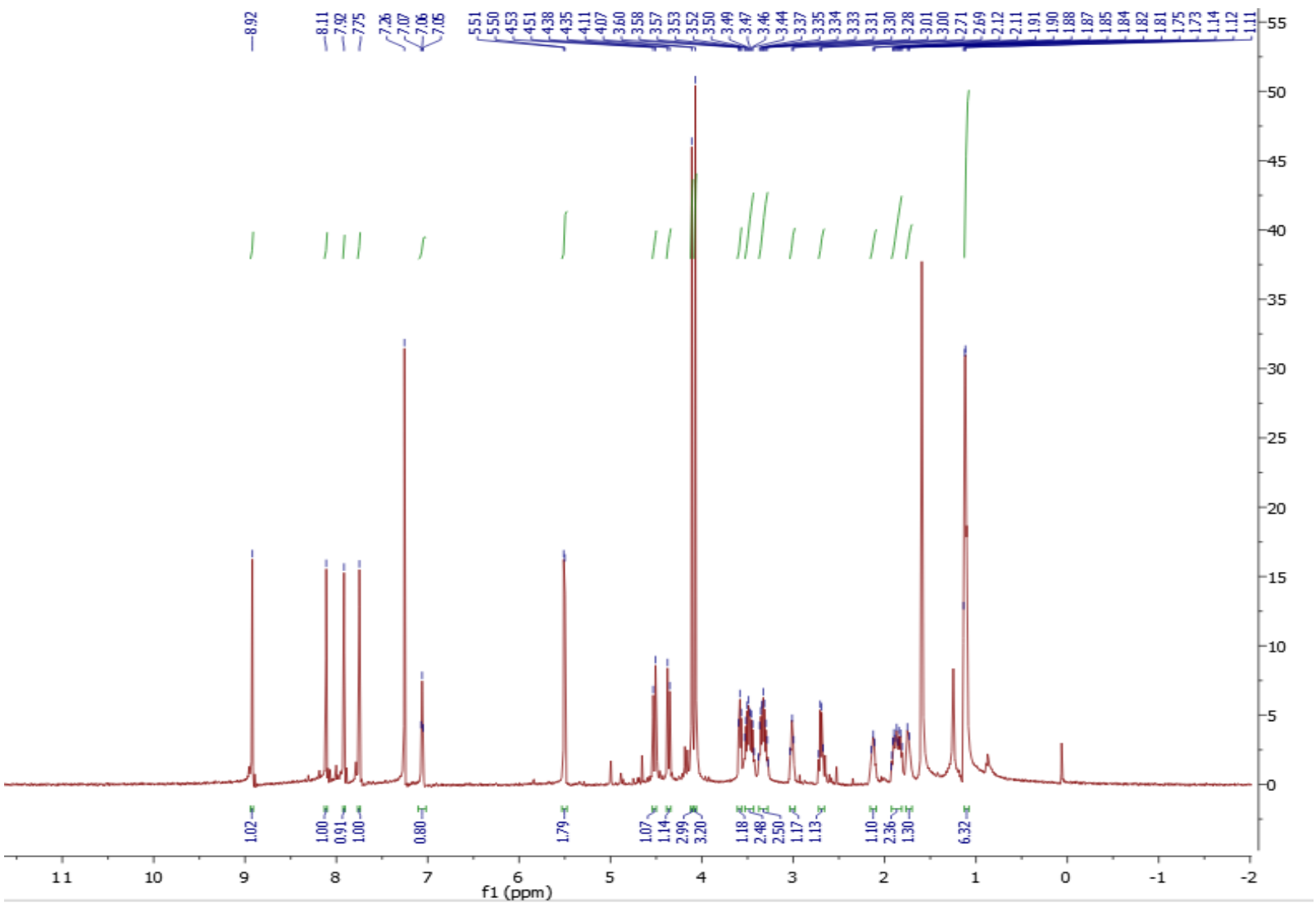

Figure 18. Cont'd.

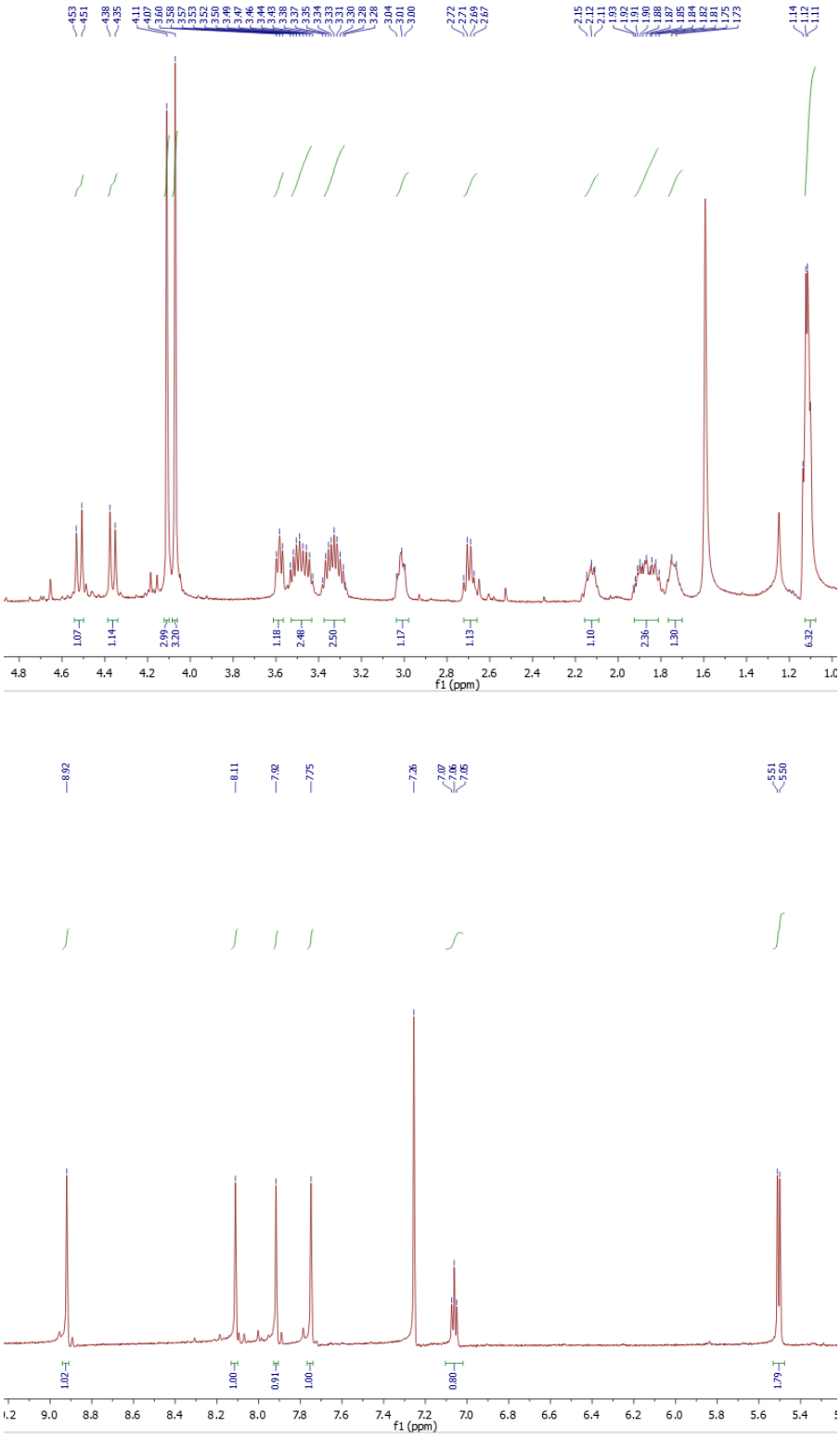

Figure 18. Cont'd.

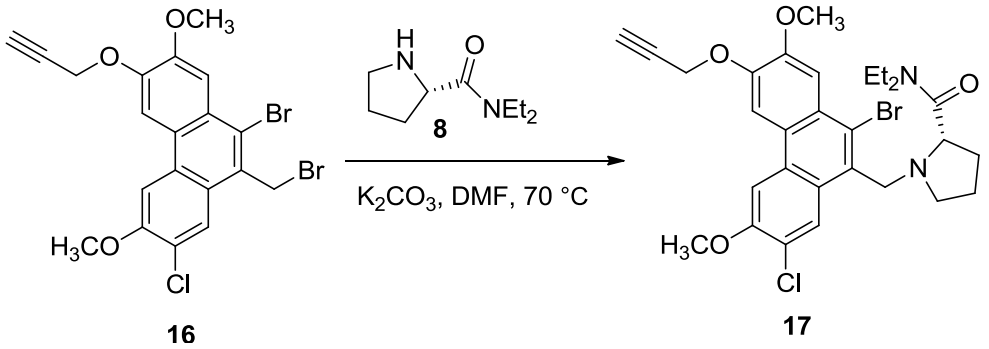

Scheme 21. The synthesis of intermediate 17.

3.4. The Synthesis of DCB-3510 (18).

The synthesis of DCB-3510 was carried out utilizing conditions similar to those used in preparing **10**. However, one additional equivalent of *n*-BuLi was used to compensate the possible consumption by the terminal alkyne. The final product was obtained with no major difficulty, and a yield of 94.1% was achieved without the observation of any possible side reactions caused by the acetylide. The overall yield of the synthesis of DCB-3510 (**18**) is 20.5%. It was also confirmed by HPLC and NMR spectroscopy that the major product was optically pure as shown in Figure 19, as no observable diastereomer was formed.

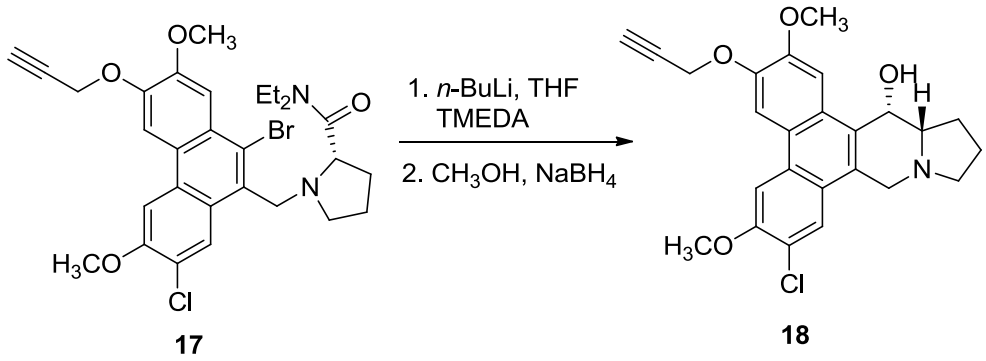

Scheme 22. The synthesis of DCB-3510 (18).

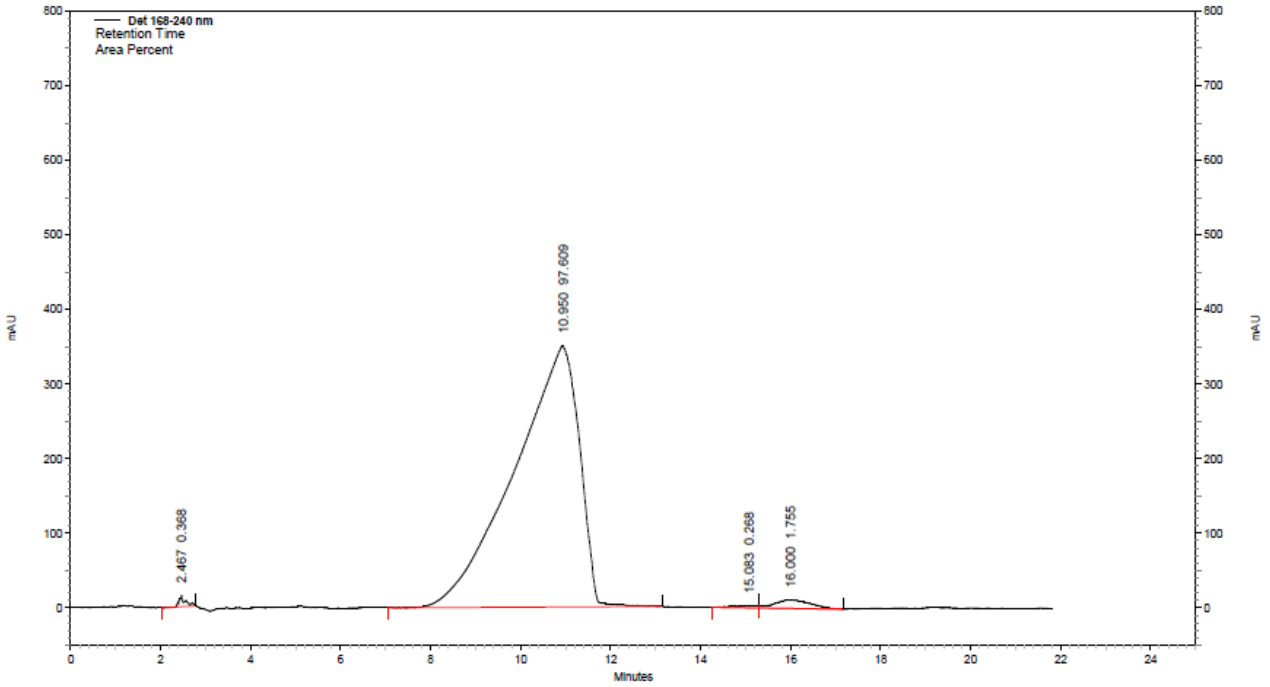

Figure 19. The HPLC analysis of DCB-3510 (18).

4. The Synthesis of DCB-3512 (20a).

4.1. The Selection of the Synthetic Targets.

Two triazole-modified analogues (**20** and **22**) shown in Figure 20 were selected as the synthetic targets from the aforementioned triazole analogues designed by the CoMFA model based on both the CoMFA prediction results, which was to increase the volume and decrease the electron density at the 3-position, and the assessment of the feasibility of synthesizing these molecules. The selected analogues ranged from the simple acyl triazole to a more complex

aromatic acyl-substituted triazole group. However, before carrying out the synthesis of **22**, the synthesis of compound **21** was firstly attempted.

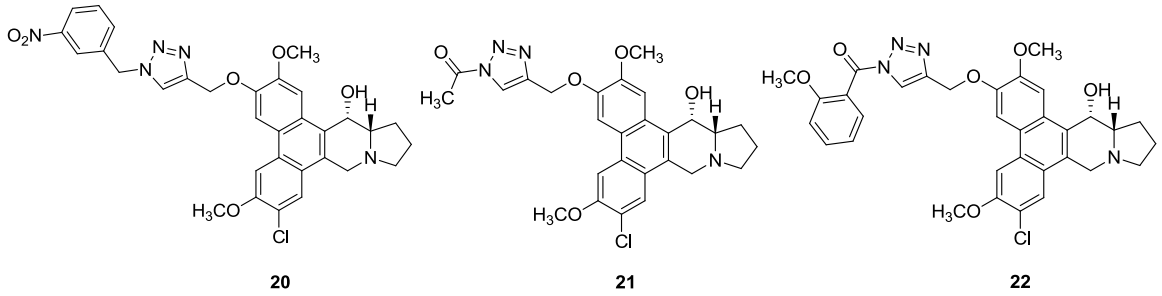

Figure 20. The structures of compounds 20, 21 and 22.

4.2. The Attempted Synthesis of Intermediates 21 and 22.

The first synthesis was carried out on acetyl azide by refluxing acetyl chloride and sodium azide in a water–THF solvent system.[40] However, only a trace amount of product was detected by mass spectrometry, and due to the volatility of the acetyl chloride and explosive potential of this small molecular weight organic azide, a decision was made to abandon the attempted synthesis of **21**.

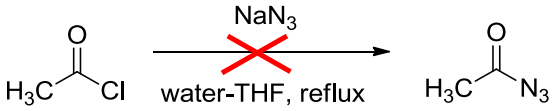

Scheme 23. The proposed synthesis of acetyl azide.

The focus was then switched to the synthesis of 2-methoxybenzoyl azide by introducing *t*-BuOCl as an oxidative reagent and NaN_3 as the azide source.[41] The *t*-BuOCl prepared *in situ* was stirred with NaN_3 for 24 h, and column chromatography was performed to isolate the pure organic azide product.[42] A longer reaction time aimed at increasing the yield was tried; however instead of increasing the yield, a byproduct from the Curtius rearrangement, 2-methoxyaniline, was detected. Another method to synthesize 2-methoxybenzoyl azide starting from 2-methoxybenzoic acid using cyanuric chloride was attempted as well; unfortunately, it gave an unsatisfactory result.[43] After obtaining 2-methoxybenzoyl azide, although in an unsatisfactory yield, the copper(I)-catalyzed alkyne–azide cycloaddition (CuAAC) was carried out on DCB-3510 and 2-methoxybenzoyl azide using a more affordable salt, $CuSO_4 \cdot 5H_2O$, as the catalyst and sodium ascorbate as the reducing agent.[44] However, only starting material (DCB-3510) and the 3-hydroxy DCB-3510 analogue, which resulted from ripping off of the propargyl group, were recovered from the reaction mixture. By suspecting the catalytic ability of the combination of Cu(II) salt and sodium ascorbate, Cu(I) salt (CuI) was introduced directly.[45] Again the starting material, DCB-3510, was recovered from the reaction mixture with no sign of the cycloaddition product.

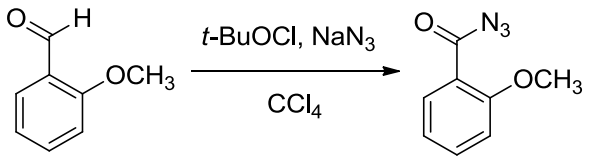

Scheme 24. The attempted synthesis of 2-methoxybenzoyl azide.

By failing to obtain either compound **21** or **22**, the synthetic target was switched to making solely alkyl triazole analogues since suspicion was falling on the feasibility of conducting CuAAC on an acyl azide largely due to its unreactive nature. Therefore, the synthesis of compound **20** was attempted.

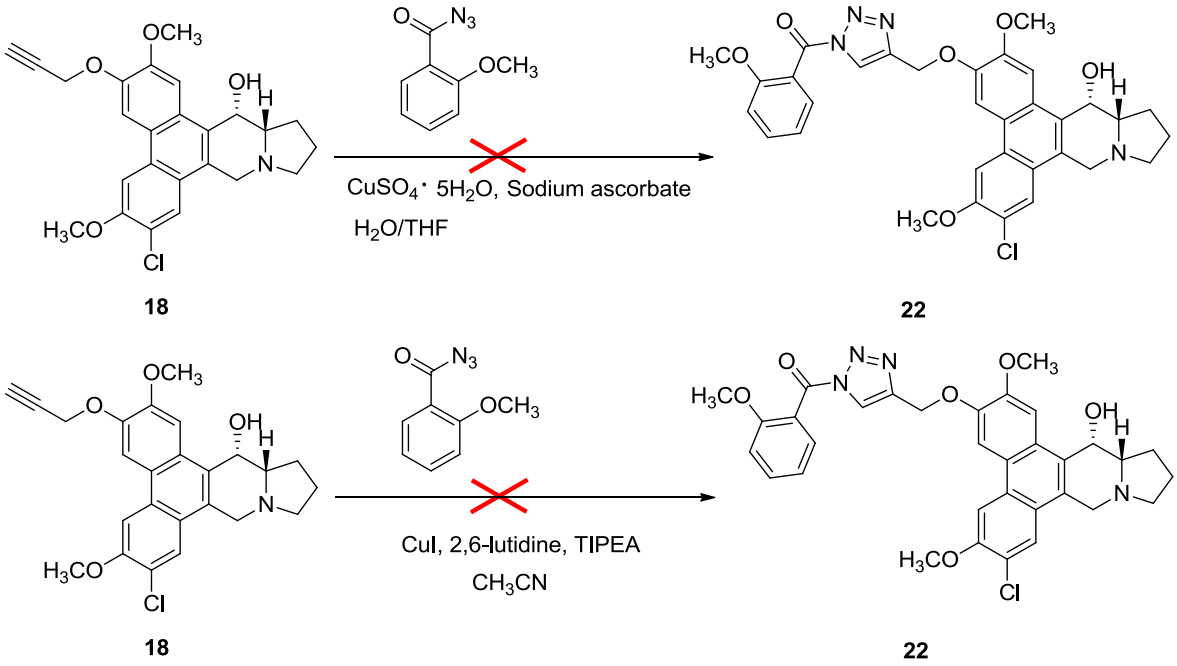

Scheme 25. The attempted synthesis of compound 22 via CuAAC (Top: indirect introduction of Cu(I) catalyst; Bottom: direct introduction of Cu(I) catalyst).

The synthesis of *N*-aralkyl-substituted **20** (Figure 20) was commenced with the preparation of 1-(azidomethyl)-3-nitrobenzene (**19**) based on the reported procedures.[46] However, only a moderate yield of 66.67% of **19** was achieved by analyzing the ^{1}H NMR integration of the spectrum, and a mixture of 3-nitrobenzyl bromide and **19** was obtained. Due to the difficulty of separating the resulting mixture containing two compounds with extremely similar polarities, together with **19**'s explosive nature and its unstable properties on silica gel, it was determined to

utilize the crude product directly in the synthesis of **20**. The CuAAC reaction was carried out using Cu(I) salt (CuI) directly as the catalyst, and the major product was isolated.[45] The purity of the product was determined by HPLC as shown in Figure 21.

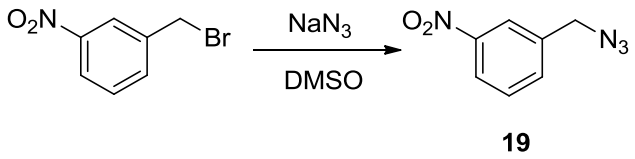

19

Scheme 26. The synthesis of intermediate 19.

Fortunately, the CuAAC reaction was successfully performed; however, what was interesting was the tertiary amine in the indolizidine moiety reacted with the 3-nitrobenzyl bromide in the crude product to yield a quaternary ammonium salt **20a** (DCB-3512) shown in Scheme 27 with a yield of 41.3%, and the majority of the rest of the impurities was confirmed to be the corresponding quaternary ammonium salt of DCB-3510 (i.e., the salt of **18**). In the beginning a salt was detected by mass spectrometry with a bromide as the negative ion and a molecule constituted of the target molecule and an extra 3-nitrobenzyl group as the positive ion. Although it was concluded the material was a single molecule by HPLC and mass spectrometric analysis, a DOSY NMR experiment was performed to further confirm that it was a single molecule. The speculation was then made that the extra benzyl CH_2 group was associated with on either the 3-nitrogen in the triazole or on the nitrogen in the indolizidine to make a 1,2,3-triazolium ion or a quaternary ammonium ion. Further NMR spectroscopy studies helped to draw the definitive conclusion that the extra 3-nitrobenzyl group was on the indolizidine nitrogen. The ^{1}H and ^{13}C NMR assignments of compound **20a** were made based on the analysis of COSY, HSQC, HMBC,

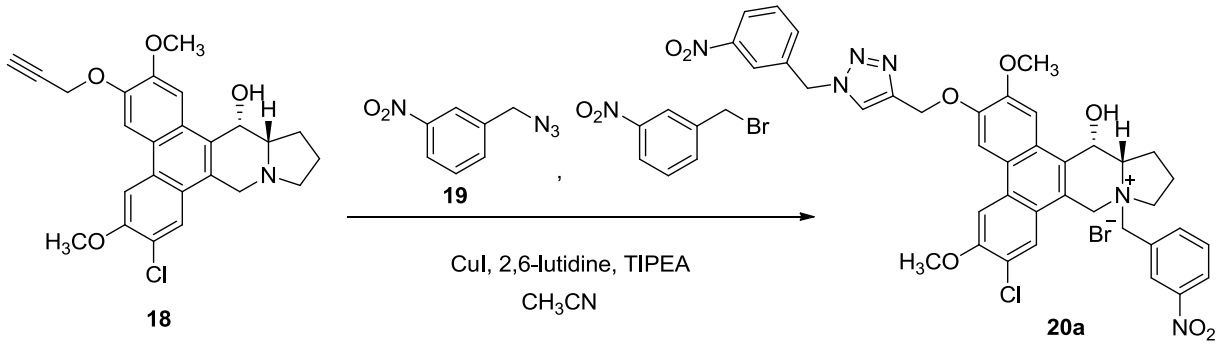

Scheme 27. The synthesis of DCB-3512 (20a).

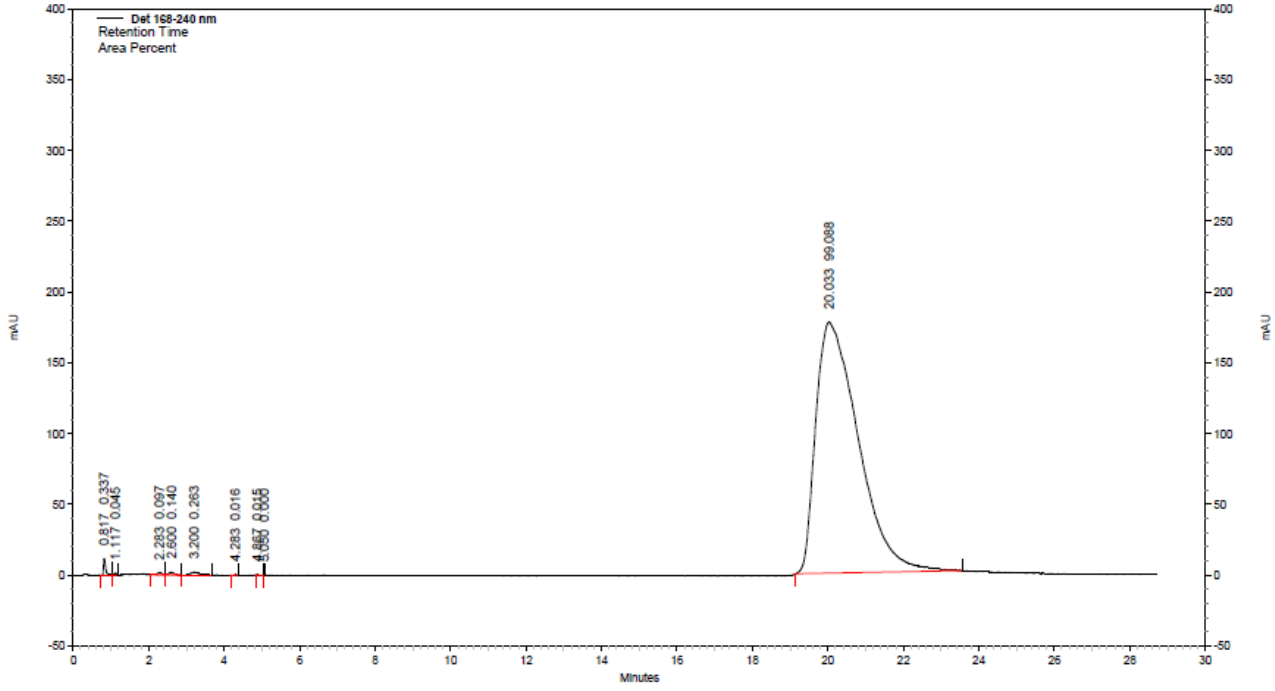

Figure 21. The HPLC analysis of DCB-3512 (20a).

H2BC, NOESY and ^{1}H-^{15}N HMBC spectra as shown in Figure 22.

The positions of two identical 3-nitrobenzyl groups **A** and **B** were made mostly based on HMBC and NOESY spectra. In the HMBC spectrum, the hydrogens of one of the two CH_2 groups with chemical shifts of 4.34 and 4.85 ppm could not only correlate to three aromatic carbons, but also to two aliphatic carbons with chemical shifts of 60.81 and 57.48 ppm, indicating its proximity to the indolizidine moiety. Therefore these two hydrogens were on the **B** 3-nitrobenzyl group. In the NOESY spectrum, the CH_2 group with a chemical shift of 5.72 ppm correlated with the triazole hydrogen (8.10 ppm), suggesting its belonging to the **A** 3-nitrobenzyl group that was proximate to the triazole moiety. In addition, one of the hydrogens of CH_2 in group **B** at the chemical shift of 4.34 ppm was also close to two hydrogens with chemical shifts of 2.69 and 2.54 ppm; meanwhile, the other hydrogen in the CH_2 group with a chemical shift of 4.85 was close to the hydrogen in the hydroxyl group at 6.30 ppm, indicating the possible position of the flexible 3-nitrobenzyl group as behind the indolizidine ring as can be shown in 3D structure constructed in the SYBYL program in Figure 23.

The unexpected compound **20a** was formed mainly due to the usage of the crude mixture of 3-nitrobenzyl azide and 3-nitrobenzyl bromide. Since a large excess crude 3-nitrobenzyl azide was used in the CuAAC reaction to assure the maximum conversion of DCB-3510, it was inevitable to introduce almost the same excess amount of 3-nitrobenyl bromide into the reaction system, which reacted with the tertiary amine to give the ammonium salt. Although the resulting product was not the desired compound **20**, it might provide a promising candidate according to the CoMFA contour map prediction. Firstly, as can be seen in the contour map in Figure 24, there was a large red area occupying the space that the 3-nitrobenzyl group **B** fell into, meaning the negatively charged groups and H-bond acceptors were favored. Fortunately, the nitro group

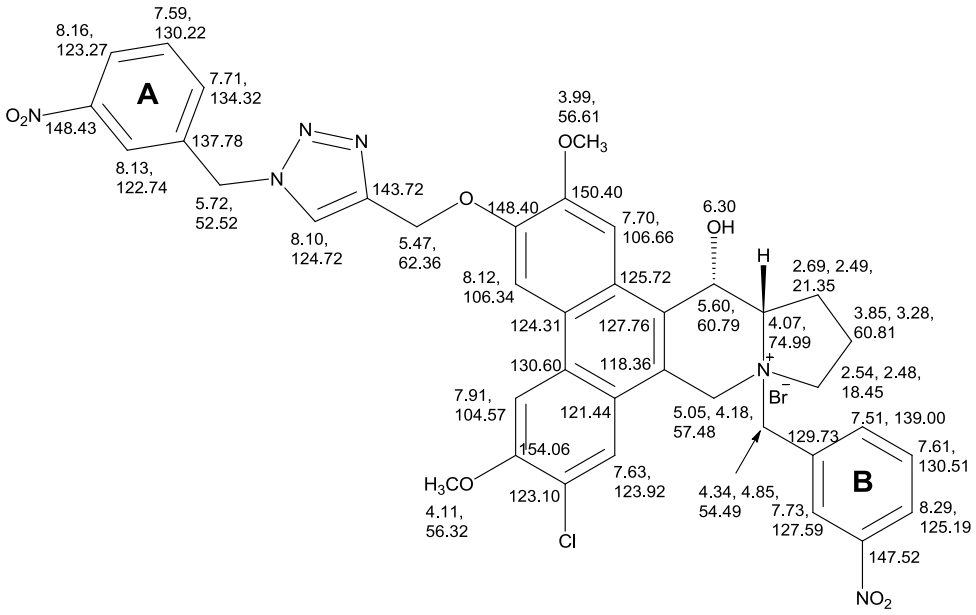

Figure 22. The ^{1}H and ^{13}C NMR chemical shift assignments of DCB-3512 (20a).

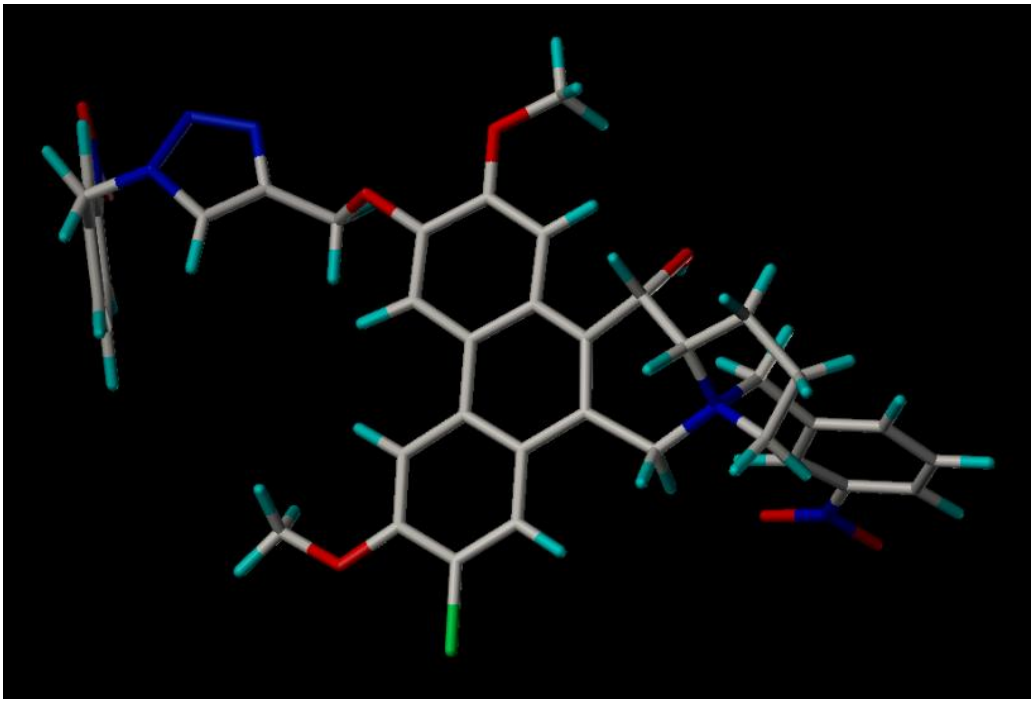

Figure 23. The energy-minimized 3D structure of DCB-3512 (20a).

in 3-nitrobenzyl group **B** was able to provide extra negatively charged groups and H-bond acceptors, making compound **20a** a possible promising candidate. Compound **20a** was also placed into the CoMFA model to predict its activity against NF-κB pathway, and a moderate result of 7.399 (pIC_{50}) was obtained. However, due to the difficulties of constructing the salt molecule and assigning the corresponding charges in the SYBYL program, and the uncertain positions of the flexible 3-nitrobenzyl group **B**, it is not feasible to accurately predict the activity of compound **20a**. Besides the CoMFA predictions, the alteration of the solubility of this analogue via its transformation into a salt also rendered **20a** a potential active candidate. One major aspect that was detrimental to the activities of tylophorine analogues was their poor solubility in either organic solvents or water; however by modifying to the corresponding salt the solubility in water might increase dramatically, which could ultimately improve the biological activity.

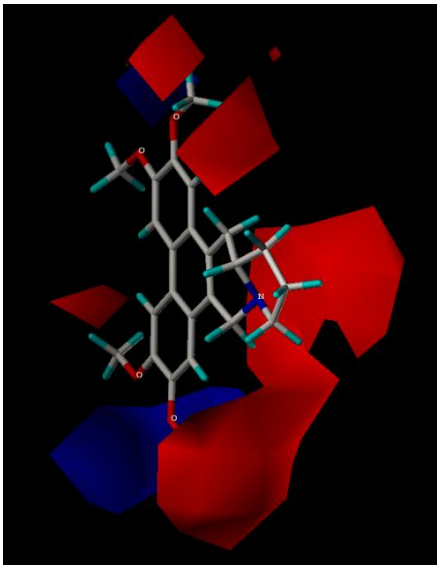

Figure 24. The electrostatic contour map in the novel CoMFA model. (Red area: negative charge and H-bond acceptors favored; Blue area: positive charge and H-bond donor favored.)

5. The Attempted Synthesis of Compound 28 (Scheme 32).

In the synthesis of compound **28**, the chlorodifluoromethoxy group was determined to be installed at an early stage as a protective group, aiming at avoiding the extra steps and the harsh conditions of protecting and deprotecting of the hydroxyl group at the late stage, where the unstable phenanthroindolizidine alkaloid might be easily decomposed.

5.1. The Synthesis of Intermediate 23.

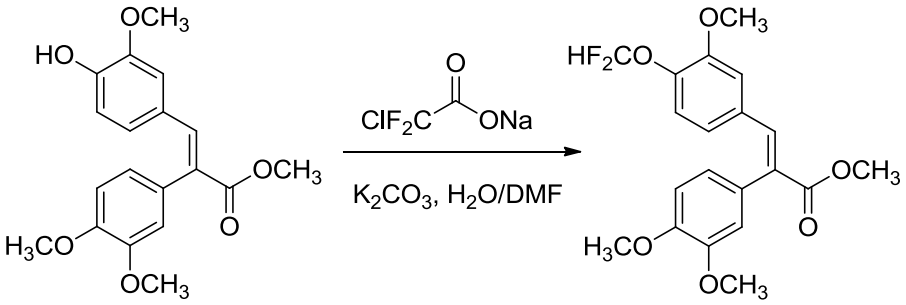

23

Scheme 28. The synthesis of intermediate 23.

The synthesis of intermediate **23** began with (*E*)-methyl 2-(3,4-dimethoxyphenyl)-3-(4-hydroxy-3-methoxyphenyl)acrylate, which was prepared based on the procedures already established in Dr. Baker's lab.[3] Sodium chlorodifluoroacetate, which functioned as a difluorocarbene precursor, was utilized under thermolysis conditions to give the difluoromethoxy group on the north ring with a yield of 34.4%.[47, 48] The difluoromethoxy ^{1}H and ^{13}C NMR peaks could be found in the spectra shown below, proving the successful installation of the difluoromethoxy group.

Figure 25. The ^{1}H NMR (500 MHz, $CDCl_3$) spectrum (first specturm) and ^{13}C NMR (125 MHz, $CDCl_3$) spectrum (second spectrum) of intermediate 23 with the enlarged view of difluoromethoxy peaks.

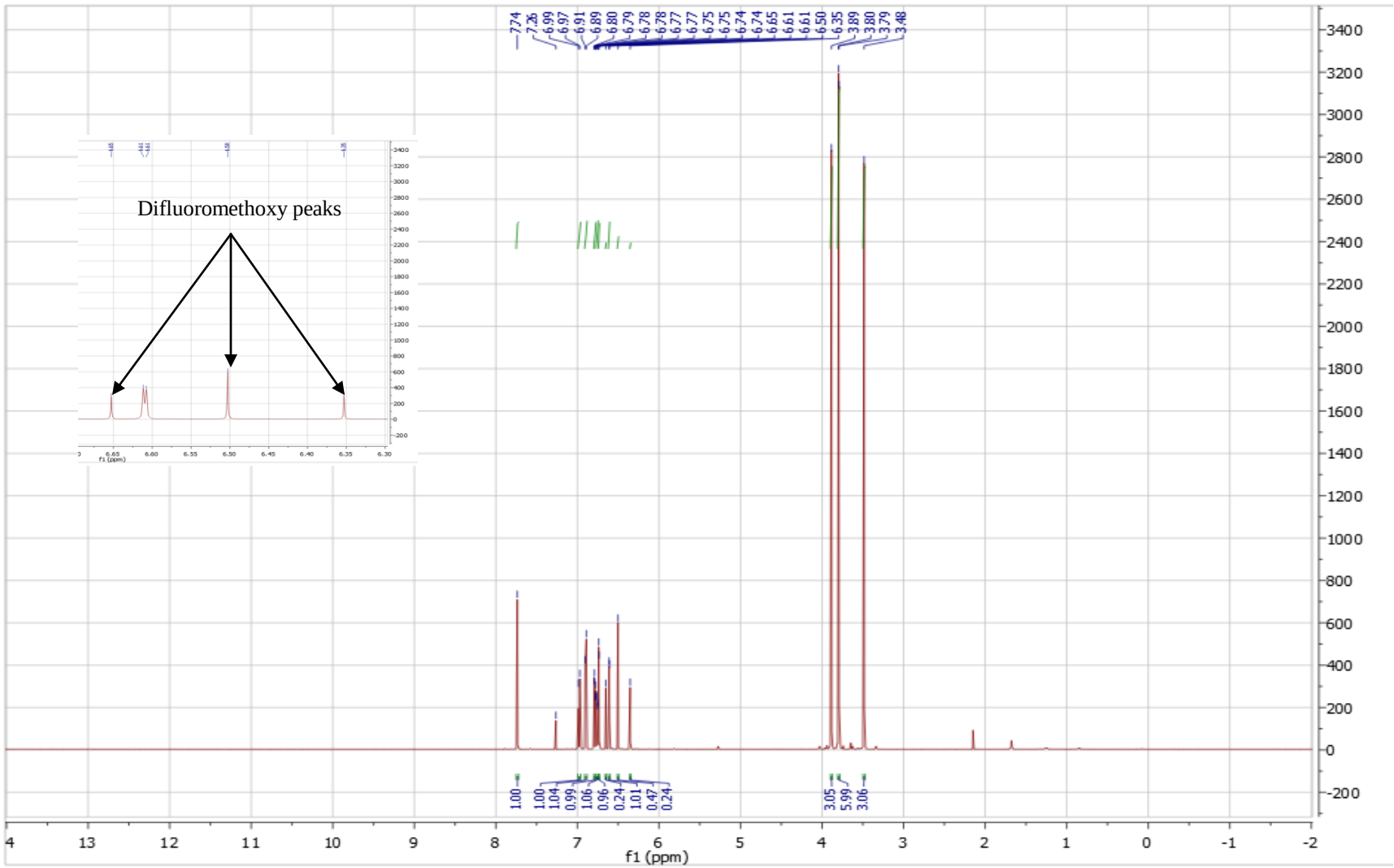

Figure 25. Cont'd.

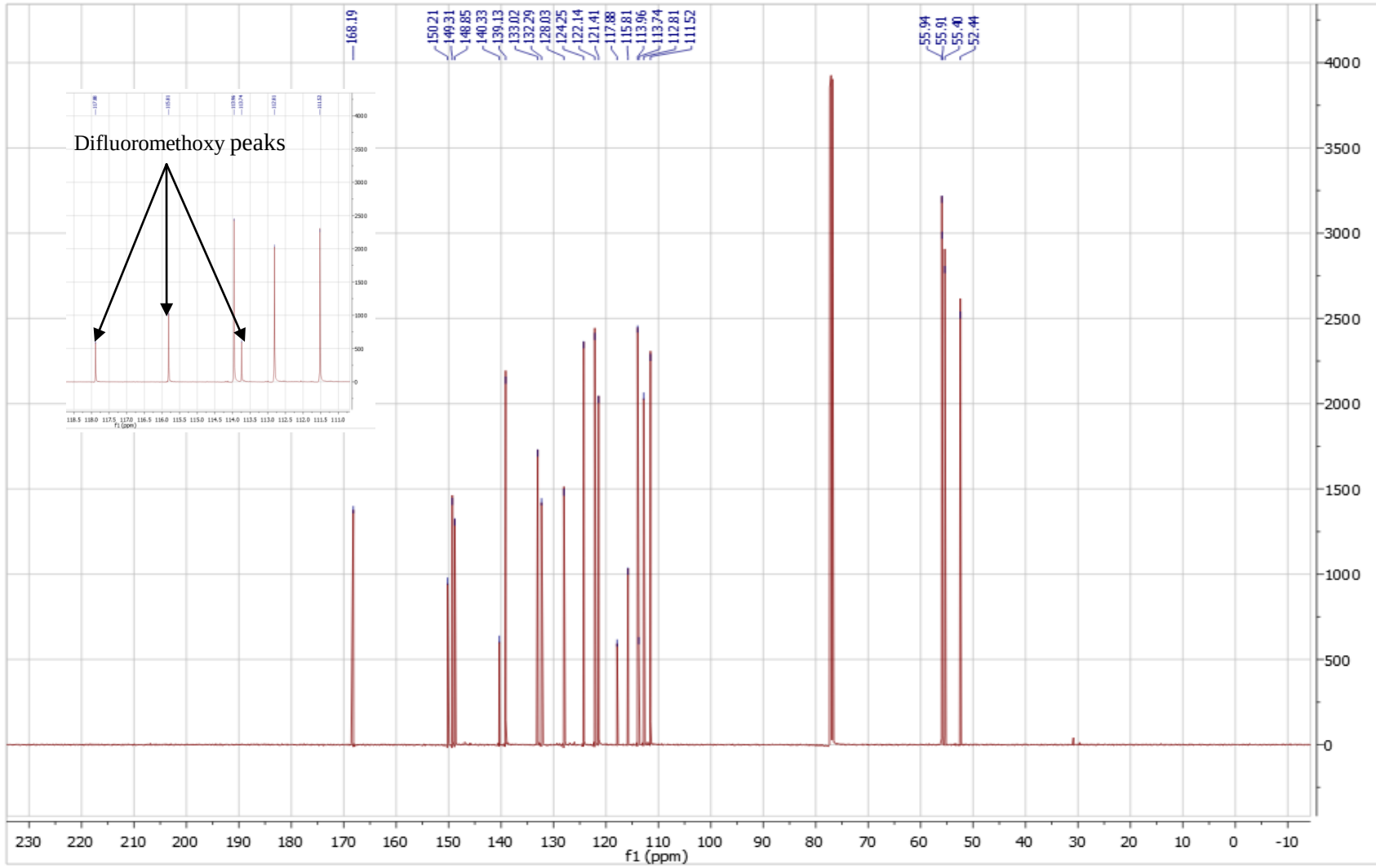

Figure 25. Cont'd.

5.2. The Synthesis of Intermediates 24 and 25.

The syntheses of intermediates **24** (a yield of 94.1%) and **25** (a yield of 98.1%) were carried out by following the same conditions used in the previous synthesis of DCB analogues. No major difficulty was encountered during the syntheses of these compounds; however, additional $FeCl_3$ was necessary in the synthesis of **24**.

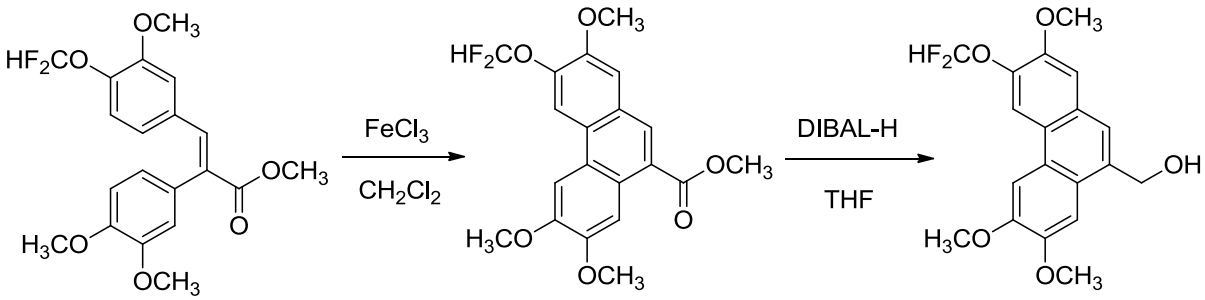

23 **24** **25**

Scheme 29. The synthesis of intermediate 24 and 25.

5.3. The Synthesis of Intermediate 26.

In the synthesis of **26** the same conditions used in preparing intermediate **6** were used, and a mixture of was obtained as expected. The major product (a yield of 60.6%) was isolated by column chromatography and analyzed by mass spectrometry and ^{1}H NMR spectroscopy, which confirmed the whole structure of the compound except the position of the bromine on the aromatic system. Unfortunately attempts to crystallize this compound for a better elucidation of its structure failed; therefore 1D NOESY NMR experiments were conducted on the Varian VNMRS 600 MHz spectrometer.

The ^{1}H NMR and four 1D NOESY NMR spectra are shown in Figures 27 and 28, and all five possible positions where the bromine might be located are labeled in Figure 26. According to the

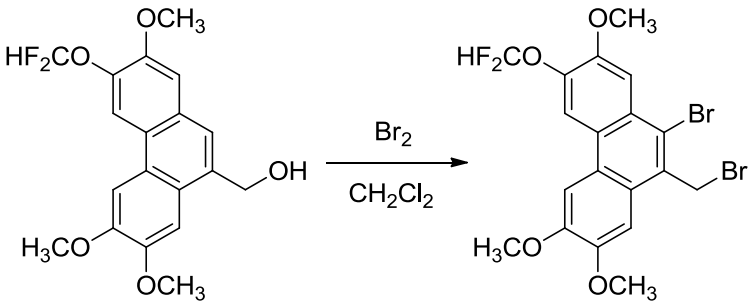

25 **26**

Scheme 30. The synthesis of intermediate 26.

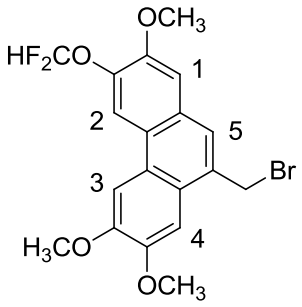

Figure 26. The five positions assigned on intermediate 26.

1D NOESY spectra, there is only one aromatic H (7.49 ppm) that was close enough to the bromomethyl H (5.26 ppm), suggesting the other bromine had to be on either 4- or 5-position. However, if the bromine were on the 4-position, there should be two pairs of aromatic Hs (1- and -5 or 2- and 3-) that are close enough to show a NOESY interaction. In the spectra shown below only one pair of aromatic Hs (8.23, 7.78 ppm) could be found, indicating the position of the bromine was not on 4-position. Therefore, the bromine had to be on 5-position, which made the Hs on 2- and 3-position close to each other. The assignment of each H could also be made according to the spectra. The H (8.23 ppm) was the one at 2-position since it was only close to one aromatic H and not close to the methoxy Hs. The H with a chemical shift of 7.93 ppm occupied the 1-position due to its proximity to the methoxy Hs and the long distance to the

bromomethyl Hs. The H (7.78 ppm) was the one at 3-position because it was close to both methoxy Hs and one aromatic H. The last H (7.49 ppm) should be the H on the 4-position based on its close distance to the methoxy Hs and bromomethyl Hs.

5.4. The Synthesis of Intermediates 27 and 28.

With intermediate **26** in hand and its structure confirmed, the synthesis of **27** was performed by the same procedure used in preparing intermediate **17** (Scheme 21) to give a yield of 83.1%.

For the synthesis of the target product **28**, the chemistry outlined in Scheme 22 for the synthesis of **18** was followed. However, in the case of **28**, a mixture was obtained after the $NaBH_4$ reduction, and no desired product was detected by either mass spectrometry or NMR spectroscopy. The *m/z* of the $[M+H]^+$ peak of one compound in the mixture was found to be 467.25479 by mass spectrometry, suggesting a structure shown in Figure 29. Speculation was that the ring-closure step was the failed step, and the reducing agent removed the difluoromethyl group. Therefore, a test was conducted to confirm the above speculation by running mass spectrometry after quenching the active aryl carbanion with CD_3OD before the addition of $NaBH_4$. As expected, an *m/z* of the $[M+H]^+$ peak at 518.28839 was found in the mixture, which indicated the proposed deuterated structure shown in Figure 30. Disappointedly the desired $[M+H]^+$ peak corresponding to the structure shown in Figure 31 was not found. Although the exact cause of the failure of the ring closure is not clear, speculation is that the difluoromethyl group, which has a strong electron-withdrawing effect, might stabilize the aryl carbanion which does form as shown by the deuteration experiment through the aromatic system and lead to its resistance of attacking the amide carbonyl group.

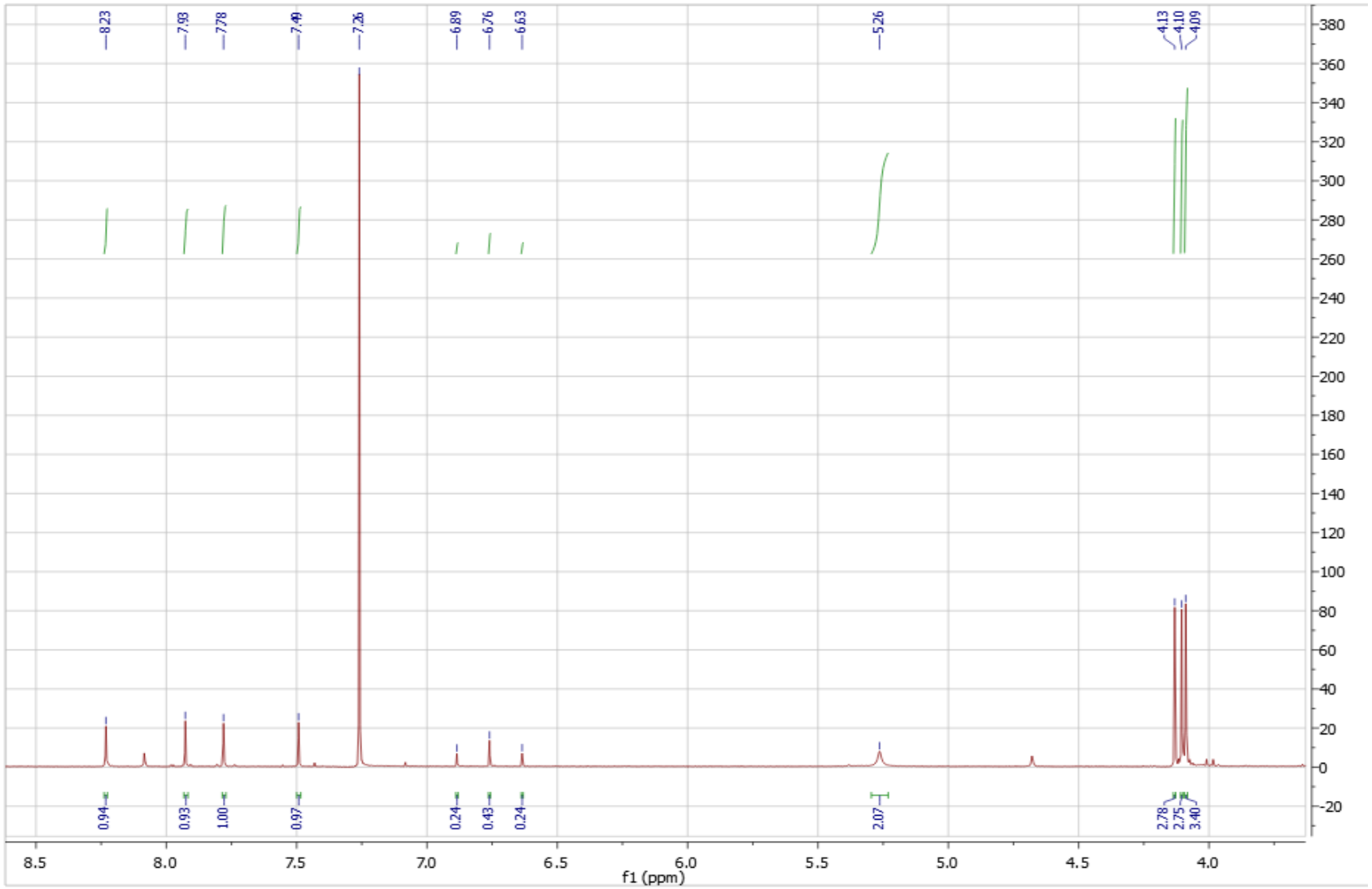

Figure 27. ^{1}H NMR (600 MHz, $CDCl_3$) spectrum of intermediate 26.

Figure 28. 1D NOESY NMR (600 MHz, $CDCl_3$) spectra of intermediate 26.

Figure 28. Cont'd.

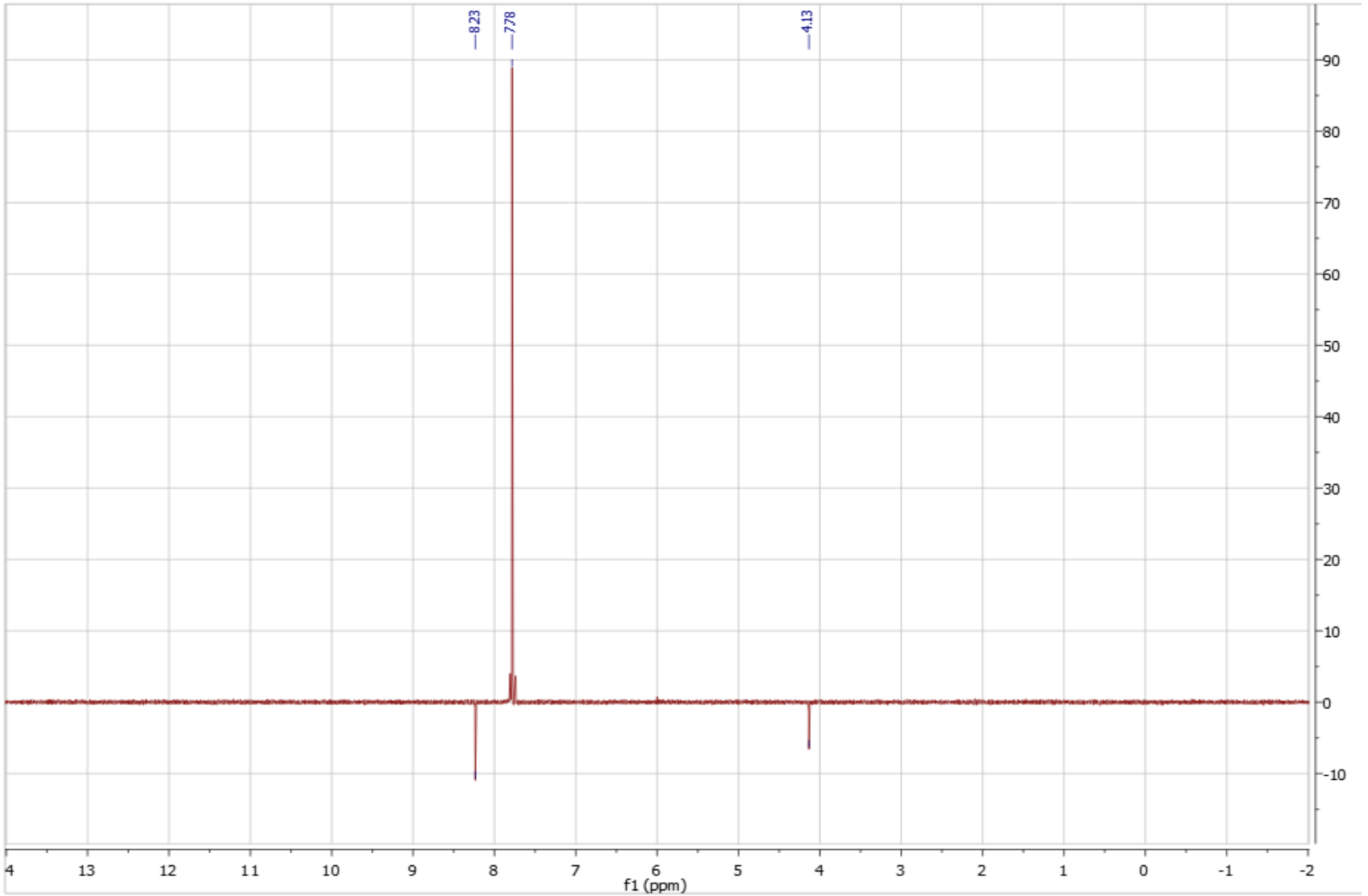

Figure 28. Cont'd.

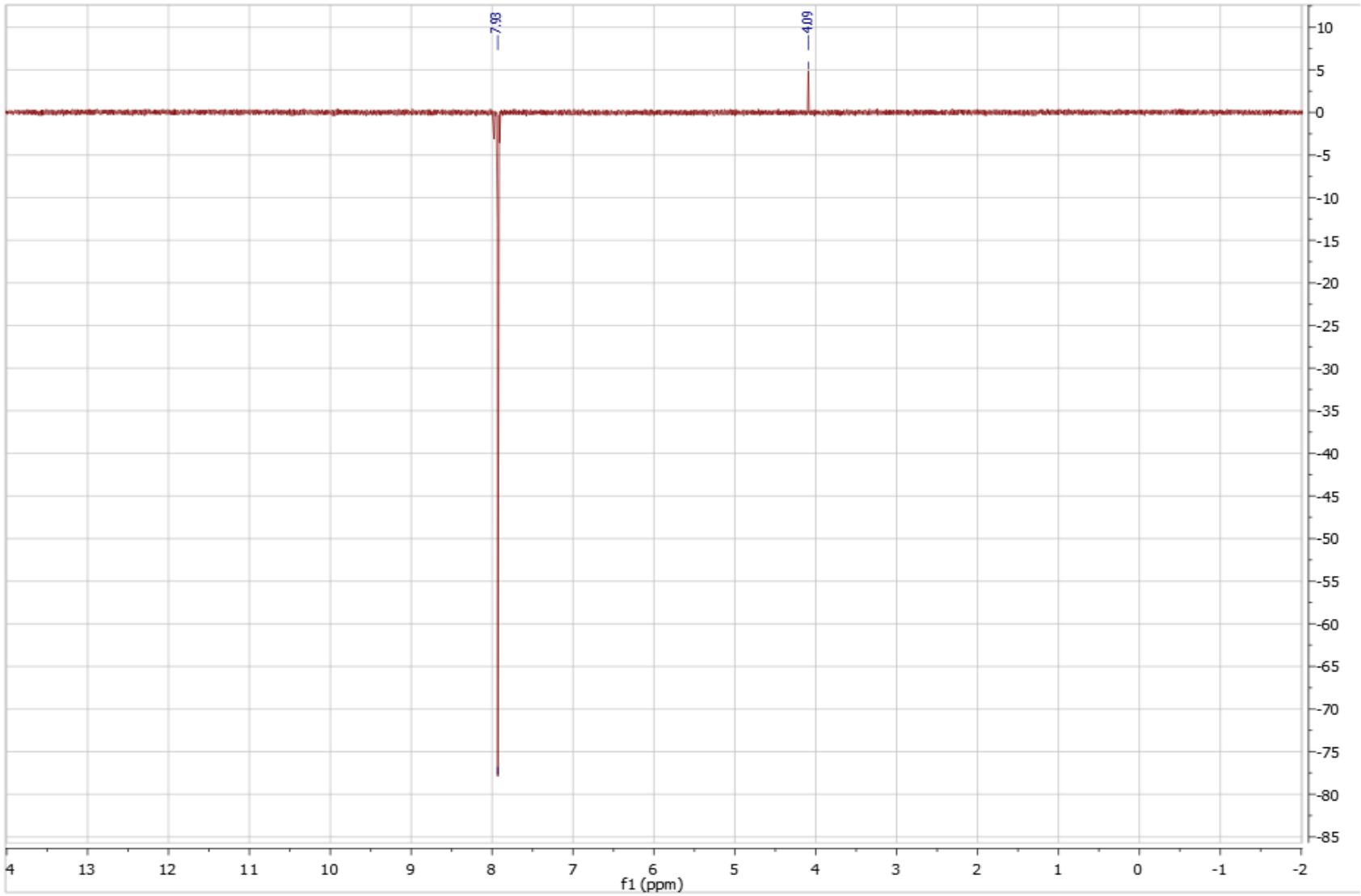

Figure 28. Cont'd.

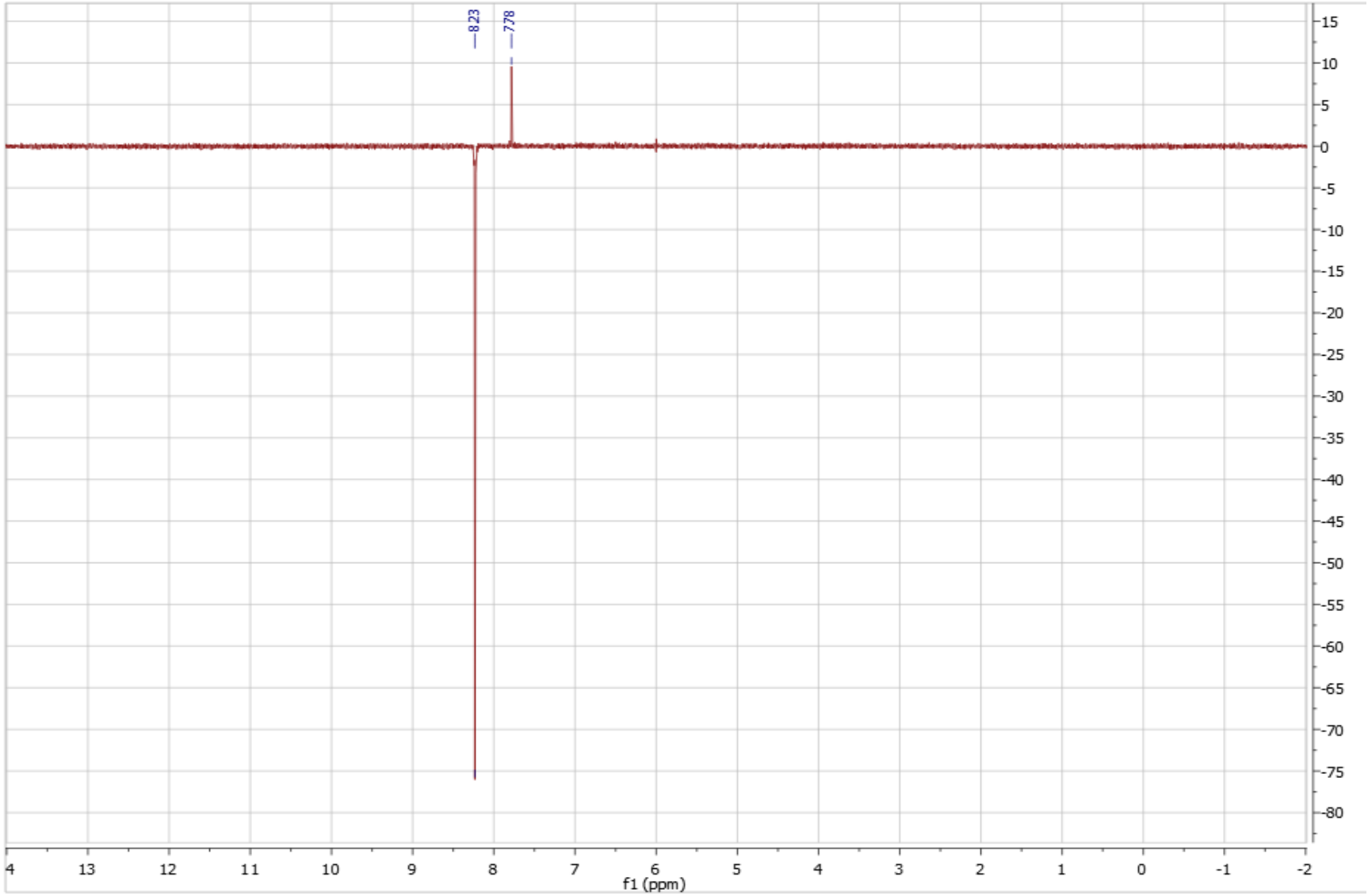

Figure 28. Cont'd.

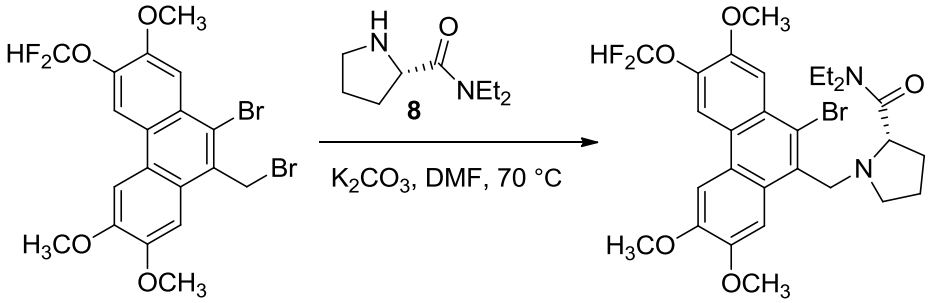

Scheme 31. The synthesis of intermediate 27.

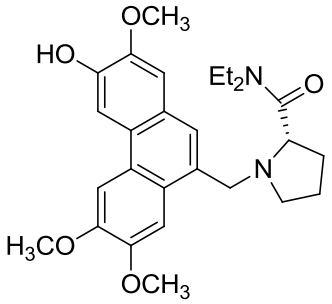

Figure 29. The unexpected product in the attempted synthesis of compound 28.

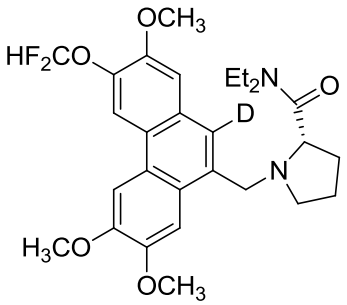

Figure 30. The deuterated intermediate in the route for the synthesis of compound 28.

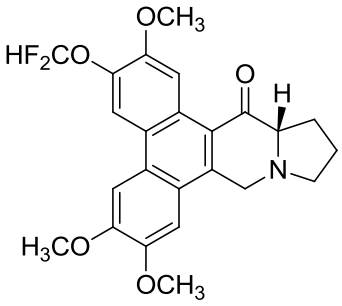

Figure 31. The ring-closed intermediate expected in the attempted synthesis of compound 28.

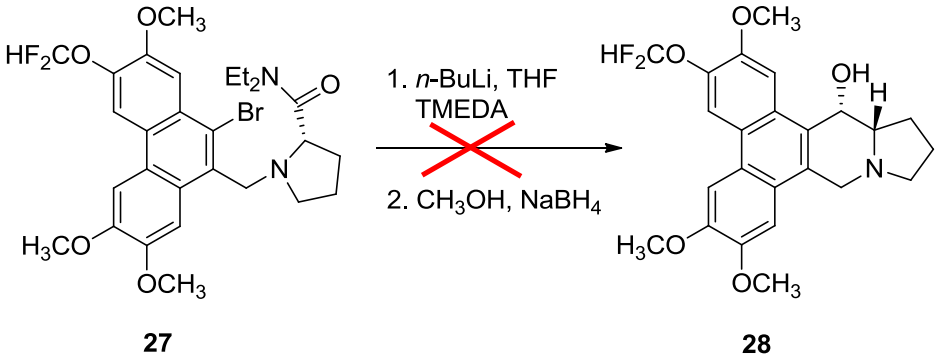

27 **28**

Scheme 32. The attempted synthesis of compound 28.

6. The Biological Studies of DCB-3510, DCB-3511 and DCB-3512

6.1. The Results of the Biological Studies.

The biological activities of the newly synthesized compounds DCB-3510, DCB-3511 and DCB-3512 were studied with DCB-3503 as a reference in Dr. Cheng's lab at Yale University School of Medicine. The cytotoxicity of these compounds against HepG2, Huh7 and HLN liver cancer cell lines and the anti-hepatitis C virus (HCV) activities were determined and the results are shown in Table 4.

Table 4. The biological activities of DCB-3510, DCB-3511, and DCB-3512.

	Cytotoxicity IC_{50} (μm)			**Anti-HCV Activity ID_{50} (μm)**
	HepG2	**Huh7**	**HLN**	**HCV**
DCB-3503	0.3 ± 0.06	0.56 ± 0.3	0.45 ± 0.1	0.03 ± 0.004
DCB-3510	5.2 ± 0.9	2.6 ± 0.9	1.7 ± 0.65	2.7 ± 0.6
DCB-3511	9.5 ± 0.2	1.7 ± 0.8	2.2 ± 0.6	1.6 ± 0.45
DCB-3512	24 ± 2.9	8.6 ± 1.8	14 ± 2.1	9.1 ± 1.9

6.2. The Analysis of the Inconsistencies of the Predictive and the Experimental Data.

To our surprise, although these three novel compounds were still active according to the results, they were not as potent as DCB-3503 either for their cytotoxicity against the cancer cell lines or on the anti-HCV activity. Meanwhile by increasing the substituent volume at the 3-

position, the activities decreased as can be seen for DCB-3510 and DCB-3512, which was not consistent with the predictions of the CoMFA model that was developed for the NF-κB pathway—not whole-cell cytotoxicity. What is interesting is that the nitrogen of the indolizidine moiety might not function as an important H-bond acceptor due to the still active biological data of DCB-3512 as an ammonium salt. However, if one takes the difference between the data used to construct the CoMFA model, which was the IC_{50} against NF-κB pathway, and the testing results data which was the IC_{50} or ID_{50} against whole cells into consideration, it is possible that these data are not suitable to evaluate the accurate prediction ability of CoMFA. Although these analogues are believed to affect the NF-κB pathway, other pathways cannot be ruled out. Additionally even if the NF-κB pathway was the only pathway being affected, it was still possible multiple proteins in this pathway could be the targets, not to mention the possibility of the existence of multiple binding sites on one protein.

Although it was difficult to give direct proof of the above analysis, one screening result from another independent group might shed light on it. In the study conduct by Wang's group, it was found the same modifications would bring the opposite effect on tylophorine and DCB-3503. The cytotoxicity against the A549 cell line of several tylophorine analogues are shown in Figure 32.[17] It is obvious that if there was no hydroxyl group at 14-position, the 7-methoxy compounds were less potent than the 7-hydrogen one. However, by adding a hydroxyl group at the 14-position rendering the *S* configuration, the 7-methoxy compound was more active than the 7-hydrogen one. It is possible that by adding a hydroxyl group the total mechanism of the resulting analogue is changed, and the previous study has shown that the addition of a 14-hydroxyl group at least changed the pharmacokinetics.[7] Although the molecules used to construct the CoMFA model in the training set were believed to function by way of the NF-κB pathway, the 14-

hydroxyl ones and 14-hydrogen ones might bind to different proteins or different sites on the same protein, which eventually made the CoMFA model not that predictable.

The prediction made by the CoMFA that by decreasing the substituent volume at the 7-position the activity increases came from merely the molecules without 14-hydroxyl groups due to a lack of available experimental data, and this lack of experimental data for a larger variety of molecules, together with their complicated and varied mechanisms, made the model not as predictable as desired. Additionally the non-rigid and flexible triazole arm at the 3-position made it more difficult to accurately predict the activity due to the multiple positions of the arm that could be placed in the calculated CoMFA field. Based on the above analysis, although the ligand-based approach utilizing CoMFA model might not be the ideal tool for designing novel tylophorine analogues due to the lack of diversity in the molecules in the training set, and the lack of corresponding data and the uncertain mechanisms that occur with structural changes, it still shed light on the complexity and diversity of the possible anti-cancer mechanisms of DCB-3503.

Compound No.	A549 GI_{50} (μm)
A	0.70
B	0.30
C	0.50
D	0.01
E	0.06
F	<0.001
G	0.67
H	>10
I	0.40
J	1.00

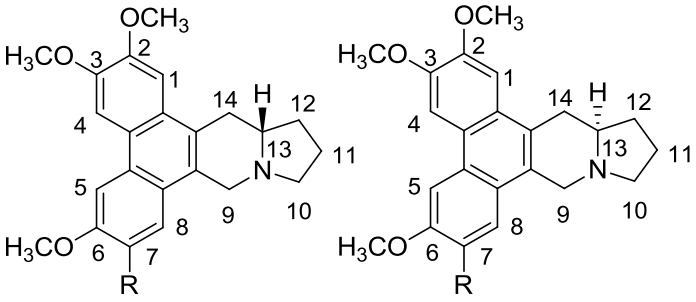

A R = OCH_3 **C** R = OCH_3

B R = H **D** R = H

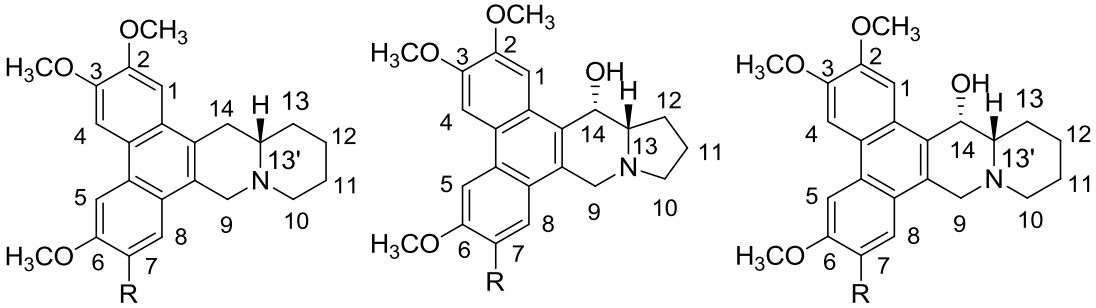

E R = OCH_3 **G** R = OCH_3 **I** R = OCH_3

F R = H **H** R = H **J** R = H

Figure 32. The analysis of the inconsistencies of the experimental and predictive biological activities of the novel DCB-3503 analogues.

V. EXPERIMENTAL

The analytical TLC was performed on 0.2-mm aluminum-backed plates (Sorbent Technologies, Norcross, GA), and the detection was carried out by 254 nm UV light and/or dipping–heating with *p*-anisaldehyde–sulfuric acid dip.[49] Column chromatography was run by utilizing silica gel, 63–200 mesh (Sorbent Technologies, Norcross, GA). ^{1}H and ^{13}C NMR spectra were acquired at 25 °C on a Varian VNMRS 500 spectrometer at 500 MHz and 125 MHz, respectively, or a Varian VNMRS 600 spectrometer at 600 MHz and 150 MHz, respectively. Chemical shifts are reported in δ (ppm) units relative to the signal of $CDCl_3$, THF-d_8 or CD_3CN for ^{1}H or ^{13}C. All 2D NMR spectra were obtained on Varian VNMRS 500 or Varian VNMRS 600 instruments. High-resolution mass spectra were acquired on a JEOL AccuTOF-DART spectrometer with an ESI source or on a Q-Star TOF spectrometer with an ESI source.

1. The Construction of the Novel CoMFA Model.

The inhibitory activities against NF-κB pathway of a series of tylophorine analogues obtained from Dr. Cheng's lab, all of which were believed to function through the same mechanism, were selected as the training set of this model.[11, 14] The IC_{50} data in M^{-1} scale were then converted to pIC_{50} values before the application in the model. The two enantiomers of cryptopleurine were considered as equally effective as they were tested as a racemic mixture.

The model was constructed using the SYBYL-X 2.1 molecular modeling program (Tripos International, St. Louis, MO). All the molecular structures were constructed by the Sketcher in SYBYL-X 2.1, and their energies were minimized in MMFF94s force field after the assignment of MMFF94 charges.

All the prepared molecules were then superimposed on a common core shown in Figure 8 with (−)-antofine as the template, which was selected due to its second highest pIC_{50} that might represent the most bioactive conformation of this series of analogues. The reason why cryptopleurine was not chosen was because its IC_{50} was obtained from a racemic mixture, making it impossible to differentiate which isomer possesses a higher value.

The already aligned molecules were then placed in a 3D grid with a spacing of 2 Å, and the Tripos standard field was used to calculate the steric (Lennard-Jones potential) and electrostatic (Coulomb potential) energies by introducing an sp^3 carbon with a + 1 charge as the probe. The truncation cutoffs of the steric and electrostatic fields were both 30.0 kcal/mol. A partial least square (PLS) analysis was then carried out using the default setting in SYBYL-X 2.0. A leave-one-out (LOO) cross-validation was firstly calculated to give the q^2 and the optimal number of components, the latter of which provided the highest q^2 and lowest standard error. The optimal number of components was then used in non-cross-validation to give conventional correlation coefficient r^2.

After completion of the model the contour maps could be examined, and the correlated modifications could be made. All the novel molecules designed from the contour maps were also built in the Sketcher in SYBYL-X.2.1, and their corresponding energies were minimized in the MMFF94s force field after the assignment of the MMFF94 charges. The alignment of the testing set molecules were carried out using the same common core; however, (−)-antofine was added to the testing set as the alignment template to maintain the consistency.

2. The Synthesis of the Novel DCB-3503 Analogues.

Preparation of 2-(3-chloro-4-methoxyphenyl)acetic acid (1)

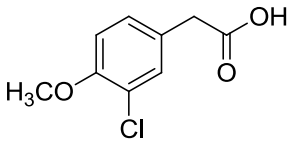

A solution of 2-(4-methoxyphenyl)acetic acid (0.850 g, 5.12 mmol) in 8.5 mL acetone was added Oxone® (3.15 g, 10.2 mmol), and the resulting suspension was stirred for 15 min at room temperature. Then an aqueous solution of NaCl (1.19 g, 20.4 mmol, in 8.5 mL H_2O) was added dropwise to the suspension, and the reaction mixture was stirred for 6 h at room temperature. Afterwards the solvent was removed by rotary evaporation, and the residue was diluted with H_2O (43 mL) and extracted by ethyl acetate (3 × 30 mL). The combined organic layer was then dried with anhyd $MgSO_4$ and concentrated in vacuo to yield crude 2-(3-chloro-4-methoxyphenyl)acetic acid (**1**, a yield of >80.0% by ^{1}H NMR integration) as a yellowish red solid. ^{1}H NMR (500 MHz, $CDCl_3$) δ 7.27 (d, *J* = 2.5 Hz, 1H), 7.10 (dd, *J* = 8.5, 2.0 Hz, 1H), 6.85 (d, *J* = 8.5 Hz, 1H), 3.84 (s, 1H), 3.54 (s, 1H). ^{13}C NMR (125 MHz, $CDCl_3$) δ 39.71, 56.11, 112.14, 122.35, 126.22, 128.78, 131.07, 154.26, 177.94. HRDARTMS: Calcd for $C_9H_9ClO_3$ *m/z* 200.02402; $[M-H]^+$ *m/z* 199.01547 (calcd 199.01620).

Preparation of (*E*)-2-(3-chloro-4-methoxyphenyl)-3-(3,4-dimethoxyphenyl)acrylic acid (2)

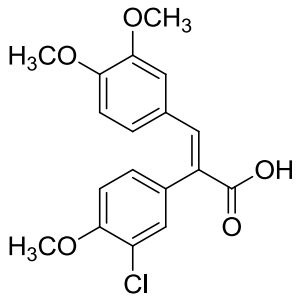

To a suspension of 2-(3-chloro-4-methoxyphenyl)acetic acid (**1**, 1.50 g, 7.50 mmol) and 3,4-dimethoxybenzaldehyde (1.25 g, 7.50 mmol) in acetic anhydride (4.14 mL, 43.7 mmol), triethylamine (2.63 mL, 18.7 mmol) was added, and the mixture was stirred at 100 °C for 24 h. Afterwards the reaction was allowed to cool to room temperature and H_2O (3.75 mL) was slowly added, then the mixture was cooled to room temperature again and extracted with CH_2Cl_2 (3 × 15 mL). The organic layer was then dried over $MgSO_4$ and concentrated in vacuo. The residue was further purified by column chromatography (9:1 CH_2Cl_2:EtOAc) to give (*E*)-2-(3-chloro-4-methoxyphenyl)-3-(3,4-dimethoxyphenyl)acrylic acid (**2**, 1.20 g, 3.45 mmol, 46.0% yield) as a light-yellow precipitate. ^{1}H NMR (500 MHz, $CDCl_3$) δ 7.88 (s, 1H), 7.33 (d, *J* = 2.0 Hz, 1H), 7.14 (dd, *J* = 8.5, 2.0 Hz, 1H), 6.97 (d, *J* = 8.5 Hz, 1H), 6.85 (dd, *J* = 8.5, 2.0 Hz, 1H), 6.74 (d, *J* = 8.5 Hz, 1H), 6.55 (d, *J* = 2.0 Hz, 1H), 3.92 (s, 3H), 3.86 (s, 3H), 3.51 (s, 3H). ^{13}C NMR (125 MHz, $CDCl_3$) δ 55.24, 55.83, 56.22, 110.62, 112.27, 112.60, 122.79, 125.86, 126.81, 127.29, 128.86, 129.54, 131.81, 142.92, 148.34, 150.59, 154.68, 172.69. HRDARTMS: Calcd for $C_{18}H_{17}ClO_5$ *m/z* 348.07645; $[M+H]^+$ *m/z* 349.08376 (calcd 349.08428).

Preparation of (*E*)-methyl 2-(3-chloro-4-methoxyphenyl)-3-(3,4-dimethoxyphenyl)acrylate (3)

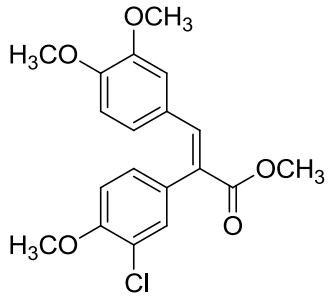

(*E*)-2-(3-chloro-4-methoxyphenyl)-3-(3,4-dimethoxyphenyl)acrylic acid (**2**, 4.66 g, 13.4 mmol) was dissolved in dry methanol (230 mL), and to this solution concd H_2SO_4 (4.60 mL) was added and the resulting solution was stirred for 12 h at 65 °C. Afterwards the reaction mixture was concentrated via rotary evaporation, and the slurry was purified by column chromatography (9:1 CH_2Cl_2:EtOAc) to give (*E*)-methyl 2-(3-chloro-4-methoxyphenyl)-3-(3,4-dimethoxyphenyl)acrylate (**3**, 4.47 g, 12.4 mmol, 92.5% yield) as a pale-yellow solid. ^{1}H NMR (500 MHz, $CDCl_3$) δ 7.77 (s, 1H), 7.29 (d, *J* = 2.0 Hz, 1H), 7.10 (dd, *J* = 8.5, 2.5 Hz, 1H), 6.95 (d, *J* = 8.5 Hz, 1H), 6.80 (dd, *J* = 8.5, 2.0 Hz, 1H), 6.71 (d, *J* = 8.5 Hz, 1H), 6.50 (d, *J* = 2.5 Hz, 1H), 3.90 (s, 3H), 3.83 (s, 3H), 3.77 (s, 3H), 3.49 (s, 3H). ^{13}C NMR (125 MHz, $CDCl_3$) δ 52.32, 55.21, 55.79, 56.19, 110.61, 112.25, 112.47, 122.68, 125.37, 127.08, 128.26, 129.45, 129.47, 131.73, 140.94, 148.27, 150.16, 154.53, 168.16. HRDARTMS: Calcd for $C_{19}H_{19}ClO_5$ *m/z* 362.09210; $[M+H]^+$ *m/z* 363.10008 (calcd 363.09993).

Preparation of methyl 7-chloro-2,3,6-trimethoxyphenanthrene-9-carboxylate (4)

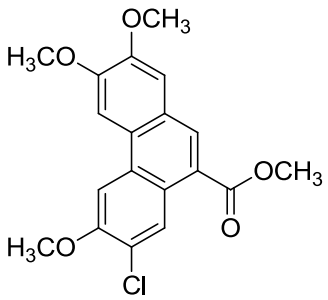

A solution of (*E*)-methyl 2-(3-chloro-4-methoxyphenyl)-3-(3,4-dimethoxyphenyl)acrylate (**3**, 4.05 g, 11.2 mmol) in CH_2Cl_2 (250 mL) was cooled to -10 °C, and to this solution a freshly prepared solution of $FeCl_3$ (13.0 g, 80.8 mmol) in EtOAc (250 mL) was added dropwise, and the resulting mixture was stirred overnight at room temperature. Then the reaction was checked by TLC. If compound **3** could still be found, then an equal amount of $FeCl_3$ (13.0 g, 80.8 mmol) in EtOAc (250 mL) was added with stirring until all the starting material was consumed. Then H_2O (272 mL) was added, and the reaction mixture was stirred for 3 h at room temperature. Afterwards the mixture was extracted by CH_2Cl_2 (3 × 200 mL), and the combined organic layer was dried with anhyd $MgSO_4$ and concentrated via rotary evaporator. The pure methyl 7-chloro-2,3,6-trimethoxyphenanthrene-9-carboxylate (**4**, 3.62 g, 10.1 mmol, 90.2% yield) could then be obtained as a white solid by column chromatography (9:1 CH_2Cl_2:hexanes). ^{1}H NMR (500 MHz $CDCl_3$) δ 9.06 (s, 1H), 8.27 (s, 1H), 7.70 (s, 1H), 7.67 (s, 1H), 7.20 (s, 1H), 4.11 (s, 3H), 4.09 (s, 3H), 4.03 (s, 3H), 4.00 (s, 3H). ^{13}C NMR (125 MHz, $CDCl_3$) δ 52.13, 55.97, 56.06, 56.10, 102.80, 103.02, 109.29, 122.39, 123.45, 123.59, 125.45, 126.36, 128.05, 129.96, 130.55, 149.78, 151.20, 153.30, 167.61. HRDARTMS: Calcd for $C_{19}H_{17}ClO_5$ *m/z* 360.07645; $[M+H]^+$ *m/z* 361.08364 (calcd 361.08428).

Preparation of (7-chloro-2,3,6-trimethoxyphenanthren-9-yl)methanol (5)

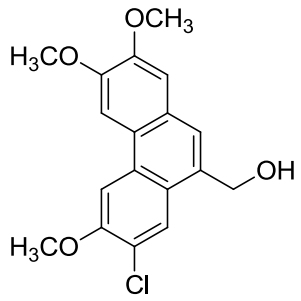

Methyl 7-chloro-2,3,6-trimethoxyphenanthrene-9-carboxylate (**4**, 2.00 g, 5.56 mmol) was dissolved in THF (150 mL), and the solution was maintained under N_2 atmosphere in an ice bath. To this solution a solution of 1.0 M DIBAL-H in hexanes (22.4 mL, 22.4 mmol) was then added dropwise, and the reaction mixture was allowed to stir overnight at room temperature. Afterwards the reaction was again cooled in an ice bath and $Na_2SO_4 \cdot 10H_2O$ was carefully added until the formation of bubbles came to a stop. The resulting mixture was then filtered through Celite and concentrated by rotary evaporation to give (7-chloro-2,3,6-trimethoxyphenanthren-9-yl)methanol (**5**, 1.62 g, 4.88 mmol, 87.8% yield) as a white solid. ^{1}H NMR (500 MHz, $CDCl_3$) δ 8.14 (s, 1H), 7.80 (s, 1H), 7.74 (s, 1H), 7.55 (s, 1H), 7.16 (s, 1H), 5.06 (s, 2H), 4.11 (s, 3H), 4.10 (s, 3H), 4.02 (s, 3H). ^{13}C NMR (125 MHz, $CDCl_3$) δ 55.92, 56.11, 56.26, 63.99, 103.15, 103.72, 108.48, 122.70, 123.98, 124.11, 124.50, 125.93, 126.93, 130.05, 131.89, 149.44, 149.70, 153.31. HRDARTMS: Calcd for $C_{18}H_{17}ClO_4$ *m/z* 332.08154; $[M]^+$ *m/z* 332.08076 (calcd 332.08154).

Preparation of 9-bromo-10-(bromomethyl)-2-chloro-3,6,7-trimethoxyphenanthrene (6)

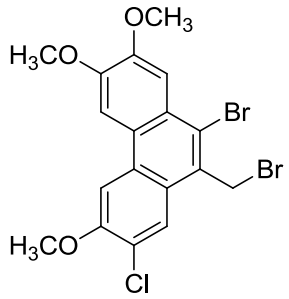

To a solution of 7-chloro-2,3,6-trimethoxyphenanthren-9-yl)methanol (**5**, 2.00 g, 6.02 mmol) in CH_2Cl_2 (50 mL) at 0 °C was added a solution of Br_2 (1.00 g, 6.26 mmol) in CH_2Cl_2 (10 mL). The resulting reaction mixture was then stirred overnight at room temperature. Afterward the solvent was removed by rotary evaporation, and column chromatography (6:4 CH_2Cl_2:hexanes followed by pure CH_2Cl_2) was performed to give bromo-10-(bromomethyl)-2-chloro-3,6,7-trimethoxyphenanthrene (**6**, 1.10 g, 2.33 mmol, 38.7% yield) as a white solid. ^{1}H NMR (500 MHz, $CDCl_3$) δ 8.15 (s, 1H), 7.83 (s, 1H), 7.81 (s, 1H), 7.77 (s, 1H), 5.20 (s, 2H), 4.14 (s, 3H), 4.13 (s, 3H), 4.09 (s, 3H). ^{13}C NMR (125 MHz, $CDCl_3$) δ 32.28, 56.07, 56.20, 56.33, 103.10, 103.68, 109.67, 123.76, 123.80, 124.26, 125.12, 126.01, 126.32, 128.67, 129.33, 150.40, 150.43, 153.87. HRDARTMS: Calcd for $C_{18}H_{15}Br_2ClO_3$ *m/z* 471.90765; $[M+H]^+$ *m/z* 472.91725 (calcd 472.91547).

Preparation of (*S*)-benzyl 2-(diethylcarbamoyl)pyrrolidine-1-carboxylate (7)

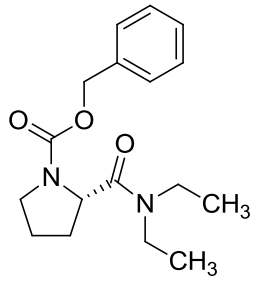

To an ice-cold solution of (*S*)-1-((benzyloxy)carbonyl)pyrrolidine-2-carboxylic acid (1.00 g, 4.02 mmol) in CH_2Cl_2 (8.0 mL), a solution of *N,N'*-dicyclohexylcarbodiimide (0.880 g, 4.27 mmol) in CH_2Cl_2 (8.0 mL) was added dropwise. After the formation of a white precipitate, a solution of diethylamine (0.420 mL, 4.03 mmol) in CH_2Cl_2 (8.0 mL) was added dropwise, and the resulting mixture was allowed to stir overnight at room temperature. Afterwards the reaction mixture was filtered, and the resulting filtrate was further purified by column chromatography (4:6 EtOAc:hexanes) to give (*S*)-benzyl 2-(diethylcarbamoyl)pyrrolidine-1-carboxylate (**7**, 0.740 g, 2.43 mmol, 60.4% yield) as a colorless liquid. $[\alpha]_D^{20} = -30.4$ (*c* = 1.2, MeOH). ^{1}H NMR (500 MHz, $CDCl_3$) δ 7.10–6.99 (m, 5H), 4.83 (dd, *J* = 90.7, 12.2 Hz, 1H), 4.82 (t, *J* = 12.0 Hz, 1H), 4.32 (ddd, *J* = 61.7, 8.2, 3.5 Hz, 1H), 3.45–3.38 (m, 1H), 3.33–3.09 (m, 3H), 3.01–2.86 (m, 2H), 1.97–1.75 (m, 2H), 1.63–1.53 (m, 2H), 0.94 (dt, *J* = 73.7, 7.2 Hz, 3H), 0.72 (dt, *J* = 33.0, 7.0 Hz, 3H). ^{13}C NMR (125 MHz, $CDCl_3$) δ 12.69, 13.95, 23.25, 29.91, 41.32, 46.53, 56.17, 66.35, 127.31, 127.52, 127.67, 127.92, 128.03, 128.14, 136.37, 153.92, 171.35. HRDARTMS: Calcd for $C_{17}H_{24}N_2O_3$ *m/z* 304.17869; $[M+H]^+$ *m/z* 305.18648 (calcd 305.18652).

Preparation of (*S*)-*N*,*N*-diethylpyrrolidine-2-carboxamide (8)

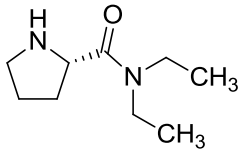

Pd/C (0.06 g, 10% Pd) was added to a solution of (*S*)-benzyl 2-(diethylcarbamoyl)pyrrolidine-1-carboxylate (**7**, 0.600 g, 1.97 mmol) in C_2H_5OH (60 mL), and the resulting mixture was stirred under H_2 atmosphere for 4 h. Afterwards the mixture was filtered, and the solvent in the filtrate was removed via rotary evaporation to give (*S*)-*N*,*N*-diethylpyrrolidine-2-carboxamide (**8**, 0.330 g, 1.94 mmol, 98.5% yield) as a colorless liquid. $[\alpha]_D^{20} = -92.2$ (*c* = 1.1, MeOH). ^{1}H NMR (500 MHz, $CDCl_3$) δ 3.64 (t, *J* = 7.7 Hz, 1H), 3.35–3.28 (m, 1H), 3.27–3.19 (m, 1H), 3.17–3.09 (m, 2H), 3.04–2.99 (m, 1H), 2.62 (dt, *J* = 11.0, 7.0 Hz, 1H), 1.95–1.88 (m, 1H), 1.68–1.51 (m, 2H), 1.48–1.42 (m, 1H), 1.04 (t, *J* = 7.2 Hz, 3H), 0.96 (t, *J* = 7.2 Hz, 3H). ^{13}C NMR (125 MHz, $CDCl_3$) δ 12.73, 14.16, 26.50, 31.25, 40.04, 40.94, 47.63, 57.98, 173.03. HRDARTMS: Calcd for $C_9H_{18}N_2O$ *m/z* 170.14191; $[M+H]^+$ *m/z* 171.14979 (calcd 171.14974).

Preparation of (*S*)-1-((10-bromo-7-chloro-2,3,6-trimethoxyphenanthren-9-yl)methyl)-*N*,*N*-diethylpyrrolidine-2-carboxamide (9)

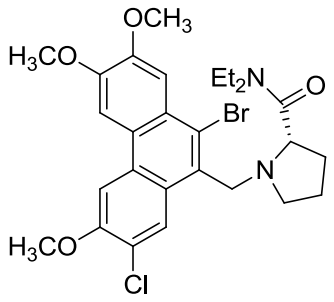

A mixture of 9-bromo-10-(bromomethyl)-2-chloro-3,6,7-trimethoxyphenanthrene (**6**, 0.800 g, 1.70 mmol), (*S*)-*N*,*N*-diethylpyrrolidine-2-carboxamide (**8**, 0.320 g, 1.88 mmol) and K_2CO_3 (1.04 g, 7.53 mmol) in DMF (24 mL) was heated to reflux for 8 h. Afterwards the mixture was allowed to cool to room temperature, and a filtration was carried out. The resulting filtrate was then concentrated by rotary evaporation to give a residue, from which (*S*)-1-((10-bromo-7-chloro-2,3,6-trimethoxyphenanthren-9-yl)methyl)-*N*,*N*-diethylpyrrolidine-2-carboxamide (**9**, 0.650 g, 1.16 mmol, 68.2% yield) could be obtained by column chromatography (4:6 EtOAc:hexanes) as a pale yellow solid. $[\alpha]_D^{20} = -57.9$ (*c* = 2.7, CH_2Cl_2). ^{1}H NMR (500 MHz, $CDCl_3$) δ 8.85 (s, 1H), 7.81 (s, 1H), 7.71 (s, 1H), 7.68 (s, 1H), 4.39 (dd, *J* = 73.7, 10.2 Hz, 2H), 4.10 (s, 3H), 4.09 (s, 3H), 4.06 (s, 3H), 3.61–3.41 (m, 3H), 3.37–3.26 (m, 2H), 3.03–2.97 (m, 1H), 2.73–2.64 (m, 1H), 2.18–2.06 (m, 1H), 1,91–1.70 (m, 3H), 1.13–1.08 (m, 6H). ^{13}C NMR (125 MHz, $CDCl_3$) δ 13.07, 14.53, 22.98, 29.44, 40.28, 41.21, 55.18, 55.96, 56.13, 56.18, 60.35, 64.06, 102.76, 103.03, 109.87, 123.03, 123.16, 124.69, 125.89, 126.38, 128.70, 128.90, 130.75, 149.51, 149.87, 153.45, 171.10. HRDARTMS: Calcd for $C_{27}H_{32}BrClN_2O_4$ *m/z* 562.12340; $[M+H]^+$ *m/z* 563.13146 (calcd 563.13122).

Preparation of (13a*S*,14*S*)-7-chloro-2,3,6-trimethoxy-9,11,12,13,13a,14-hexahydrodibenzo[*f*,*h*]pyrrolo[1,2-*b*]isoquinolin-14-ol (10)

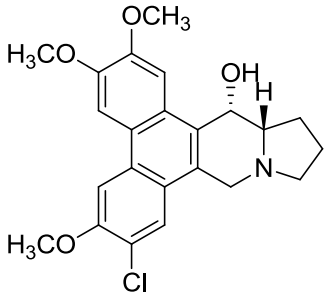

TMEDA (0.660 g, 5.68 mmol) was added to a solution of (*S*)-1-((10-bromo-7-chloro-2,3,6-trimethoxyphenanthren-9-yl)methyl)-*N*,*N*-diethylpyrrolidine-2-carboxamide (**9**, 1.35 g, 2.40 mmol) in dry THF (54 mL), and to this mixture a solution of 2.5 M *n*-BuLi in hexanes (1.94 mL, 4.85 mmol) was added carefully at -78 °C under an N_2 atmosphere. The resulting mixture was allowed to stir for 4 h. Then methanol (13.5 mL) was added, followed by $NaBH_4$ (0.460 g, 12.2 mmol), and the reaction mixture was stirred at -40 °C for 1 h and at room temperature for 8 h. H_2O (27 mL) was then added to quench the reaction at ice bath temperature. The mixture was extracted with CH_2Cl_2 (3 × 30 mL), and the combined organic layer was dried over anhyd $MgSO_4$ and concentrated in vacuo. The resulting residue was further purified by column chromatography (98:2 CH_2Cl_2:CH_3OH) to give (13a*S*,14*S*)-7-chloro-2,3,6-trimethoxy-9,11,12,13,13a,14-hexahydrodibenzo[*f*,*h*]pyrrolo[1,2-*b*]isoquinolin-14-ol (**10**, 0.890 g, 2.15 mmol, 89.6% yield) as a white solid. ^{1}H NMR (500 MHz, THF-d_8) δ 7.94 (s, 1H), 7.93 (s, 1H), 7.78 (s, 1H), 7.23 (s, 1H), 4.77 (s, 1H), 4.10 (s, 3H), 4.07 (s, 3H), 3.99 (s, 3H), 3.66–3.56 (m, 1H), 3.30 (t, *J* = 8.2 Hz, 1H), 3.13 (d, *J* = 15.0 Hz, 1H), 2.45–2.41 (m, 1H), 2.33–2.23 (m, 2H),

2.01–1.93 (m, 1H), 1.86–1.81 (m, 2H). ^{13}C NMR (125 MHz, THF-d_8) δ 21.72, 23.72, 53.10, 54.85, 55.00, 55.10, 55.29, 64.42, 65.65, 103.04, 103.96, 105.76, 121.45, 123.01, 123.49, 123.79, 126.34, 127.29, 129.41, 129.46, 149.19, 150.22, 152.91. HRDARTMS: Calcd for $C_{23}H_{24}ClNO_4$ *m/z* 413.13939; $[M+H]^+$ *m/z* 414.14737 (calcd 414.14721).

Preparation of (*E*)-3-(4-acetoxy-3-methoxyphenyl)-2-(3-chloro-4-methoxyphenyl)acrylic acid (11)

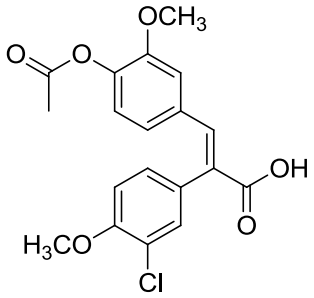

Triethylamine (16.8 mL, 119 mmol) was carefully added to a suspension of 2-(3-chloro-4-methoxyphenyl)acetic acid (**1**, 8.40 g, 42.0 mmol) and 4-hydroxy-3-methoxybenzaldehyde (6.39 g, 42.0 mmol) in acetic anhydride (23.5 mL, 248 mmol), and the resulting mixture was stirred at 100 °C for 24 h. Afterwards the reaction was allowed to cool to room temperature, and H_2O (21.0 mL) was added dropwise. The resulting mixture was cooled to room temperature again and extracted with CH_2Cl_2 (3 × 80 mL). The organic layer was then dried over $MgSO_4$ and concentrated in vacuo. The resulting residue was further purified by column chromatography (9:1 CH_2Cl_2:EtOAc) to give (*E*)-3-(4-acetoxy-3-methoxyphenyl)-2-(3-chloro-4-methoxyphenyl)acrylic acid (**11**, 12.6 g, 33.6 mmol, 80.0% yield) as a light-yellow solid. ^{1}H

NMR (500 MHz, $CDCl_3$) δ 7.88 (s, 1H), 7.33 (d, *J* = 2.0 Hz, 1H), 7.11 (dd, *J* = 8.5, 2.0 Hz, 1H), 6.95 (d, *J* = 8.5 Hz, 1H), 6.91 (d, *J* = 8.0 Hz, 1H), 6.81 (dd, *J* = 8.5, 1.5 Hz, 1H), 6.66 (d, *J* = 1.5 Hz, 1H), 3.91 (s, 3H), 3.49 (s, 3H), 2.28 (s, 3H). ^{13}C NMR (125 MHz, $CDCl_3$) δ 20.60, 55.36, 56.21, 112.27, 113.94, 122.79, 122.83, 124.54, 128.19, 129.41, 129.71, 131.64, 132.72, 140.87, 142.09, 150.64, 154.85, 168.65, 172.27. HRDARTMS: Calcd for $C_{19}H_{17}ClO_6$ *m/z* 376.07137; $[M+H]^+$ *m/z* 377.07892 (calcd 377.07919).

Preparation of (*E*)-methyl 2-(3-chloro-4-methoxyphenyl)-3-(4-hydroxy-3-methoxyphenyl)acrylate (12)

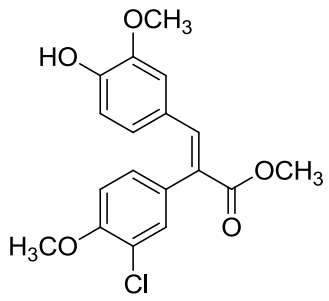

To a solution of (*E*)-3-(4-acetoxy-3-methoxyphenyl)-2-(3-chloro-4-methoxyphenyl)acrylic acid (**11**, 0.500 g, 1.33 mmol) in dry methanol (25 mL) was added 0.50 mL concd H_2SO_4, the reaction mixture was allowed to stir at 65 °C for 12 h. The mixture was then concentrated in vacuo, and the resulting residue was purified by column chromatography (9:1 CH_2Cl_2:EtOAc) to give (*E*)-methyl 2-(3-chloro-4-methoxyphenyl)-3-(4-hydroxy-3-methoxyphenyl)acrylate (**12**, 0.430 g, 1.24 mmol, 93.2% yield) as a pale-yellow solid. ^1H NMR (500 MHz, $CDCl_3$) δ 7.76 (s, 1H), 7.29 (d, *J* = 2.0 Hz, 1H), 7.10 (dd, *J* = 8.5, 2.0 Hz, 1H), 6.95 (d, *J* = 8.5 Hz, 1H), 6.76 (s, 1H), 6.46 (s,

1H), 5.88 (s, 1H), 3.91 (s, 3H), 3.77 (s, 3H), 3.50 (s, 1H). ^{13}C NMR (125 MHz, $CDCl_3$) δ 52.34, 55.33, 56.20, 112.08, 112.28, 114.31, 122.66, 126.08, 126.62, 127.90, 129.49, 131.74, 141.16, 145.98, 147.11, 154.52, 168.25. HRDARTMS: Calcd for $C_{18}H_{17}ClO_5$ *m/z* 348.07645; $[M+H]^+$ *m/z* 349.08511 (calcd 349.08428).

Preparation of (*E*)-methyl 2-(3-chloro-4-methoxyphenyl)-3-(3-methoxy-4-(prop-2-yn-1-yloxy)phenyl)acrylate (13)

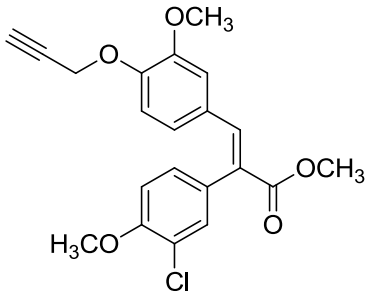

(*E*)-methyl 2-(3-chloro-4-methoxyphenyl)-3-(3-methoxy-4-(prop-2-yn-1-yloxy)phenyl)acrylate (**12**, 5.76 g, 16.5 mmol) was dissolved in 350 mL of acetone, followed by the addition of K_2CO_3 (21.3 g, 154 mmol). The resulting mixture was allowed to stir for 15 min at room temperature, then a solution of 80 wt.% propargyl bromide in toluene (14.6 g, 98.2 mmol) was added dropwise. The reaction was then stirred for 12 h at 65 °C and filtered after cooling to room temperature. The resulting filtrate was concentrated by rotary evaporation and purified by column chromatography (8:2 hexanes:EtOAc) to give (*E*)-methyl 2-(3-chloro-4-methoxyphenyl)-3-(3-methoxy-4-(prop-2-yn-1-yloxy)phenyl)acrylate (**13**, 5.94 g, 15.4 mmol, 93.3% yield) as a white solid. ^{1}H NMR (500 MHz, $CDCl_3$) δ 7.74 (s, 1H), 7.26 (d, *J* = 2.0 Hz,

1H), 7.07 (dd, *J* = 8.0, 2.0 Hz, 1H), 6.92 (d, *J* = 8.5 Hz, 1H), 6.84 (d, *J* = 8.0 Hz, 1H), 6.76 (dd, *J* = 8.0, 1.5 Hz, 1H), 6.49 (d, *J* = 2.0 Hz, 1H), 4.68 (d, *J* = 2.0 Hz, 2H), 3.86 (s, 3H), 3.74 (s, 3H), 3.45 (s, 3H), 2.48 (t, *J* = 2.3 Hz, 1H). ^{13}C NMR (125 MHz, $CDCl_3$) δ 52.33, 55.20, 56.16, 56.39, 76.23, 78.01, 112.27, 112.93, 113.07, 122.65, 124.92, 128.17, 128.77, 129.28, 129.45, 131.65, 140.66, 147.84, 148.76, 154.55, 168.02. HRDARTMS: Calcd for $C_{21}H_{19}ClO_5$ *m/z* 386.09210; $[M+H]^+$ *m/z* 387.09970 (calcd 387.09993).

Preparation of methyl 7-chloro-2,6-dimethoxy-3-(prop-2-yn-1-yloxy)phenanthrene-9-carboxylate (14)

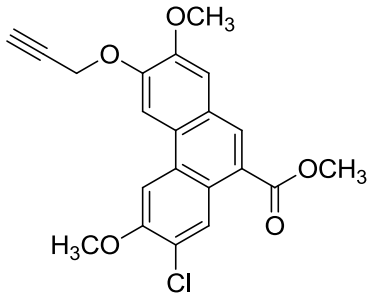

To a solution of (*E*)-methyl 2-(3-chloro-4-methoxyphenyl)-3-(3-methoxy-4-(prop-2-yn-1-yloxy)phenyl)acrylate (**13**, 1.42 g, 3.68 mmol) in CH_2Cl_2 (83 mL) was added dropwise a freshly prepared solution of $FeCl_3$ (4.32 g, 26.6 mmol) in EtOAc (83 mL) at -10 °C, and the reaction mixture was allowed to stir overnight at room temperature. Afterwards H_2O (92 mL) was added, and the mixture was stirred for 3 h at room temperature. It was then extracted with CH_2Cl_2 (3 × 70 mL), and the combined organic layer was dried over anhyd $MgSO_4$ and concentrated in vacuo. The resulting residue was purified by column chromatography (pure CH_2Cl_2) to give methyl 7-chloro-2,6-dimethoxy-3-(prop-2-yn-1-yloxy)phenanthrene-9-carboxylate (**14**, 1.35 g, 3.51 mmol,

95.4% yield) as a white solid. ^{1}H NMR (500 MHz, $CDCl_3$) δ 9.08 (s, 1H), 8.33 (s, 1H), 8.04 (s, 1H), 7.81 (s, 1H), 7.27 (s, 1H), 5.01 (d, *J* = 2.5 Hz, 2H), 4.11 (s, 3H), 4.03 (s, 3H), 4.01 (s, 3H), 2.63 (t, *J* = 2.3 Hz, 1H). ^{13}C NMR (125 MHz, $CDCl_3$) δ 52.20, 56.00, 56.05, 57.16, 76.64, 77.95, 103.16, 106.46, 109.72, 123.10, 123.41, 123.70, 126.12, 126.29, 128.11, 130.17, 130.41, 148.89, 150.22, 153.50, 167.61. HRDARTMS: Calcd for $C_{21}H_{17}ClO_5$ *m/z* 384.07645; $[M+H]^+$ *m/z* 385.08342 (calcd 385.08428).

Preparation of (7-chloro-2,6-dimethoxy-3-(prop-2-yn-1-yloxy)phenanthren-9-yl)methanol (15)

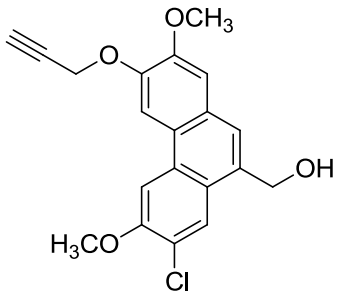

A solution of methyl 7-chloro-2,6-dimethoxy-3-(prop-2-yn-1-yloxy)phenanthrene-9-carboxylate (**14**, 2.42 g, 6.30 mmol) in dry THF (170 mL) was maintained under N_2 atmosphere in an ice bath, and to this solution was added 1.0 M DIBAL-H in hexanes (25.2 mL, 25.2 mmol) dropwise. The resulting reaction mixture was stirred overnight at room temperature. Then the reaction was cooled in an ice bath, and $Na_2SO_4 \cdot 10H_2O$ was added slowly until there was no bubbles forming. The mixture was then filtered over Celite and concentrated in vacuo to give (7-chloro-2,6-dimethoxy-3-(prop-2-yn-1-yloxy)phenanthren-9-yl)methanol (**15**, 1.80 g, 5.06 mmol, 80.3% yield) as a white solid. ^{1}H NMR (500 MHz, $CDCl_3$) δ 8.17 (s, 1H), 8.08 (s, 1H), 7.88 (s, 1H),

7.60 (s, 1H), 7.23 (s, 1H), 5.11 (s, 2H), 4.99 (d, *J* = 2.5 Hz, 2H), 4.12 (s, 3H), 4.03 (s, 3H), 2.61 (t, *J* = 2.5 Hz, 1H). ^{13}C NMR (125 MHz, $CDCl_3$) δ 55.94, 56.19, 57.37, 63.99, 76.32, 78.29, 103.82, 107.28, 108.91, 122.82, 123.83, 123.96, 124.44, 125.92, 127.89, 130.23, 132.50, 147.12, 150.25, 153.49. HRDARTMS: Calcd for $C_{20}H_{17}ClO_4$ *m/z* 356.08154; $[M]^+$ *m/z* 356.08157 (calcd 356.08154).

Preparation of 9-bromo-10-(bromomethyl)-2-chloro-3,7-dimethoxy-6-(prop-2-yn-1-yloxy)phenanthrene (16)

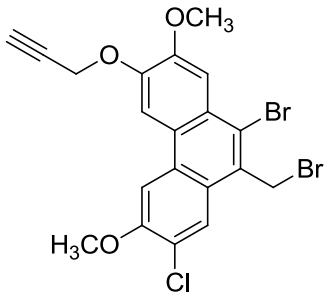

A solution of Br_2 (0.230 g, 1.44 mmol) in CH_2Cl_2 (2.3 mL) was added to a solution of (7-chloro-2,6-dimethoxy-3-(prop-2-yn-1-yloxy)phenanthren-9-yl)methanol (**15**, 0.500 g, 1.40 mmol) in CH_2Cl_2 (12.0 mL) at 0 °C, and the resulting mixture was stirred overnight at room temperature. Afterwards the solvent was removed in vacuo, and the residue was purified by column chromatography (6:4 CH_2Cl_2:hexanes) to give 9-bromo-10-(bromomethyl)-2-chloro-3,7-dimethoxy-6-(prop-2-yn-1-yloxy)phenanthrene (**16**, 0.370 g, 0.750 mmol, 53.6% yield) as a white solid. ^{1}H NMR (500 MHz, $CDCl_3$) δ 8.16 (s, 1H), 8.09 (s, 1H), 7.85 (s, 1H), 7.85 (s, 1H), 5.21 (s, 2H), 5.02 (d, *J* = 2.5 Hz, 2H), 4.13 (s, 3H), 4.09 (s, 3H), 2.62 (t, *J* = 2.5 Hz, 1H). ^{13}C

NMR (125 MHz, $CDCl_3$) δ 32.11, 56.09, 56.22, 57.31, 76.68, 77.92, 103.74, 106.94, 110.08, 123.57, 123.83, 124.19, 124.86, 126.30, 126.85, 129.27, 129.48, 148.04, 150.83, 153.99. HRDARTMS: Calcd for $C_{20}H_{15}Br_2ClO_3$ *m/z* 495.90765; $[M+H]^+$ *m/z* 496.91644 (calcd 496.91547).

Preparation of (*S*)-1-((10-bromo-7-chloro-2,6-dimethoxy-3-(prop-2-yn-1-yloxy)phenanthren-9-yl)methyl)-*N*,*N*-diethylpyrrolidine-2-carboxamide (17)

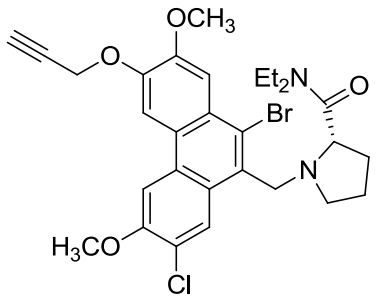

A mixture of 9-bromo-10-(bromomethyl)-2-chloro-3,7-dimethoxy-6-(prop-2-yn-1-yloxy)phenanthrene (**16**, 0.630 g, 1.27 mmol), (*S*)-*N*,*N*-diethylpyrrolidine-2-carboxamide (**8**, 0.240 g, 1.41 mmol) and K_2CO_3 (0.770 g, 5.58 mmol) in DMF (18 mL) was stirred overnight at 70 °C. Then the mixture was allowed to cool to room temperature and filtered. The resulting filtrate was concentrated in vacuo, and the residue was further purified by column chromatography (pure CH_2Cl_2 followed by 8:2 EtOAc:hexanes) to give (*S*)-1-((10-bromo-7-chloro-2,6-dimethoxy-3-(prop-2-yn-1-yloxy)phenanthren-9-yl)methyl)-*N*,*N*-diethylpyrrolidine-2-carboxamide (**17**, 0.670 g, 1.14 mmol, 89.8% yield) as a pale-yellow solid. $[\alpha]_D^{20} = -46.9$ (*c* = 2.0, CH_2Cl_2). ^1H NMR (500 MHz, $CDCl_3$) δ 8.92 (s, 1H), 8.09 (s, 1H), 7.88 (s, 1H), 7.78 (s, 1H),

5.00 (d, *J* = 2.0 Hz, 2H), 4.43 (dd, *J* = 79.7, 12.2 Hz, 2H), 4.11 (s, 3H), 4.07 (s, 3H), 3.59–3.42 (m, 3H), 3.39–3.28 (m, 2H), 3.03–2.97 (m, 1H), 2.72–2.65 (m, 1H), 2.62 (t, *J* = 2.0 Hz, 1H), 2.17–2.09 (m, 1H), 1.93–1.70 (m, 3H), 1.17–1.07 (m, 6H). ^{13}C NMR (125 MHz, $CDCl_3$) δ 13.10, 14.57, 22.96, 29.68, 40.29, 41.22, 51.88, 55.25, 56.00, 56.13, 57.32, 64.12, 76.50, 78.13, 102.87, 107.02, 110.36, 122.83, 123.24, 124.53, 126.42, 126.95, 128.82, 129.10, 131.48, 147.17, 150.37, 153.61, 172.42. HRDARTMS: Calcd for $C_{29}H_{32}BrClN_2O_4$ *m/z* 586.12340; $[M+H]^+$ *m/z* 587.13118 (calcd 587.13122).

Preparation of (13a*S*,14*S*)-7-chloro-2,6-dimethoxy-3-(prop-2-yn-1-yloxy)-9,11,12,13,13a,14-hexahydrodibenzo[*f*,*h*]pyrrolo[1,2-*b*]isoquinolin-14-ol (18)

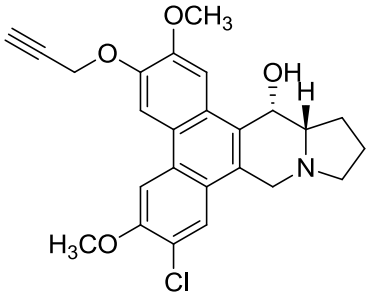

To a solution of (*S*)-1-((10-bromo-7-chloro-2,6-dimethoxy-3-(prop-2-yn-1-yloxy)phenanthren-9-yl)methyl)-*N*,*N*-diethylpyrrolidine-2-carboxamide (**17**, 0.600 g, 1.02 mmol) in dry THF (34 mL) was added TMEDA (0.420 g, 3.61 mmol), and a solution of 2.5 M *n*-BuLi in hexanes (1.23 mL, 3.08 mmol) dropwise at -78 °C under N_2 protection. The resulting mixture was stirred for 4 h at this temperature. Afterwards methanol (8.50 mL) and $NaBH_4$ (0.190 g, 5.02 mmol) was added, and the reaction mixture was allowed to stir at -40 °C for 1 h and at room temperature overnight.

H_2O (13.0 mL) was then added carefully at 0 °C, and the mixture was extracted with CH_2Cl_2 (3 × 15 mL). The combined organic layer was dried with anhyd $MgSO_4$, and the solvent was removed by rotary evaporation. The resulting residue was then further purified by column chromatography (99:1 CH_2Cl_2:*i*-PrOH) to give (13a*S*,14*S*)-7-chloro-2,6-dimethoxy-3-(prop-2-yn-1-yloxy)-9,11,12,13,13a,14-hexahydrodibenzo[*f*,*h*]pyrrolo[1,2-*b*]isoquinolin-14-ol (**18**, 0.420 g, 0.960 mmol, 94.1% yield) as a white solid. ^{1}H NMR (500 MHz, THF-d_8) δ 8.02 (s, 1H), 7.92 (s, 1H), 7.58 (s, 1H), 6.75 (s, 1H), 5.04–4.96 (m, 2H), 4.55 (d, *J* = 8.0 Hz, 1H), 4.08 (s, 3H), 3.99 (s, 3H), 3.18 (t, *J* = 7.7 Hz, 1H), 3.09 (t, *J* = 2.5 Hz, 1H), 2.86 (dd, *J* = 94.7, 14.7 Hz, 2H), 2.45–2.37 (m, 1H), 2.10–2.00 (m, 2H), 1.99–1.89 (m, 1H), 1.78–1.67 (m, 2H). ^{13}C NMR (125 MHz, THF-d_8) δ 21.46, 23.52, 52.71, 54.88, 54.93, 55.31, 56.89, 64.30, 65.62, 76.01, 78.95, 102.71, 106.02, 107.55, 121.31, 122.62, 123.25, 123.50, 126.72, 128.02, 128.84, 129.34, 146.91, 150.51, 152.79. HRDARTMS: Calcd for $C_{25}H_{24}ClNO_4$ *m/z* 437.13939; $[M+H]^+$ *m/z* 438.14650 (calcd 438.14721).

Preparation of 1-(azidomethyl)-3-nitrobenzene (19)

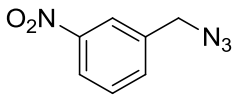

A stock solution of 0.5 M NaN_3 (0.144 g, 2.22 mmol) in DMSO (4.4 mL) was firstly prepared by stirring at room temperature for 24 h. Afterwards 2.2 mL of this stock solution (NaN_3, 0.072 g, 1.1 mmol) was obtained, and 1-(bromomethyl)-3-nitrobenzene (0.430 g, 2.00 mmol) was added.

The resulting mixture was allowed to stir overnight at room temperature, and H_2O (5.0 mL) was then added dropwise. The mixture was cooled to room temperature and extracted with Et_2O (3 × 3.0 mL). The resulting combined organic layer was washed with water (2 × 3.0 mL) and brine (3.0 mL), and the organic layer was dried over $MgSO_4$ and concentrated via rotary evaporation to give the crude 1-(azidomethyl)-3-nitrobenzene (**19**, a yield of 66.7% by ^{1}H NMR integration). The crude product was used in the following step without further purification. HRDARTMS: Calcd for $C_7H_6N_4O_2$ *m/z* 178.04908; $[M+H]^+$ *m/z* 179.05668 (calcd 179.05690).

Preparation of (13a*S*,14*S*)-7-chloro-14-hydroxy-2,6-dimethoxy-10-(2-nitrobenzyl)-3-((1-(3-nitrobenzyl)-1*H*-1,2,3-triazol-4-yl)methoxy)-10,11,12,13,13a,14-hexahydro-9*H*-dibenzo[*f*,*h*]pyrrolo[1,2-*b*]isoquinolin-10-ium bromide (20a)

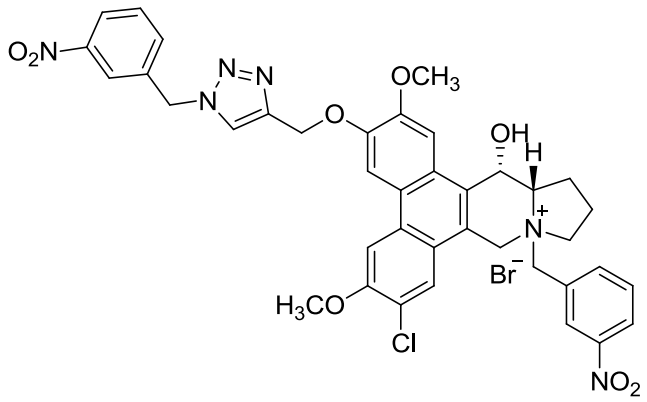

To a solution of (13a*S*,14*S*)-7-chloro-2,6-dimethoxy-3-(prop-2-yn-1-yloxy)-9,11,12,13,13a,14-hexahydrodibenzo[*f*,*h*]pyrrolo[1,2-*b*]isoquinolin-14-ol (**18**, 0.200 g, 0.460 mmol) in CH_3CN

(12.5 mL) was added crude 1-(azidomethyl)-3-nitrobenzene (**19**, 0.160 g, 0.600 mmol based on ^{1}H NMR integration), *N*,*N*-diisopropylethylamine (0.340 mL, 1.95 mmol) and 2,6-lutidine (0.230 mL, 1.99 mmol). The mixture was stirred for 5 min and CuI (0.01g, 0.05 mmol) was added. The resulting mixture was stirred for 12 h at room temperature, and the solvent was then removed by rotary evaporation. The residue was purified by column chromatography (9:1 CH_2Cl_2:EtOH) to give (13a*S*,14*S*)-7-chloro-14-hydroxy-2,6-dimethoxy-10-(2-nitrobenzyl)-3-((1-(3-nitrobenzyl)-1*H*-1,2,3-triazol-4-yl)methoxy)-10,11,12,13,13a,14-hexahydro-9*H*-dibenzo[*f*,*h*]pyrrolo[1,2-*b*]isoquinolin-10-ium bromide (**20a**, 0.160 g, 0.190 mmol, 41.3% yield) as a light-yellow solid. $[\alpha]_D^{20}$ = +98.0 (*c* = 0.6, CH_3CN). ^{1}H NMR (600 MHz, CD_3CN) δ 8.30–8.28 (m, 1H), 8.17–8.15 (m, 1H), 8.14–8.12 (m, 2H), 8.10 (s, 1H), 7.91 (s, 1H), 7.74–7.70 (m, 3H), 7.63–7.57 (m, 3H), 7.51 (d, *J* = 7.8 Hz, 1H), 5.72 (s, 2H), 5.63–5.60 (m, 1H), 5.51–5.45 (m, 2H), 5.05 (d, *J* = 16.2 Hz, 1H), 4.85 (d, *J* = 13.2 Hz, 1H), 4.34 (d, *J* = 14.4 Hz, 1H), 4.18 (d, *J* = 16.2 Hz, 1H), 4.11 (s, 3H), 4.09–4.05 (m, 1H), 3.99 (s, 3H), 3.89–3.85 (m, 1H), 3.32–3.25 (m, 1H), 2.74–2.66 (m, 1H), 2.58–2.43 (m, 3H). ^{13}C NMR (150 MHz, CD_3CN) δ 18.45, 21.35, 52.52, 54.49, 56.32, 56.61, 57.48, 60.79, 60.81, 62.36, 74.99, 104.57, 106.34, 106.66, 118.36, 121.44, 122.74, 123.10, 123.27, 123.92, 124.31, 124.72, 125.19, 125.72, 127.59, 127.76, 129.73, 130.22, 130.51, 130.60, 134.32, 137.78, 139.00, 143.72, 147.52, 148.40, 148.43, 150.40, 154.06. HRMS: Calcd for $C_{39}H_{36}ClN_6O_8^+$ *m/z* 751.2283; $[M]^+$ *m/z* 751.2040 (calcd 751.2283); Calcd for Br^- *m/z* 78.9183; $[M]^-$ *m/z* 78.9184 (calcd 78.9183).

Preparation of (*E*)-methyl 3-(4-(difluoromethoxy)-3-methoxyphenyl)-2-(3,4-dimethoxyphenyl)acrylate (23)

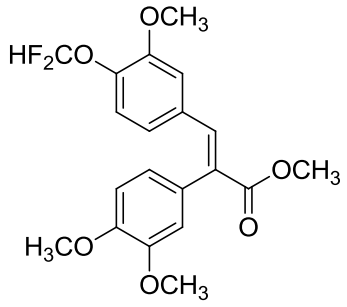

To a solution of (*E*)-methyl 2-(3,4-dimethoxyphenyl)-3-(4-hydroxy-3-methoxyphenyl)acrylate (1.14 g, 3.31 mmol) in DMF (24 mL) was added K_2CO_3 (0.930 g, 6.73 mmol) and H_2O (1.20 mL). Sodium chlorodifluoroacetate (1.12 g, 7.35 mmol) was carefully added to the resulting suspension, and the mixture was heated to 80 °C and stirred for 16 h. After cooling to room temperature the reaction was diluted with H_2O and extracted with CH_2Cl_2 (3 × 20 mL). The combined organic layer was washed with water and brine, dried over $MgSO_4$, filtered and concentrated in vacuo. The residue was then purified by column chromatography (9:1 CH_2Cl_2:hexanes) to give (*E*)-methyl 3-(4-(difluoromethoxy)-3-methoxyphenyl)-2-(3,4-dimethoxyphenyl)acrylate (**23**, 0.450 g, 1.14 mmol, 34.4% yield) as a white solid. ^{1}H NMR (500 MHz, $CDCl_3$) δ 7.74 (s, 1H), 6.98 (d, *J* = 8.0 Hz, 1H), 6.90 (d, *J* = 8.0 Hz, 1H), 6.78 (dd, *J* = 8.0, 2.0 Hz, 1H), 6.76 (dd, *J* = 8.5, 2.0 Hz, 1H), 6.74 (d, *J* = 1.5 Hz, 1H), 6.61 (d, *J* = 2.0 Hz, 1H), 6.50 (t, *J* = 75.0 Hz, 1H), 3.89 (s, 3H), 3.80 (s, 3H), 3.79 (s, 1H), 3.48 (s, 3H). ^{13}C NMR (125 MHz, $CDCl_3$) δ 52.44, 55.40, 55.91, 55.94, 111.52, 112.81, 113.96, 115.81 (t, *J* = 258.9 Hz),

121.41, 122.14, 124.25, 128.03, 132.29, 133.02, 139.13, 140.33, 148.85, 149.31, 150.21, 168.19. HRDARTMS: Calcd for $C_{20}H_{20}F_2O_6$ *m/z* 394.12279; $[M+H]^+$ *m/z* 395.13045 (calcd 395.13062).

Preparation of methyl 3-(difluoromethoxy)-2,6,7-trimethoxyphenanthrene-9-carboxylate (24)

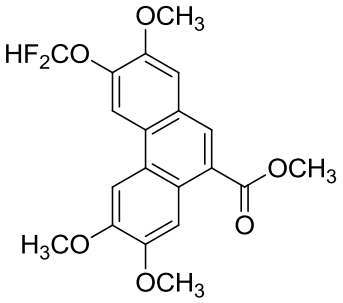

A solution of (*E*)-methyl 3-(4-(difluoromethoxy)-3-methoxyphenyl)-2-(3,4-dimethoxyphenyl)acrylate (**23**, 4.70 g, 11.9 mmol) in CH_2Cl_2 (280 mL) was cooled to -10 °C, and to this solution was added a freshly prepared solution of $FeCl_3$ (15.5 g, 95.6 mmol) in EtOAc (280 mL), and the resulting mixture was stirred overnight at room temperature. Afterwards H_2O (250 mL) was added and the mixture was stirred for 3 h at room temperature. Extraction of the mixture with CH_2Cl_2 (3 × 200 mL) was carried out, and the combined organic layer was dried over $MgSO_4$ and concentrated in vacuo. The residue was purified by column chromatography (pure CH_2Cl_2) to give methyl 3-(difluoromethoxy)-2,6,7-trimethoxyphenanthrene-9-carboxylate (**24**, 4.40 g, 11.2 mmol, 94.1% yield) as a light-yellow solid. ^{1}H NMR (500 MHz, $CDCl_3$) δ 8.42 (s, 1H), 8.16 (s, 1H), 7.98 (s, 1H), 7.54 (s, 1H), 7.14 (s, 1H), 6.74 (t, *J* = 75.0 Hz, 1H), 4.05 (s, 3H), 4.03 (s, 3H), 3.99 (s, 3H), 3.95 (s, 3H). ^{13}C NMR (125 MHz, $CDCl_3$) δ 52.08, 55.74, 55.75,

55.88, 102.37, 106.57, 110.30, 114.94, 116.23 (t, J = 258.4 Hz), 123.52, 124.35, 125.10, 126.08, 127.83, 129.41, 141.64, 149.24, 149.31, 149.60, 167.79. HRDARTMS: Calcd for $C_{20}H_{18}F_2O_6$ *m/z* 392.10714; $[M+H]^+$ *m/z* 393.11451 (calcd 393.11497).

Preparation of (3-(difluoromethoxy)-2,6,7-trimethoxyphenanthren-9-yl)methanol (25)

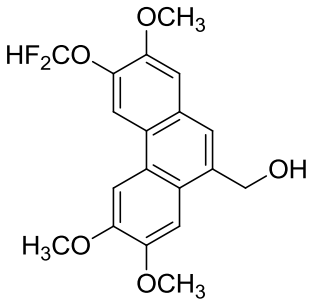

To a solution of methyl 3-(difluoromethoxy)-2,6,7-trimethoxyphenanthrene-9-carboxylate (**24**, 4.15 g, 10.6 mmol) in dry THF (285 mL) maintained under an N_2 atmosphere at 0 °C was added a solution of 1.0 M DIBAL-H in hexanes (42.0 mL, 42.0 mmol). The resulting mixture was allowed to stir overnight at room temperature. The mixture was then cooled to 0 °C, and $Na_2SO_4 \cdot 10H_2O$ was added to quench the reaction (until there were no bubbles forming). The resulting mixture was filtered over Celite and concentrated in vacuo to give (3-(difluoromethoxy)-2,6,7-trimethoxyphenanthren-9-yl)methanol (**25**, 3.80 g, 10.4 mmol, 98.1% yield) as a white solid. ^{1}H NMR (500 MHz, $CDCl_3$) δ 8.17 (s, 1H), 7.77 (s, 1H), 7.58 (s, 1H), 7.46 (s, 1H), 7.25 (s, 1H), 6.72 (t, J = 75.3 Hz, 1H), 5.11 (s, 2H), 4.11 (s, 3H), 4.04 (s, 3H), 4.00 (s, 3H). ^{13}C NMR (125 MHz, $CDCl_3$) δ 55.94, 55.98, 55.99, 64.38, 103.23, 104.61, 109.56, 115.62, 116.40 (t, J = 258.1 Hz), 123.09, 124.17, 124.28, 125.12, 129.58, 134.39, 140.00, 149.07,

149.44, 149.75. HRDARTMS: Calcd for $C_{19}H_{18}F_2O_5$ *m/z* 364.11223; $[M]^+$ *m/z* 364.11246 (calcd 364.11223).

Preparation of 9-bromo-10-(bromomethyl)-6-(difluoromethoxy)-2,3,7-trimethoxyphenanthrene (26)

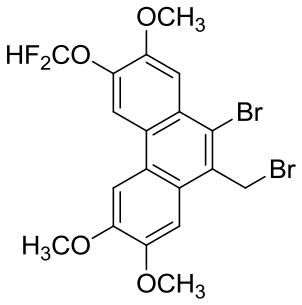

A solution of Br_2 (0.230 g, 1.44 mmol) in CH_2Cl_2 (2.5 mL) was added to a solution of (3-(difluoromethoxy)-2,6,7-trimethoxyphenanthren-9-yl)methanol (**25**, 0.500 g, 1.37 mmol) in CH_2Cl_2 (12.0 mL) at 0 °C, and the resulting mixture was stirred overnight at room temperature. Afterwards the solvent was removed by rotary evaporation, and the residue was purified by column chromatography (pure CH_2Cl_2) to give 9-bromo-10-(bromomethyl)-6-(difluoromethoxy)-2,3,7-trimethoxyphenanthrene (**26**, 0.420 g, 0.830 mmol, 60.6% yield) as a light-yellow solid. ^{1}H NMR (600 MHz, $CDCl_3$) δ 8.23 (s, 1H), 7.92 (s, 1H), 7.78 (s, 1H), 7.49 (s, 1H), 6.76 (t, *J* = 75.0 Hz, 1H), 5.26 (s, 2H), 4.13 (s, 3H), 4.10 (s, 3H), 4.09 (s, 3H). ^{13}C NMR (150 MHz, $CDCl_3$) δ 32.64, 56.07, 56.11, 56.15, 103.20, 105.22, 110.94, 115.68, 116.09 (t, *J* = 259.5 Hz), 122.47, 124.38, 124.50, 125.20, 128.56, 131.12, 140.97, 149.61, 150.02, 150.45.

HRDARTMS: Calcd for $C_{19}H_{16}Br_2F_2O_4$ *m/z* 503.93834; $[M+H]^+$ *m/z* 504.94661 (calcd 504.94617).

Preparation of (*S*)-1-((10-bromo-3-(difluoromethoxy)-2,6,7-trimethoxyphenanthren-9-yl)methyl)-*N*,*N*-diethylpyrrolidine-2-carboxamide (27)

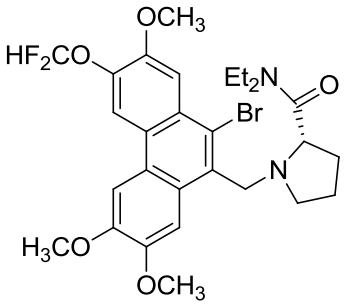

To a solution of 9-bromo-10-(bromomethyl)-6-(difluoromethoxy)-2,3,7-trimethoxyphenanthrene (**26**, 1.40 g, 2.78 mmol) in DMF (50 mL), (*S*)-*N*,*N*-diethylpyrrolidine-2-carboxamide (**8**, 0.560 g, 3.29 mmol) and K_2CO_3 (1.68 g, 12.2 mmol) were added, and the resulting mixture was allowed to stir overnight at 70 °C. Afterwards the mixture was cooled to room temperature and filtered, the resulting filtrate was concentrated via rotary evaporation. The residue was further purified by column chromatography (pure CH_2Cl_2 followed by 6:4 EtOAc:hexanes) to give (*S*)-1-((10-bromo-3-(difluoromethoxy)-2,6,7-trimethoxyphenanthren-9-yl)methyl)-*N*,*N*-diethylpyrrolidine-2-carboxamide (**27**, 1.37 g, 2.31 mmol, 83.1% yield) as a white solid. $[\alpha]_D^{20} = -41.5$ (*c* = 3.5, CH_2Cl_2). ^{1}H NMR (600 MHz, $CDCl_3$) δ 8.56 (s, 1H), 8.20 (s, 1H), 7.93 (s, 1H), 7.68 (s, 1H), 6.74 (t, *J* = 75.0 Hz, 1H), 4.45 (dd, *J* = 108.3, 12.3 Hz, 2H), 4.20 (s, 3H), 4.10 (s, 3H), 4.06 (s, 3H), 3.48–3.42 (m, 2H), 3.41–3.31 (m, 3H), 2.90–2.87 (m, 1H), 2.65 (q, *J* = 8.4 Hz, 1H), 2.15–

2.09 (m, 1H), 1.88–1.67 (m, 3H), 1.17 (t, J = 6.9 Hz, 3H), 1.12 (t, J = 6.9 Hz, 3H). ^{13}C NMR (150 MHz, $CDCl_3$) δ 13.16, 14.81, 22.81, 29.75, 40.29, 41.34, 51.60, 55.91, 56.04, 56.15, 56.95, 64.12, 102.05, 108.48, 111.19, 115.46, 116.29 (t, J = 258.5 Hz), 121.73, 123.89, 124.98, 126.82, 128.57, 133.46, 140.13, 149.46, 149.70, 149.83, 172.05. HRDARTMS: Calcd for $C_{28}H_{33}BrF_2N_2O_5$ *m/z* 594.15409; $[M+H]^+$ *m/z* 595.16142 (calcd 595.16192).

PART TWO. THE STRUCTURE-BASED APPROACH

ABSTRACT

In the structure-based approach, a biotinylated DCB-3503 analogue was designed and synthesized previously in Dr. David Baker's lab, and it was utilized by our collaborators, Dr. Yung-Chi Cheng of Yale University School of Medicine, to snare a protein targeted by DCB-3503 type compounds. In order to explore a new dimension, the biotinylated DCB-3503 was used to study the hepatitis C virus (HCV), which is closely associated with the development of hepatic (liver) cancer and may be an etiologic factor in hepatic cancer development. A cellular heat shock cognate protein 70 (Hsc70) was identified as one of the target proteins of DCB-3503 in the anti-HCV study. The target protein was then synthesized without and with ^{15}N labeling in our lab, and the thermodynamic and NMR studies of its interactions with DCB-3503 were carried out. However, failure to elucidate the specific DCB-3503 and Hsc70 interactions by NMR studies prompted us to turn to computational simulations, where two docking models, including the one based on DCB-3503 and the ATP-state Hsc70 nucleotide binding domain (NBD), and another based on DCB-3503 and the apo-state Hsc70 NBD, were constructed. The most reasonable docking pose of DCB-3503 was generated in the ATP-state protein based on the analysis of both the experimental observations and the docking scores. Design of more promising active candidates can likely be realized in the future through the study of the aforementioned docking pose.

I. BACKGROUND

1. The Identification of the Target of DCB-3503.

Based on the facts that no specific target for DCB-3503 had been identified, a structure-based approach was launched by collaborating with Dr. Yung-Chi Cheng of Yale University School of Medicine. A biotinylated DCB-3503 was designed and synthesized in Dr. Baker's group from DCB-3509 with a biotin probe installed via CuAAC click chemistry as shown in Scheme 33. The biotin probe was determined to be installed at the 3-position on DCB-3503 due to the previous structure–activity studies and CoMFA predictions.[14] Extensive structure–activity studies on phenanthroindolizidine alkaloids all point to the indolizidine ring system, as opposed to the phenanthrene system, as the pharmacophoric group.[15-18] With the biotinylated DCB-3503 in hand, our collaborators in Dr. Cheng's lab opted to investigate a new system—the hepatitis C virus (HCV), which is closely associated with the development of hepatic (liver) cancer and may be an etiologic factor in hepatic cancer development.[50] By studying the anti-HCV related activities of DCB-3503, it was hoped to open a new dimension to explore, as a promising drug candidate with both anti-viral and anticancer activities could possibly be derived. It is worth noting that due to a lack of the corresponding anti-HCV activities of the tylophorine analogues used in construction of the previous CoMFA models, a ligand-based approach is not feasible here.

The procedures to identify the target of DCB-3503 are described in the flowchart below. The biotinylated DCB-3503 was firstly immobilized on the streptavidin resin through the binding between biotin and streptavidin, which possesses an unusually high affinity ($K_d = 10^{-15}$ M).[51] In a typical experiment the resulting matrix with biotinylated-tethered DCB-3503 as the probe is

incubated with the cell lysate of interest whereby the target protein binds to the corresponding probe, which would be the DCB-3503 moiety. The target protein–biotinylated DCB-3503–streptavidin complex could then be denatured and eluted by SDS-PAGE loading buffer, and the resulting affinity-purified complex could be further resolved via SDS-PAGE analysis. The target protein bands obtained from SDS-PAGE analysis can be further analyzed by mass spectrometry to identify the target protein. After the identification of the protein a western blot analysis is carried out on the elution buffer obtained from respectively passing the cell lysate and the recombinant target protein through the DCB-3503 affinity matrix to confirm the identity of the protein.

DCB-3503 and its analogues show an inhibitory effect against HCV. The mode of action of the inhibition is at the elongation phase of protein synthesis and the replication of HCV on the

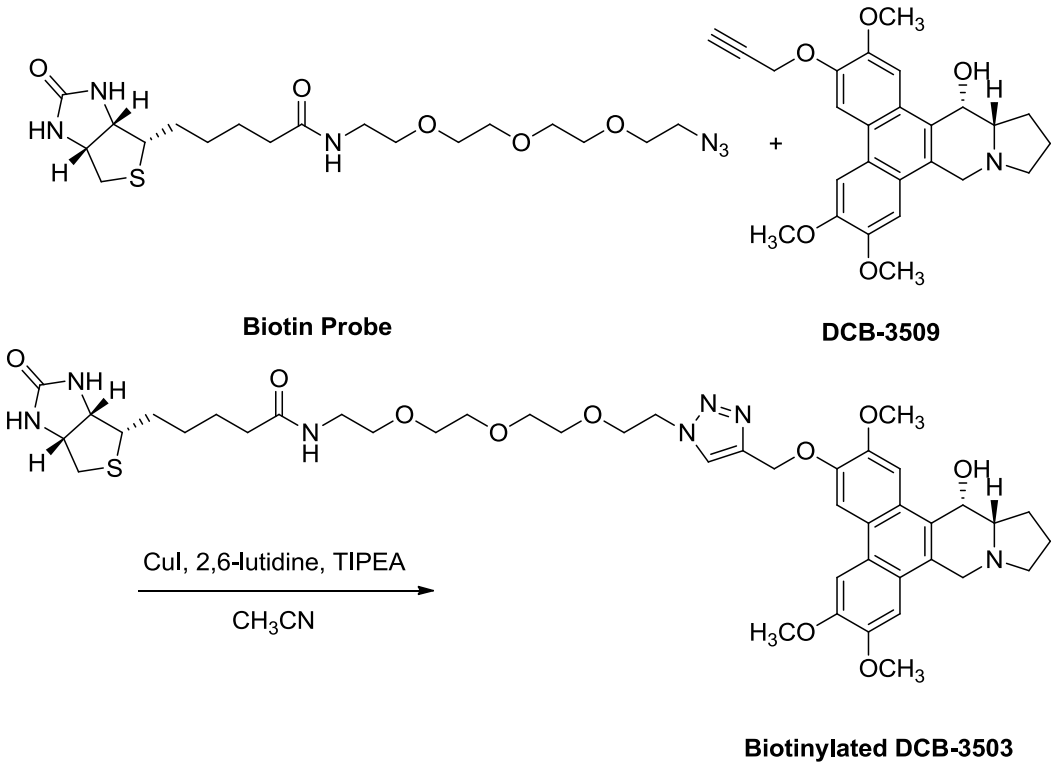

Scheme 33. The synthesis of biotinylated DCB-3503.[3]

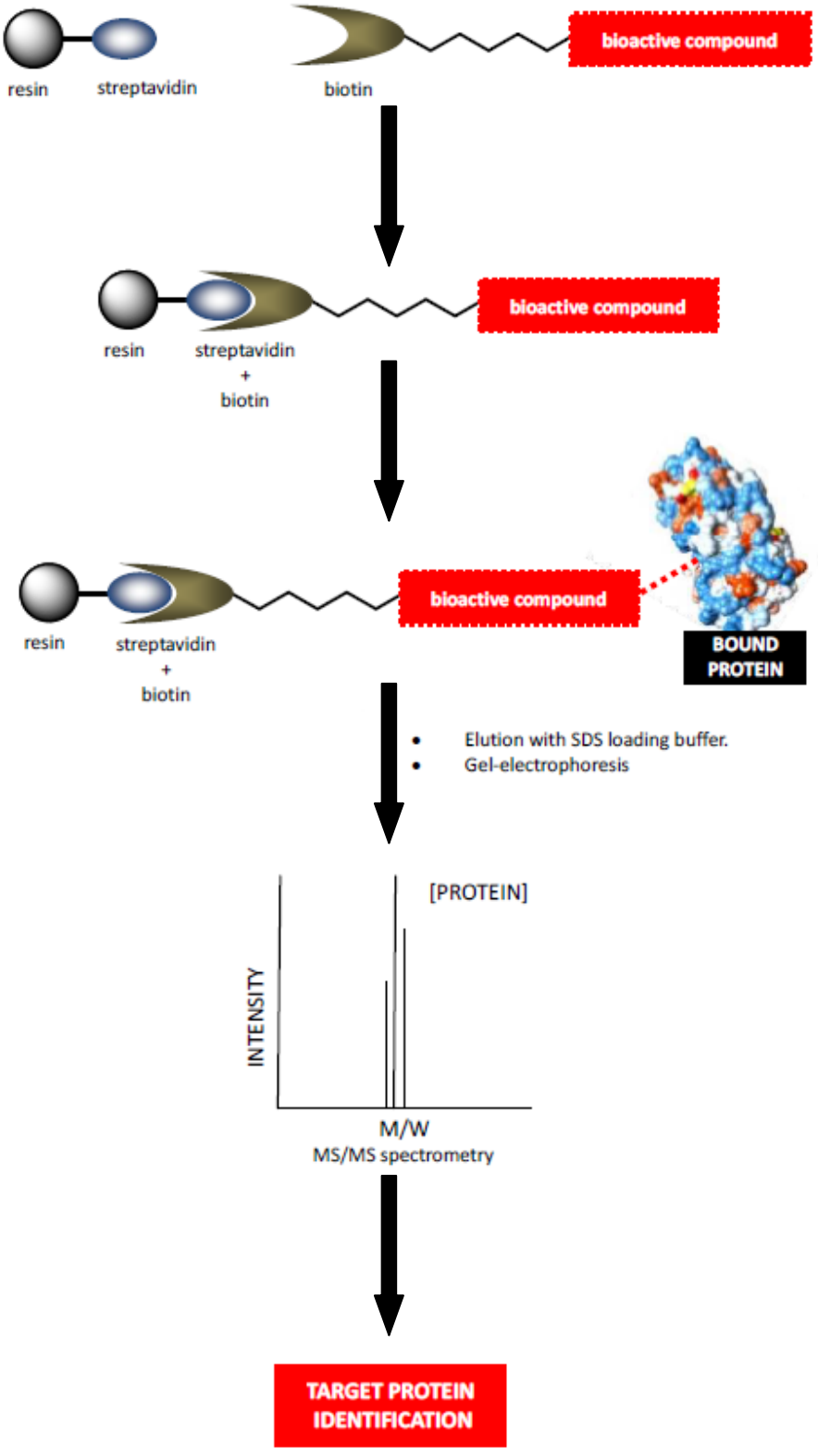

Figure 33. The workflow of DCB-3503 target protein identification.[3]

endoplasmic reticulum (ER).[52] The above-mentioned procedure using the DCB-3503 probe was carried out by incubating the streptavidin-biotin-DCB-3503 matrix in Huh-luc/neo-ET cell lysate, and the cellular heat shock cognate protein 70 (Hsc70) was successfully identified as one of the target proteins of DCB-3503. The exact binding domain of Hsc70 interacted with DCB-3503 was confirmed to be the N-terminal nucleotide binding domain (NBD) in further studies.[52]

2. The Studies of Hsc70 and Its Interactions with DCB-3503.

The Hsc70 protein is a constitutively expressed chaperone protein belonging to the family of heat shock protein 70 (Hsp70), which is classified based on the molecular weight in the units of kDa. Hsc70 is constituted of a 44 kDa N-terminal nucleotide-binding domain (NBD) and an 18 kDa substrate-binding domain (SBD) connected via a flexible linker, and a 10 kDa C-terminal domain functioning as a "lid" of the SBD. Although Hsc70 and Hsp70 proteins share 85% amino acids similarity with the major distinction appearing on the C-terminal domain, the two are believed to have different functions.[53]

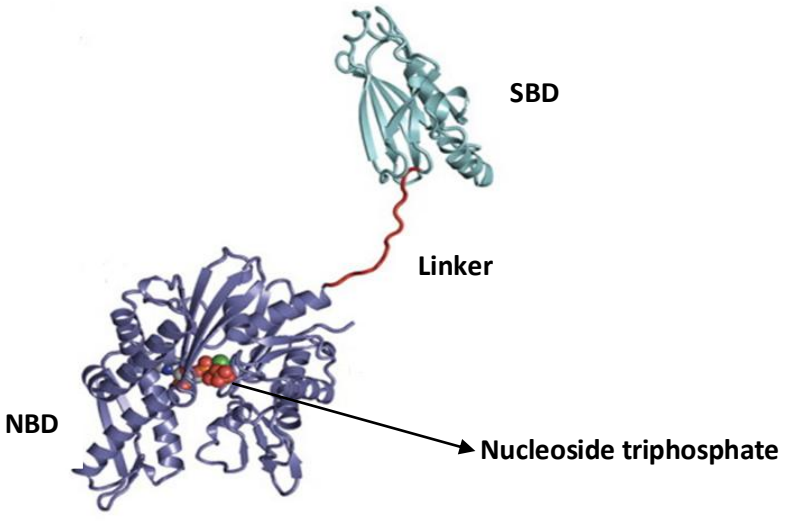

Figure 34. The structure of *E. Coli* Hsp70 (DnaK) in ADP-bound state.[4]

As one of the Hsp70 molecular chaperone family of proteins presented in all domains of life, Hsc70 is involved in signal transduction in cells and apoptosis, growth and differentiation of cells by folding, refolding and trafficking proteins through an allosteric mechanism associated with ATP hydrolysis.[54-56] Recently it was discovered that the Hsp70 family is linked to the development of cancer and neurodegenerative diseases such as Alzheimer's, Parkinson's and Huntington's.[57] It is believed that by binding ATP on the NBD of Hsc70, the SBD was able to capture and release the substrate rapidly, whereas by hydrolyzing of ATP to ADP at the NBD, the SBD could seize the substrate tightly. As can be seen in Figure 35, the chaperone activity could be realized by repeating the cycle of catching the substrate at SBD by hydrolyzing ATP to ADP, releasing of ADP and binding of new ATP molecule in order to release the substrate.

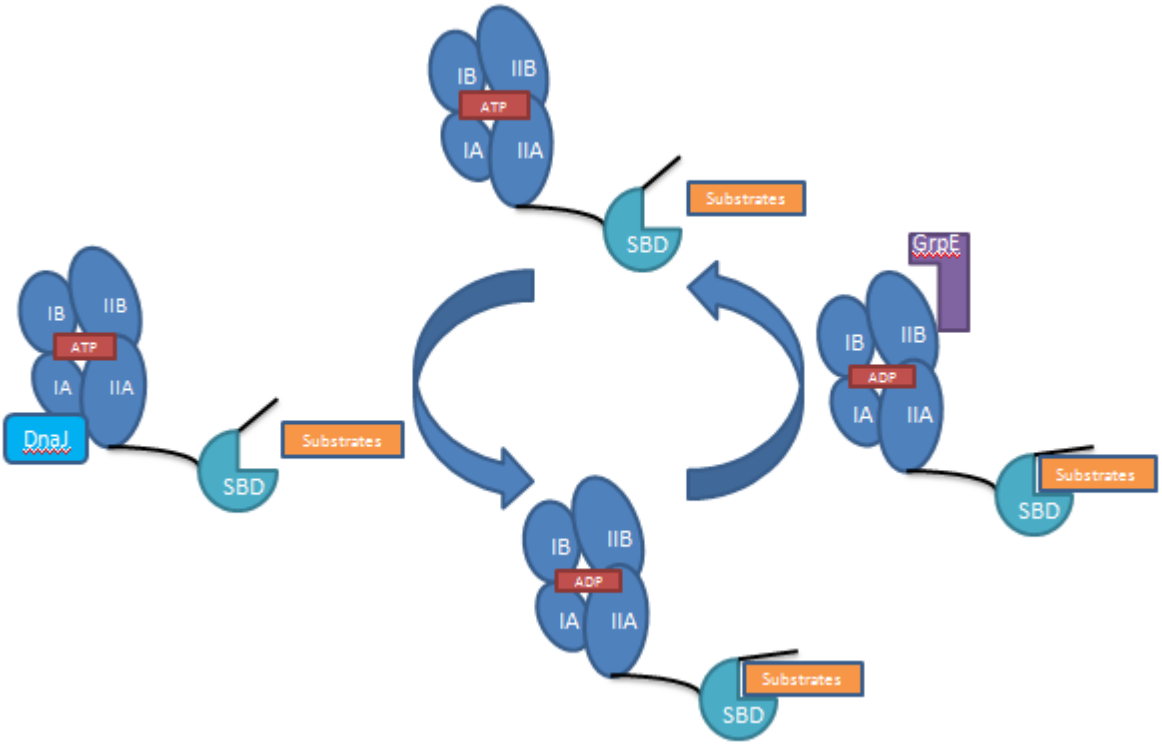

Figure 35. The functional cycle of Hsc70.

However, due to the slow rate of releasing ADP by Hsc70 itself, nucleotide exchange factors (NEFs) such as GrpE, Hsp110s and Bcl-2-associated athanogene (BAG) family proteins usually play a significant role in the cycle.[56, 58] In addition, J co-chaperones, including J domain protein, could accelerate the cycle via stimulating the hydrolysis of ATP by binding to the NBD.[59] Several studies have been conducted in attempts to elucidate the specific mechanisms by which conformational change of NBD results from the hydrolysis of ATP. The process ultimately leads to the allosteric conformational change of the SBD, quite possibly through the linker, the majority of the steps in the process still remains unknown.[4, 54, 55, 57, 60]

Studies of how DCB-3503 interacting with Hsc70 NBD were carried out in Dr. Cheng's lab after the successful identification of the target protein. In their studies it was found DCB-3503 was bound to the NBD of Hsc70 but not to the ATPase-active pocket to stimulate the ATPase activity. This was supported by the introduction of the mutation D206S at the ATPase pocket, which did not affect the binding of DCB-3503. However, the binding might be affected by ATP concentration and ionic strength. Additionally, it was found Hsc70 SBD bound to the poly U/UC motif of HCV RNA, which is essential to the efficient translation and replication of HCV in host cells. Given the results obtained and the fact that host chaperones and co-chaperones play important roles in the assembly of the HCV viral replication complex, a model was proposed about the mechanism of how DCB-3503 exhibits its anti-HCV activity. Upon treatment, DCB-3503 binds to the NBD of Hsc70 to stimulate ATP hydrolysis in the presence of the poly U/UC motif of HCV RNA, resulting in the tight binding of the corresponding HCV RNA to the SBD, which ultimately inhibits the translation of HCV in the host cells. However, due to the narrow selective index of approximate 3-fold (EC_{50} against HCV replication to IC_{50} against Huh-luc/neo-ET cell), DCB-3503 may not be significantly beneficial as an antiviral drug to the

patients already infected with HCV, but will have a special advantage toward the treatment of cancer or autoimmune diseases in patients already infected with HCV.[52]

II. STATEMENT OF THE PROBLEM

Although the target protein of DCB-3503 was successfully identified, the specific binding site and mode are still unknown due to the difficulty to obtain the co-crystal of DCB-3503 and Hsc70 NBD for further X-ray crystallographic analysis. Therefore, the decision was made to conduct ^{1}H-^{15}N HSQC NMR analysis to locate the specific binding site and possibly develop a docking model for further drug design and screening. Several small molecules targeting the NBD of some Hsp70 family proteins, functioning as either inhibitors or agonist, had been already studied by NMR spectroscopy.[61-63]

1. The Overexpression and Purification of Hsc70 NBD.

The *E. coli* cell strain with the recombinant Hsc70 NBD plasmid cloned was obtained from Dr. Cheng's lab. The protocol of overexpression and purification of the corresponding protein would be tested and established.

2. The Thermodynamic Studies of Hsc70 NBD.

Due to the necessity to confirm the binding between DCB-3503 and Hsc70 and the lack of the corresponding activity assay, two types of thermodynamic experiments would be carried out. Differential scanning calorimetry (DSC) would be conducted to confirm the ATPase activity, and any possible binding pattern observed could also be studied. The isothermal titration calorimetry (ITC) would also be performed to study the binding pattern in a more direct way, and the corresponding thermodynamic statistics could be obtained from ITC as well. In both of

the experiments the combination of different concentrations of ligand and protein would be tested, and the interactions of the ligand with protein in different states would also be studied.

3. The Elucidation of the Interactions between DCB-3503 and Hsc70.

Once the binding was confirmed, the ^{1}H-^{15}N HSQC NMR experiments would be conducted aiming at unveiling the specific interaction patterns. With the Hsc70 NBD ^{1}H-^{15}N HSQC NMR assignments provided by Dr. Erik R.P. Zuiderweg (University of Michigan, Ann Arbor), the residues involved in the possible binding site could be located via the comparison of the NMR chemical shifts. Since the NMR assignments offered by Dr. Zuiderweg were made on the ADP-bound state protein, our NMR experiments would be carried out on ADP-bound Hsc70 as well.

4. The Construction of the Docking Model.

With the specific residues of possible binding site, a docking molecular model could be constructed in Dr. Jerome Baudry's lab. The evaluation of different docking poses would be made, and further designing and screening of novel compounds based on DCB-3503 could be carried out.

III. DISCUSSION

1. The Overexpression and Purification of Hsc70 NBD.

The overexpression procedures of Hsc70 NBD were modified from the protocol provided by our collaborator in Dr. Cheng's lab. The first test of the overexpression of Hsc70 NBD was carried out utilizing the conditions provided by our collaborator in 500 mL of lysogeny broth (LB) media. After sufficient growth of the cells, an attempt to induce the overexpression of Hsc70 NBD was performed at a final concentration of IPTG (isopropyl β-D-1-thiogalactopyranoside) of 1.0 mM at 25 ℃ for 6 h (**c**). The cells were then harvested and lysed via the freeze/thaw method in 50 mM Tris-HCl (pH 7.4 at 4 °C) buffer, and the resulting lysate was centrifuged, and the supernatant and the pellet were collected. Meanwhile other possible conditions for the overexpression of Hsc70 were tested as well. Three different conditions, which were final concentration of IPTG 0.5 mM at 25 ℃ for 6 h (**a**), final concentration of IPTG 0.5 mM at 37 °C for 4 h (**b**), final concentration of IPTG 1.0 mM at 37 °C for 4 h (**d**), were used to overexpress the Hsc70 NBD in 200 mL of LB media.

The three groups of cells were then harvested and lysed via the same method used in the first test, and the corresponding supernatant and pellets were collected. An SDS-PAGE analysis of the supernatant and pellets was carried out, and the result is shown in Figure 36. As can be seen, an intense band around 45 kDa utilizing the standard lane as a reference could be observed in all four supernatant lanes, and in combination with the weight of Hsc70 NBD (44 kDa) this band was determined to be the target protein band. In addition, such a band could not be found in the pellet lanes, suggesting a good solubility of Hsc70 NBD. It was not difficult to conclude that no

major difference could be identified between four supernatant lanes in terms of their relative intensities; therefore, the optimum set of conditions was selected as condition **b**, which consumed the least IPTG and time. What is worth noting is that although the bands of the supernatant in condition **c** was more intense than the others, the protein concentration of which was regarded as the same as the others when the relative intensities were considered. The reason behind these observations was that almost 500 mL of cell culture was lysed in condition **c**, while only 200 mL of cell culture was in use for the other three, which resulted in a significant difference between the concentrations of the first batches of protein and the other three.

The purification procedures utilizing on Ni-Sepharose column were then performed. After loading and washing the crude lysate with wash buffer, the target protein Hsc70 NBD was eluted

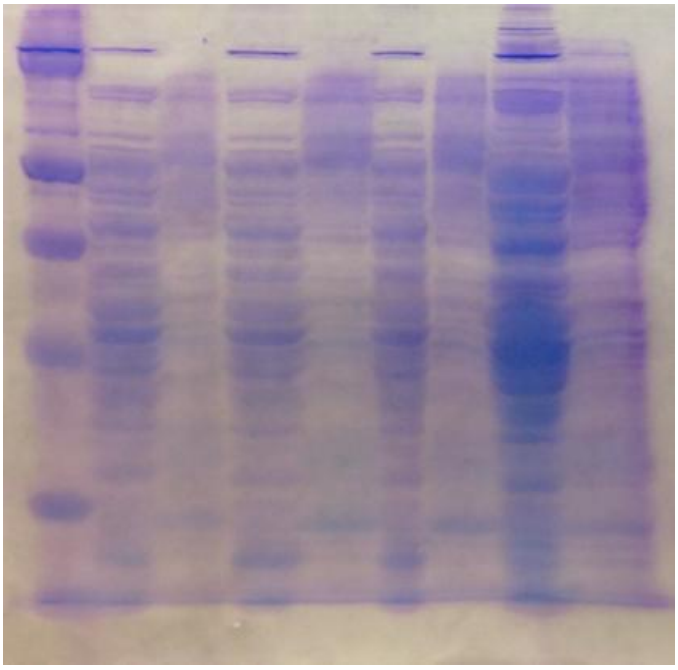

Figure 36. The SDS-PAGE analysis of the overexpression of Hsc70 NBD under different conditions. (From left to right: standard, condition a supernatant, condition a pellet, condition b supernatant, condition b pellet, condition d supernatant, condition d pellet, condition c supernatant, condition c pellet.)

with an imidazole gradient buffer made in a 100-mL gradient maker from gradient buffer **A** (50 mM Tris-HCl (pH 7.4 at 4 ℃), 500 mM NaCl, 100 mM imidazole) and gradient buffer **B** (50 mM Tris-HCl (pH 7.4 at 4 °C), 500 mM NaCl, 500 mM imidazole), and every 1-mL fractions were collected. The concentration of the protein in every fraction was measured by absorbance at 280 nM, and the fractions with the highest absorbance were analyzed by SDS-PAGE analysis with the results shown in Figure 37. Apparently Hsc70 NBD was primarily eluted in fractions from 19 to 24 according to the isolated intense bands shown in Figure 37. However, in order to obtain a clearer picture of the elution of the protein, another SDS-PAGE analysis was carried out on fractions 12 to 24. Unfortunately not only the target protein, but also some impurities, were eluted together by the gradient imidazole buffer according to the SDS-PAGE analysis. It was therefore difficult to elute Hsc70 NBD exclusively using a buffer with a fixed concentration of imidazole if the gradient buffer would not achieve a satisfactory result. The decision was then made to elute most of the target protein bound to the Ni-Sepharose resin by utilizing an elution buffer constituted of 50 mM Tris-HCl (pH 7.4 at 4 ℃), 250 mM imidazole and 500 mM NaCl, in which the imidazole concentration was estimated from the concentration of imidazole that was able to start eluting the target protein in the SDS-PAGE analysis shown in Figure 38. By collecting this eluted solution we were able to obtain the protein with the least impurities according to the SDS-PAGE analysis.

In order to further purify the target protein from the protein mixture obtained from the Ni-Sepharose column, gel filtration chromatography was performed by taking advantage of the size difference between Hsc70 NBD and the rest of the impurities. The gel filtration chromatography buffer was selected as the same buffer being used in the experiment in the next step (50 mM Tris-HCl (pH 7.4 at 4 °C) and 100 mM NaCl or 50 mM MOPS (pH 7.4 at 4 °C) and100 mM

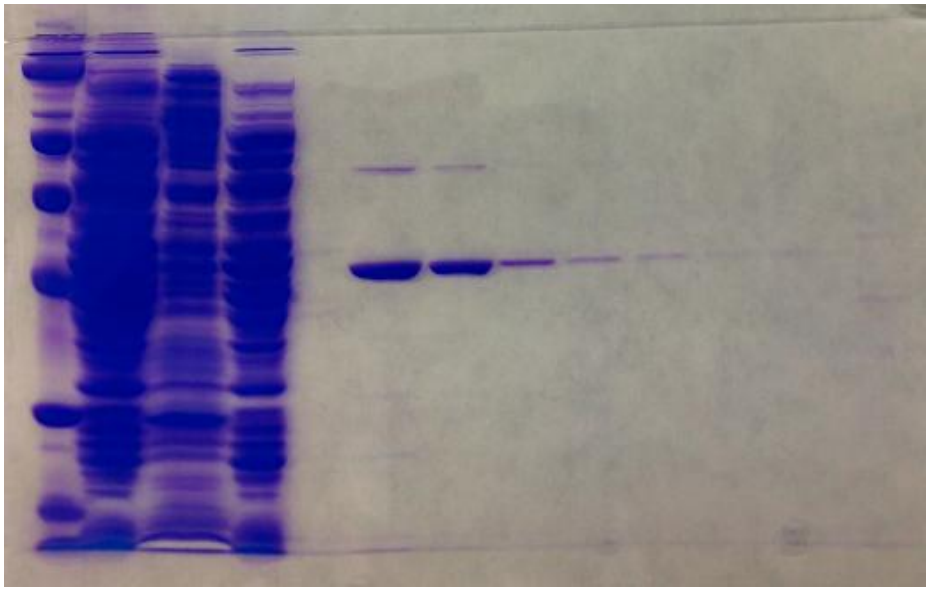

Figure 37. The SDS-PAGE analysis of the purification of Hsc70 NBD via a Ni-Sepharose column. (From left to right: standard, supernatant, pellet, supernatant flow-through, wash buffer flow-through, fractions 19, 21, 24, 26, 28, 31, stripping buffer flow-through.)

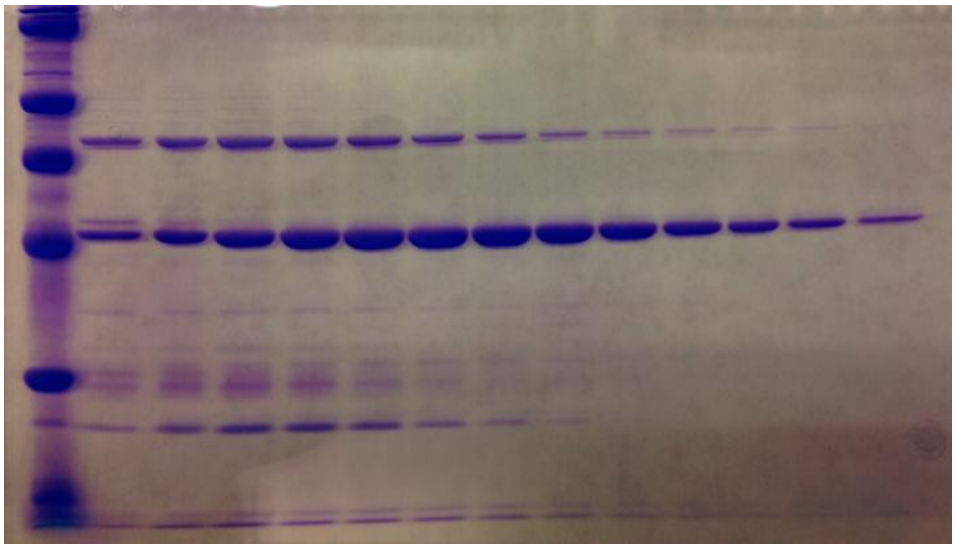

Figure 38. The SDS-PAGE analysis of the fractions 12 to 24 obtained from a Ni-Sepharose column. (From left to right: standard, fractions 12 to 24.)

NaCl based on different usages of the protein) so as to eliminate the further dialysis procedures. The results of the separation are shown in Figure 39, and fractions from each peak were analyzed by SDS-PAGE. It was apparent that the second peak in the gel filtration chromatogram contained Hsc70 NBD and the third peak was determined to be the peak of imidazole as seen in Figure 40. In addition fractions from 5 to 19 were also analyzed by SDS-PAGE to assist in making the decision to collect and pool fractions from 9 to 14 together. Although a small amount of impurities were still presented in the pooled fraction, the protein was determined to be pure enough to be utilized in future experiments.

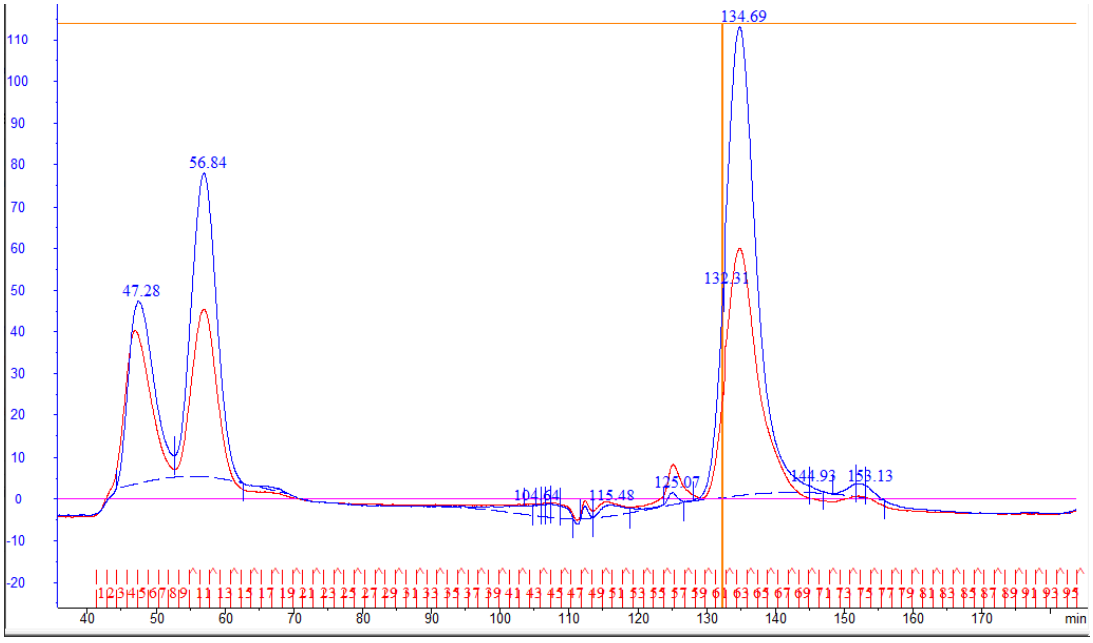

Figure 39. Separation of Hsc70 NBD obtained from gel filtration chromatography.

2. Differential Scanning Calorimetry (DSC) Studies.

Four DSC experiments were carried out aiming at studying the activities of Hsc70 NBD and the corresponding interactions with DCB-3503. In each of the experiments the thermal unfolding

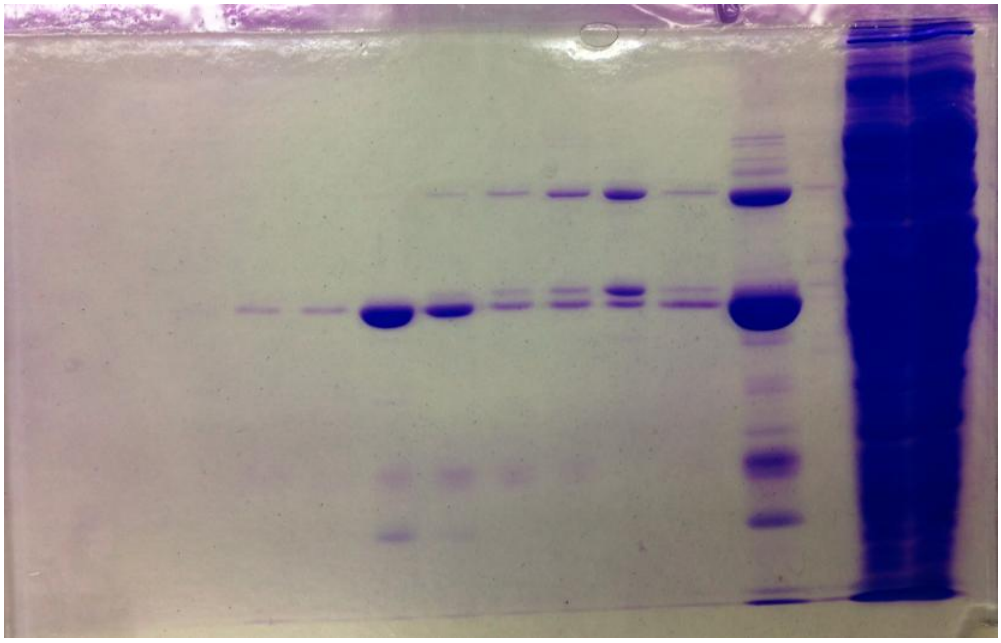

Figure 40. The SDS-PAGE analysis of the gel filtration chromatography. (From right to left: supernatant, supernatant flow-through, wash buffer flow-through, elution buffer flow-through, stripping buffer flow-through, fractions of 4, 7, 8, 9, 11, 16, 17, 56, 64 and 74.)

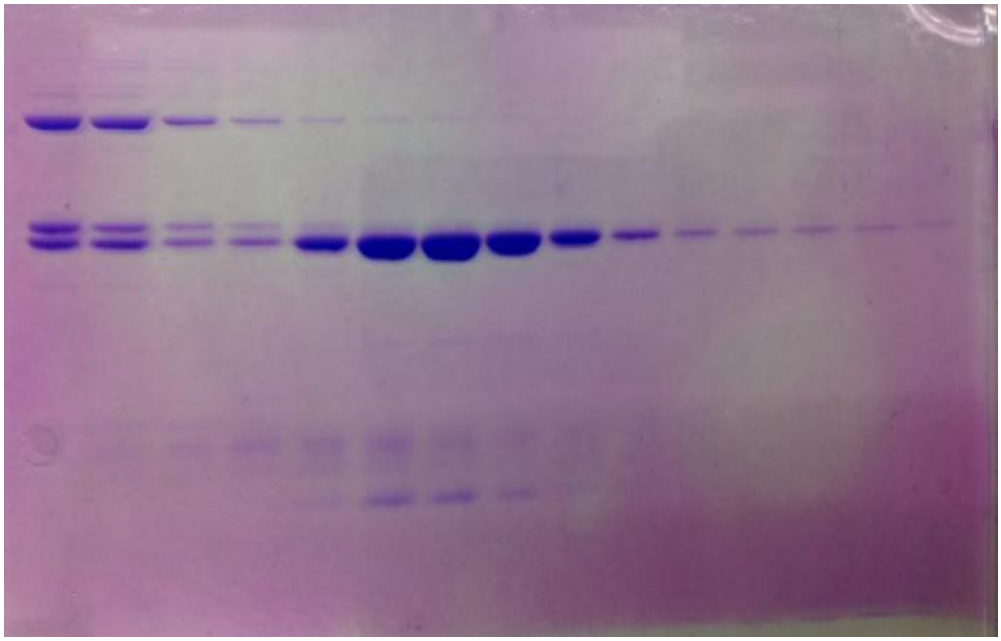

Figure 41. The SDS-PAGE analysis of the consecutive fractions obtained from gel filtration chromatography. (From left to right: fraction 5 to 19.)

("melting") temperature T_m of the protein in different states was measured using the identical pure buffer as a reference. Two chambers containing the protein solution and buffer were slowly heated, and more heat was allowed to flow into the chamber with protein solution as the protein began to unfold, which provided a thermogram of heat flow *vs*. temperature with the T_m as the temperature at the peak. In Figure 42 four resulting thermograms with the T_m of apo (**A**), DCB-3503-bound (**B**), ADP-bound (**C**) and ADP- plus DCB-3503-bound (**D**) states proteins are shown. It is apparent that the T_m of the protein increased dramatically from 47 ℃ to 57 ℃ after the binding of ADP by comparing diagrams **A** and **C**, suggesting the ATPase activity of the isolated Hsc70 NBD. The same trend was observed in diagrams **B** and **D** as well. However, when it came to the comparison of **A** and **B** or **C** and **D**, which indicated the binding pattern of DCB-3503 to the protein, no obvious changes of T_m were observed. Although at the beginning section of the diagram the curves between **A** and **B** or **C** and **D** were slightly different, the binding of DCB-3503 would not affect the T_m of the protein, an indication of a weaker binding, possibly on the surface of the protein. Compared with the already known ADP binding pattern, which was deep into the cleft of the protein, DCB-3503 might only bind to the surface of the protein, making it unable to influence the unfolding process of the protein. What is worth mentioning is that all four protein solutions turned cloudy after the experiment, suggesting the denaturation of this protein is irreversible.

3. Isothermal Titration Calorimetry (ITC) Studies.

The ITC experiment, which is a more direct way to detect the binding of DCB-3503 to Hsc70 NBD, was carried out. In ITC experiments the ligand solution is titrated into the protein solution

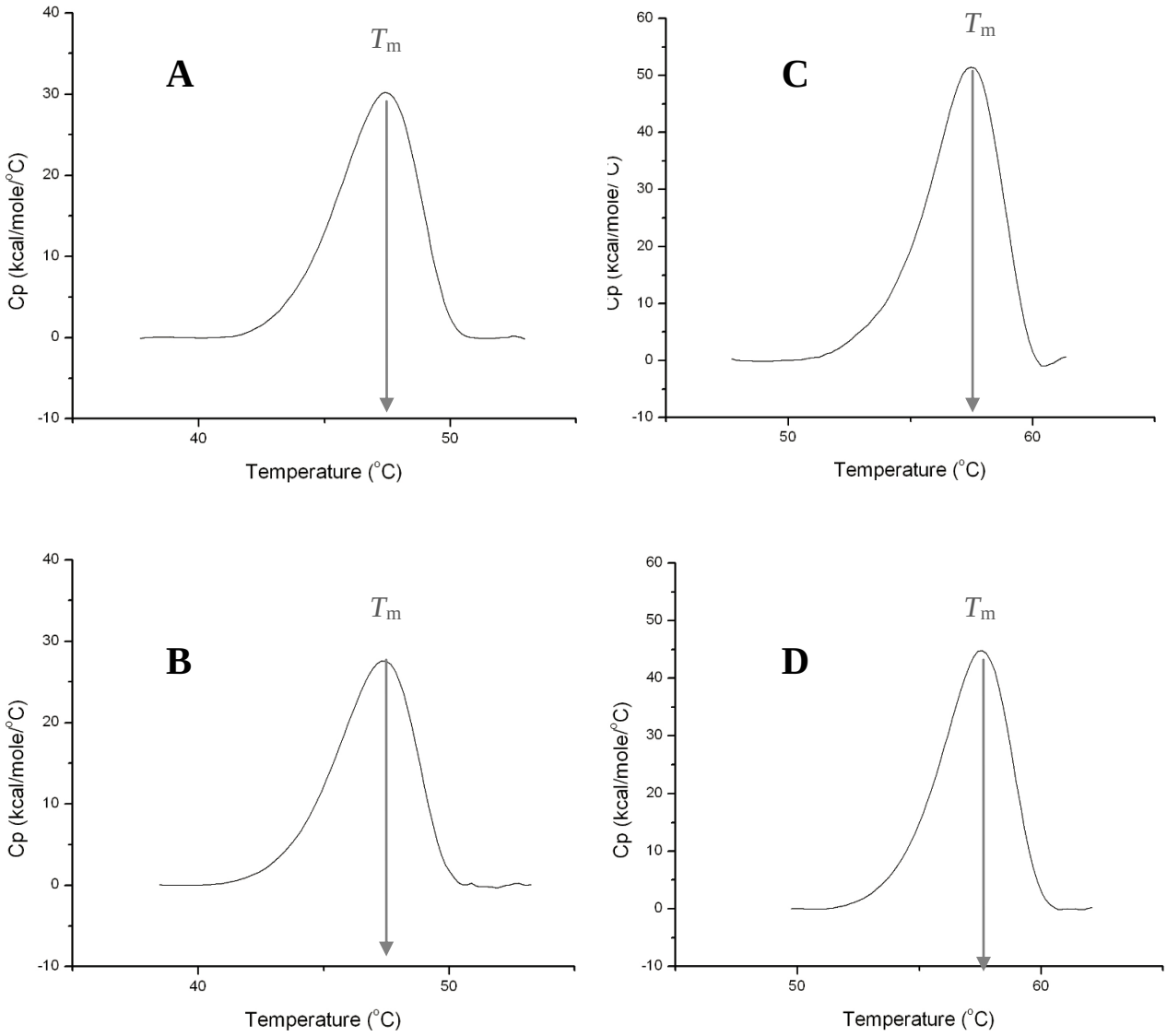

Figure 42. DSC studies of the interactions between ATP, DCB-3503 and Hsc70 NBD. (A: apo; B: DCB-3503 bound; C: ADP bound; D: DCB-3503 and ADP bound.)

sitting in a cell, and the heat generated by the interactions of the ligand and protein is measured in comparison with the reference cell, and the corresponding thermodynamic statistics are derived. Therefore, it was extremely important to keep the buffer components in the ligand solution identical to the ones in the protein solution to avoid unnecessary noise heat.

Due to the poor solubility of DCB-3503 in aqueous media, DMSO was used to dissolve a quantitative amount of ligand by gentle heating, and the DMSO solution was further diluted by addition to aqueous buffer at room temperature. Additionally, the DCB-3503 DMSO stock solution was prepared freshly before the experiments because of the instability of this ligand. Since the final concentration of DMSO (v/v 5%) should be the same in both the ligand solution and the protein solution, DMSO was slowly added into the protein solution to make the final concentration as 5%.

The first attempted group of ITC experiments started with the titration of 250 µM DCB-3503 solution, the concentration of which was estimated to saturate the protein, into a 25 µM apo Hsc70 NBD solution. All the raw ITC data were processed by the NITPIC program. From the ITC data, however, it was obvious that saturation was not reached and no baseline could be drawn to further calculate the thermodynamics. Therefore, a more concentrated DCB-3503 DMSO stock solution was prepared, and the corresponding concentration of the 5% DMSO aqueous DCB-3503 solution was increased to 500 µM. The titration was done on the 25 µM apo protein solution as well. To our surprise the saturation of the titration was still not reached, even with the ligand concentration doubled. Thus new ITC experiments were designed.

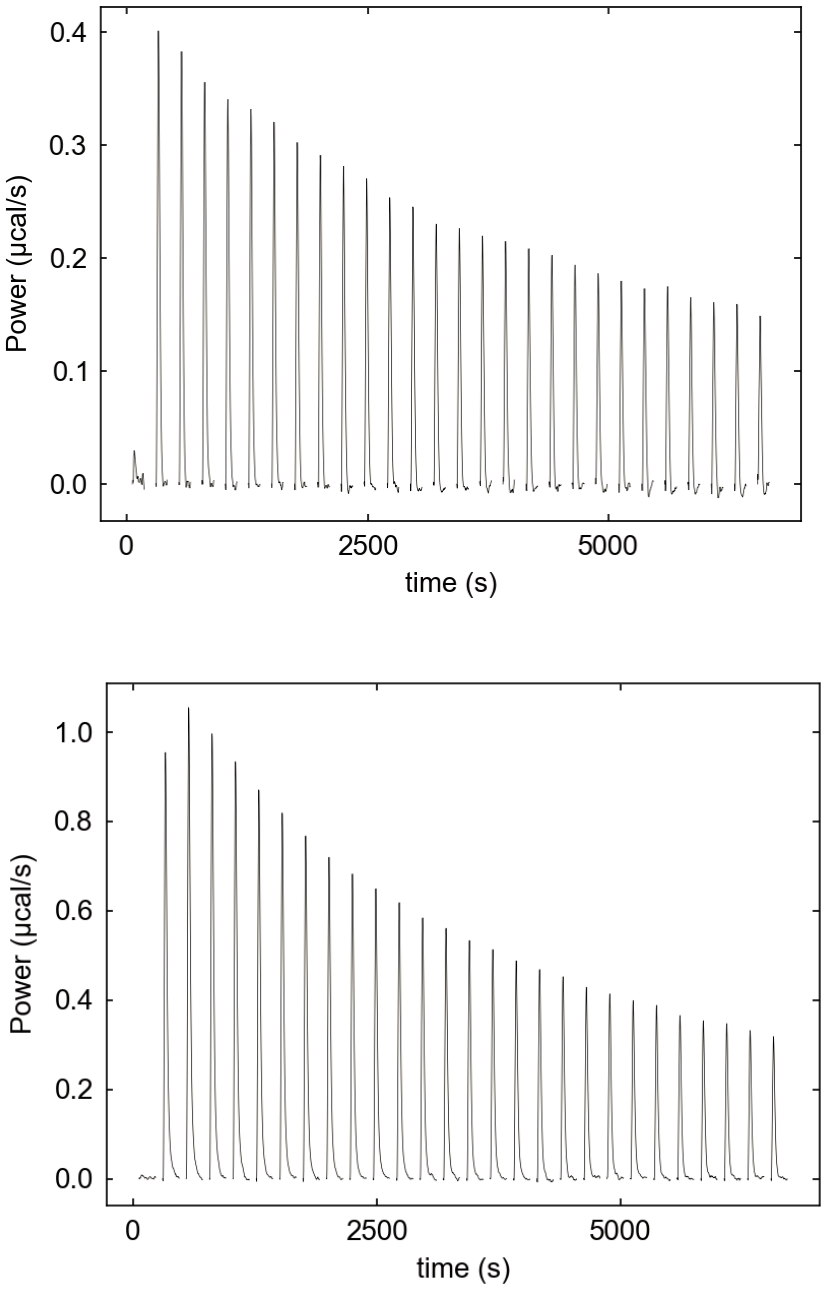

Figure 43. The results obtained from the first group of ITC studies. (Top: titration of 250 µM DCB-3503 into 25 µM apo Hsc70 NBD; Bottom: titration of 500 µM DCB-3503 into 25 µM apo Hsc70 NBD.)

In order to saturate the protein solution, a protein solution with lower concentration than the one used previously was prepared. An experiment of titrating 500 μM DCB-3503 solution into 15 μM apo protein solution was performed. As can be seen in Figure 44 no saturation was reached in the experiment. Thus two more experiments of titrating 500 μM DCB-3503 solution into 7.5 μM apo protein solution and 5 μM apo protein solution respectively were carried out. Surprisingly in neither of the experiments was saturation reached. The suspicion then fell onto the possible heat generated by dilution of DCB-3503 into a larger quantity of water. Then one more experiment was performed to prove the above-mentioned theory, as 500 μM DCB-3503 solution was titrated into pure 5% DMSO buffer without the presence of any protein. As predicted, significant heat signals were observed in the experiment as can be seen in Figure 44. Thus it was concluded due to the highly hydrophobic structure of DCB-3503, although it was diluted into aqueous buffer before titration, it could still bring significant enthalpy change into the system when it was further diluted, which generated huge level noise in the results.

By knowing the cause of the problem, an additional group of experiments were carried out, in which one was the titration of 500 μM DCB-3503 into 5% DMSO buffer and one was the titration of 500 μM ligand into 31 μM apo protein solution with 5% DMSO. It was important to point out that a single batch of DCB-3503 aqueous solution was prepared from one DMSO stock solution freshly prepared, and in both of the experiments the DCB-3503 solution used to titrate the protein was obtained from the above-mentioned single batch in order to eliminate possible differences in the concentration of the ligand between solutions prepared in two batches, which could generate huge errors in the ITC studies. The raw ITC data were processed by the NITPIC and SEDPHAT programs, and a global fit was carried out on both experiments. The injection heat data was obtained by subtracting the reference data from the data obtained with protein

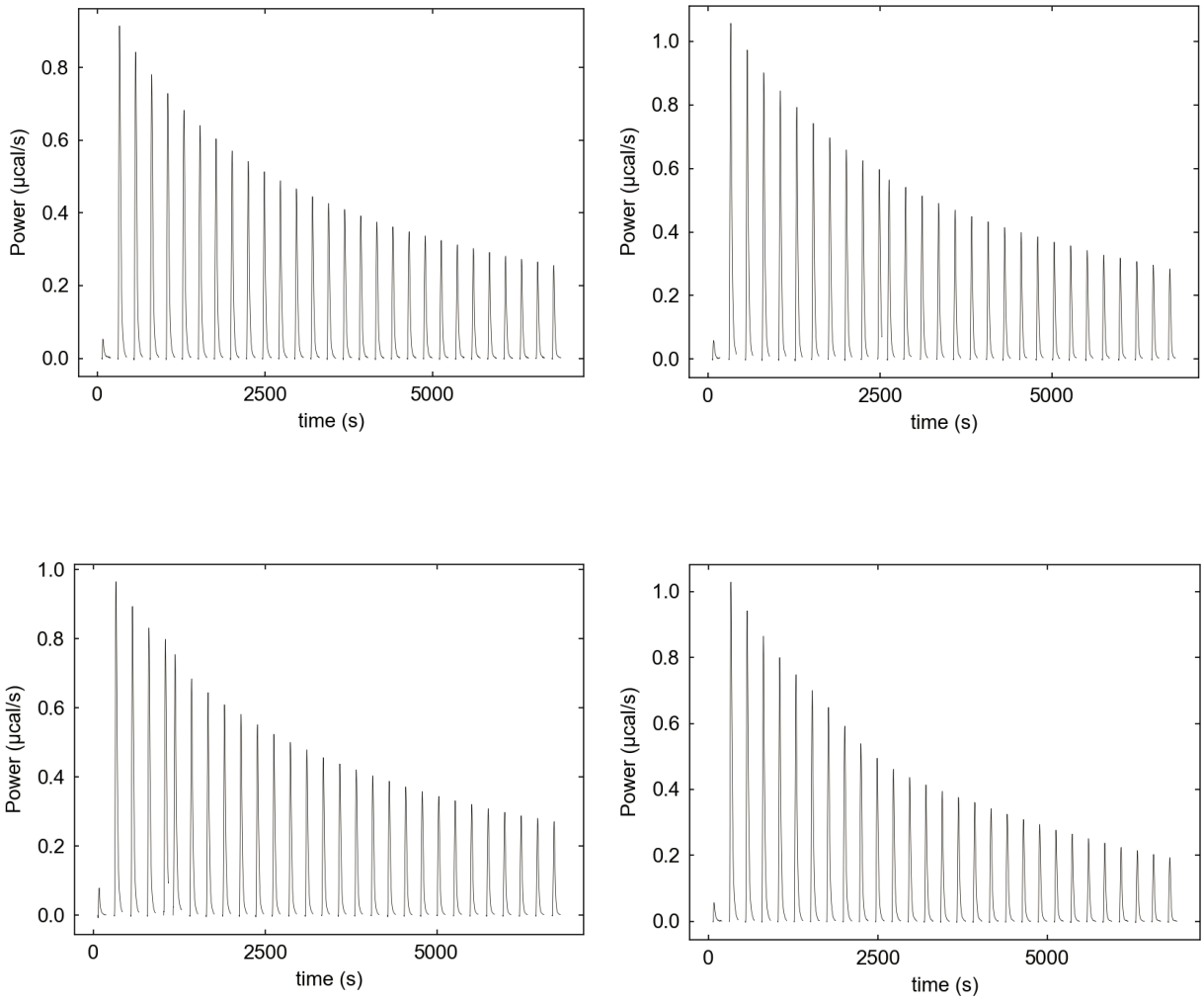

Figure 44. The results obtained from the second group of ITC studies. (Top left: titration of 500 µM DCB-3503 into 15 µM apo Hsc70 NBD; Bottom left: titration of 500 µM DCB-3503 into 7.5 µM apo Hsc70 NBD; Top right: titration of 500 µM DCB-3503 into 5 µM apo Hsc70 NBD; Bottom right: titration of 500 µM DCB-3503 into buffer.)

solution, and the resulting data were plotted as shown in Figure 45. It was apparent that no baseline was able to be reached in this group of experiments; therefore, the corresponding thermodynamics were not obtained. A second group of experiments conducted on ADP-bound protein was also performed, as ADP was added into both reference and actual experiments to a same final concentration of 290 μM. As can be seen in Figure 45, the data from the reference experiment show no considerable differences from those of the reference sample in the apo protein experiment. However, the binding pattern changed significantly when ADP was present, as an endothermic signal increased with the injection to compete with the heat generated by dilution of DCB-3503. It was concluded that a complex binding pattern was obtained when DCB-3503 interacts with the ADP-bound protein, which precludes the calculation of the thermodynamic parameters.

Although problems were present in titration of Hsc70 NBD by DCB-3503, the binding pattern of DCB-3503 to both apo and ADP-bound protein revealed the existence of the binding, and a complicated mechanism is indicated between the macromolecule and the small ligand, especially in the presence of ADP where an endothermic signal played a large role at the end of the titration. The major problems could be illustrated as the following. First of all, because of the poor solubility of DCB-3503, it was not possible to further increase the ligand concentration. Additionally, in order to keep the protein active the concentration of the protein needed to be kept above 22 μM (1 mg/mL). Those facts made the saturation of the titration difficult to achieve, especially in a weak-binding pattern scenario. Secondly, the preliminary ITC results showed an entropy-driven binding instead of an enthalpy-driven one. The lack of abundant H-bond donors and the large aromatic system made the interactions more likely to be hydrophobic in nature rather hydrophilic involving H-bond breaking and formation, which make the process an

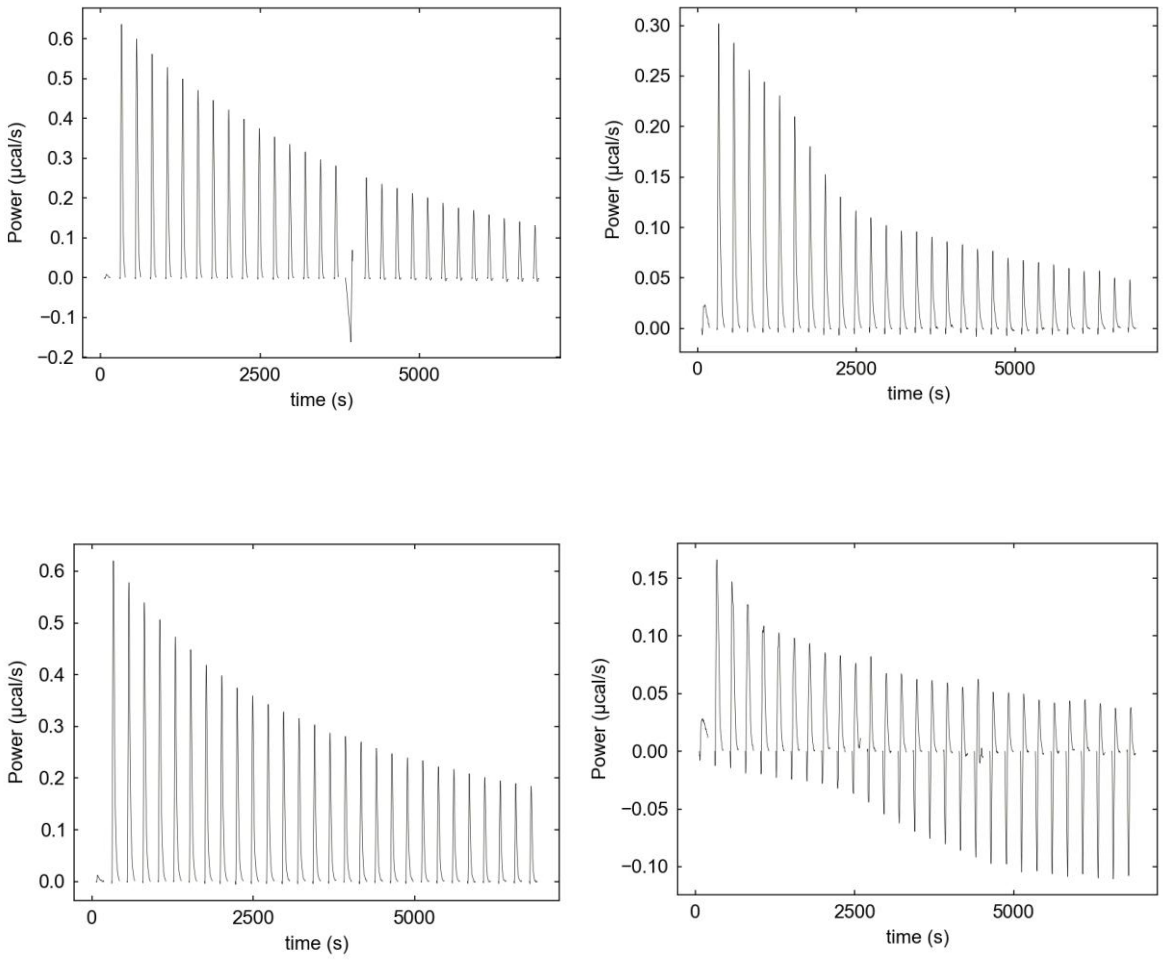

Figure 45. The results obtained from the third group of ITC studies. (Top left: titration of 500 µM DCB-3503 into buffer; Bottom left: titration of 500 µM DCB-3503 into 31 µM apo Hsc70 NBD; Top right: titration of 500 µM DCB-3503 into buffer with ADP; Bottom right: titration of 500 µM DCB-3503 into 31 µM ADP bound Hsc70 NBD.)

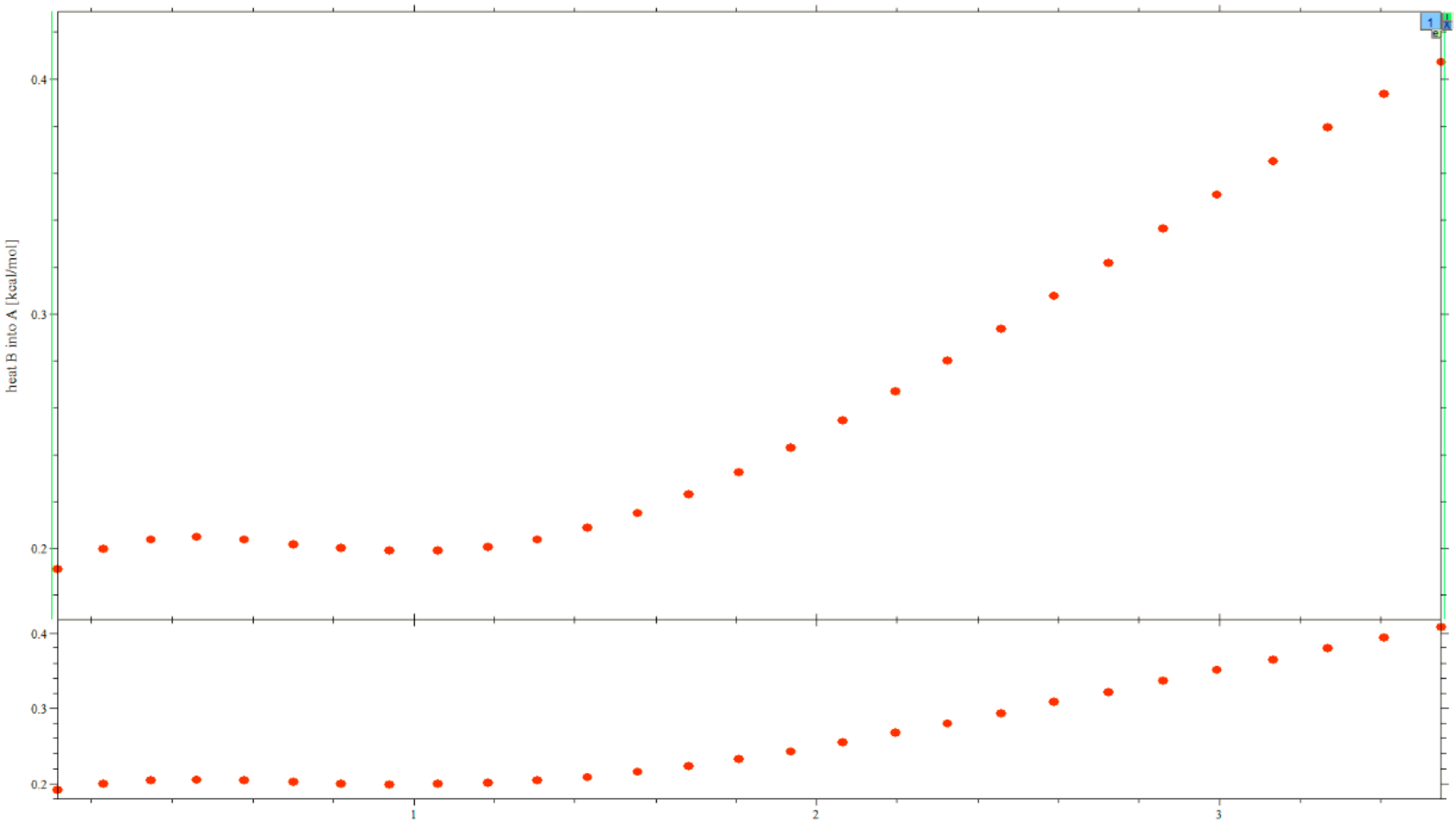

Figure 46. The ITC data plot obtained from the subtraction of apo Hsc70 data (bottom left in Figure 43) from the reference data (top left in Figure 43).

entropy-driven one. Since the heat released and observed in ITC was largely a change in enthalpy, with a high heat of dilution from the ligand as a huge background noise, it was difficult to accurately measure the enthalpy change of the ligand–protein interactions.

4. NMR (^{1}H-^{15}N HSQC) Studies.

Three ^{1}H-^{15}N HSQC experiments were carried out on the ADP-bound Hsc70 NBD in order to best correlate the assignments provided by Dr. Zuiderweg that were obtained on the ADP-bound protein. The results are shown in Figure 47, as the spectrum of the ADP-bound protein (**A**) was firstly collected, then the spectra of the ADP-bound protein with an estimation of 50% (**B**) and 100% (**C**) DCB-3503 saturation were collected after the injection of the corresponding DCB-3503 DMSO solution. To better analyze the results, alignments of spectra **A** and **B**, **A** and **C, B** and **C** and **A**, **B** and **C** were performed. However, no significant changes of the chemical shifts of the peaks were observed. In addition, compared with the ^{1}H-^{15}N NMR assignments of the chemical shifts of Hsc70 provided by Dr. Zuiderweg, a considerable number of peaks were missing in the current spectra. It was considered that these spectra were the ones of soluble dimers of Hsc70 due to the peaks crowding in the center area, and these soluble dimers were believed to be formed during the inevitable concentration step where high pressure was applied to the protein solution obtained from gel filtration chromatography. Although the concentration of the protein measured on spectrophotometer at the absorbance of 280 nM was high enough to obtain a good NMR spectrum, most likely it was the soluble dimer that contributed to the high concentration, leaving not enough monomer in the solution to give an adequate spectrum. However, because of the similar protein preparation procedures and the observed activities in the

Figure 47. ^{1}H-^{15}N HSQC spectra and the corresponding alignments. (I. A; II. B; III. C; IV. A and B; V. A and C; VI. B and C; VII. A, B and C.)

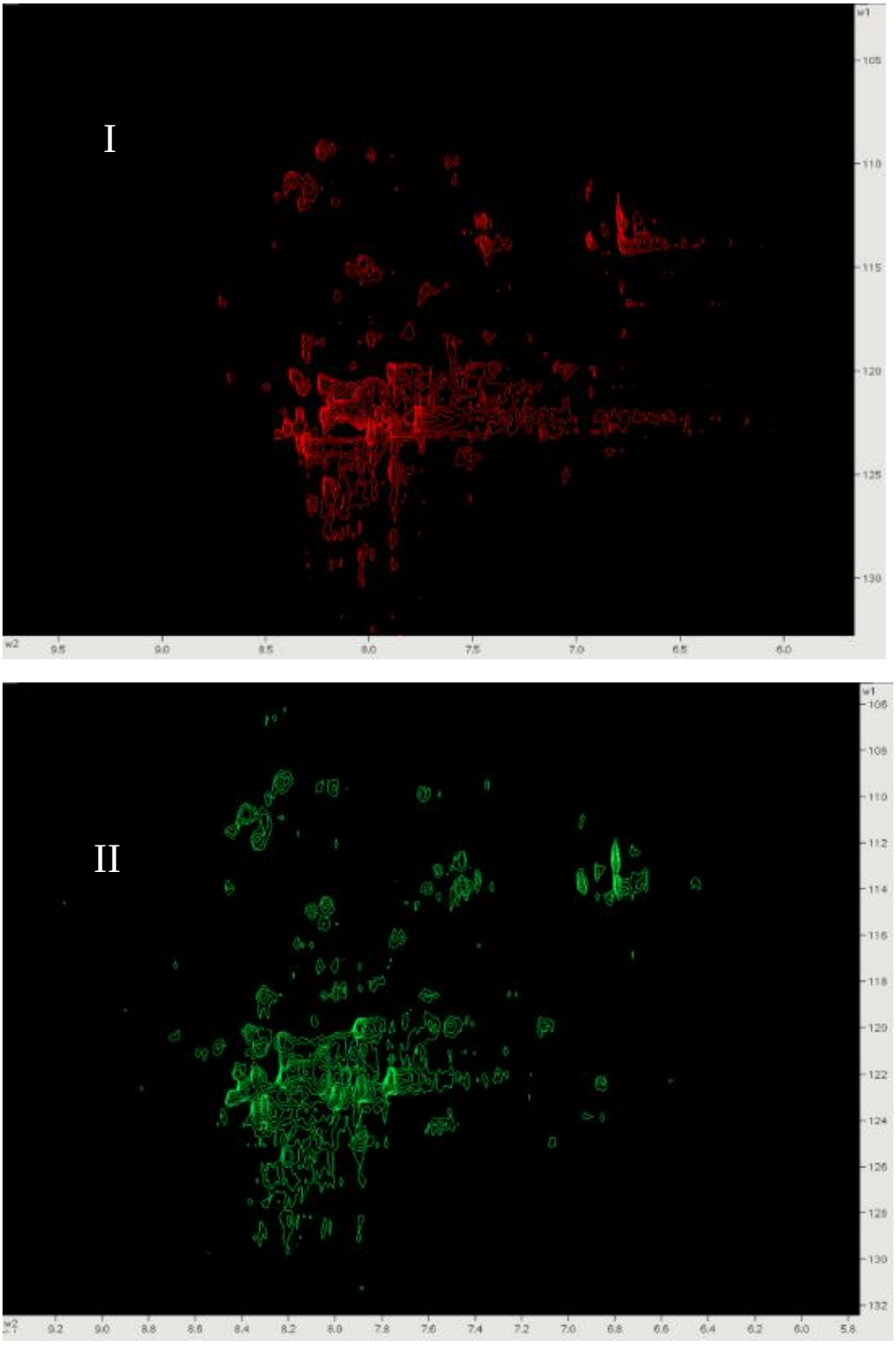

Figure 47. Cont'd.

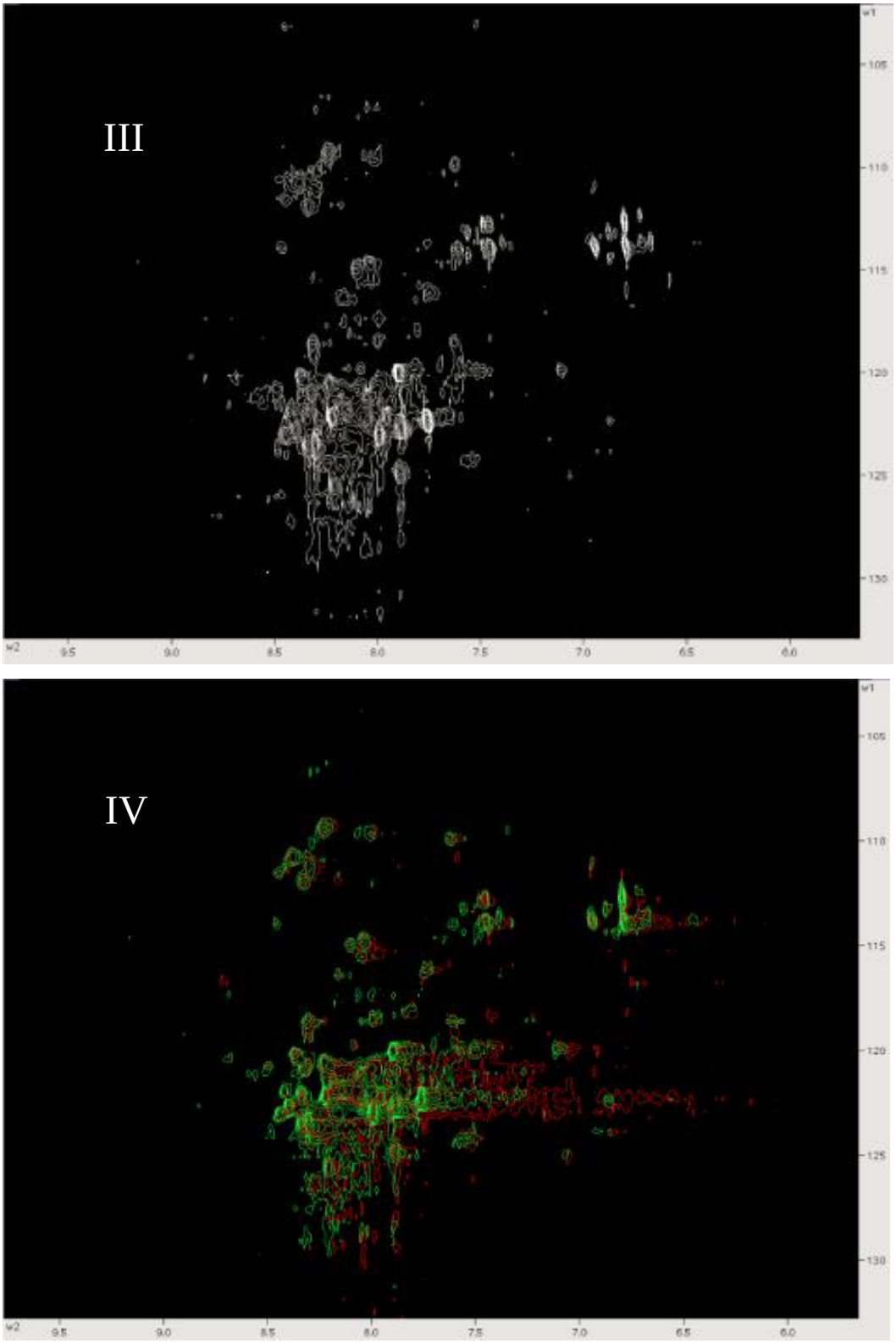

Figure 47. Cont'd.

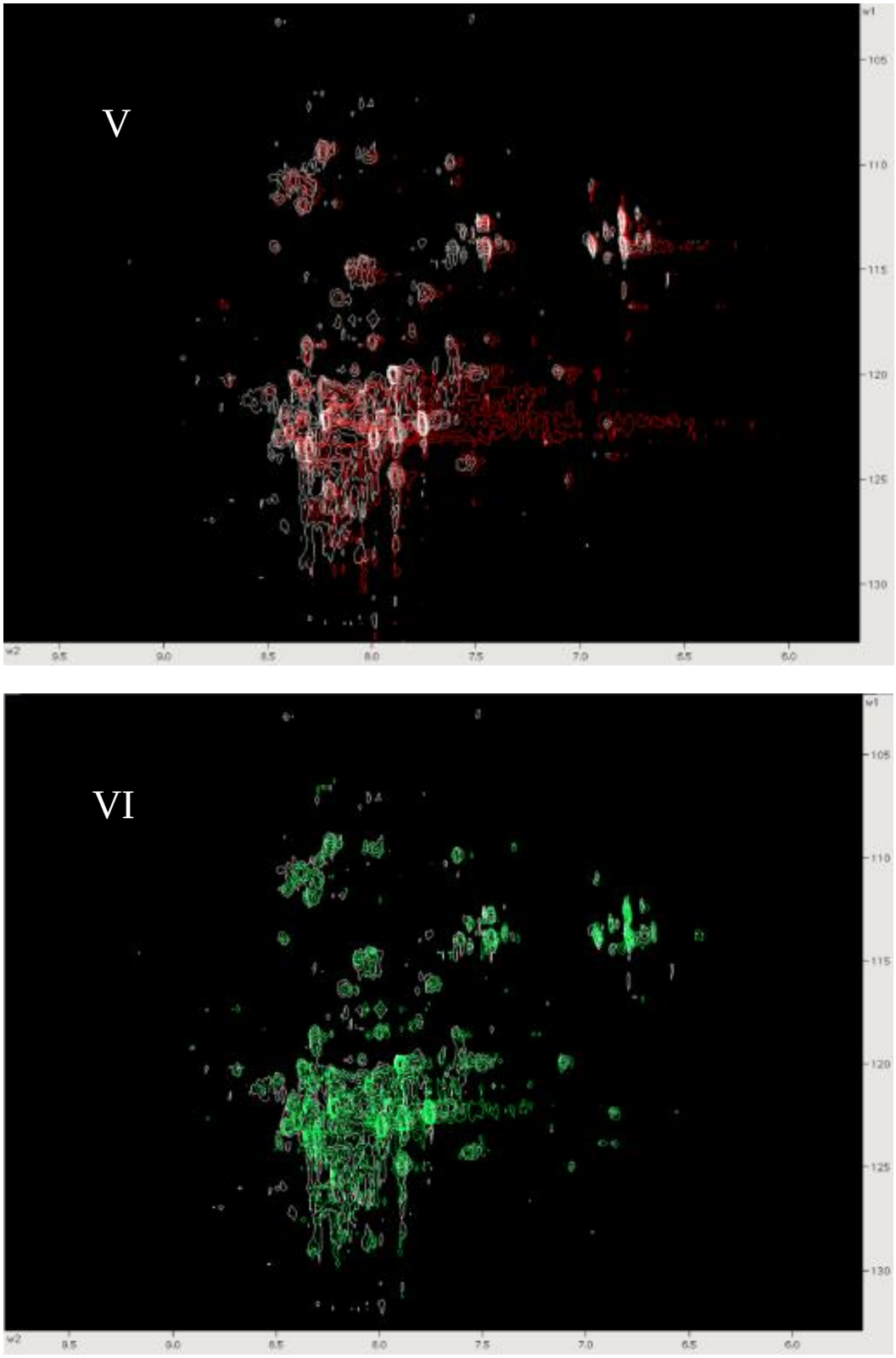

Figure 47. Cont'd.

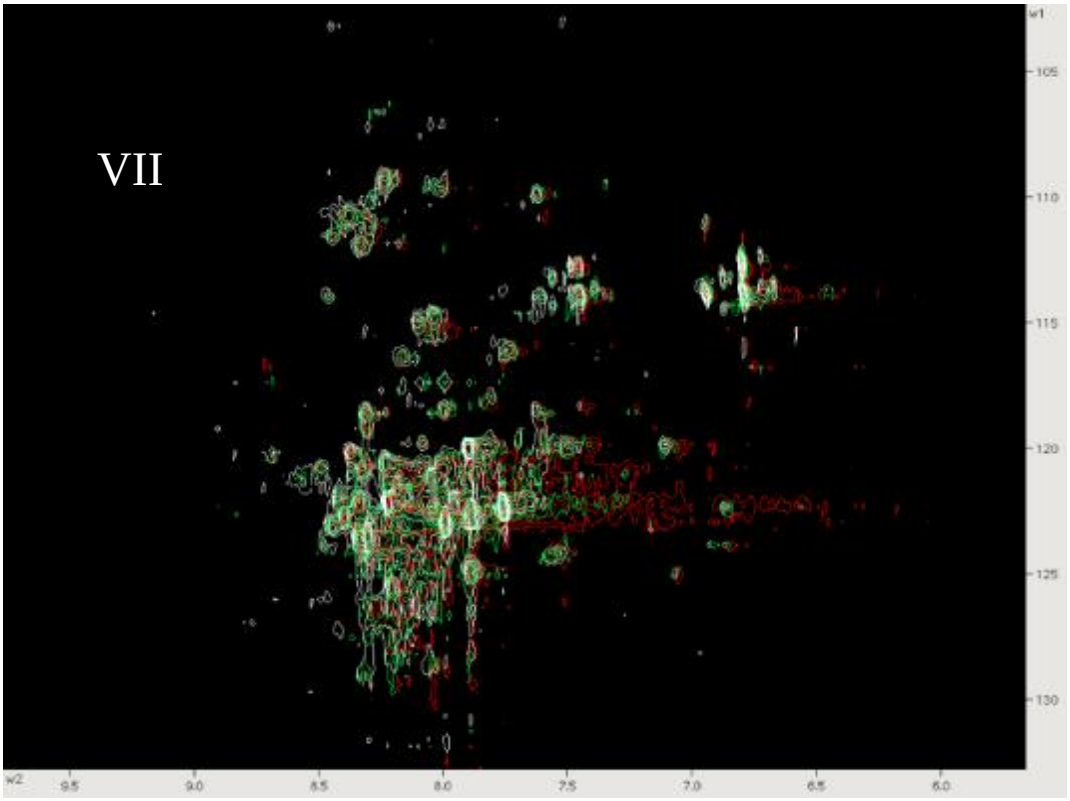

Figure 47. Cont'd.

DSC and ITC experiments, the surface of the monomer where the dimers joined were believed to be a considerable distance away from the ATP or DCB-3503 binding sites.

5. Construction of the Docking Models.

5.1. The Introduction of Docking.

Docking is an important tool designed for structure-based drug design with the purpose of simulating the interactions between a small-to-medium-size molecule (ligand) and a not-too-flexible macromolecular target (receptor), which is usually a protein. It is able to generate different orientations and conformations of the ligand within the binding site of the target molecule to calculate the optimal binding geometries and energies for further optimization of the ligand molecules. In the docking model, several poses of the ligand can be generated, and the score of each will be calculated as a free energy of binding. The docking model in our study was built in a MOE 2012.10 environment. A reliable docking model can be built when the ligand has limited flexibility (up to 10 rotatable bonds) and the active binding site is allowed to move (side chains can be flexible, while the backbone is always fixed).[64]

Unfortunately, in our study not enough experimental information was obtained to elucidate the specific binding site of DCB-3503 to Hsc70 NBD; therefore Site Finder was utilized to identify the potential binding site. Site Finder is a program devised to calculate the possible active binding site in a receptor from the 3D atomic coordinates of the receptor. It is a geometric method to identify the potential binding site with a work flow shown as follows: 1. Identify the tight atomic packing regions as potential sites and exclude the ones “too exposed” to solvent; 2. Classify the sites as hydrophobic and hydrophilic; 3. Calculate and eliminate the inappropriate

alpha spheres, which are the associated spheres generated by the collection of four points produced by the triangulation of the 3D points in the selected sites; 4. Classify the alpha spheres as hydrophobic and hydrophilic followed by the corresponding clustering to produce the sites; 5. Rank these sites by the amino acid composition of the pocket.[64]

5.2. The Docking Model Constructed with ATP.

Before the construction of the model, the ligand and protein need to be properly prepared. The ligand DCB-3503 was built by Molecule Builder in MOE 2012.10, and the corresponding energy was minimized by the MMFF94x force field. The X-ray crystal structure of Hsc70 NBD was obtained from the Protein Data Bank (PDB) with the code of 1NGE. The protein was then prepared in MOE via protein structure preparation tools (Structure Preparation, Protonate 3D and LigX). The purpose of preparing the 3D protein structure is to fix the missing or poorly resolved atomic data. Prior to the preparation of the protein structure, all the water molecules and other solvent molecules were deleted.

In the previous study conducted in Dr. Cheng's lab the conclusion was made that DCB-3503 was able to stimulate the hydrolysis of ATP in Hsc70 NBD; therefore, a docking model that includes the ATP molecule at the ATPase site was firstly constructed. The ATP was retained and prepared together with the protein molecule, and the Site Finder was utilized to detect the potential binding site of Hsc70 NBD in the presence of the ATP molecule. In Figure 48 the most potential binding site [with the largest size and highest propensity for ligand binding (PLB) score as 3.56] is shown as highlighted in the alpha sphere centers and pocket surface, respectively. The alpha sphere centers depiction is viewed from the front of the protein, while the pocket surface one is viewed from the side of the protein rotated 45° counterclockwise from the front view. In

these two figures, the red spheres or surface indicated hydrophilic atoms, and the white ones suggested hydrophobic atoms. Additionally, the ATP molecule is highlighted in light purple in the figures. It is obvious that the most potential site was at the "entrance" of the protein cleft, whereas the ATPase active site is at the end of the cavity. Meanwhile, the existence of a large hydrophobic area indicates the possibility of binding of DCB-3503, which has a significant amount of hydrophobic surface. It is worth noting that except for this site of highest potential and a site ranking the second with a PLB score at 2.19, all the rest of the sites calculated by the program had negative PLB scores, suggesting that these are not potential binding sites. Although the second best site had a positive PLB score, due to its significantly smaller size of 83 (in receptor atoms) compared with a size of 209 of the first site, the considerable quantity of hydrophilic surface and the proximity to the ATPase active site residing the D206S mutation, where DCB-3503 is not supposed to bind to according to the corresponding studies in Dr. Cheng's lab, it was not considered as a potential binding site.

With the potential binding site calculated, the docking with DCB-3503 was carried out. There were 26 poses selected by the program as potential binding poses, with the final docking scores ranking from -7.7315 to -5.0414 kcal/mol. The more negative the score, the more favorable the pose is considered to be. Even though the score plays an important role in the evaluation of the poses, whether or not the pose is able to explain the experimental observation is also a vital aspect to take into consideration. After carefully examining all the poses based on the criteria mentioned above, the pose with the second lowest score was considered to be the most reasonable one based on a number of considerations. The most important point in selecting a reasonable pose is to ensure the exposure of the 3-methoxy group of DCB-3503 on the protein surface, as a biotinylated-tethered DCB-3503 molecule with a biotin linker modified from

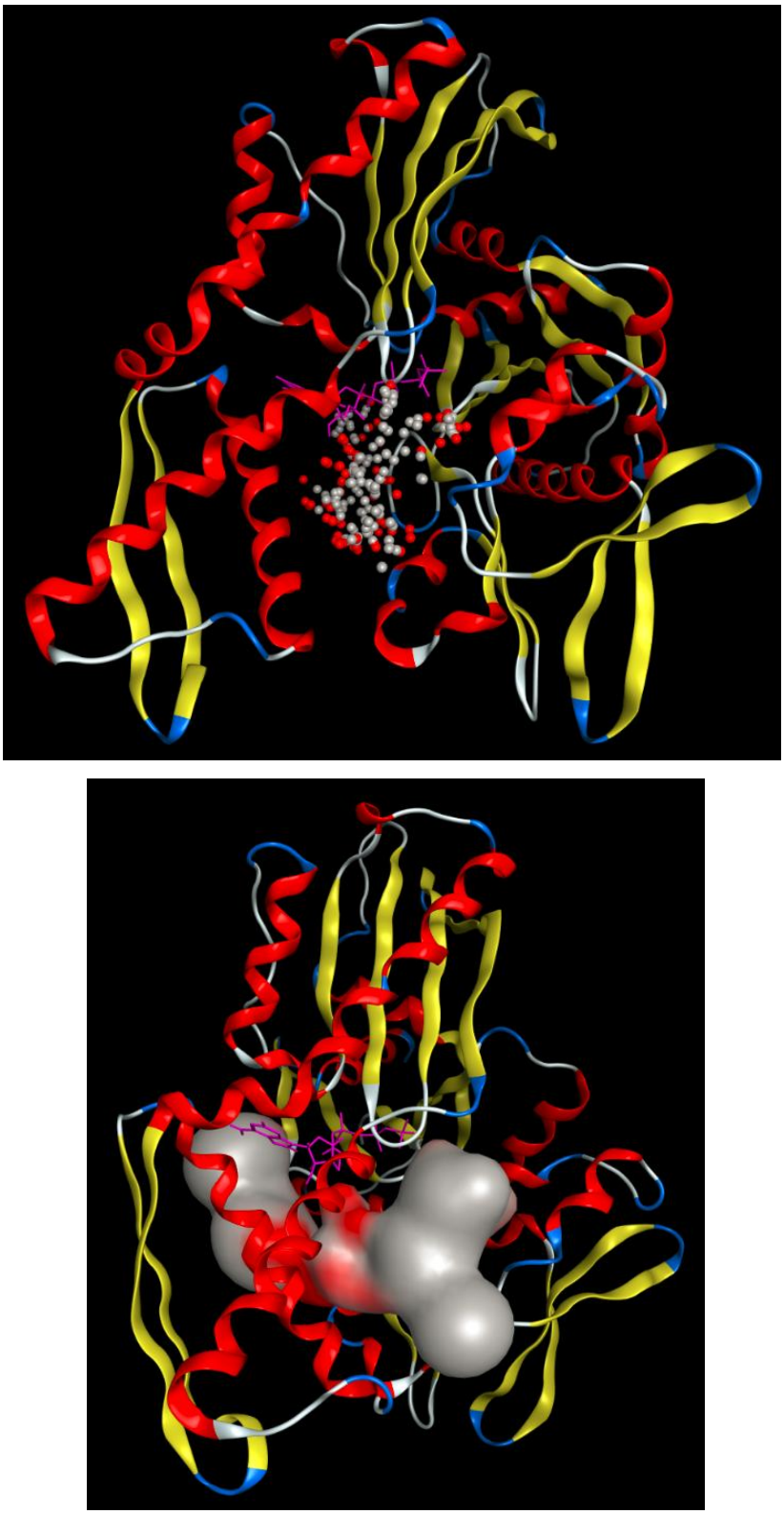

Figure 48. The binding site of greatest potential of apo Hsc70 NBD identified by Site Finder. (Top alpha sphere center view; Bottom: pocket surface view.)

a 3-methoxy group buried deep into the protein would not be able to "fish" the Hsc70 out from the cell lysate. Although the best pose given by the program had a score of -7.7315 compared with the second one as -7.3548, the second pose was to be considered the one of greatest potential. Most of the poses ranking after the second one had their 3-methoxy groups buried into the protein. The overall views of the docking pose without and with the detailed binding pocket are shown in Figures 49 and 50, where the ATP molecule is in light purple. In Figure 49 the overall binding is shown as the front view and the top view, respectively. It is clear that the binding appears at the "entrance" of the ATPase active site cleft, where ATP is on the back top side of DCB-3503. The overall view of the binding results with the amino acid residues constituting of the binding pocket visible is shown here as well, as DCB-3503 is colored light blue, and the nonpolar hydrogens on the protein are hidden.

Two enlarged views of the binding are displayed as well. In the first view in Figure 51, the detailed interactions (H-bonding, hydrophobic) between DCB-3503 and the residues in the pocket could be observed. A weak arene-H interaction between Arg264 and the B aromatic ring, and two H-bonds including the one between the 14-hydroxyl group and Glu231 with a distance of 3.08 Å, and the one between the nitrogen and Arg264 with a distance of 3.35 Å were generated. Although the 3-methoxy group was close to the surface generated by His87 in the second figure showing the surface interactions, the C–O bond could be rotated to avoid the collision, while the linker attached to the 3-position could still be exposed. All the above information, including the exposure of the 3-methoxy group, could be obtained from the 2D ligand interactions analysis as well except for the arene-H interaction, which is too weak to show.

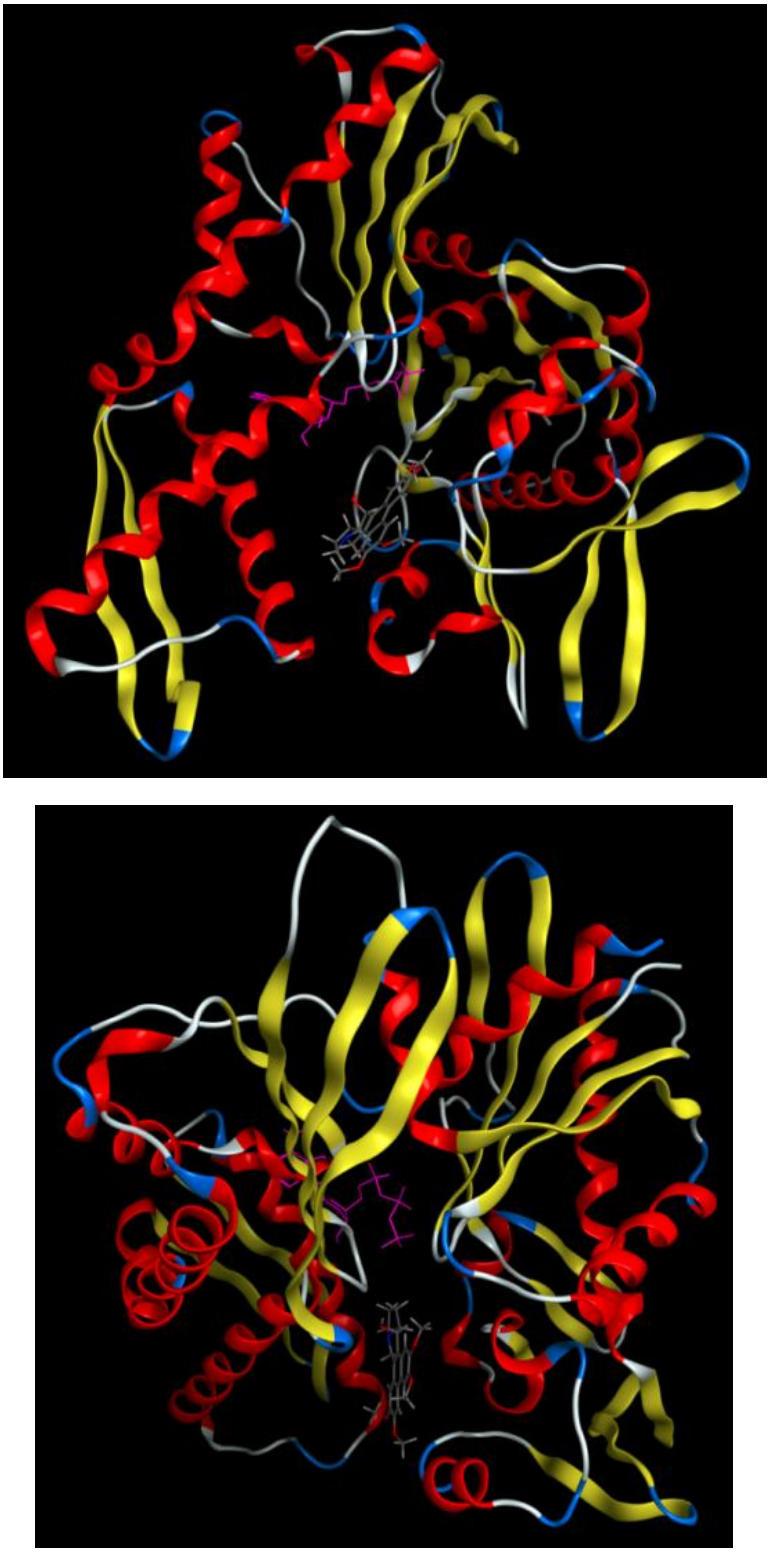

Figure 49. The overall views of the docking pose of greatest potential of DCB-3503 with ATP in light purple. (Top: front view; Bottom: top view.)

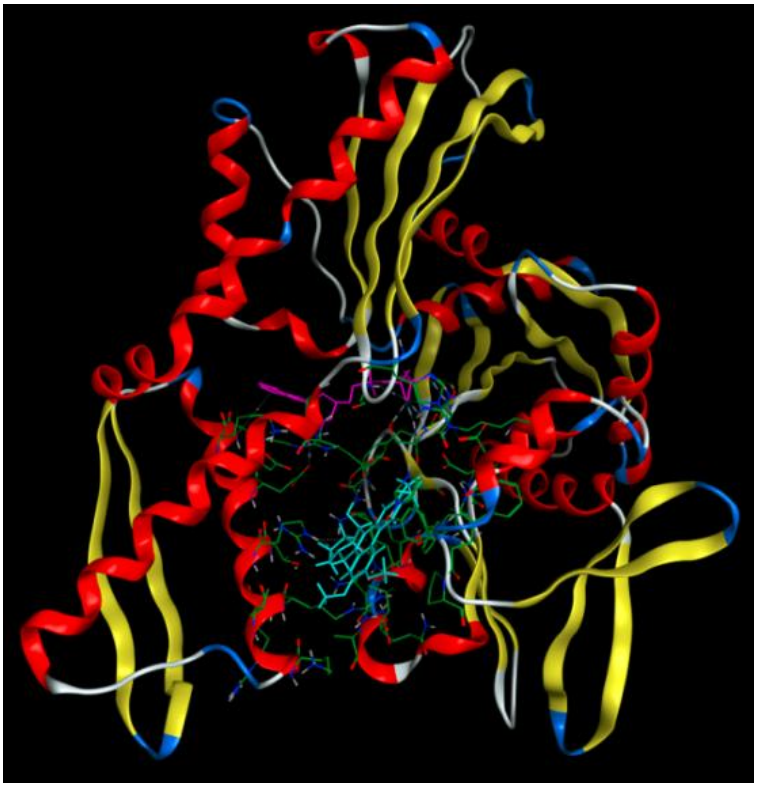

Figure 50. The overall view of the docking pose of greatest potential of DCB-3503 (in light blue) with ATP (in light purple) in the detailed binding pocket.

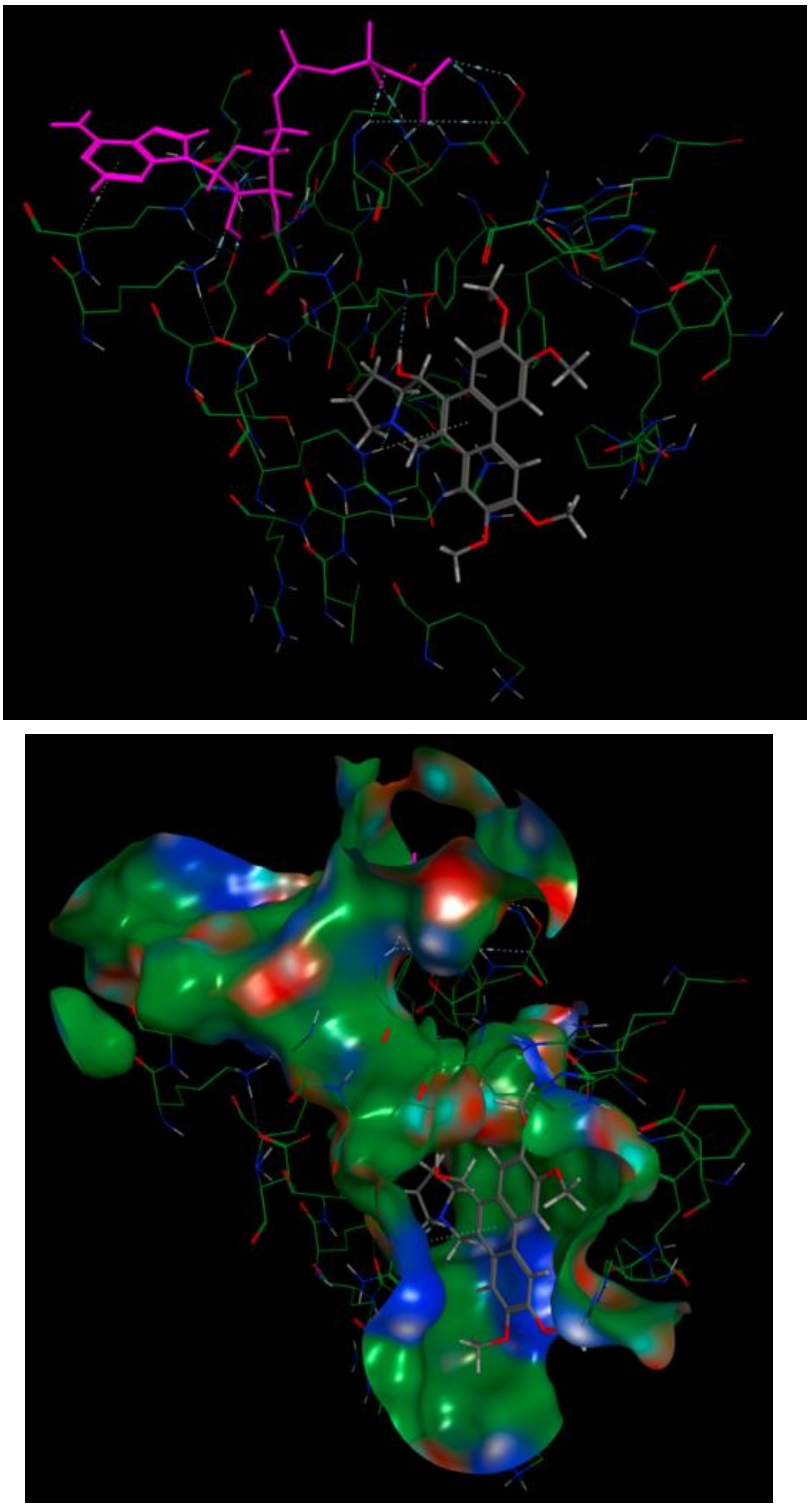

Figure 51. The detailed view of the interactions between DCB-3503 and the binding pocket of Hsc70 NBD. (Top: regular view of the detailed interactions; Bottom: surface view of the detailed interactions.)

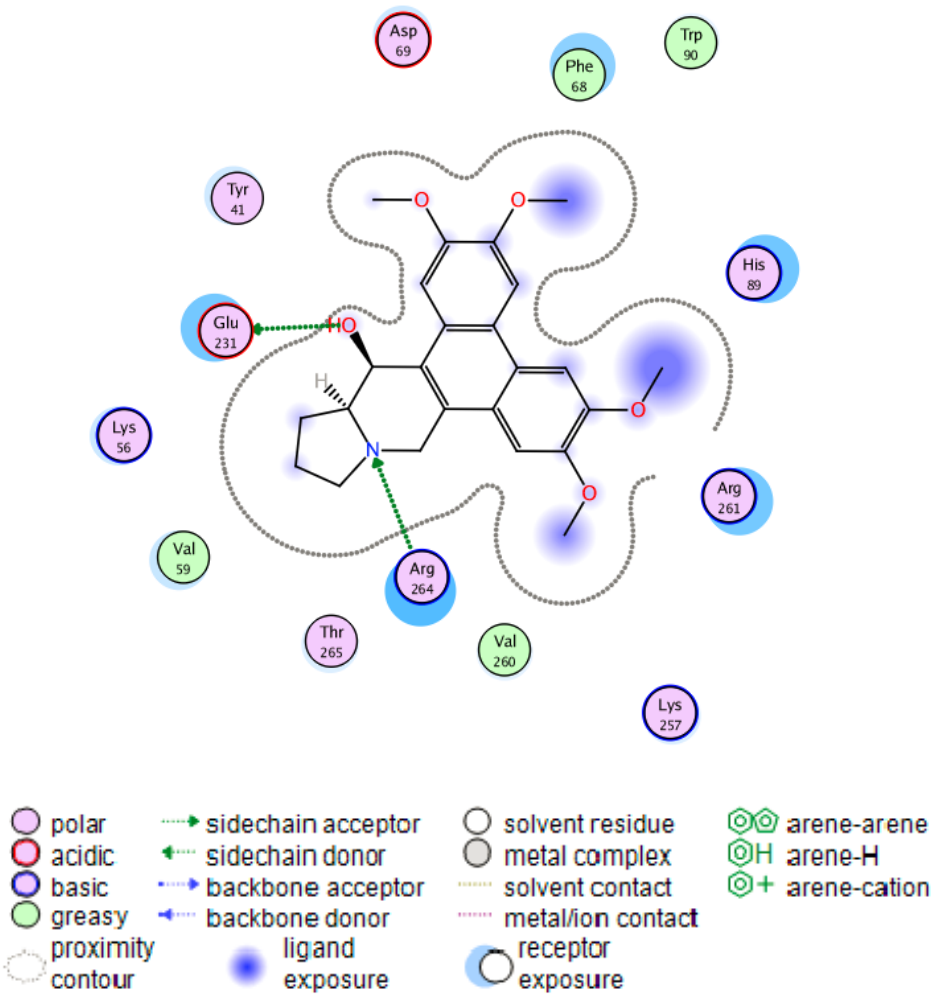

Figure 52. The 2D view of the interactions between DCB-3503 and the binding pocket of Hsc70 NBD with the legend shown below.

The docking pose could also explain some of our experimental observations. The most important question remaining is how DCB-3503 stimulates the ATP hydrolysis via binding to Hsc70 at a site other than ATPase active site. Further studies of the docking model were carried out through the overlapping of the DCB-3503-ATP-binding pocket complex with the originally prepared ATP-protein before docking. By aligning the docking results with the original protein, it was expected to observe the position changes brought by DCB-3503 onto Hsc70 and ATP. In the overall view the backbone carbons of the original protein are shown in grey with the corresponding ATP as light purple, and the carbons in the pocket resulting from docking are colored as green with the related ATP as light blue. It is apparent that considerable shifts are observed on both the amino acid residues and the ATP molecule, and by carefully examining the details, it is found that several new H-bonding and hydrophobic interactions are created and several old ones are eliminated. A clearer comparison is displayed in Figure 54 by 2D ligand interactions analysis, and it is obvious that more interactions are generated between the triphosphates and the residues constituted of the ATPase active site. Thus a model is proposed as the following: due to the binding of DCB-3503 at the "entrance" of the cleft, the positions of the corresponding residues are shifted, which results in allosteric position changes of the ATPase active site residues and the ATP molecule, and as a result more interactions are built around the triposphates moiety, which ultimately serve to accelerate the ATP hydrolysis. A similar allosteric mechanism has been proposed before, as the binding of the ligand at the entrance of the ATPase cleft of DnaK NBD far from the active site led to the disruption of the interaction between DnaJ and DnaK.[63]

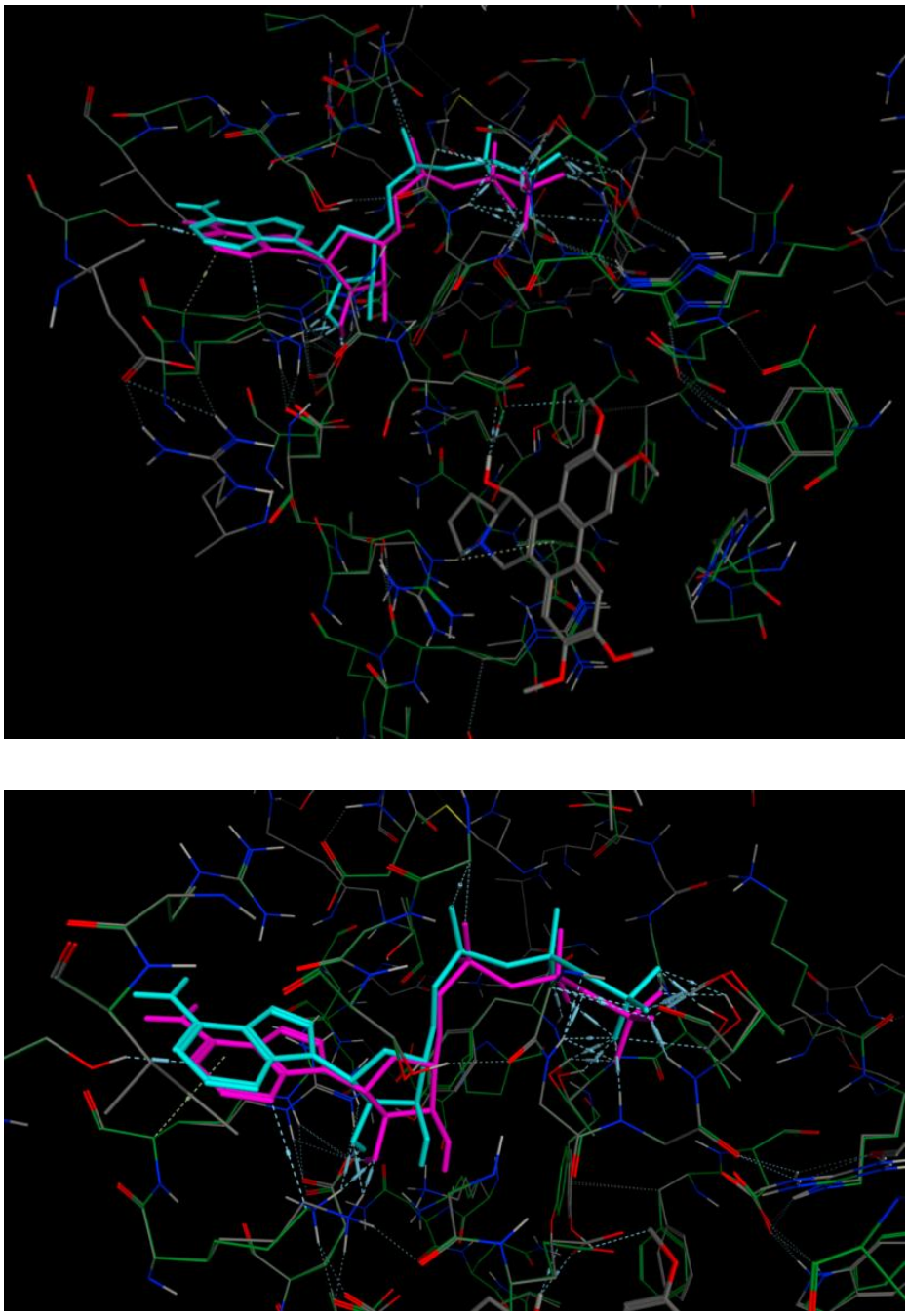

Figure 53. The overall and detailed views of the alignment of the ATP-binding pocket after docking with the one before docking. (The pocket with the green backbone carbons and light blue ATP resulted from docking; the one with the grey backbone carbons and light purple ATP belongs to the original one.)

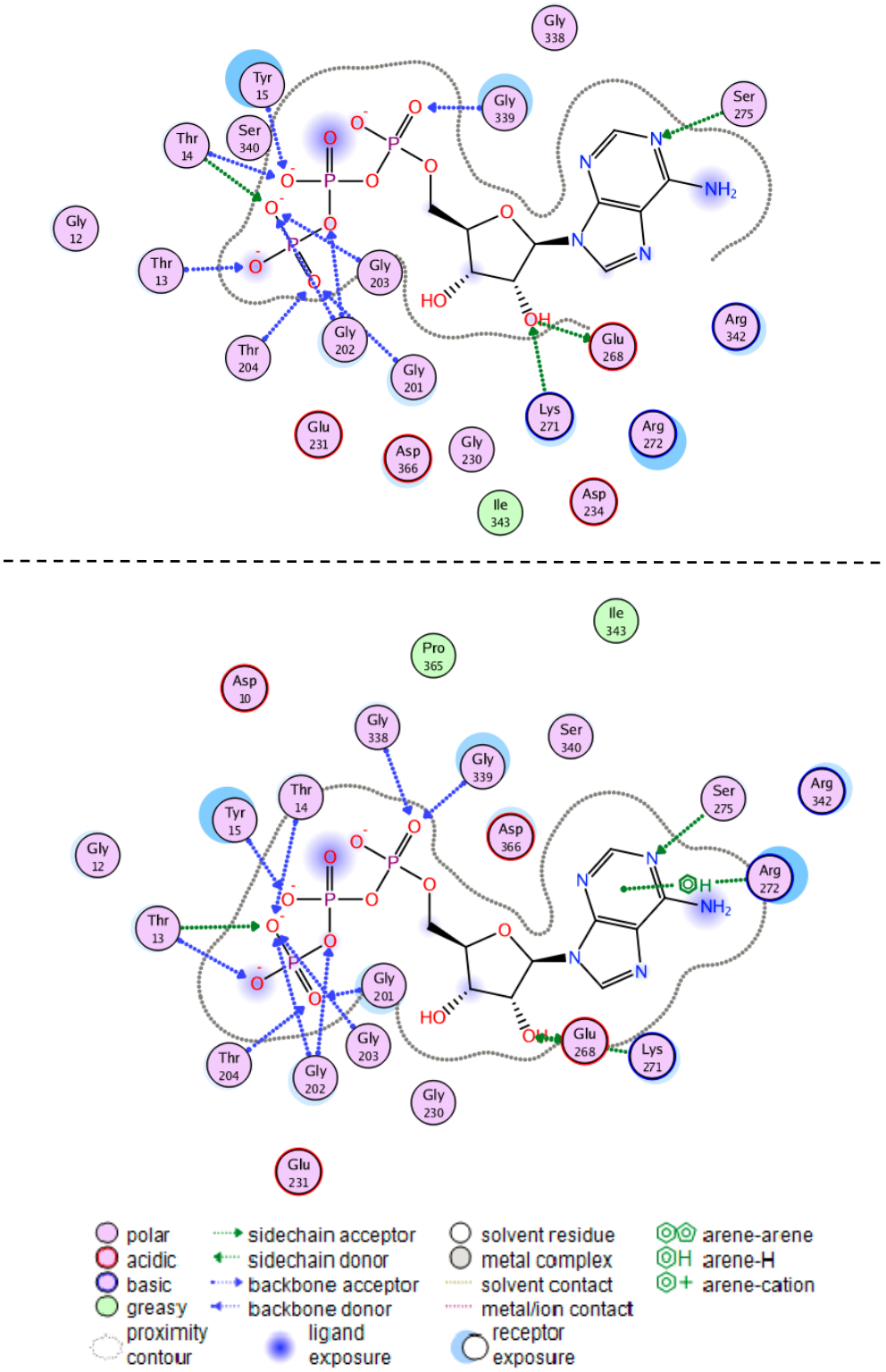

Figure 54. The 2D views of the interactions between ATP and the binding pocket. (Top: before docking; Bottom: after docking.)

Several experimental observations could also be explained by the proposed model. In the ITC experiment, after the binding of DCB-3503 to the protein in the presence of ADP, a secondary event was observed primarily due to the construction of the new interactions between the ADP molecule and the protein. Under the assumption that the same binding site and pattern were obtained without the presence of ATP or ADP, it was not a surprise that the heat generated in the apo state ITC experiment is not significantly large as only weak binding is present due to the small number of H-bonds being constructed. Additionally its weak binding nature and its exposure on the surface of the protein explains the inability of DCB-3503 to alter the melting point of the protein in the DSC study.

In addition, the blockage at the entrance of the cleft that is considerably distant from the ATPase active site from the results of the D206S mutation study mentioned in the introduction. It is therefore not impossible to elute the protein bound to the biotin matrix by a high concentration of ATP as observed in Dr. Cheng's lab, as large number of ATP molecules would overcrowd the cleft or alter the conformation of the protein that serves to break up the DCB-3503–protein complex. Meanwhile the two H-bonds once again emphasized the importance of the stereochemistry of the HO- at 14-position and the nitrogen in the tertiary amino group.

5.3. The Docking Model Constructed without ATP.

Based on the previous conclusion that DCB-3503 derived its activity by stimulating ATP hydrolysis, it was reasonable to construct the docking model with the protein with ATP already bound. However, a docking model without ATP at the active site was also built to better compare the two states.

Similar procedures and the same protein structure from the first model were utilized for building the new model; however, before the preparation of the protein, the ATP molecule was deleted together with water molecules. Site Finder was applied to locate the potential binding site, and the site of greatest potential was identified as shown in Figure 55 with a PLB score of 4.29 and a size of 399. By making careful observations it was found this large binding site was actually the combination of the ATPase active site and the potential DCB-3503 binding site identified in the previous model. Since the occupation of the ATP in the previous model, the site below the ATPase active site was identified instead of the whole larger binding site.

A docking model was attempted at the large binding site, and the general view of the pose of DCB-3503 (in light blue) with the best score (-8.3457 kcal/mol) is shown in Figure 56. It is not surprising to find the overlapping of the adenine moiety of ATP (in light purple) and DCB-3503 when the protein obtained after docking was aligned with the original protein with the ATP molecule included. The docking details are shown in Figure 56 on the right and in Figure 57 in a regular view and two surface views, respectively. It was obvious that DCB-3503 preferably bound to the most hydrophobic site on the protein, i.e., the cavity where the adenine of ATP resided, over the site identified in the previous model, as both of DCB-3503 and adenine possess abundant aromatic systems. It is unlikely for DCB-3503 to bind to the adenine binding site if ATP was already in place; likewise, it was impossible for ATP to bind to the ATPase active site when DCB-3503 already occupied the hydrophobic pocket within such a narrow space. Although this hydrophobic binding site is far away from the D206S mutant in the ATP hydrolysis site, in consideration of the non-competitive mechanism of DCB-3503, this site was not regarded as the possible binding site of DCB-3503. However, the possibility should not be excluded that DCB-3503 would function as an inhibitor to apo Hsc70 NBD according to the above analysis, and the

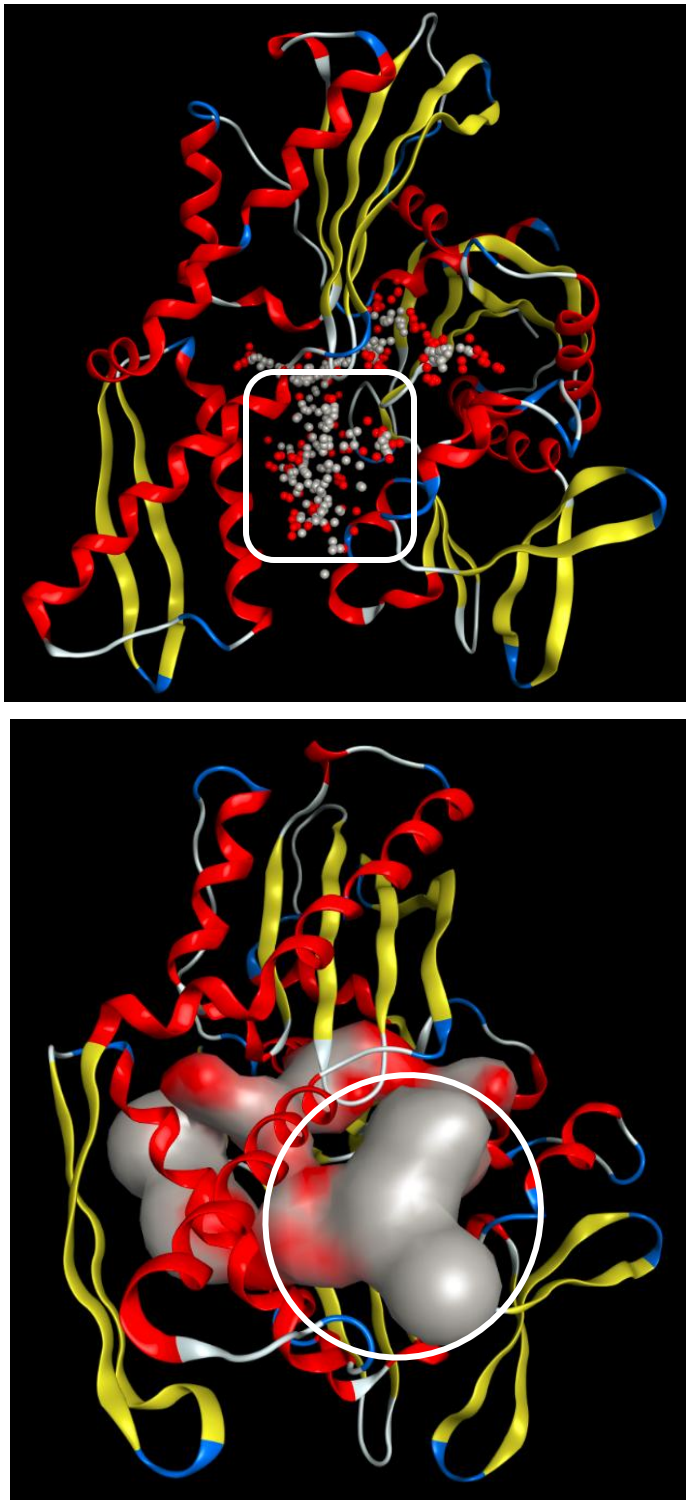

Figure 55. The binding site of greatest potential of Hsc70 NBD in the presence of ATP identified by Site Finder. (Left: alpha sphere center view; Right: pocket surface view. The site within the white circles is the potential site identified in the previous model.)

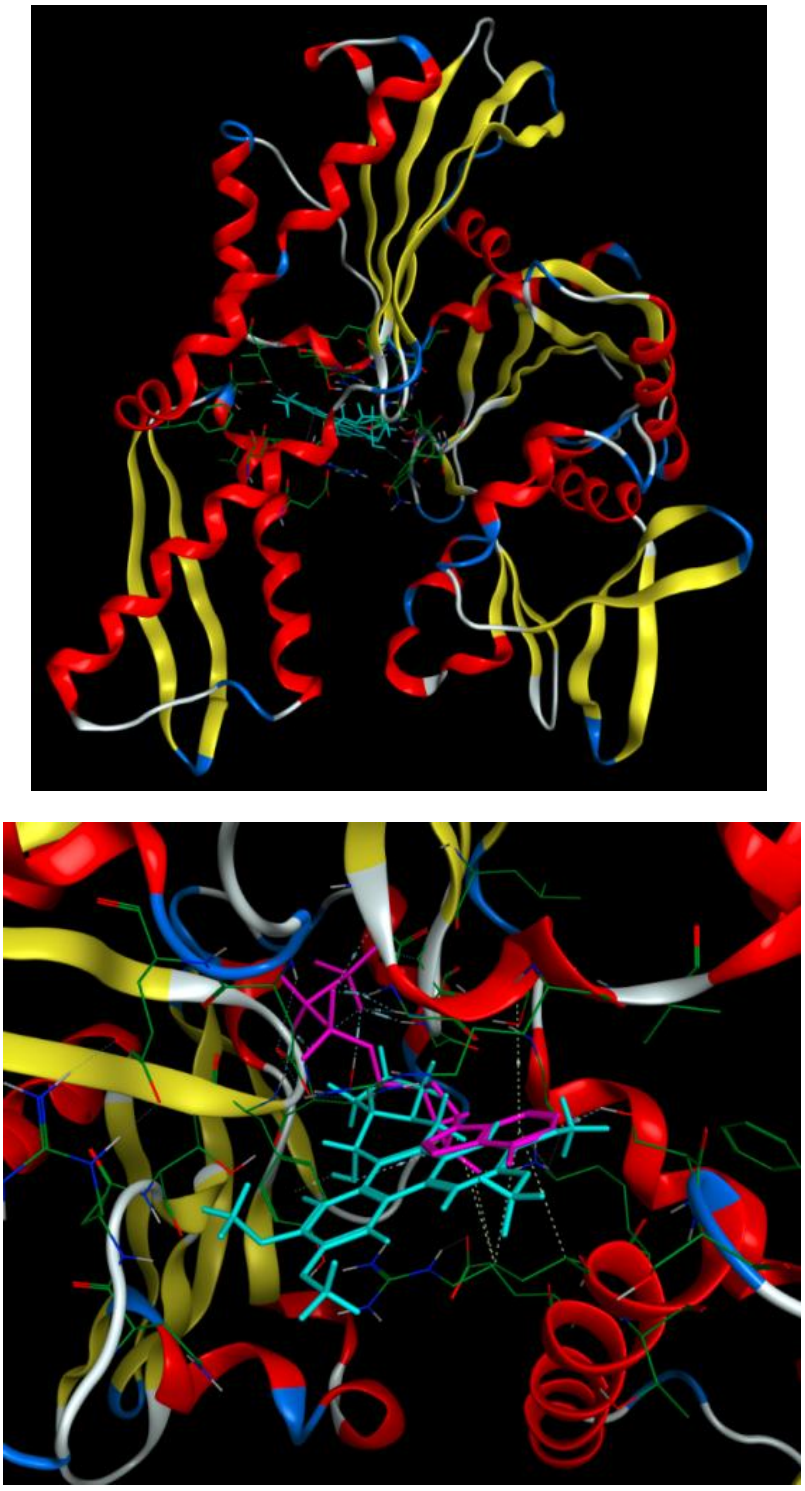

Figure 56. The general (top) and detailed (bottom) views of the binding pose of greatest potential for DCB-3503 with ADP-bound Hsc70 NBD.

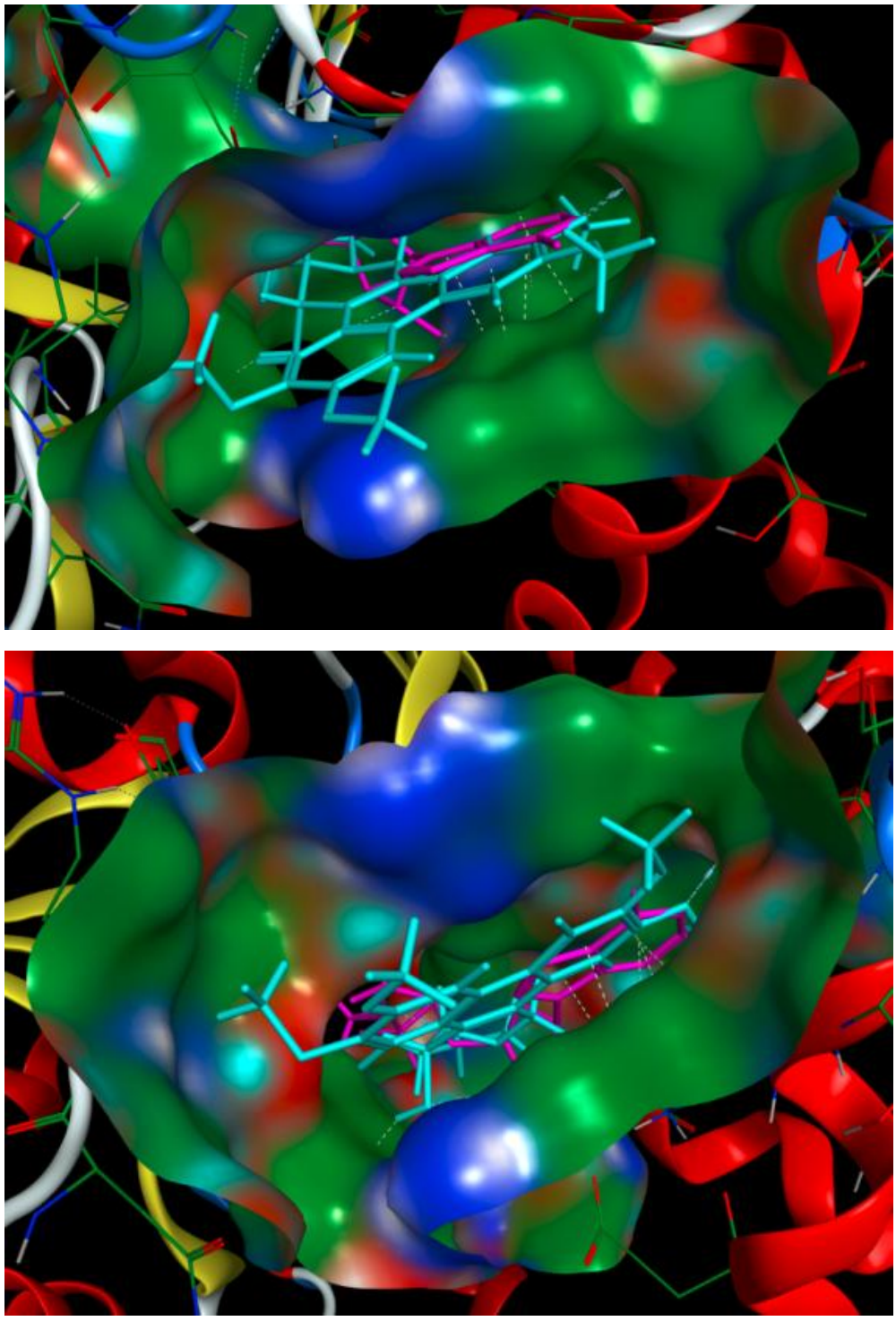

Figure 57. The detailed surface views of the binding pose of greatest potential for DCB-3503 with ADP-bound Hsc70 NBD. (Top: top view; Bottom: bottom view.)

rational design of such an inhibitor competing at the adenine binding site has been already described.[65] It is not impossible for DCB-3503 to bind to multiple sites on the apo protein, whereas on the ATP-bound protein the most reasonable binding site is at the "entrance" of the cleft. Further studies need to be conducted on the possible inhibition activity of DCB-3503 against apo Hsc70 NBD. The construction of this docking model of the apo protein and examination of the possible model of DCB-3503–apo protein binding in light of the results of experimental observations further confirm the rational nature of the first model built on the ATP-bound protein.

V. EXPERIMENTAL

1. The Overexpression and Purification of Hsc70 NBD.

The *E. coli* BL21 (DE3) pLysS cell strain with the six-His-tagged NBD of the recombinant Hsc70 protein plasmid cloned in was first inoculated on a sterilized lysogeny broth (LB) agar plate containing 50 µg/mL kanamycin and 20 µg/mL chloramphenicol as antibiotics, and the cells were allowed to grow overnight at 37 ℃. Afterwards an isolated colony grown on an LB agar plate was transferred into 1 mL of LB with 50 µg/mL kanamycin and 20 µg/mL chloramphenicol, and the subculture was incubated for 6–8 h at 37 ℃ until cloudiness in the vial was observed. Then the 1 mL of subculture was transferred into 200 mL of LB containing 50 µg/mL kanamycin and 20 µg/mL chloramphenicol, and the resulting subculture was allowed to grow overnight at 37 ℃. The overnight subculture was then transferred into 4000 mL of LB containing 25 µg/mL kanamycin and 20 µg/mL chloramphenicol and grown at 37 ℃ until the optical density was ~0.6 at 600 nm. Then the expression of the protein was induced by the addition of isopropyl β-D-1-thiogalactopyranoside (IPTG) to a final concentration of 0.5 mM, and the cells were centrifuged after 4 h of induction at 37 ℃. The cells were resuspended in 1600 mL 0.85% (w/v) NaCl solution and centrifuged again to give the cells ready to be stored at -80 ℃.

For the overexpression of the ^{15}N labeled Hsc70 NBD, a 200-mL subculture was grown in LB media followed the same procedure for preparation of the regular protein, and the cells were then centrifuged and resuspended in 4000 mL of M9 minimal media (with 1 g/L $^{15}NH_4Cl$) with 25 µg/mL kanamycin and 20 µg/mL chloramphenicol in and allowed to grow at 37 ℃ until the

optical density was ~0.6 at 600 nm. Afterwards induction of the expression of the protein was carried out utilizing IPTG at a final concentration of 0.5 mM for 4 h, the cells were then harvested by the procedures stated above.

The purification of Hsc70 NBD began with dissolving 0.5 L cell culture into 15 mL lysis buffer (100 mM NaCl, 20 mM imidazole, 1mM phenylmethanesulfonylfluoride (PMSF), 1 mM $MgCl_2$, 20 µg/mL DNase I, 50 mM Tris-HCl (pH 7.4 at 4 °C)), and the resulting suspension was homogenized. Afterwards the suspended cells were lysed with 3 cycles of freeze and thaw in liquid N_2. The lysate was then centrifuged at 17,000 RPM for 1 h and the cleared supernatant was transfer to a clean Falcon tube. The supernatant was loaded onto 1 mL of a Ni-Sepharose (GE Healthcare Life Science, Pittsburgh, PA) column and was then washed with 150 mL of wash buffer (100 mM NaCl, 20 mM imidazole, 50 mM Tris-HCl (pH 7.4 at 4 °C)). The Hsc70 NBD protein bound to the Ni-Sepharose was then eluted with buffer containing 500 mM NaCl, 250 mM imidazole and 50 mM Tris-HCl (pH 7.4 at 4 °C). The SDS-PAGE analysis showed multiple impurities were eluted together with the target protein, and gel filtration chromatography was used to further purify the protein. The gel filtration buffer with 100 mM KCl, 5 mM $MgCl_2$, 5 mM K_3PO_4 and 50 mM MOPS (pH 7.4 at 4 °C) was utilized, and the resulting protein was further concentrated under nitrogen pressure to give pure Hsc70 NBD. The final yield of the protein was consistently between 2.2 to 2.7 mg/L of induced cell culture.

2. Differential Scanning Calorimetry (DSC).

The DSC experiments were carried out on a VP-DSC microcalorimeter (MicroCal, Inc.) at an external pressure of 25 psi. The starting temperature and the final temperature were set to 15 °C

and 75 °C, respectively, and the heating rate was 1 °C/min. All the solutions were degassed at 20 ℃ for 15 min, and any possible precipitate was spinned down before the experiment.

A solution of Hsc70 NBD at a concentration of 23 μM in MOPS buffer (100 mM KCl, 5 mM $MgCl_2$, 5 mM K_3PO_4, 50 mM MOPS (pH 7.4 at 4 °C)) was used. The first experiment was performed by using the above-mentioned apo-state protein solution directly. Then the ADP-state protein solution was prepared by adding 12 μL of 20 mM ADP aqueous stock solution to 1.2 mL of apo protein solution to make the ADP final concentration as 200 μM, and this solution was used in the ADP-state protein experiments. The third experiment testing the interactions between Hsc70 NBD and DCB-3503 was carried out utilizing a solution prepared by adding 10 μL of 10 mM DCB-3503 DMSO stock solution into 1.2 mL of apo-state protein solution. The final concentration of DCB-3503 was 83 μM in the solution. The solution used in the last experiment was then prepared by adding 12 μL of 20 mM ADP aqueous stock solution and 10 μL of 10 mM DCB-3503 DMSO stock solution in 1.2 mL apo protein solution, making the final concentration of ADP and DCB-3503 as 200 μM and 83 μM, respectively.

3. Isothermal Titration Calorimetry (ITC).

The ITC experiments were performed on a VP-ITC microcalorimeter (MicroCal, Inc.) at 25 ℃, and the total number of injections was set to 29. The solutions to be placed in the cell and the syringe were degassed for 15 min at 20 ℃ and any possible precipitate was centrifuged before the experiment. All the experiments were performed based on the procedures used in the last two groups of experiments described in detail below. The corresponding components and concentration of buffers were adjusted accordingly in each individual experiment.

In each of the last two groups of experiments, a reference experiment and an experiment with the protein were performed. The same protein solution (100 mM KCl, 5 mM $MgCl_2$, 5 mM K_3PO_4, 50 mM MOPS (pH 7.4 at 4 ℃)) at a concentration of 33 µM was used in every experiment, and the same ADP aqueous stock solution with a concentration of 40 mM was used as well. In order to avoid the possible decomposition of DCB-3503 in DMSO over a long duration of time, and to maintain a consistent and accurate concentration of the DCB-3503 stock solution, two batches of DCB-3503 powder for two groups of experiments were accurately weighed. The ligand powder was dissolved right before the experiment, and the resulting DCB-3503 DMSO stock solution was then used to prepare the ligand solution used in two experiments in one group. In the two experiments of the first group, the same ligand solution (500 µM DCB-3503, 5% DMSO, 100 mM KCl, 5 mM $MgCl_2$, 5 mM K_3PO_4, 50 mM MOPS (pH 7.4 at 4 °C)) was placed in the syringe of the VP-ITC instrument. However, a solution of protein (31 µM Hsc70 NBD, 5% DMSO, 100 mM KCl, 5 mM $MgCl_2$, 5 mM K_3PO_4, 50 mM MOPS (pH 7.4 at 4 °C)) and pure buffer (5% DMSO, 100 mM KCl, 5 mM $MgCl_2$, 5 mM K_3PO_4, 50 mM MOPS (pH 7.4 at 4 ℃)) were used, respectively, in the protein experiment and in the reference experiment. Similar procedures and solutions were used in the second group of experiments except for the usage of 40 mM ADP stock solution. In both of the protein solution (31 µM Hsc70 NBD, 5% DMSO, 100 mM KCl, 5 mM $MgCl_2$, 5 mM K_3PO_4, 50 mM MOPS (pH 7.4 at 4 °C)) and the reference buffer (5% DMSO, 100 mM KCl, 5 mM $MgCl_2$, 5 mM K_3PO_4, 50 mM MOPS (pH 7.4 at 4 ℃)), the corresponding ADP stock solution was added to make the final concentration as 300 µM. In the preparation of the ligand solution (500 µM DCB-3503, 5% DMSO, 100 mM KCl, 5 mM $MgCl_2$, 5 mM K_3PO_4, 50 mM MOPS (pH 7.4 at 4 ℃)), extra ddH_2O was required in order to keep the concentration consistent with the new concentration of

buffer components in the protein solution generated by the addition of ADP stock solution as mentioned above.

4. NMR (^{1}H-^{15}N HSQC) Studies.

The ^{15}N labeled Hsc70 NBD was prepared, followed by the previously elaborated overexpression and purification procedures. However, in the gel filtration chromatography the buffer was constituted of 100 mM NaCl and 50 mM Tris-HCl (pH 7.4 at 4°C), and the same buffer was used for the NMR studies. The NMR sample was prepared by concentrating the diluted protein solution obtained from gel filtration chromatography to a more concentrated solution at 186 μM, and 400 μL of this sample was obtained and centrifuged for 5 min at 13,200 rpm. Afterwards 30 μL of 150 mM ADP D_2O solution and 5% DMSO (21.5 μL) were added to finish the preparation of the sample. All the NMR experiments were carried out at 25 °C on a 600 MHz Varian VNMR spectrometer equipped with a triple-resonance cold probe. The first ^{1}H-^{15}N HSQC spectrum was collected for 16 h with the number of scans at 272. Before the collection of the second ^{1}H-^{15}N HSQC spectrum, 4 μL of 10 mM DCB-3503 DMSO stock solution was added slowly into the sample in the Shigemi NMR tube, and the collection was set to 16 h with the number of scans at 272. The last spectrum was collected after the careful addition of an extra 5 μL of 10 mM DCB-3503 DMSO stock solution into the sample, and it was allowed to collect 23 h with the number of scans at 392. All the spectra were processed with the SPARKY program.

5. The Construction of Docking Models.

All the docking models were built in the MOE 2012.10 program (Chemical Computing Group, Montreal, Canada). The ligand DCB-3503 was constructed in Molecule Builder incorporated in MOE, and the corresponding energy was minimized in the MMFF94x force field. The X-ray crystal structure of the protein was obtained from the Protein Data Bank (PDB) with a code of 1NGE.

In the construction of the model with ATP-bound protein, water molecules were first deleted. The protein was then prepared in the Structure Preparation tool followed by Protonate 3D and LigX, and partial charges were assigned in the MMFF94x force field during the preparation. Afterwards Site Finder was utilized to identify the most potential binding site, and instead of selecting only receptor atoms, all atoms including those of the ATP were involved in the calculation. Then the best potential binding site was selected, and dummy atoms were created at the alpha sphere centers. When doing docking, these dummy atoms were chosen as the receptor site, and the rigid receptor protocol was selected with the placement as a triangle matcher. The London dG was selected as rescoring 1, while GBVI/WSA dG was used as rescoring 2. The default setting of refinement was utilized except for the tether, which was set to 0.1 as to increase the flexibility of the side chains.

In the construction of the model without ATP, the same ligand and protein and similar procedures and settings were adopted. However, the protein was prepared after the deletion of both water molecules and the ATP molecule, and all remaining atoms were selected when Site Finder was used to locate the binding site of greatest potential.

CONCLUSION

In the ligand-based approach, a CoMFA model was built based on a group of tylophorine analogues that were believed to function on the NF-κB pathway. Several DCB-3503 analogues with higher projective activities were designed via the CoMFA model, and the corresponding syntheses were performed using a modification of a novel route. These novel DCB-3503 analogues were further studied by our collaborator, Dr. Yung-Chi Cheng of Yale University School of Medicine, on their antitumor and anti-HCV activities. The analysis of the inconsistencies of the predictive and the experimental data was made in the condition of a lack of experimental data against NF-κB pathway, and a more complicated than anticipated mechanism of the antitumor activities of DCB-3503 and its analogues were brought to light.

In the structure-based approach, a target protein of DCB-3503 type compounds, Hsc70, was successfully snared by the biotinylated DCB-3503, and its active domain was subsequently identified. Due to the inability to obtain the co-crystal structure of DCB-3503 and Hsc70 NBD by our collaborator, the above protein was overexpressed and purified by us for further 1H-15N HSQC NMR studies, which could possibly aid in elucidating the specific interactions between DCB-3503 and the protein. The thermodynamic studies were also carried out on DCB-3503 and Hsc70 NBD prior to the NMR studies. However, the failure to obtain satisfactory NMR spectra prompted us to turn to the computational simulations. Two docking models were constructed on the ATP-state Hsc70 NBD and the apo-state Hsc70 NBD, respectively. The most reasonable docking pose was generated in the ATP-state protein, and more promising active candidates can likely be designed from the model in the future.

REFERENCES

1. Wang, Z. W.; Li, Z.; Wang, K. L.; Wang, Q. M. Efficient and Chirally Specific Synthesis of Phenanthro-Indolizidine Alkaloids by Parham-Type Cycloacylation. *Eur. J. Org. Chem.* **2010**, 292-299.
2. Hahn, A. Synthesis of an Antitumor Agent DCB-3509: Synthesis of Analogues via "Click Chemistry". B.S.Thesis, University of Tennessee, Knoxville, 2011.
3. Francis, S. The Design and Synthesis of Biotinylated Tylophorine Analogues for use as Affinity Probes in the Elucidation of the Cellular Targets of DCB-3503. Ph.D.Dissertation, University of Tennessee, Knoxville, 2009.
4. Chang, Y.-W.; Sun, Y.-J.; Wang, C.; Hsiao, C.-D. Crystal Structures of the 70-kDa Heat Shock Proteins in Domain Disjoining Conformation. *J. Biol. Chem.* **2008,** *283*, 15502-15511.
5. Ratnagiriswaran, A. N.; Venkatachalam, K. The chemical examination of Tylophora asthmatica and the isolation of the alkaloids tylophorine and tylophorinine. *Indian J. Med. Res.* **1935,** *22*, 433-41.
6. Kaczmarek, C. Synthetic Studies on Anticancer Compounds: The Tylophorinines. M.S.Thesis, University of Tennessee, Knoxville, 2004.
7. Gao, W. L.; Lam, W.; Zhong, S. B.; Kaczmarek, C.; Baker, D. C.; Cheng, Y. C. Novel mode of action of tylophorine analogs as antitumor compounds. *Cancer Res.* **2004,** *64*, 678-688.
8. Shiah, H. S.; Gao, W. L.; Baker, D. C.; Cheng, Y. C. Inhibition of cell growth and nuclear factor-kappa B activity in pancreatic cancer cell lines by a tylophorine analogue, DCB-3503. *Mol. Cancer Ther.* **2006,** *5*, 2484-2493.

9. You, X.; Pan, M.; Gao, W. L.; Shiah, H. S.; Tao, J.; Zhang, D. Q.; Kournpouras, F.; Wang, S.; Zhao, H. Y.; Madri, J. A.; Baker, D.; Cheng, Y. C.; Yin, Z. N. Effects of a novel tylophorine analog on collagen-induced arthritis through inhibition of the innate immune response. *Arthritis and Rheum.* **2006,** *54*, 877-886.

10. Choi, J. Y.; Gao, W. L.; Odegard, J.; Shiah, H. S.; Kashgarian, M.; McNiff, J. M.; Baker, D. C.; Cheng, Y. C.; Craft, J. Abrogation of skin disease in lupus-prone MRL/Fas(lpr) mice by means of a novel tylophorine analog. *Arthritis and Rheum.* **2006,** *54*, 3277-3283.

11. Gao, W. L.; Bussom, S.; Grill, S. P.; Gullen, E. A.; Hu, Y. C.; Huang, X. S.; Zhong, S. B.; Kaczmarek, C.; Gutierrez, J.; Francis, S.; Baker, D. C.; Yu, S. S.; Cheng, Y. C. Structure-activity studies of phenanthroindolizidine alkaloids as potential antitumor agents. *Bioorg. Med. Chem. Lett.* **2007,** *17*, 4338-4342.

12. Gilmore, T. D. Introduction to NF-kappa B: players, pathways, perspectives. *Oncogene* **2006,** *25*, 6680-6684.

13. Wang, Y.; Gao, W. L.; Svitkin, Y. V.; Chen, A. P. C.; Cheng, Y. C. DCB-3503, a Tylophorine Analog, Inhibits Protein Synthesis through a Novel Mechanism. *Plos One* **2010,** *5*.

14. Gao, W.; Chen, A. P.-C.; Leung, C.-H.; Gullen, E. A.; Fuerstner, A.; Shi, Q.; Wei, L.; Lee, K.-H.; Cheng, Y.-C. Structural analogs of tylophora alkaloids may not be functional analogs. *Bioorg. Med. Chem. Lett.* **2008,** *18*, 704-709.

15. Wang, Y.; Wong, H. C.; Gullen, E. A.; Lam, W.; Yang, X. M.; Shi, Q.; Lee, K. H.; Cheng, Y. C. Cryptopleurine Analogs with Modification of E Ring Exhibit Different Mechanism to Rac-Cryptopleurine and Tylophorine. *Plos One* **2012,** *7*.

16. Lv, H. N.; Ren, J. H.; Ma, S. G.; Xu, S.; Qu, J.; Liu, Z. J.; Zhou, Q.; Chen, X. G.; Yu, S. S. Synthesis, Biological Evaluation and Mechanism Studies of Deoxytylophorinine and Its Derivatives as Potential Anticancer Agents. *Plos One* **2012,** *7*.

17. Wang, Z. W.; Wu, M.; Wang, Y.; Li, Z.; Wang, L.; Han, G. F.; Chen, F. Z.; Liu, Y. X.; Wang, K. L.; Zhang, A.; Meng, L. H.; Wang, Q. M. Synthesis and SAR studies of phenanthroindolizidine and phenanthroquinolizidine alkaloids as potent anti-tumor agents. *Eur. J. Med. Chem.* **2012,** *51*, 250-258.

18. Niphakis, M. J.; Gay, B. C.; Hong, K. H.; Bleeker, N. P.; Georg, G. I. Synthesis and evaluation of the anti-proliferative and NF-κB activities of a library of simplified tylophorine analogs. *Bioorg. Med. Chem.* **2012,** *20*, 5893-5900.

19. Gutierrez, J. Design and Synthesis of Novel Tylophorine Analogs and their Biological Activity. Ph.D.Dissertation, University of Tennessee, Knoxville, 2009.

20. Buckley, T. F., III; Henry, R. Amino acids as chiral educts for asymmetric products. Chirally specific syntheses of tylophorine and cryptopleurine. *J. Org. Chem.* **1983,** *48*, 4222-32.

21. Cramer, R. D.; Patterson, D. E.; Bunce, J. D. Comparative Molecular-Field Analysis (Comfa) .1. Effect of Shape on Binding of Steroids to Carrier Proteins. *J. Am. Chem. Soc.* **1988,** *110*, 5959-5967.

22. Zhang, L.; Tsai, K. C.; Du, L. P.; Fang, H.; Li, M. Y.; Xu, W. F. How to Generate Reliable and Predictive CoMFA Models. *Curr. Med. Chem.* **2011,** *18*, 923-930.

23. Tsai, K. C.; Chen, Y. C.; Hsiao, N. W.; Wang, C. L.; Lin, C. L.; Lee, Y. C.; Li, M. Y.; Wang, B. H. A comparison of different electrostatic potentials on prediction accuracy in CoMFA and CoMSIA studies. *Eur. J. Med. Chem.* **2010,** *45*, 1544-1551.

24. SYBYL-X 2.1 Tutorial. Tripos International, St. Louis, MO. **2013**.

25. Parisini, E.; Metrangolo, P.; Pilati, T.; Resnati, G.; Terraneo, G. Halogen bonding in halocarbon-protein complexes: a structural survey. *Chem. Soc. Rev.* **2011,** *40*, 2267-78.

26. Hernandes, M. Z.; Cavalcanti, S. M.; Moreira, D. R.; de Azevedo Junior, W. F.; Leite, A. C. Halogen atoms in the modern medicinal chemistry: hints for the drug design. *Curr. Drug Targets* **2010,** *11*, 303-14.

27. Riley, K. E.; Hobza, P. Strength and Character of Halogen Bonds in Protein-Ligand Complexes. *Cryst. Growth Des.* **2011,** *11*, 4272-4278.

28. Xu, Z.; Yang, Z.; Liu, Y.; Lu, Y.; Chen, K.; Zhu, W. Halogen bond: its role beyond drug-target binding affinity for drug discovery and development. *J. Chem. Inf. Model.* **2014,** *54*, 69-78.

29. Purser, S.; Moore, P. R.; Swallow, S.; Gouverneur, V. Fluorine in medicinal chemistry. *Chem. Soc. Rev.* **2008,** *37*, 320-30.

30. Hopkins, C. Y.; Chisholm, M. J. Chlorination by Aqueous Sodium Hypochlorite. *Can. J. Res., Sect. B* **1946,** *24*, 208-210.

31. Mai, A.; Massa, S.; Valente, S.; Simeoni, S.; Ragno, R.; Bottoni, P.; Scatena, R.; Brosch, G. Aroyl-pyrrolyl hydroxyamides: Influence of pyrrole C4-phenylacetyl substitution on histone deacetylase inhibition. *Chemmedchem* **2006,** *1*, 225-237.

32. Wang, K. L.; Lu, M.; Yu, A.; Zhu, X. Q.; Wang, Q. M. Iron(III) Chloride Catalyzed Oxidative Coupling of Aromatic Nuclei. *J. Org. Chem.* **2009,** *74*, 935-938.

33. Brown, H. C.; Krishnam.S. Selective Reductions .14. Fast Reaction of Aryl Bromides and Iodides with Lithium Aluminum Hydride in Tetrahydrofuran . A Simple, Convenient

Procedure for Hydrogenolysis of Aryl Bromides and Iodides. *J. Org. Chem.* **1969,** *34*, 3918-&.

34. Wang, Z. W.; Wang, Q. M. Highly efficient synthesis of phenanthroquinolizidine alkaloids via Parham-type cycliacylation. *Tetrahedron Lett.* **2010,** *51*, 1377-1379.
35. Mitchell, R. H.; Lai, Y.-H.; Williams, R. V. N-Bromosuccinimide-dimethylformamide: a mild, selective nuclear monobromination reagent for reactive aromatic compounds. *J. Org. Chem.* **1979,** *44*, 4733-5.
36. Chimni, S. S.; Mahajan, D. Small organic molecule catalyzed enantioselective direct aldol reaction in water. *Tetrahedron: Asymmetry* **2006,** *17*, 2108-2119.
37. Lin, S.; Yang, Z.-Q.; Kwok, B. H. B.; Koldobskiy, M.; Crews, C. M.; Danishefsky, S. J. Total Synthesis of TMC-95A and -B via a New Reaction Leading to Z-Enamides. Some Preliminary Findings as to SAR. *J. Am. Chem. Soc.* **2004,** *126*, 6347-6355.
38. Nicholas, K. M.; Pettit, R. Alkyne protecting group. *Tetrahedron Lett.* **1971,** *37*, 3475-8.
39. Tejedor, D.; Mendez-Abt, G.; Cotos, L.; Garcia-Tellado, F. Propargyl Claisen rearrangement. Allene synthesis and beyond. *Chem. Soc. Rev.* **2013,** *42*, 458-471.
40. Swetha, M.; Ramana, P. V.; Shirodkar, S. G. Simple and Efficient Method for the Synthesis of Azides in Water-THF Solvent System. *Org. Prep. Proced. Int.* **2011,** *43*, 348-353.
41. Arote, N. D.; Akamanchi, K. G. Direct conversion of aldehydes to acyl azides using tert-butyl hypochlorite. *Tetrahedron Lett.* **2007,** *48*, 5661-5664.
42. Mintz, M. J.; Walling, C. Tert-butyl hypochlorite. *Org. Syn.* **1969,** *49*, 9-12.
43. Bandgar, B. P.; Pandit, S. S. Synthesis of acyl azides from carboxylic acids using cyanuric chloride. *Tetrahedron Lett.* **2002,** *43*, 3413-3414.

44. Himo, F.; Lovell, T.; Hilgraf, R.; Rostovtsev, V. V.; Noodleman, L.; Sharpless, K. B.; Fokin, V. V. Copper(I)-catalyzed synthesis of azoles. DFT study predicts unprecedented reactivity and intermediates. *J. Am. Chem. Soc.* **2005,** *127*, 210-216.

45. Rostovtsev, V. V.; Green, L. G.; Fokin, V. V.; Sharpless, K. B. A stepwise Huisgen cycloaddition process: Copper(I)-catalyzed regioselective "ligation" of azides and terminal alkynes. *Angew. Chem., Int. Ed.* **2002,** *41*, 2596-+.

46. Alvarez, S. G.; Alvarez, M. T. A practical procedure for the synthesis of alkyl azides at ambient temperature in dimethyl sulfoxide in high purity and yield. *Synthesis* **1997**, 413-414.

47. Williams, S. J.; Zammit, S. C.; Cox, A. J.; Shackleford, D. M.; Morizzi, J.; Zhang, Y.; Powell, A. K.; Gilbert, R. E.; Krum, H.; Kelly, D. J. 3 ',4 '-Bis-difluoromethoxycinnamoylanthranilate (FT061): An orally-active antifibrotic agent that reduces albuminuria in a rat model of progressive diabetic nephropathy. *Bioorg. Med. Chem. Lett.* **2013,** *23*, 6868-6873.

48. Derenberg, M.; Hodge, P. Action of sodium and lithium chlorodifluoroacetates on 9,10-phenanthrenedione. *J. Chem. Soc., Perkin Trans. 1* **1972**, 1056-8.

49. Schaumberg, J. P.; Hokanson, G. C.; French, J. C.; Smal, E.; Baker, D. C. 2'-Chloropentostatin, a new inhibitor of adenosine deaminase. *J. Org. Chem.* **1985,** *50*, 1651-6.

50. de, O. A. L. J.; D'Oliveira, A.; Melo, R. C.; De, S. E. C.; Costa, S. C. A.; Parana, R. Association between hepatitis C and hepatocellular carcinoma. *J. Glob. Infect. Dis.* **2009,** *1*, 33-7.

51. Weber, P. C.; Ohlendorf, D. H.; Wendoloski, J. J.; Salemme, F. R. Structural Origins of High-Affinity Biotin Binding to Streptavidin. *Science* **1989,** *243*, 85-88.

52. Wang, Y.; Lee, S.; Lam, W.; Cheng, Y.C. Unpublished Work. **2013**.

53. Liu, T.; Daniels, C. K.; Cao, S. S. Comprehensive review on the HSC70 functions, interactions with related molecules and involvement in clinical diseases and therapeutic potential. *Pharmacol. Ther.* **2012,** *136*, 354-374.

54. Kityk, R.; Kopp, J.; Sinning, I.; Mayer, M. P. Structure and dynamics of the ATP-bound open conformation of Hsp70 chaperones. *Mol. Cell* **2012,** *48*, 863-74.

55. Swain, J. F.; Dinler, G.; Sivendran, R.; Montgomery, D. L.; Stotz, M.; Gierasch, L. M. Hsp70 chaperone ligands control domain association via an allosteric mechanism mediated by the interdomain linker. *Mol. Cell* **2007,** *26*, 27-39.

56. Arakawa, A.; Handa, N.; Ohsawa, N.; Shida, M.; Kigawa, T.; Hayashi, F.; Shirouzu, M.; Yokoyama, S. The C-terminal BAG domain of BAG5 induces conformational changes of the Hsp70 nucleotide-binding domain for ADP-ATP exchange. *Structure* **2010,** *18*, 309-19.

57. Bhattacharya, A.; Kurochkin, A. V.; Yip, G. N. B.; Zhang, Y.; Bertelsen, E. B.; Zuiderweg, E. R. P. Allostery in Hsp70 Chaperones Is Transduced by Subdomain Rotations. *J. Mol. Biol.* **2009,** *388*, 475-490.

58. Sondermann, H.; Scheufler, C.; Schneider, C.; Hohfeld, J.; Hartl, F. U.; Moarefi, I. Structure of a Bag/Hsc70 complex: convergent functional evolution of Hsp70 nucleotide exchange factors. *Science* **2001,** *291*, 1553-7.

59. Jiang, J.; Maes, E. G.; Taylor, A. B.; Wang, L.; Hinck, A. P.; Lafer, E. M.; Sousa, R. Structural basis of J cochaperone binding and regulation of Hsp70. *Mol. Cell* **2007,** *28*, 422-33.

60. Jiang, J.; Prasad, K.; Lafer, E. M.; Sousa, R. Structural basis of interdomain communication in the Hsc70 chaperone. *Mol. Cell* **2005,** *20*, 513-24.

61. Rousaki, A.; Miyata, Y.; Jinwal, U. K.; Dickey, C. A.; Gestwicki, J. E.; Zuiderweg, E. R. Allosteric drugs: the interaction of antitumor compound MKT-077 with human Hsp70 chaperones. *J Mol. Biol.* **2011,** *411*, 614-32.

62. Wisen, S.; Bertelsen, E. B.; Thompson, A. D.; Patury, S.; Ung, P.; Chang, L.; Evans, C. G.; Walter, G. M.; Wipf, P.; Carlson, H. A.; Brodsky, J. L.; Zuiderweg, E. R. P.; Gestwicki, J. E. Binding of a Small Molecule at a Protein-Protein Interface Regulates the Chaperone Activity of Hsp70-Hsp40. *ACS Chem. Biol.* **2010,** *5*, 611-622.

63. Chang, L.; Miyata, Y.; Ung, P. M.; Bertelsen, E. B.; McQuade, T. J.; Carlson, H. A.; Zuiderweg, E. R.; Gestwicki, J. E. Chemical screens against a reconstituted multiprotein complex: myricetin blocks DnaJ regulation of DnaK through an allosteric mechanism. *Chem. Biol.* **2011,** *18*, 210-21.

64. MOE 2012.10 Tutorial. Chemical Computing Group, Montreal, Canada. **2012**.

65. Williamson, D. S.; Borgognoni, J.; Clay, A.; Daniels, Z.; Dokurno, P.; Drysdale, M. J.; Foloppe, N.; Francis, G. L.; Graham, C. J.; Howes, R.; Macias, A. T.; Murray, J. B.; Parsons, R.; Shaw, T.; Surgenor, A. E.; Terry, L.; Wang, Y. K.; Wood, M.; Massey, A. J. Novel Adenosine-Derived Inhibitors of 70 kDa Heat Shock Protein, Discovered Through Structure-Based Design. *J. Med. Chem.* **2009,** *52*, 1510-1513.

APPENDIX

^{1}H, ^{13}C, selected 2D NMR and mass spectra

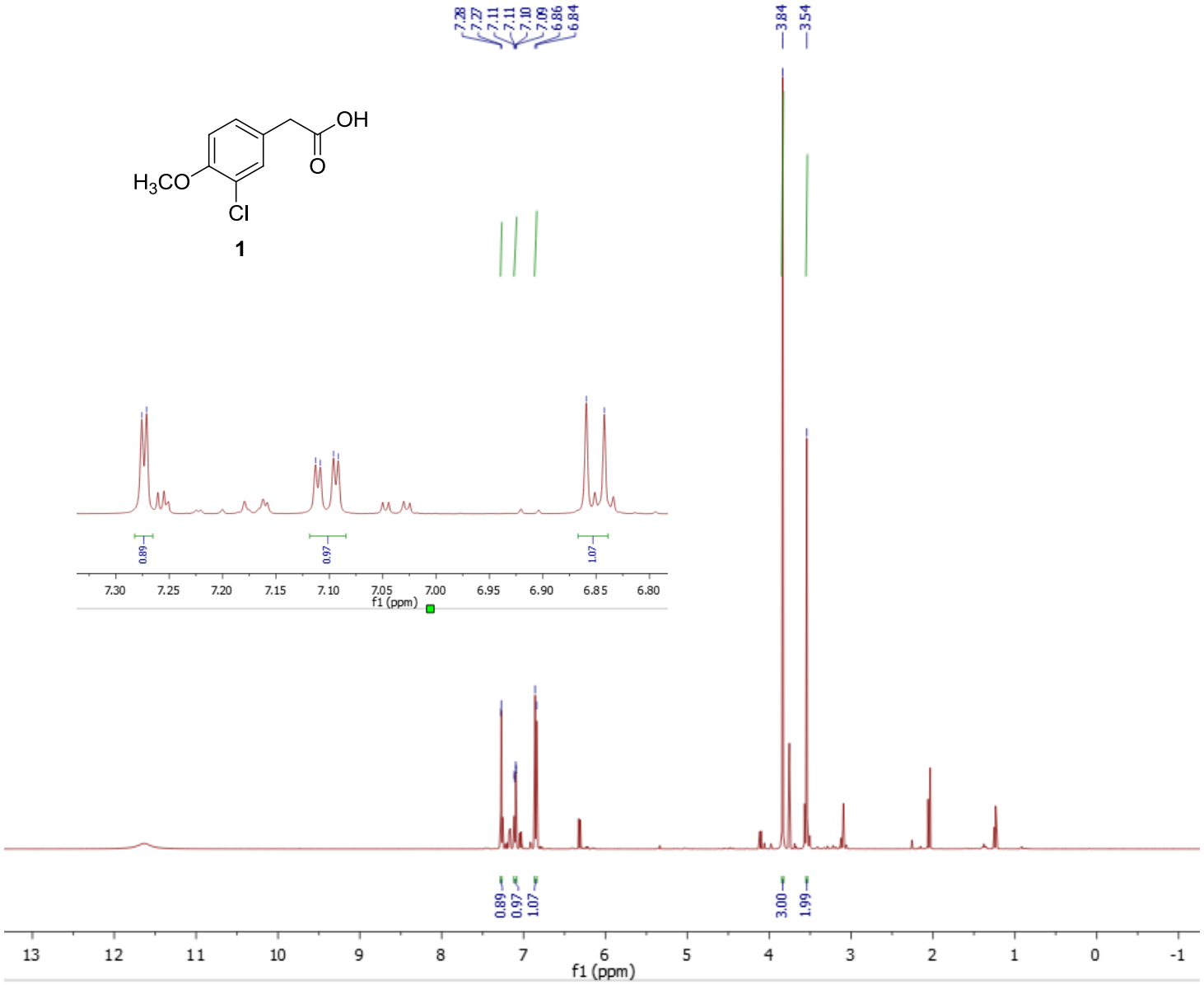

^{1}H NMR spectrum (500 MHz, $CDCl_3$) of 2-(3-chloro-4-methoxyphenyl)acetic acid (**1**).

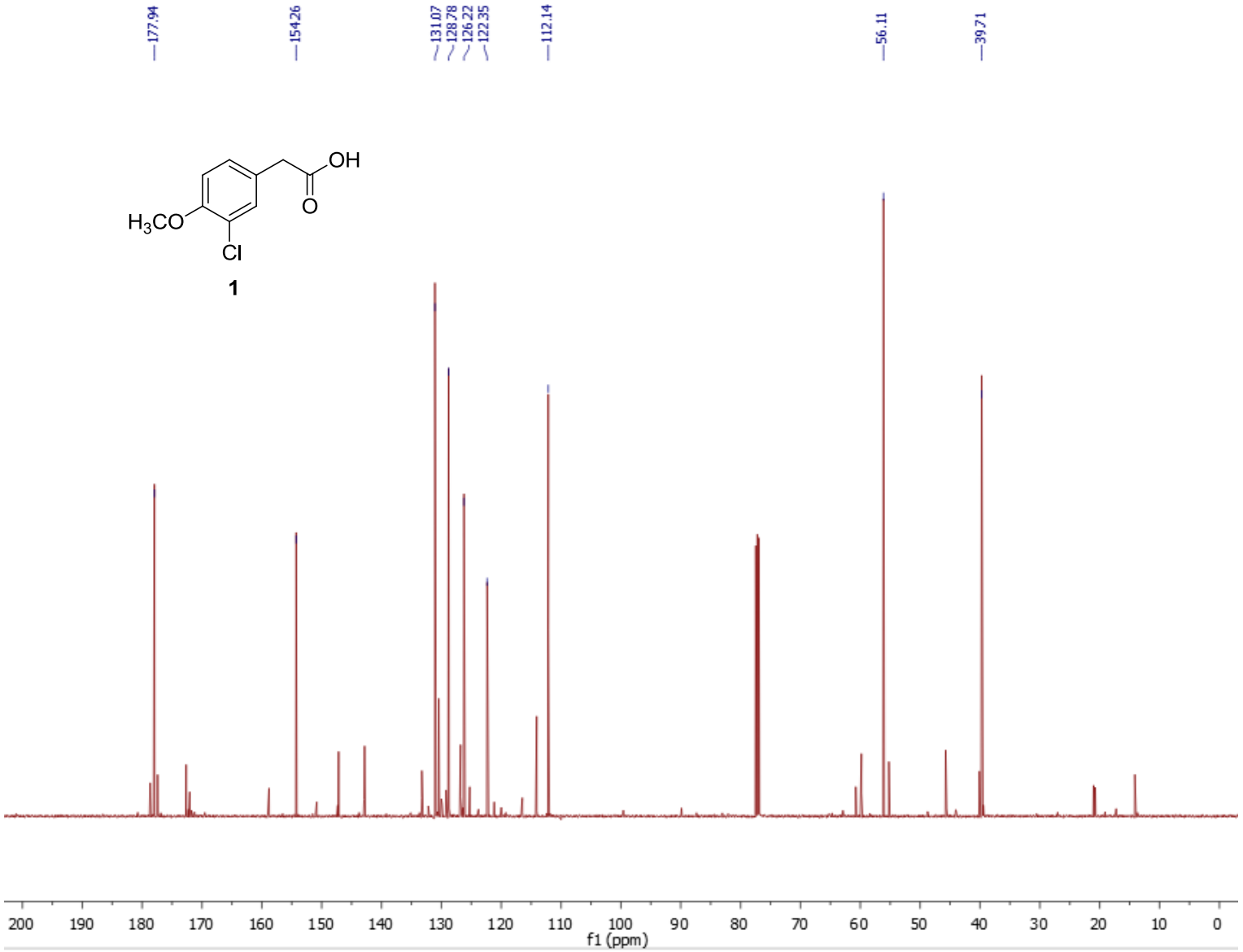

^{13}C NMR spectrum (500 MHz, $CDCl_3$) of 2-(3-chloro-4-methoxyphenyl)acetic acid (**1**).

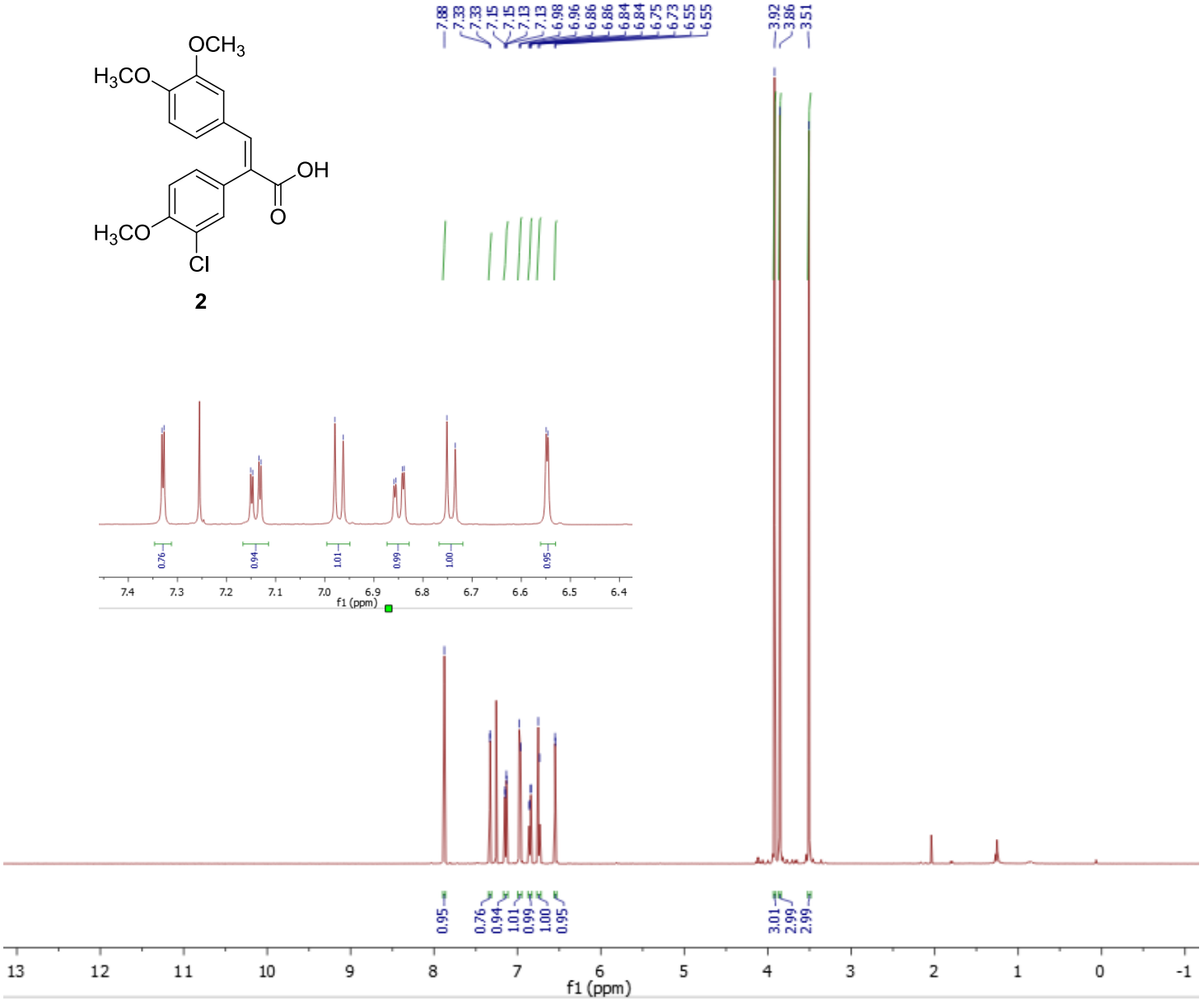

^{1}H NMR spectrum (500 MHz, $CDCl_3$) of (*E*)-2-(3-chloro-4-methoxyphenyl)-3-(3,4-dimethoxyphenyl)acrylic acid (**2**).

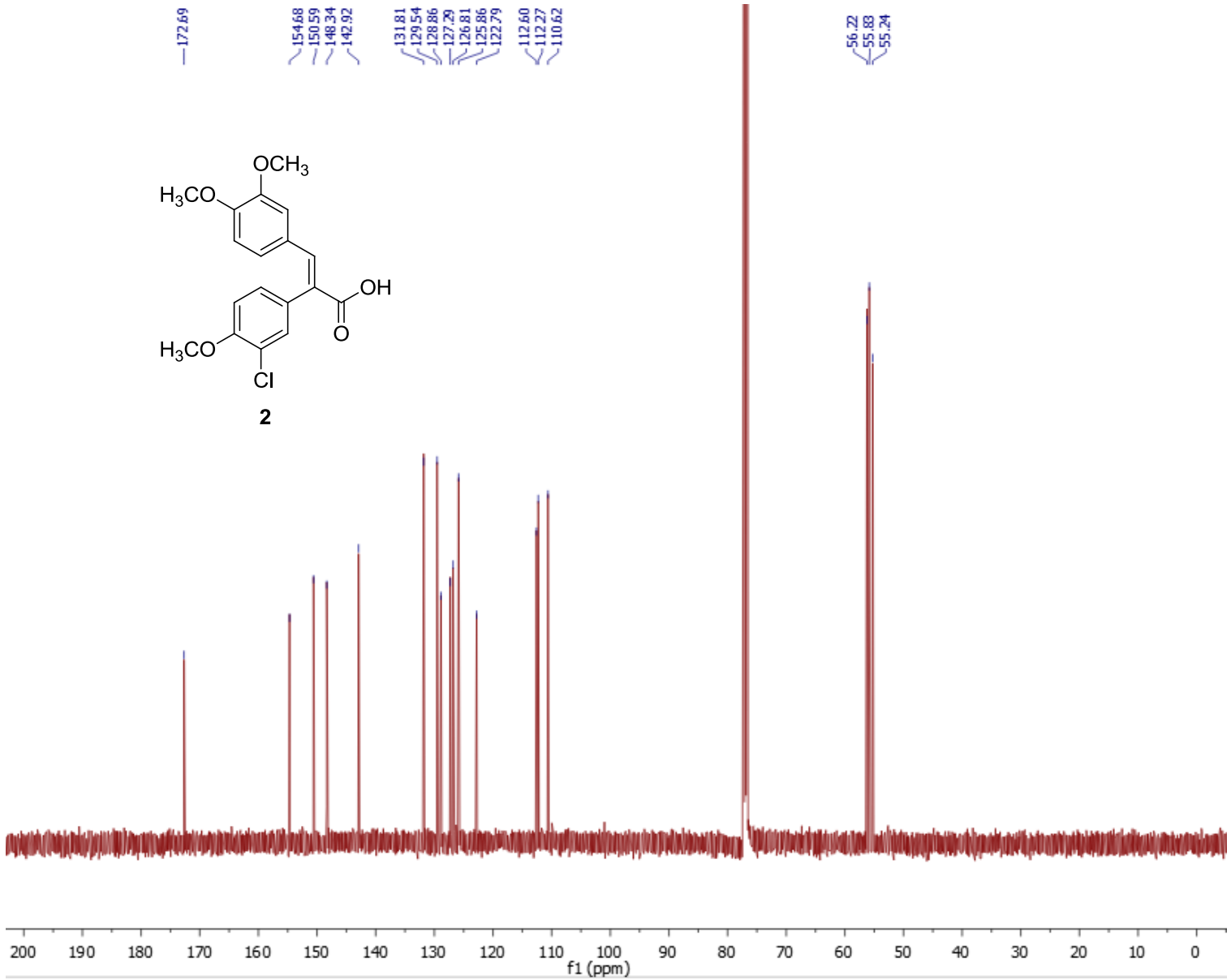

^{13}C NMR spectrum (125 MHz, $CDCl_3$) of (*E*)-2-(3-chloro-4-methoxyphenyl)-3-(3,4-dimethoxyphenyl)acrylic acid (**2**).

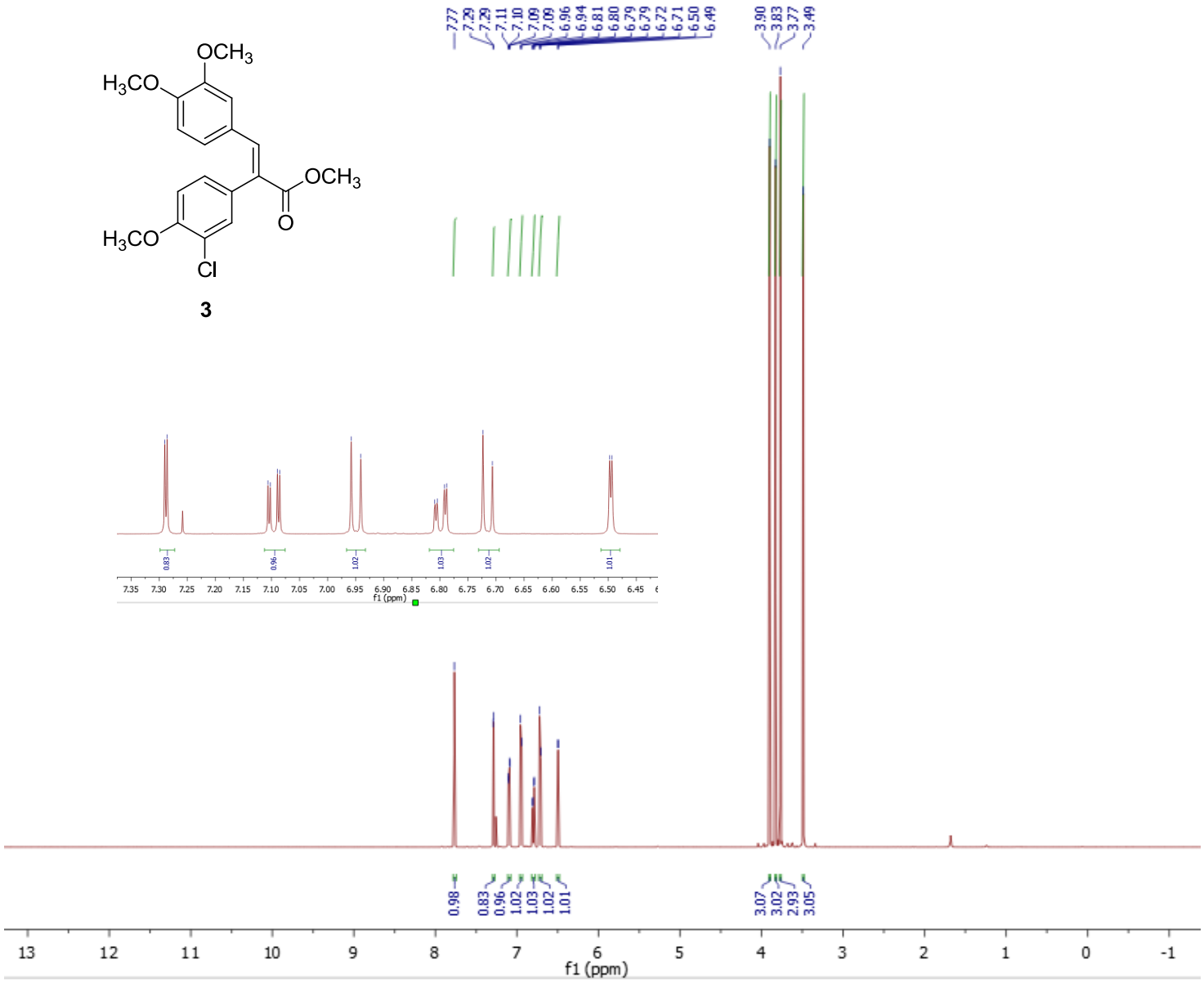

^{1}H NMR spectrum (500 MHz, $CDCl_3$) of (*E*)-methyl 2-(3-chloro-4-methoxyphenyl)-3-(3,4-dimethoxyphenyl)acrylate (**3**).

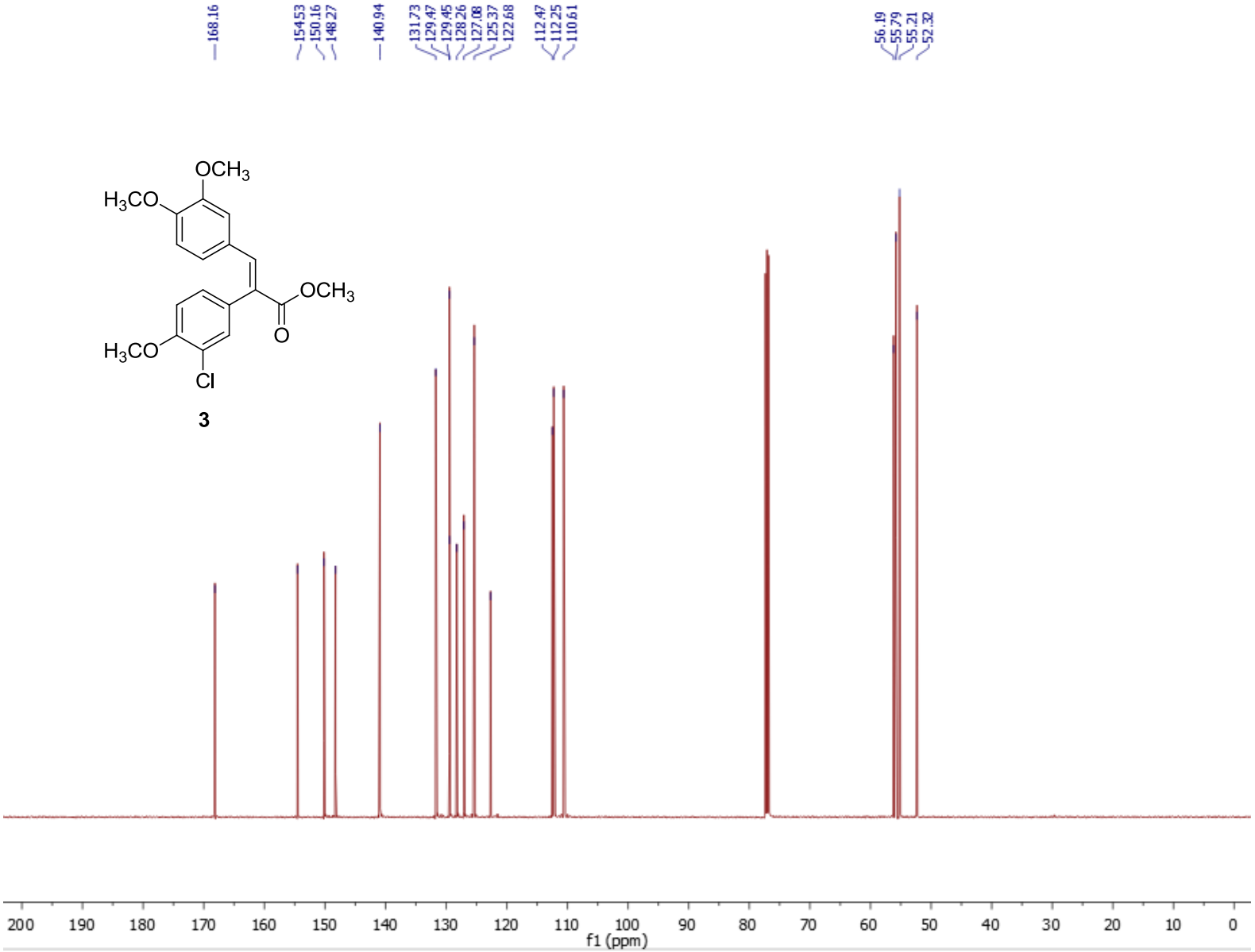

^{13}C NMR spectrum (125 MHz, $CDCl_3$) of (*E*)-methyl 2-(3-chloro-4-methoxyphenyl)-3-(3,4-dimethoxyphenyl)acrylate (**3**).

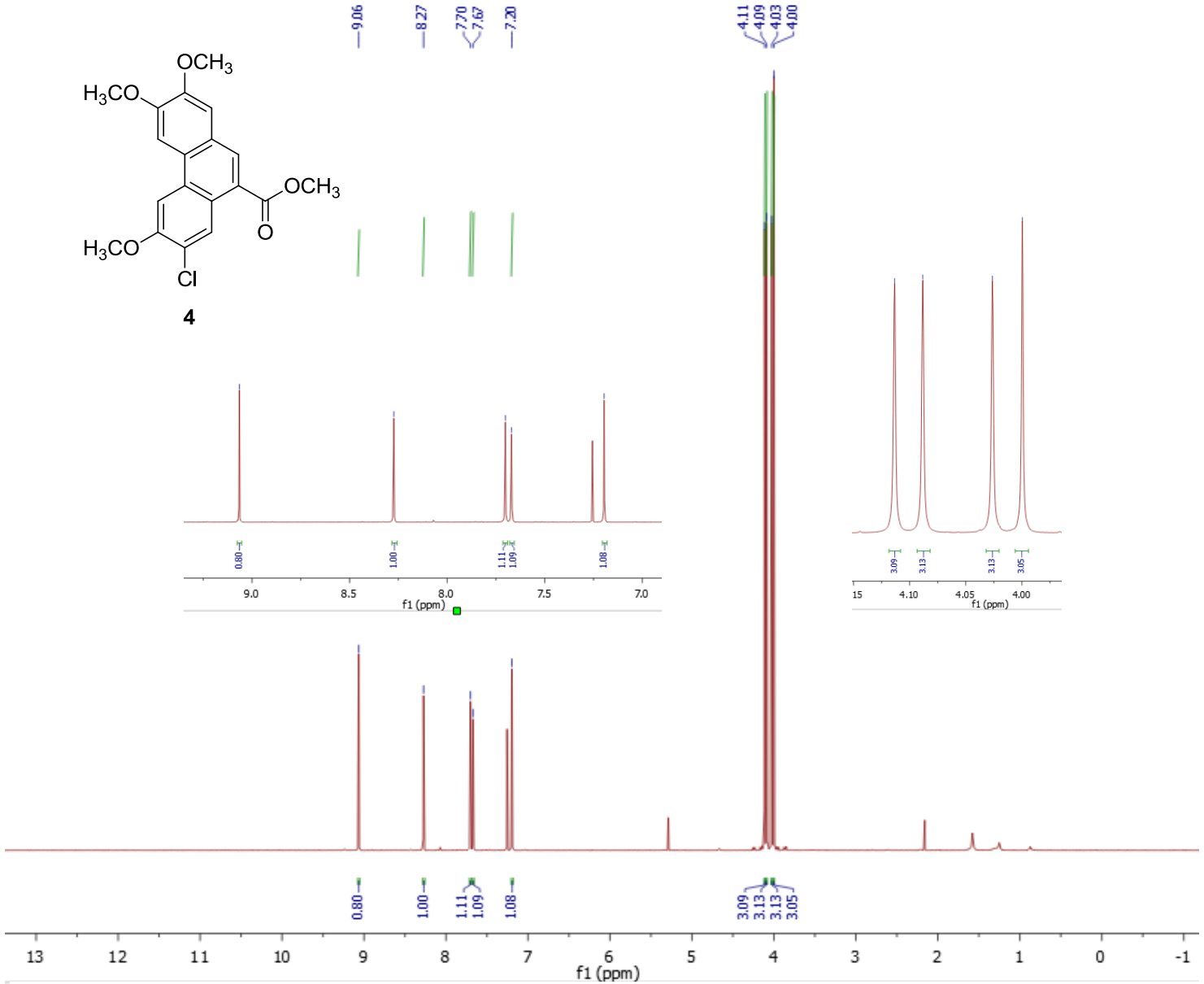

^{1}H NMR spectrum (500 MHz, $CDCl_3$) of methyl 7-chloro-2,3,6-trimethoxyphenanthrene-9-carboxylate (**4**).

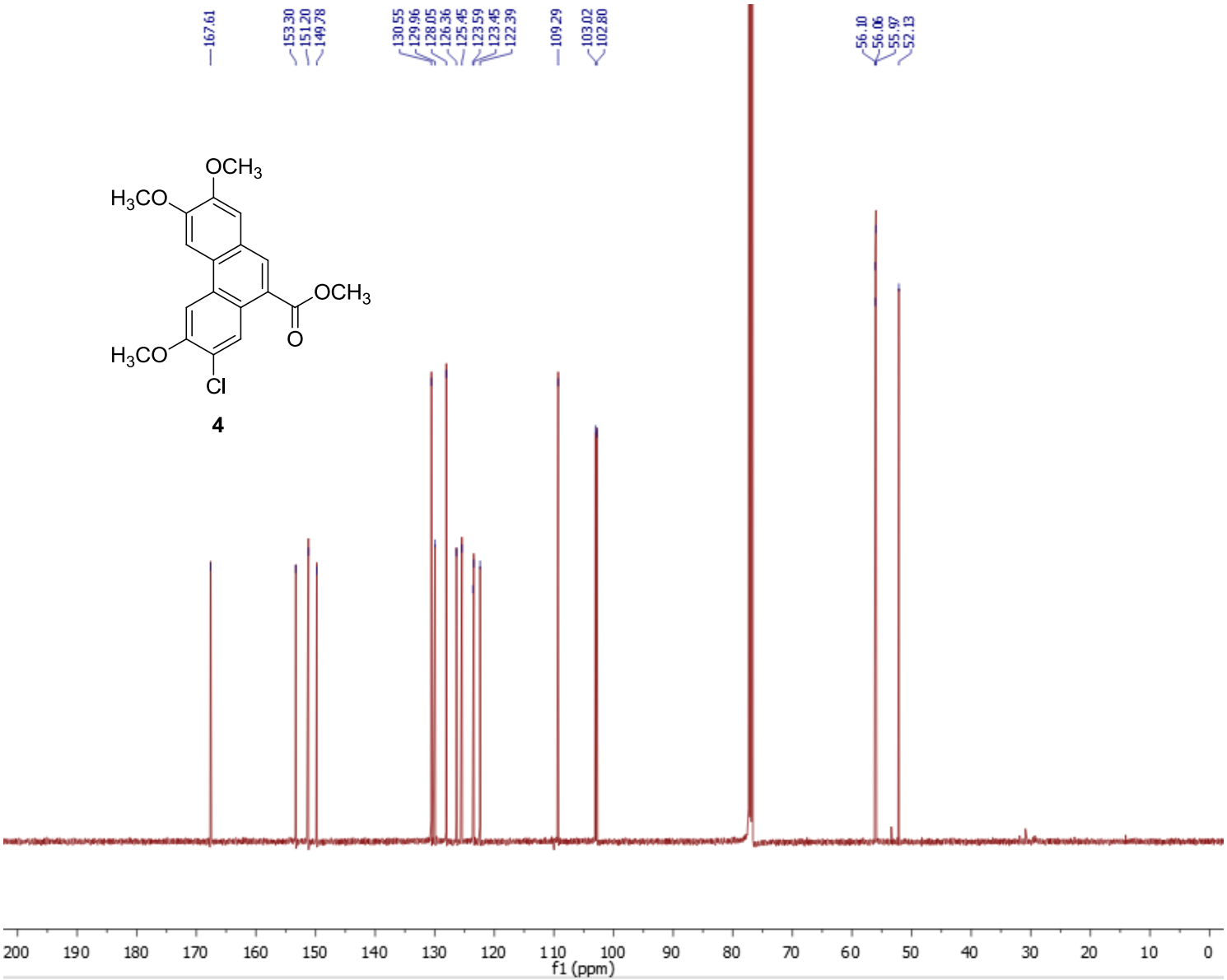

^{13}C NMR spectrum (125 MHz, $CDCl_3$) of methyl 7-chloro-2,3,6-trimethoxyphenanthrene-9-carboxylate (**4**).

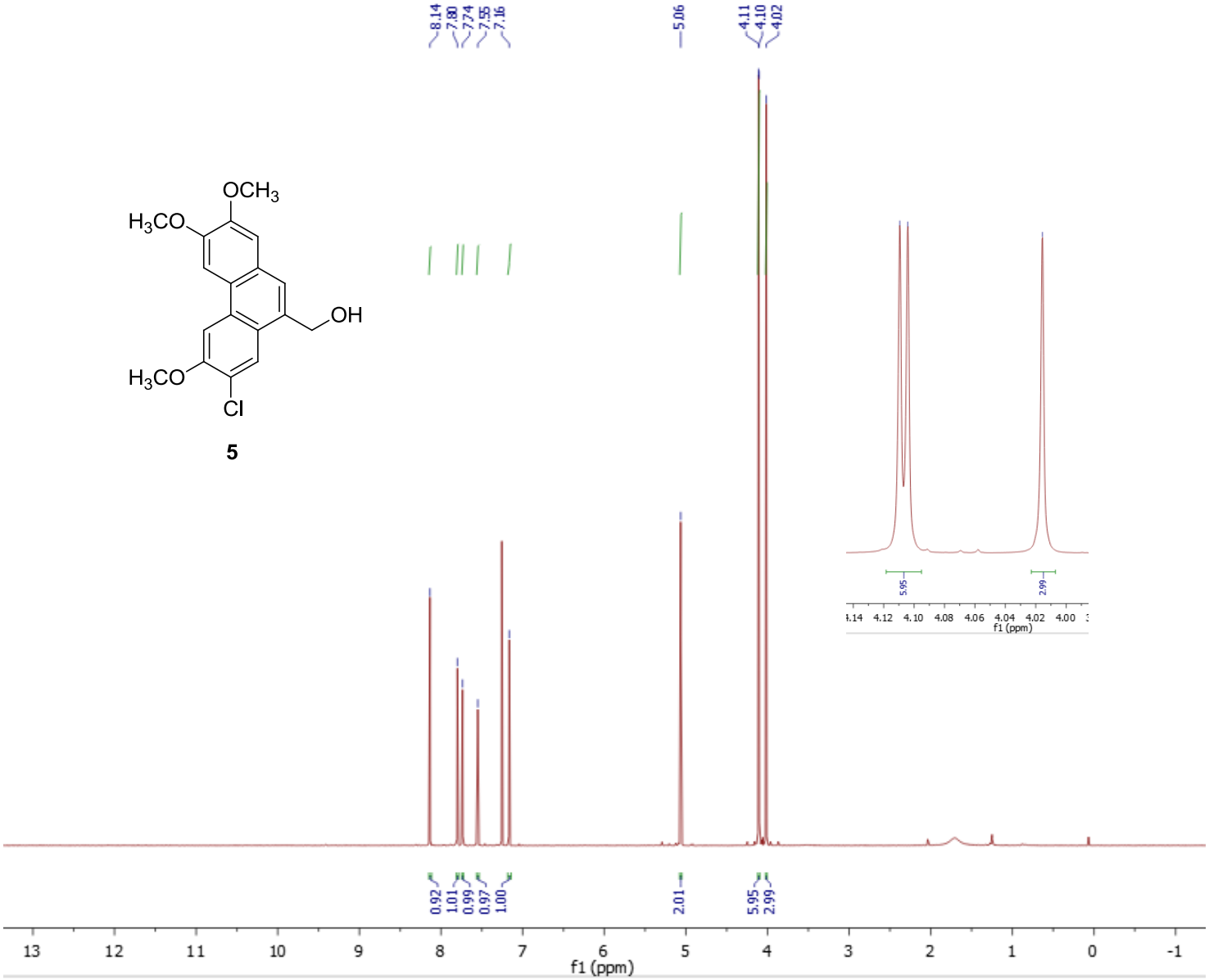

^{1}H NMR spectrum (500 MHz, $CDCl_3$) of (7-chloro-2,3,6-trimethoxyphenanthren-9-yl)methanol (**5**).

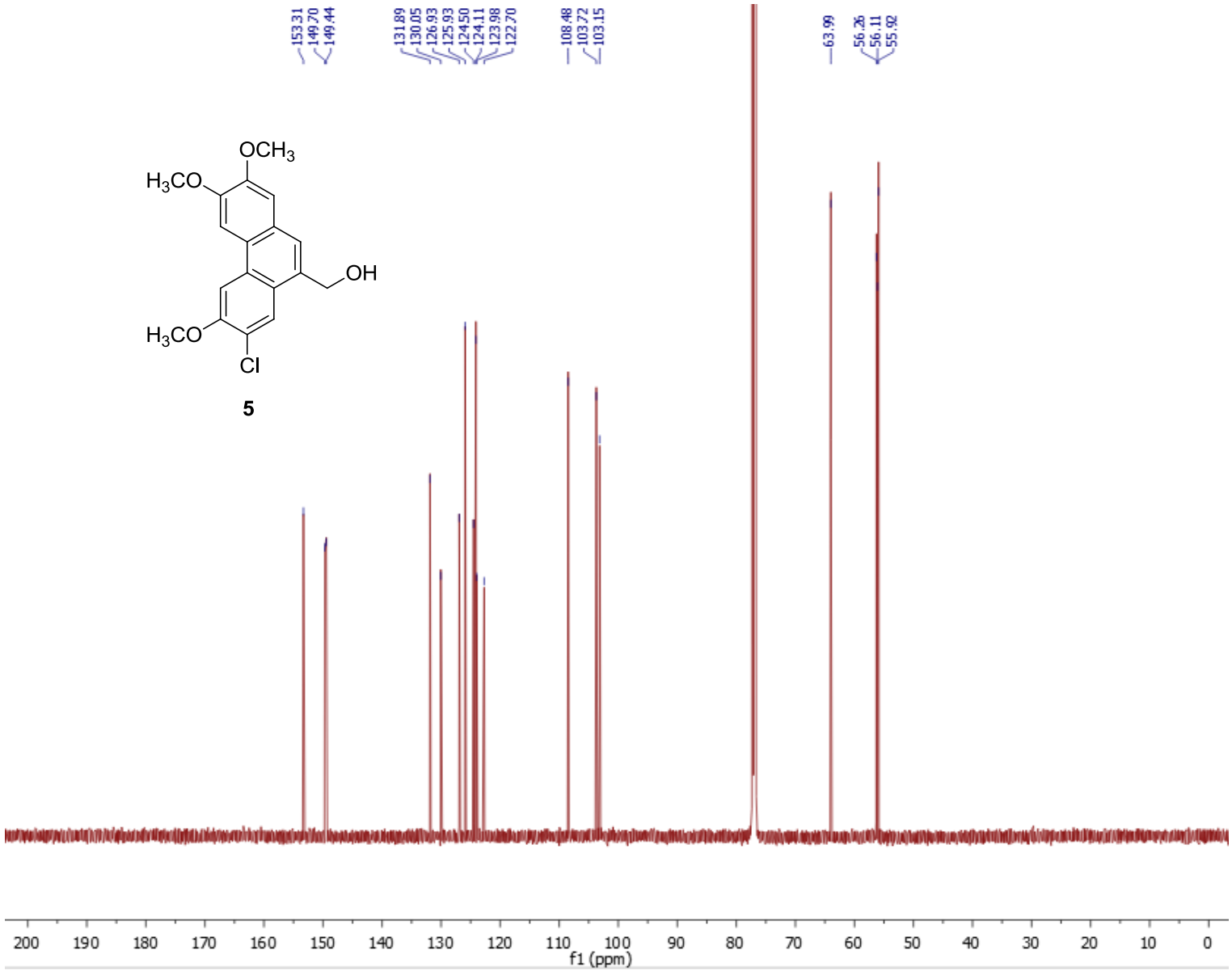

^{13}C NMR spectrum (125 MHz, $CDCl_3$) of (7-chloro-2,3,6-trimethoxyphenanthren-9-yl)methanol (**5**).

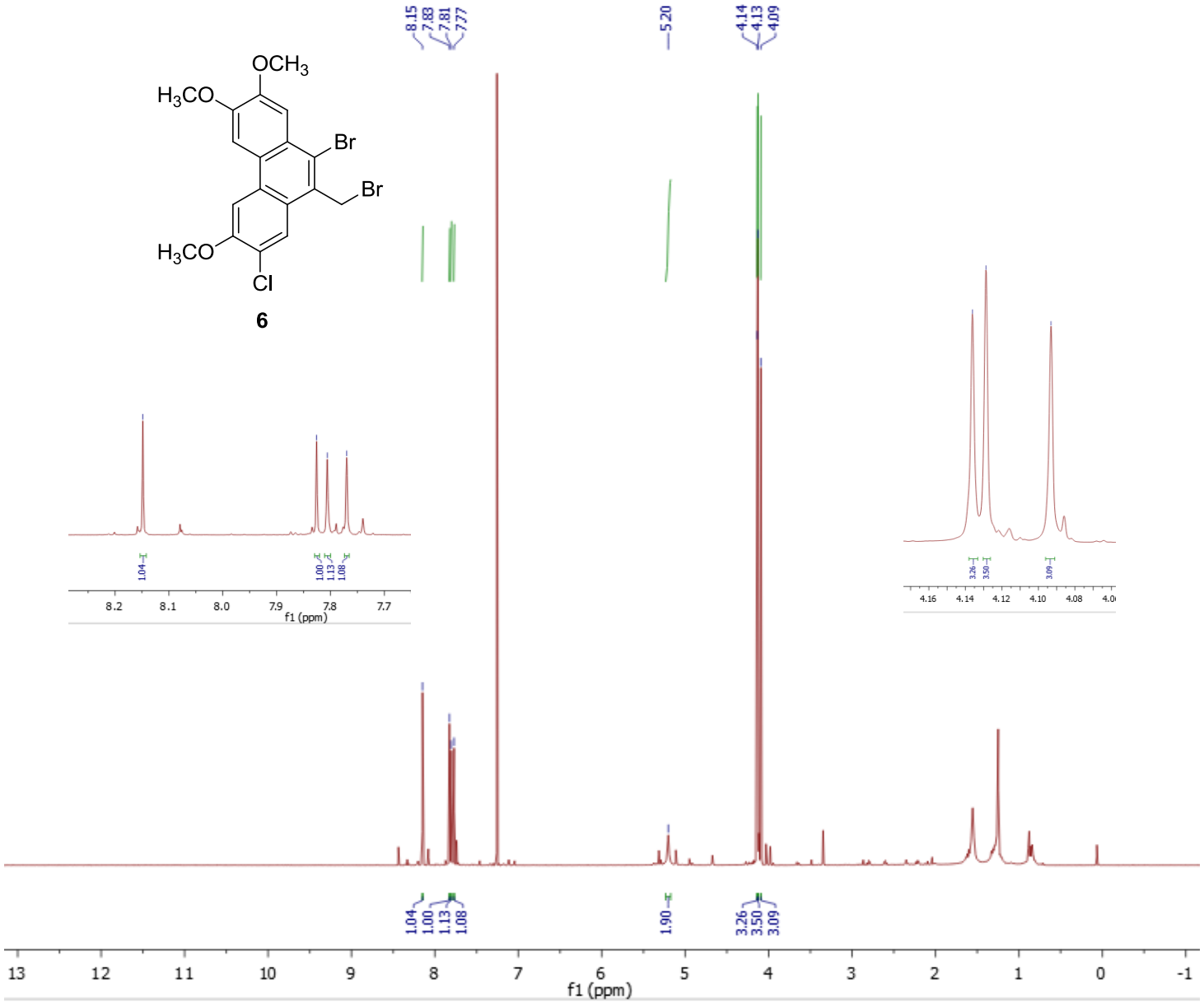

^{1}H NMR spectrum (500 MHz, $CDCl_3$) of 9-bromo-10-(bromomethyl)-2-chloro-3,6,7-trimethoxyphenanthrene (**6**).

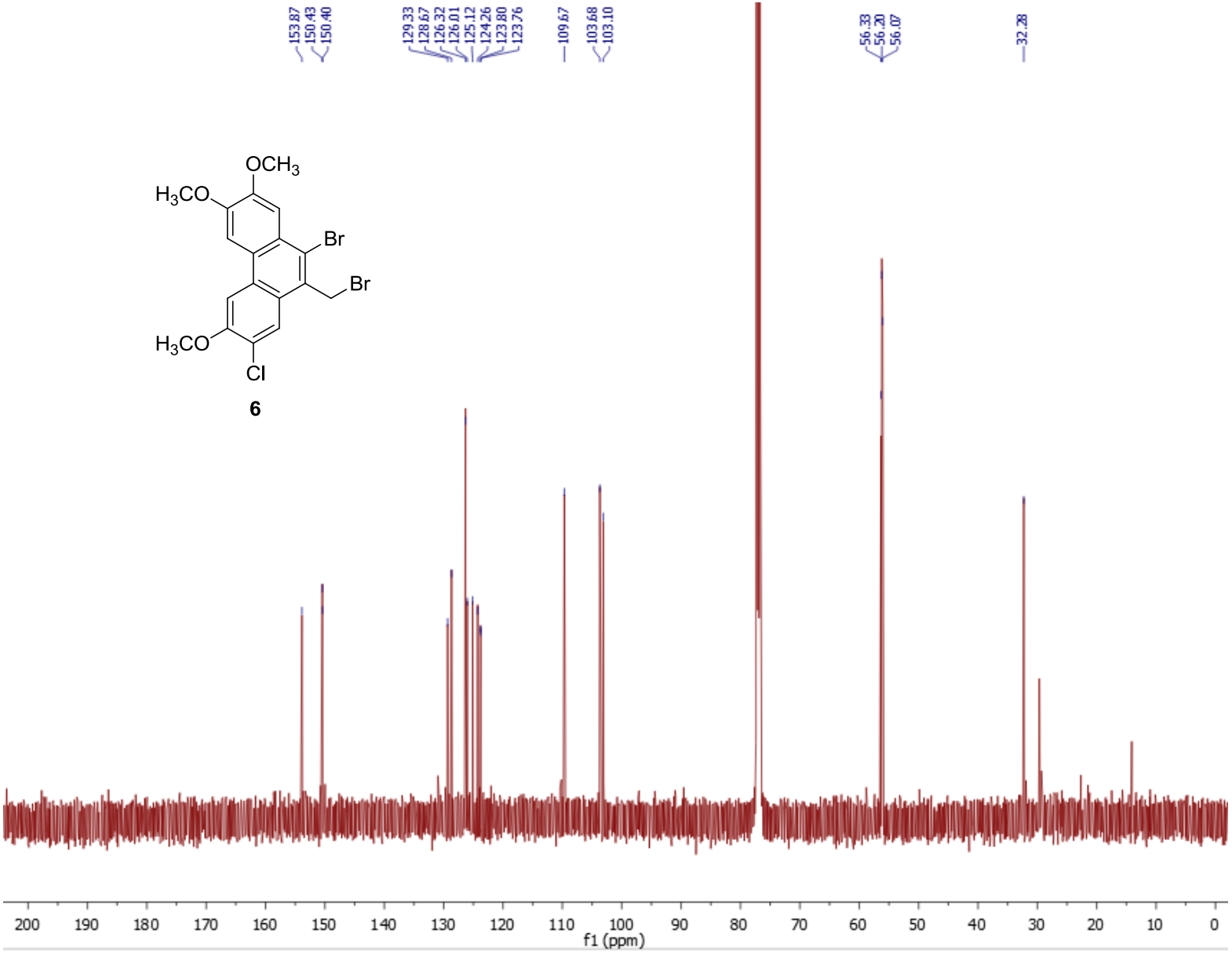

^{13}C NMR spectrum (125 MHz, $CDCl_3$) of 9-bromo-10-(bromomethyl)-2-chloro-3,6,7-trimethoxyphenanthrene (**6**).

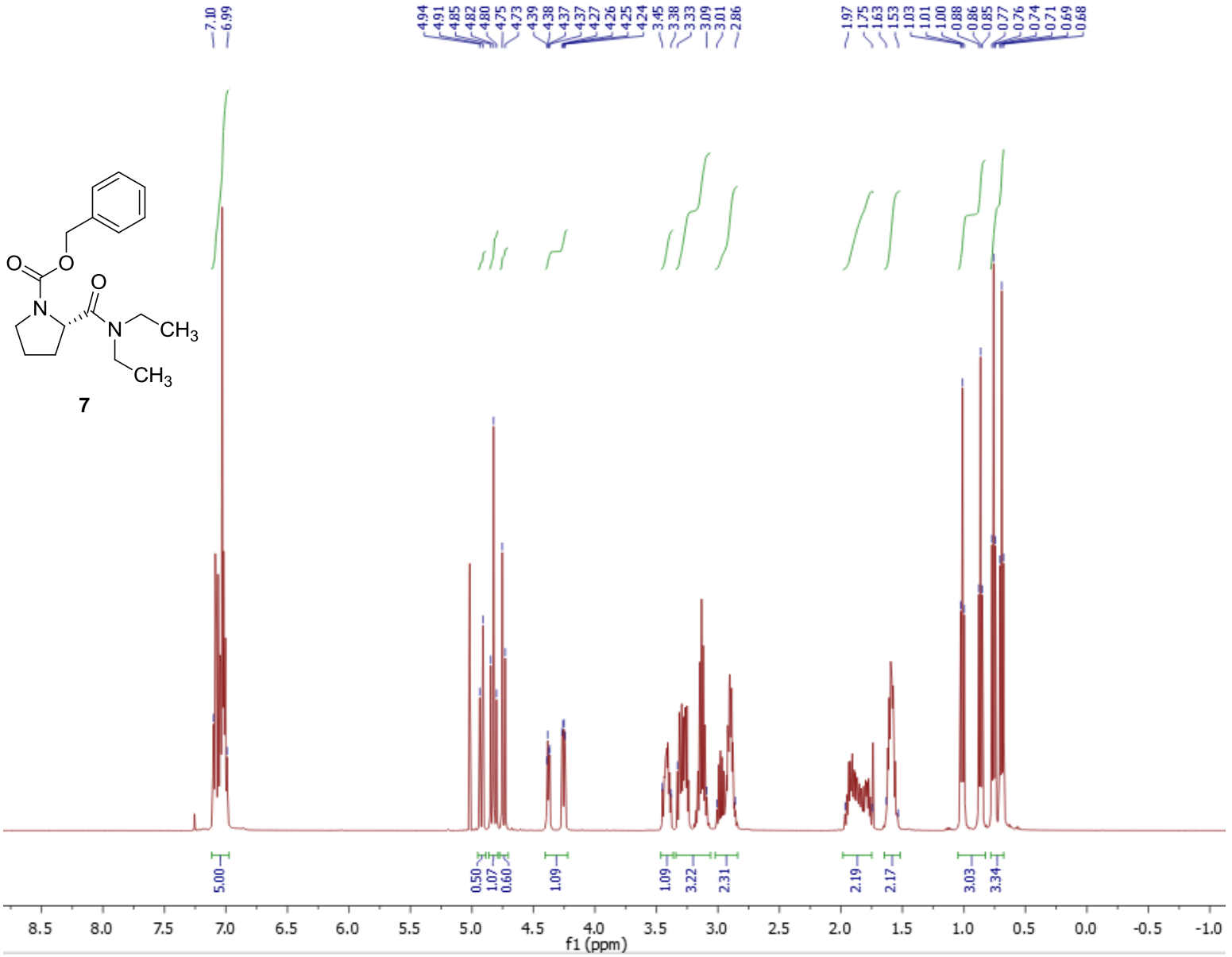

^{1}H NMR spectrum (500 MHz, $CDCl_3$) of (*S*)-benzyl 2-(diethylcarbamoyl)pyrrolidine-1-carboxylate (**7**).

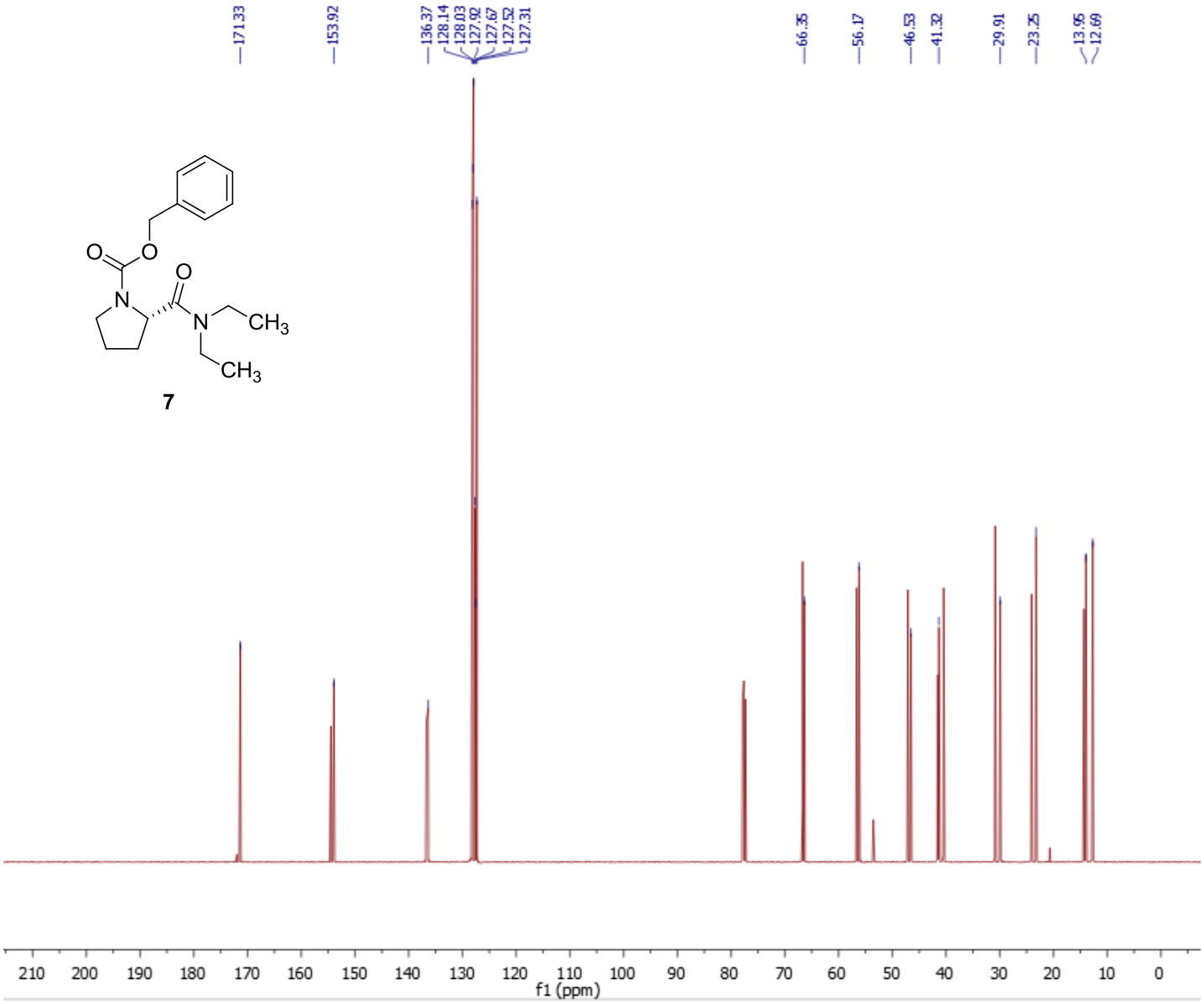

^{13}C NMR spectrum (125 MHz, $CDCl_3$) of (*S*)-benzyl 2-(diethylcarbamoyl)pyrrolidine-1-carboxylate (**7**).

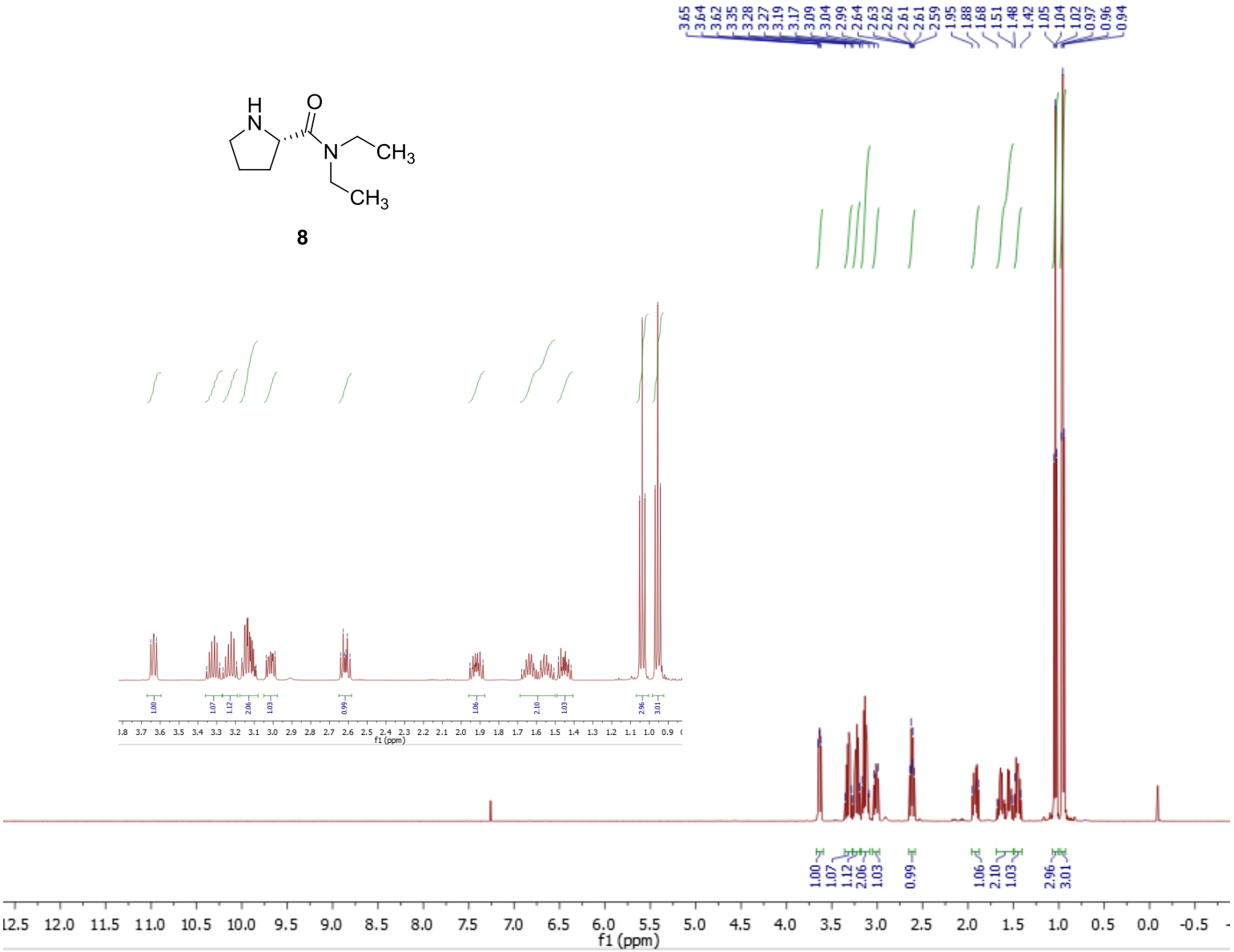

^{1}H NMR spectrum (500 MHz, $CDCl_3$) of (*S*)-*N*,*N*-diethylpyrrolidine-2-carboxamide (**8**).

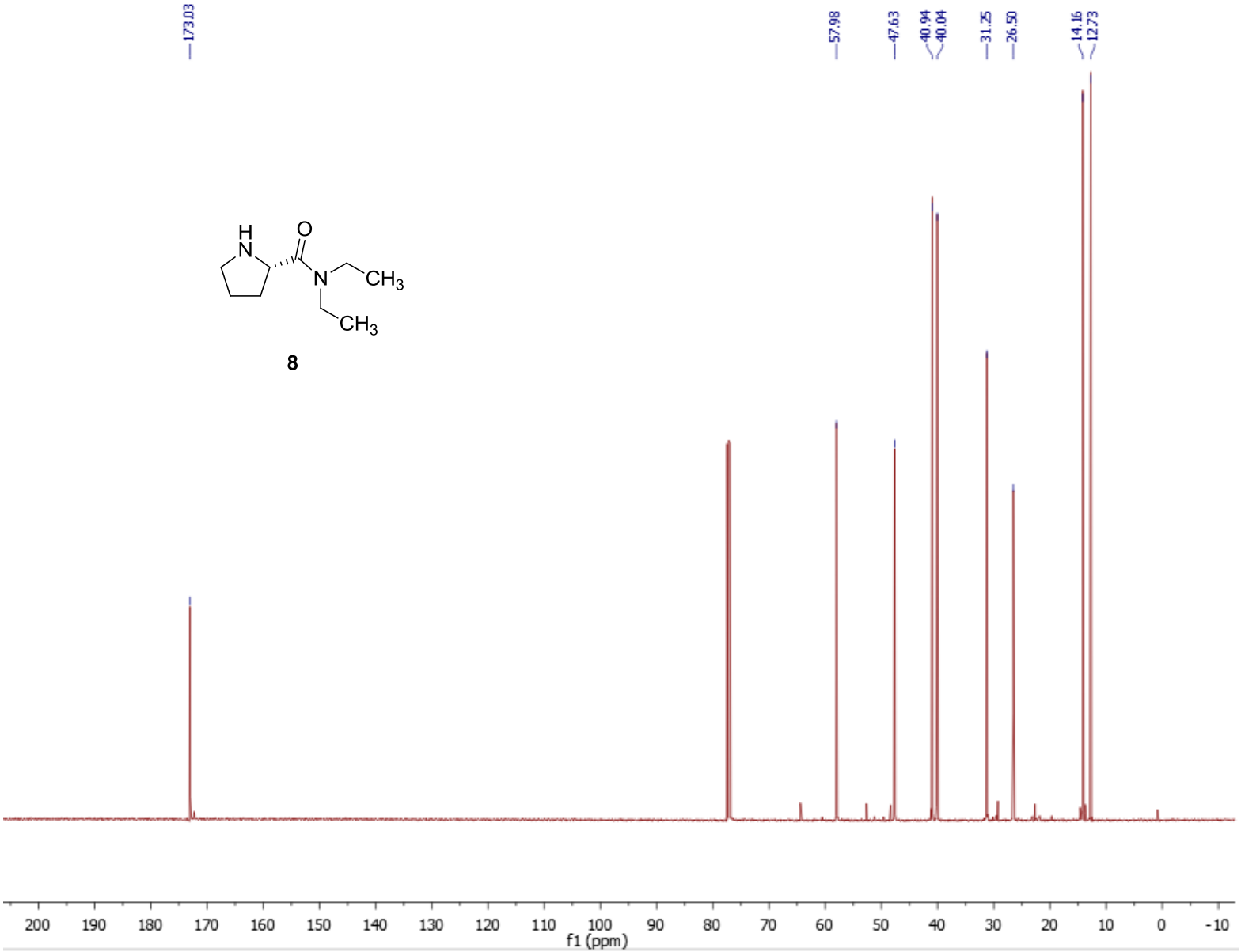

^{13}C NMR spectrum (125 MHz, $CDCl_3$) of (*S*)-*N*,*N*-diethylpyrrolidine-2-carboxamide (**8**).

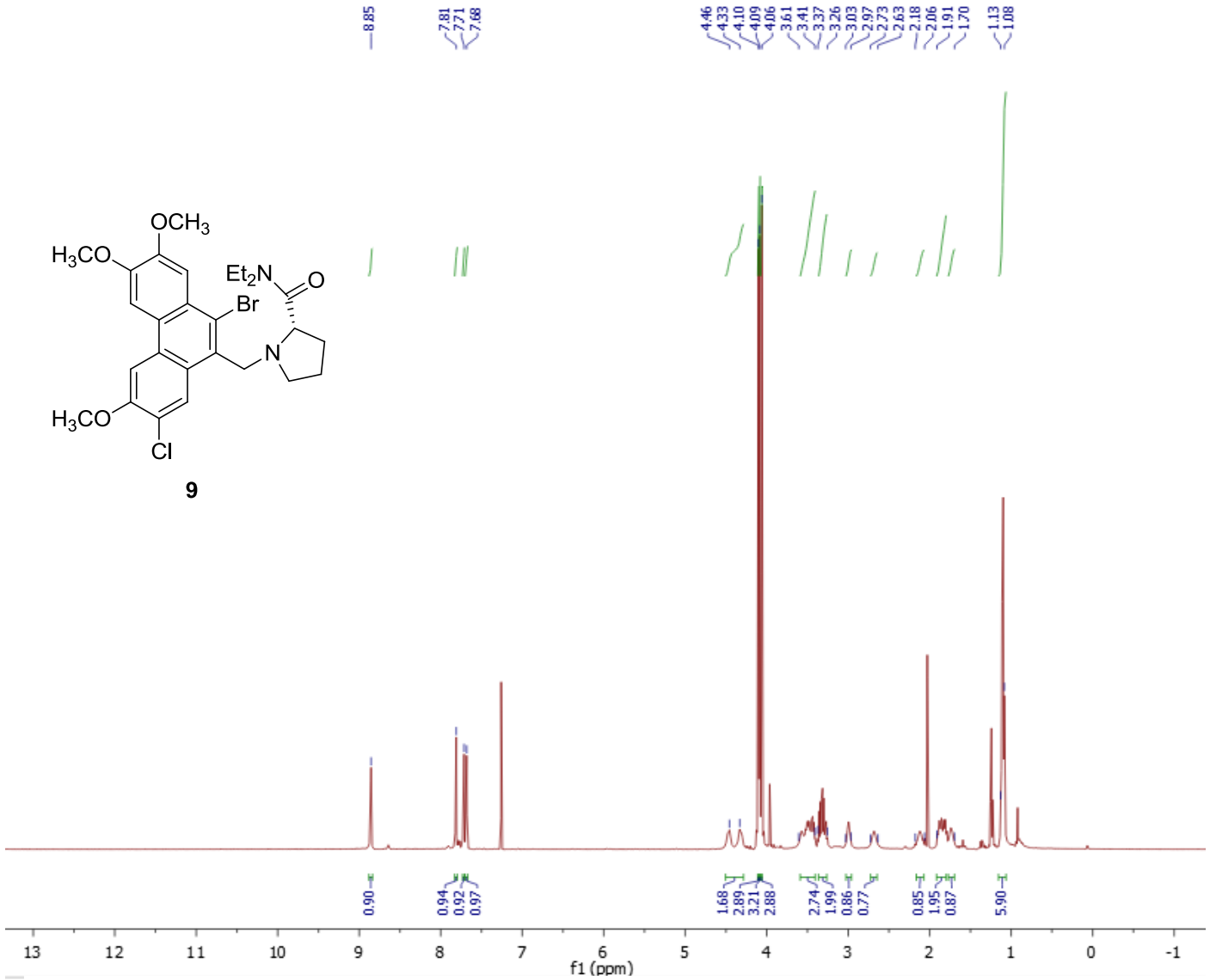

^{1}H NMR spectrum (500 MHz, $CDCl_3$) of (*S*)-1-((10-bromo-7-chloro-2,3,6-trimethoxyphenanthren-9-yl)methyl)-*N*,*N*-diethylpyrrolidine-2-carboxamide (**9**).

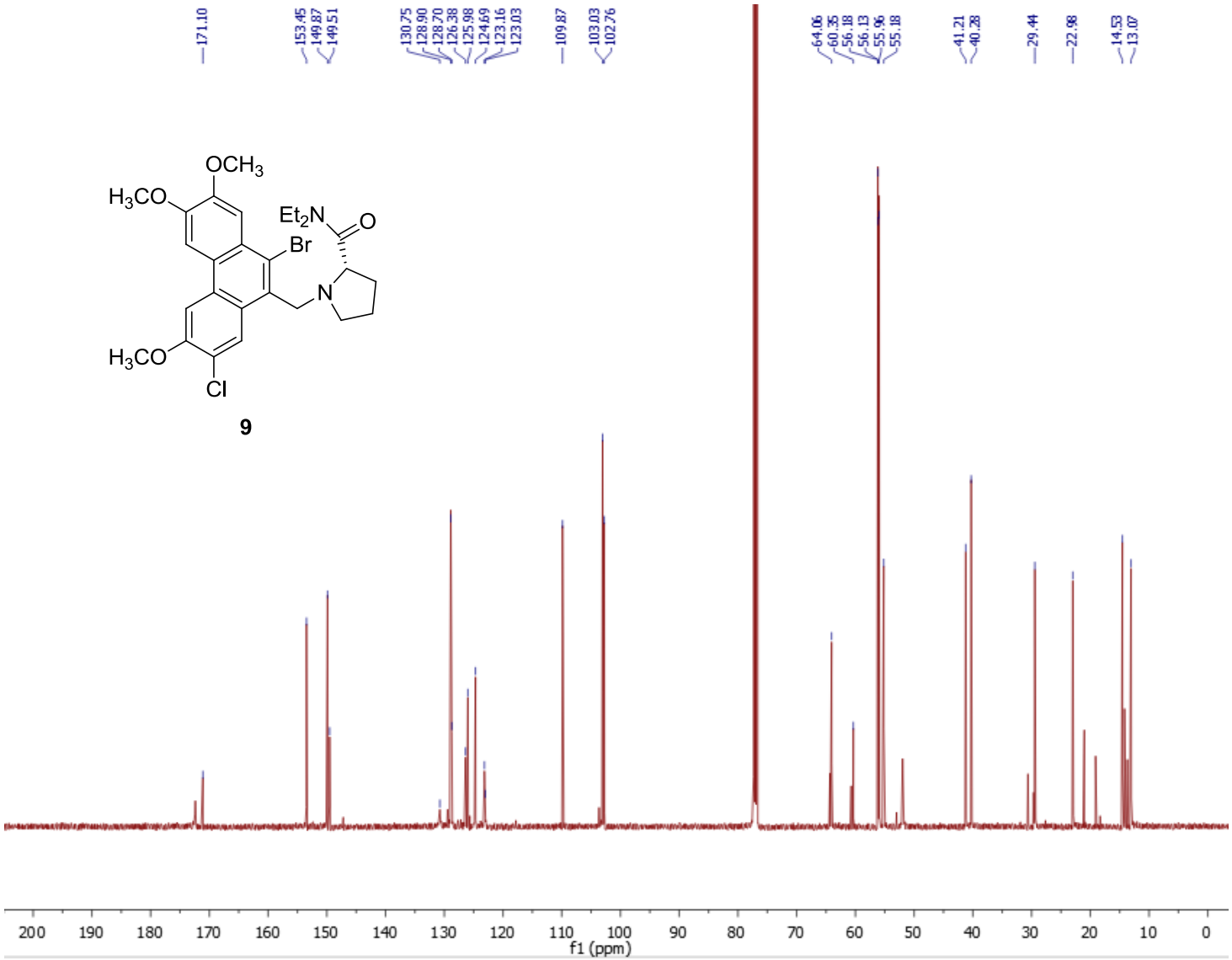

^{13}C NMR spectrum (125 MHz, $CDCl_3$) of (*S*)-1-((10-bromo-7-chloro-2,3,6-trimethoxyphenanthren-9-yl)methyl)-*N*,*N*-diethylpyrrolidine-2-carboxamide (**9**).

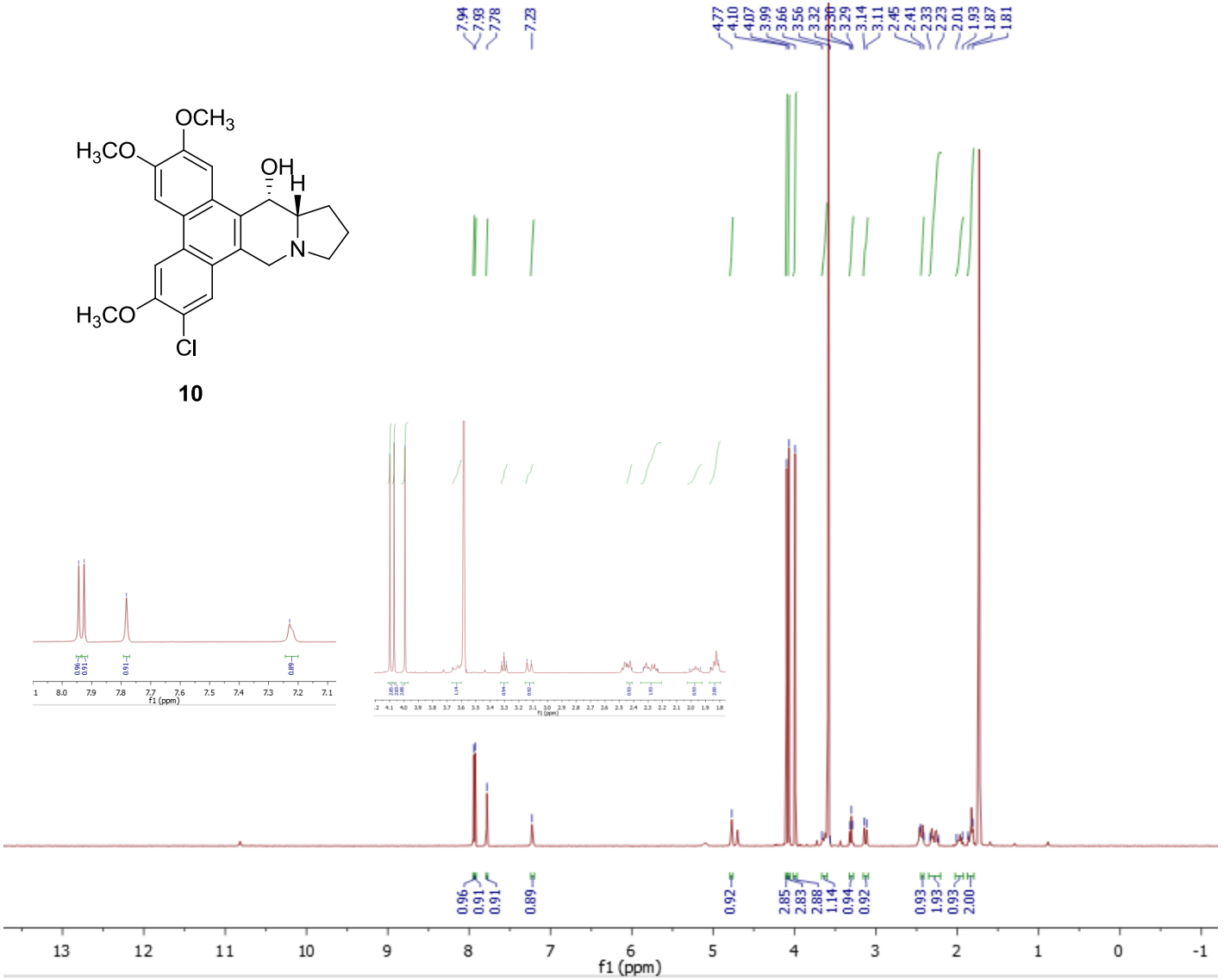

^{1}H NMR spectrum (500 MHz, THF-d_8) of (13a*S*,14*S*)-7-chloro-2,3,6-trimethoxy-9,11,12,13,13a,14-hexahydrodibenzo[*f*,*h*]pyrrolo[1,2-*b*]isoquinolin-14-ol (**10**).

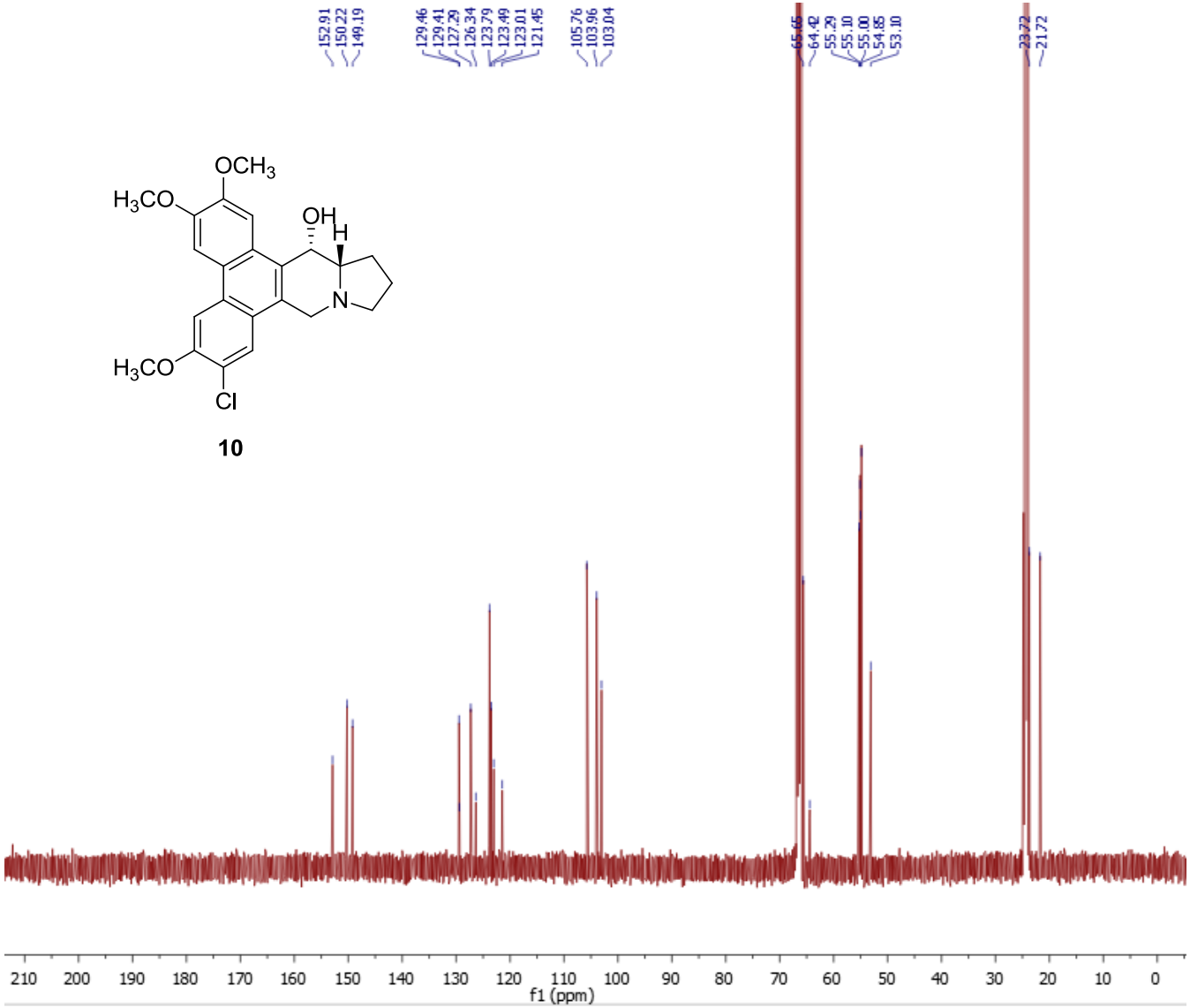

^{13}C NMR spectrum (125 MHz, THF-d_8) of (13a*S*,14*S*)-7-chloro-2,3,6-trimethoxy-9,11,12,13,13a,14-hexahydrodibenzo[*f*,*h*]pyrrolo[1,2-*b*]isoquinolin-14-ol (**10**).

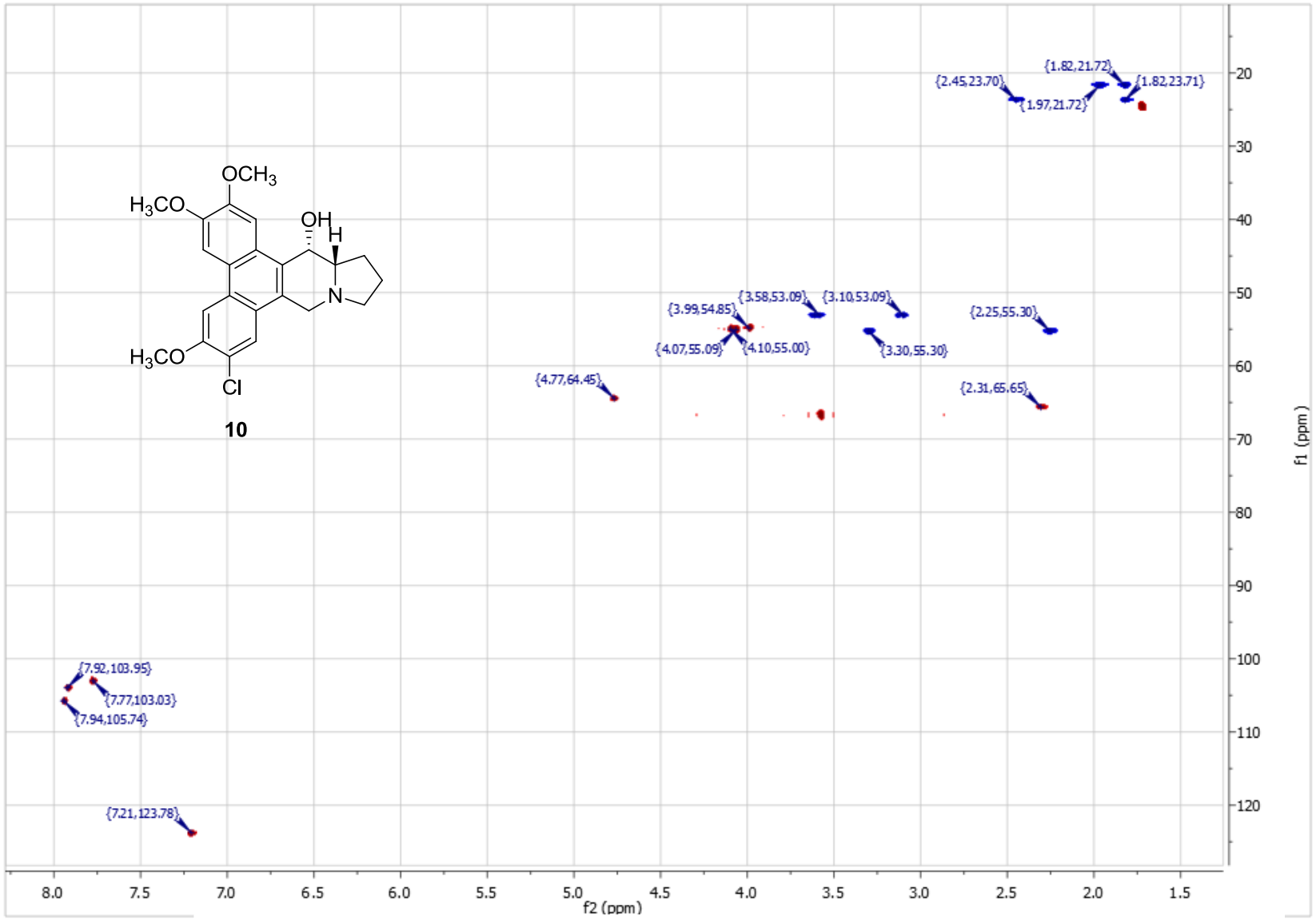

^{1}H-^{13}C HSQC NMR spectrum (500 MHz, THF-d_8) of (13a*S*,14*S*)-7-chloro-2,3,6-trimethoxy-9,11,12,13,13a,14-hexahydrodibenzo[*f*,*h*]pyrrolo[1,2-*b*]isoquinolin-14-ol (**10**).

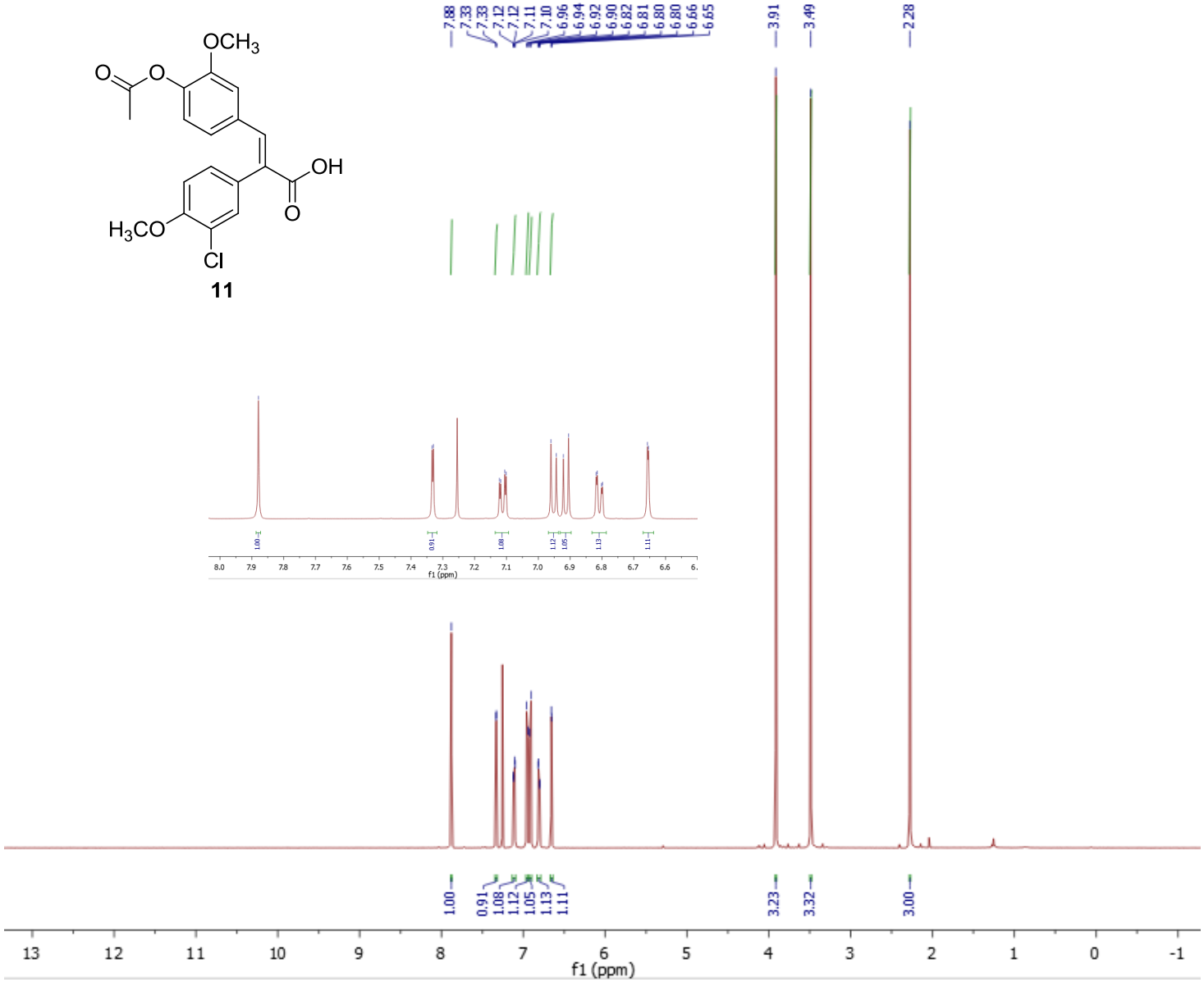

^{1}H NMR spectrum (500 MHz, $CDCl_3$) of (*E*)-3-(4-acetoxy-3-methoxyphenyl)-2-(3-chloro-4-methoxyphenyl)acrylic acid (**11**).

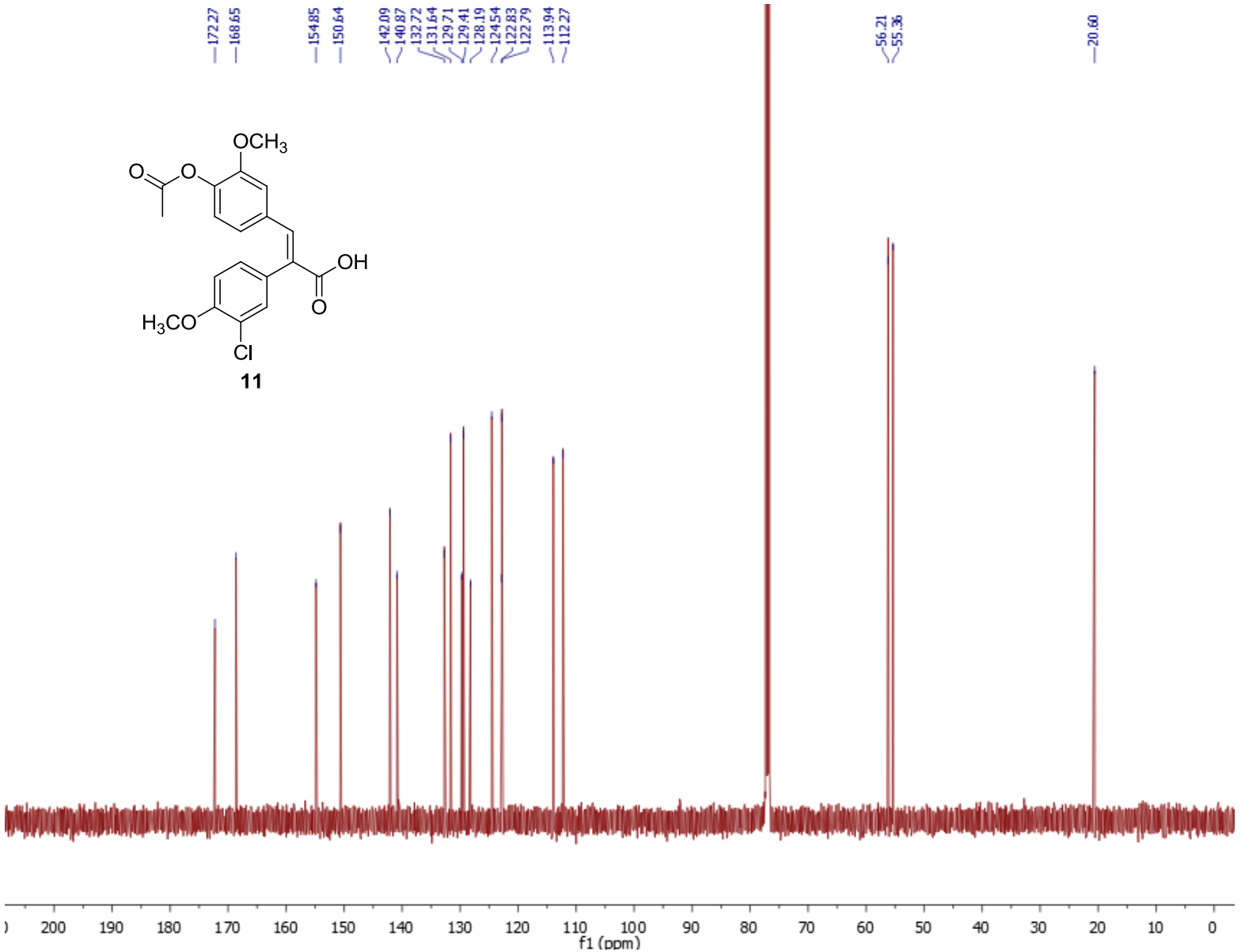

^{13}C NMR spectrum (125 MHz, $CDCl_3$) of (*E*)-3-(4-acetoxy-3-methoxyphenyl)-2-(3-chloro-4-methoxyphenyl)acrylic acid (**11**).

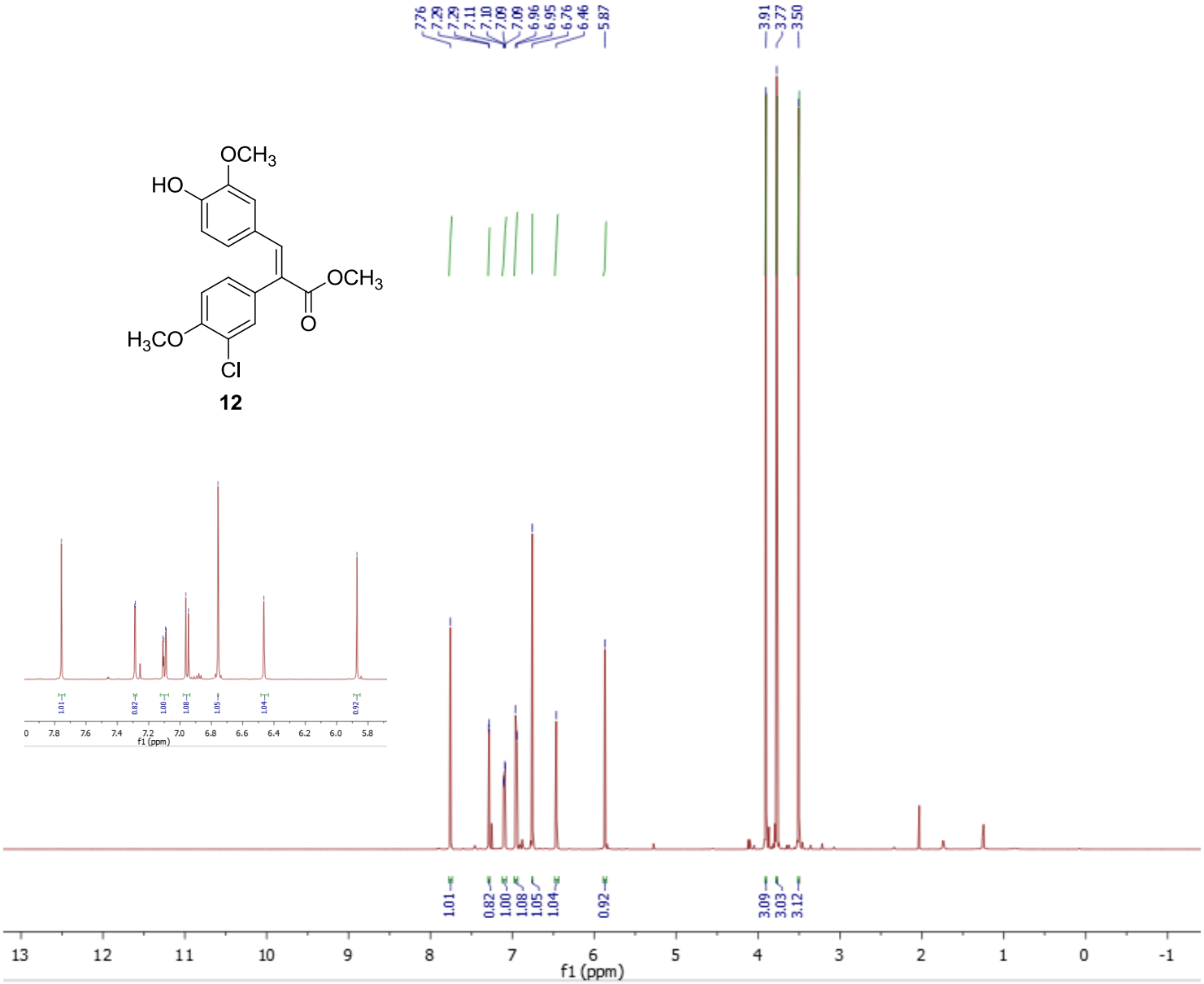

^{1}H NMR spectrum (500 MHz, $CDCl_3$) of (*E*)-methyl 2-(3-chloro-4-methoxyphenyl)-3-(4-hydroxy-3-methoxyphenyl)acrylate (**12**).

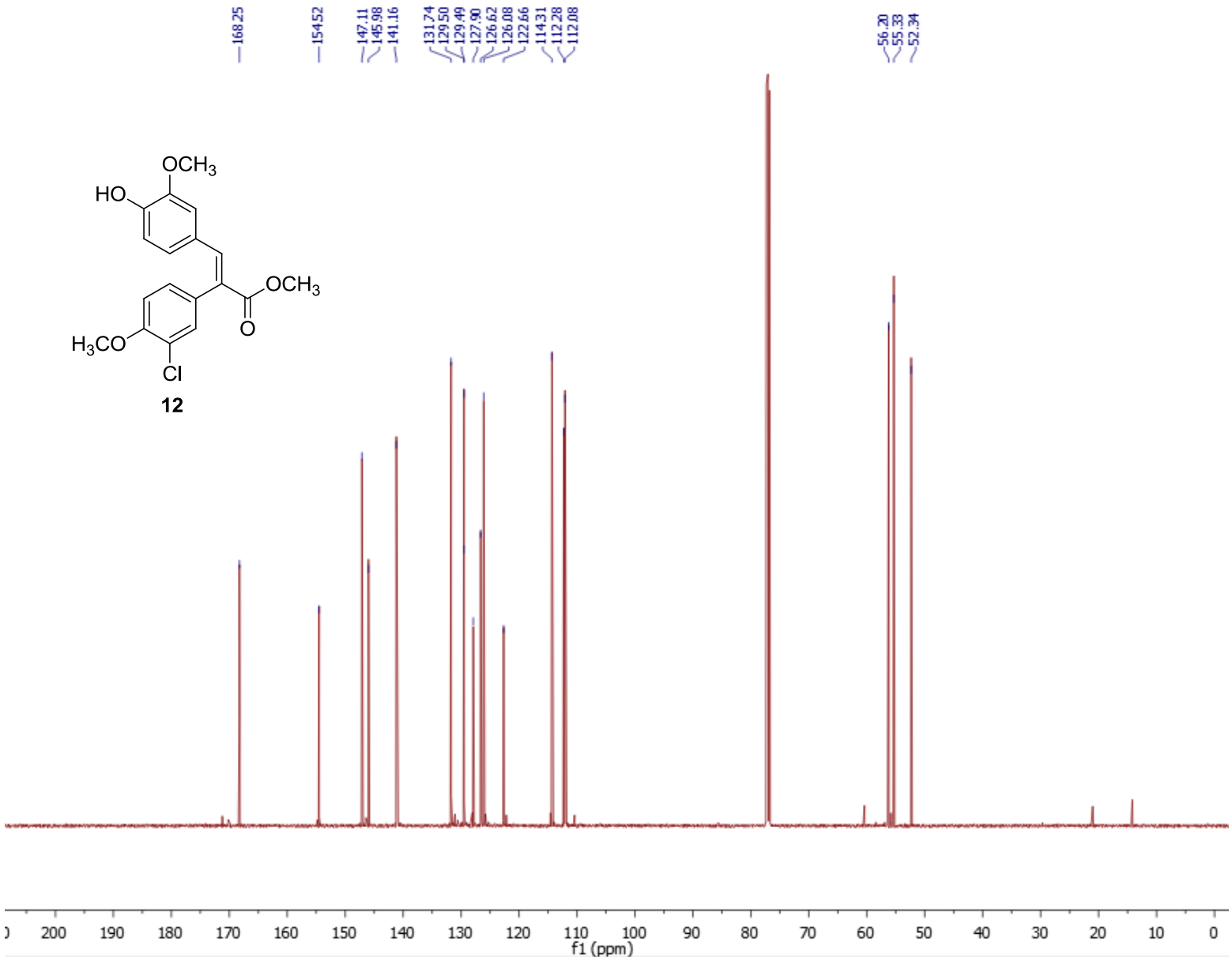

^{13}C NMR spectrum (125 MHz, $CDCl_3$) of (*E*)-methyl 2-(3-chloro-4-methoxyphenyl)-3-(4-hydroxy-3-methoxyphenyl)acrylate (**12**).

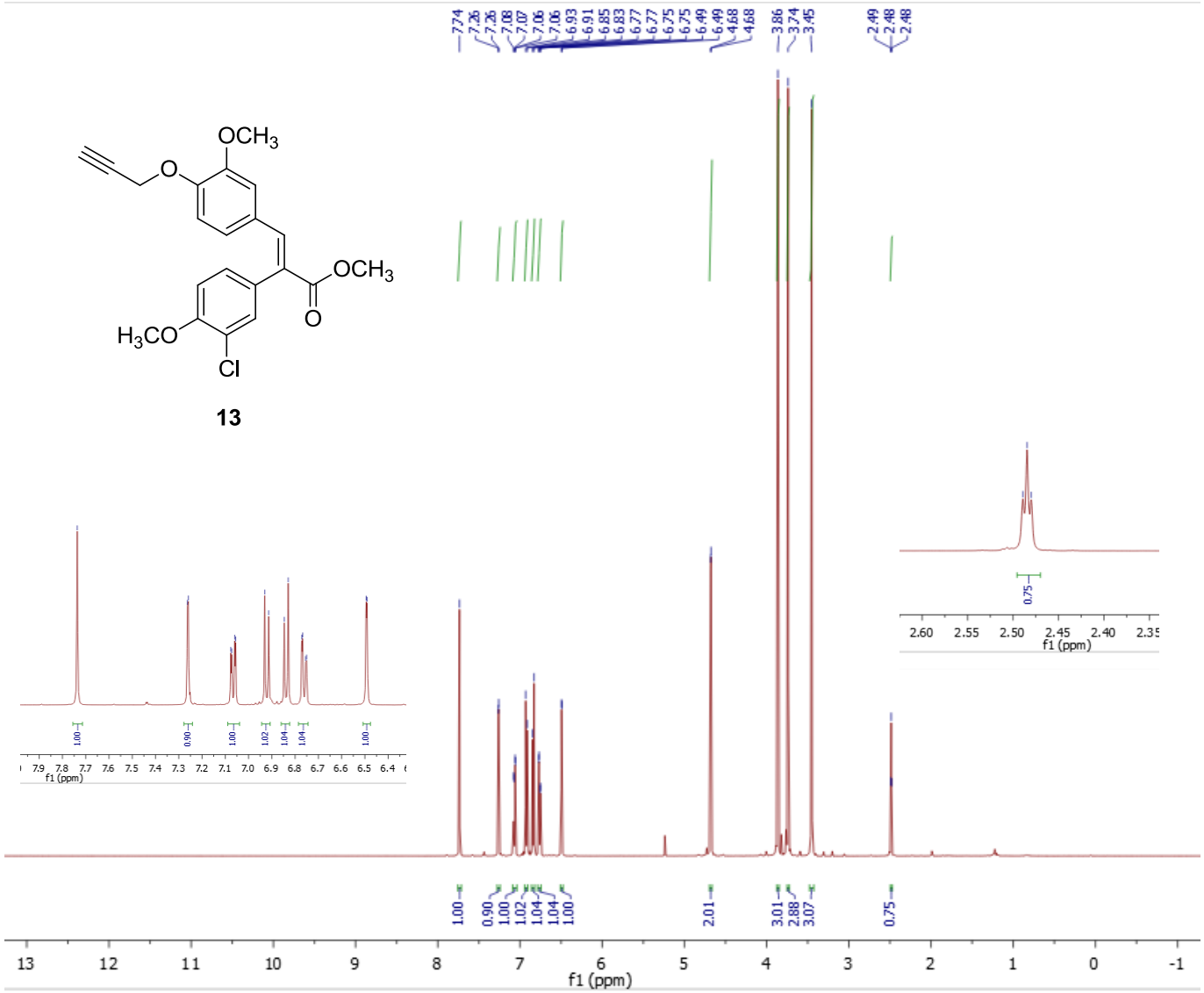

^{1}H NMR spectrum (500 MHz, $CDCl_3$) of (*E*)-methyl 2-(3-chloro-4-methoxyphenyl)-3-(3-methoxy-4-(prop-2-yn-1-yloxy)phenyl)acrylate (**13**).

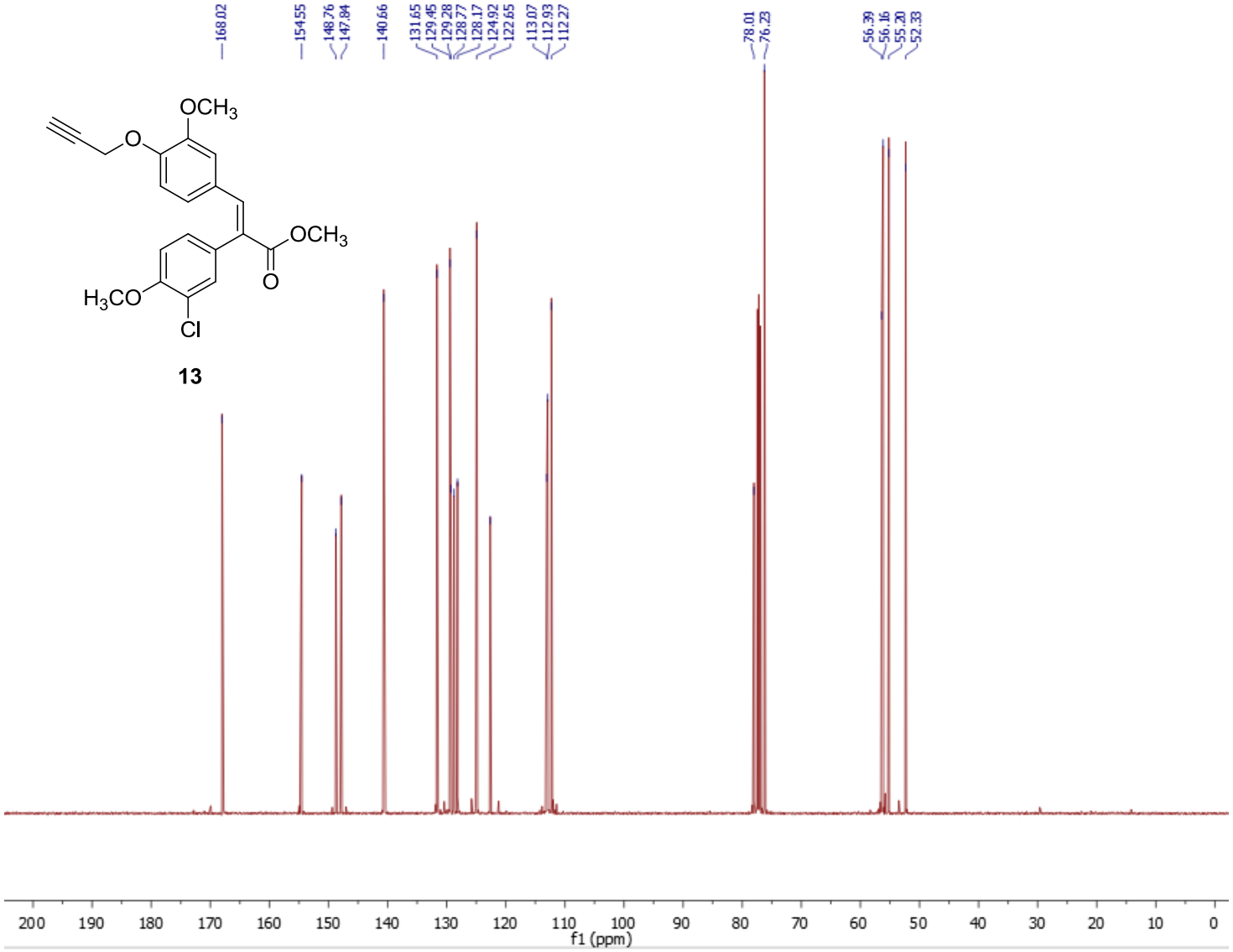

^{13}C NMR spectrum (125 MHz, $CDCl_3$) of (*E*)-methyl 2-(3-chloro-4-methoxyphenyl)-3-(3-methoxy-4-(prop-2-yn-1-yloxy)phenyl)acrylate (**13**).

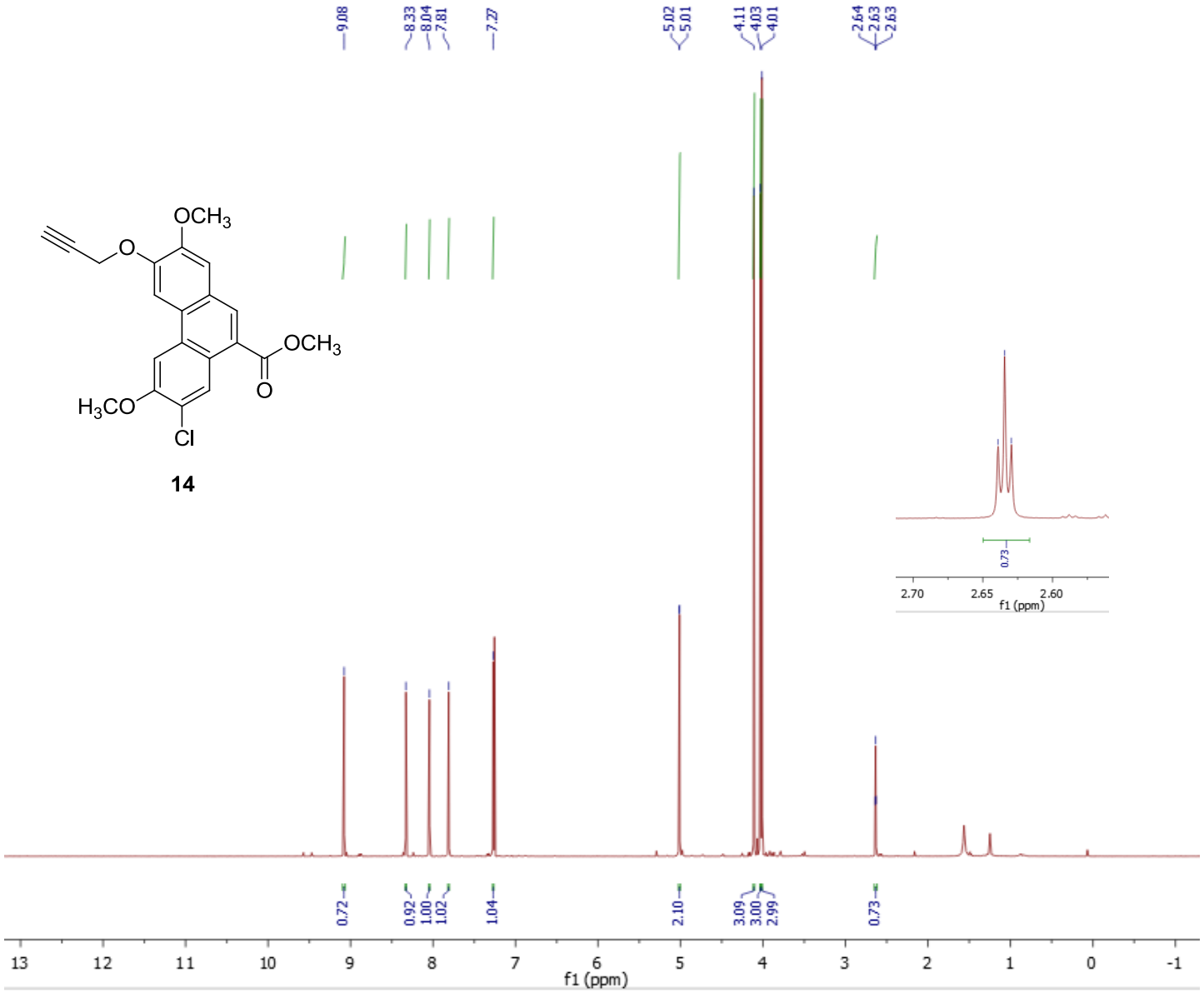

^{1}H NMR spectrum (500 MHz, $CDCl_3$) of methyl 7-chloro-2,6-dimethoxy-3-(prop-2-yn-1-yloxy)phenanthrene-9-carboxylate (**14**).

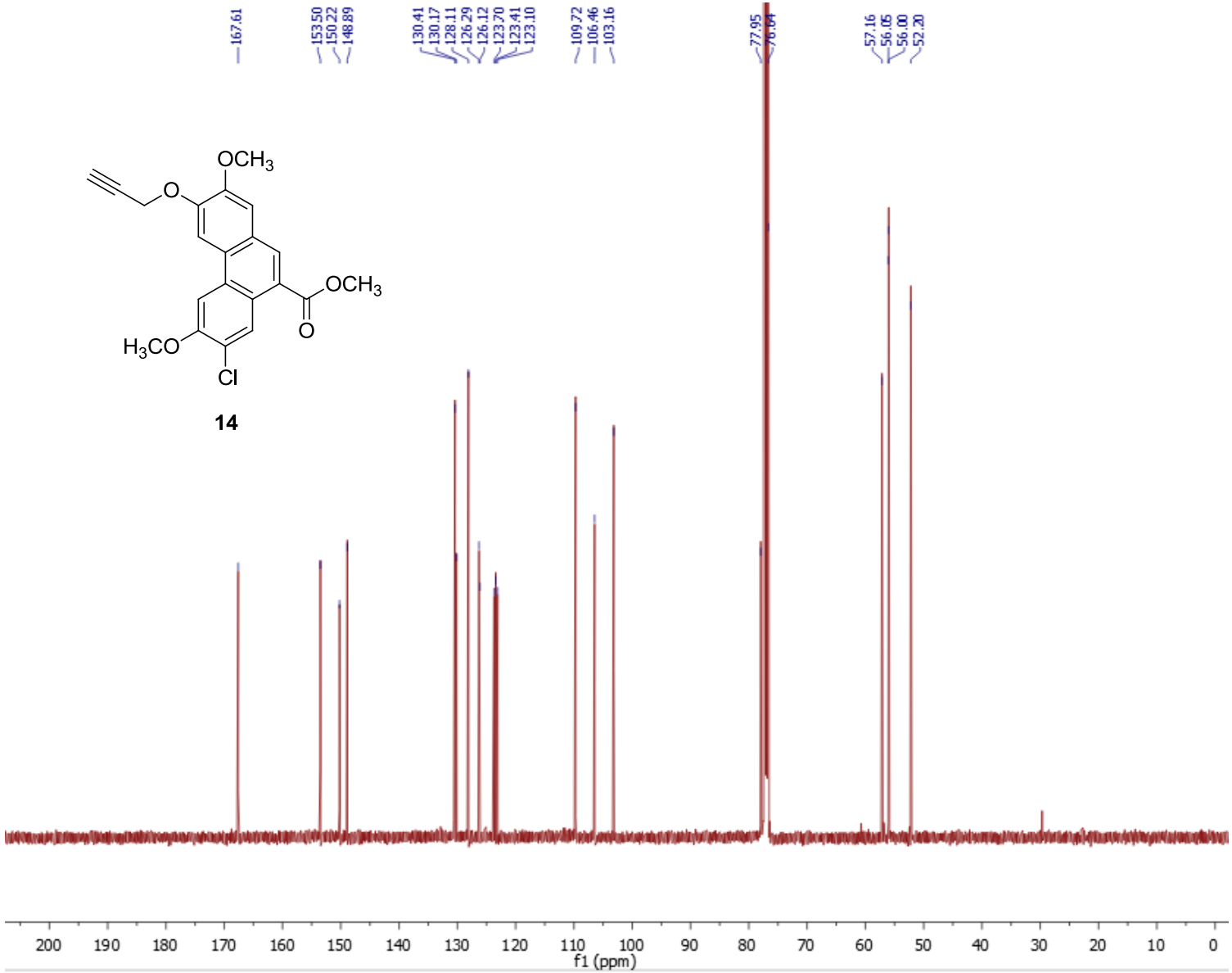

^{13}C NMR spectrum (125 MHz, $CDCl_3$) of methyl 7-chloro-2,6-dimethoxy-3-(prop-2-yn-1-yloxy)phenanthrene-9-carboxylate (**14**).

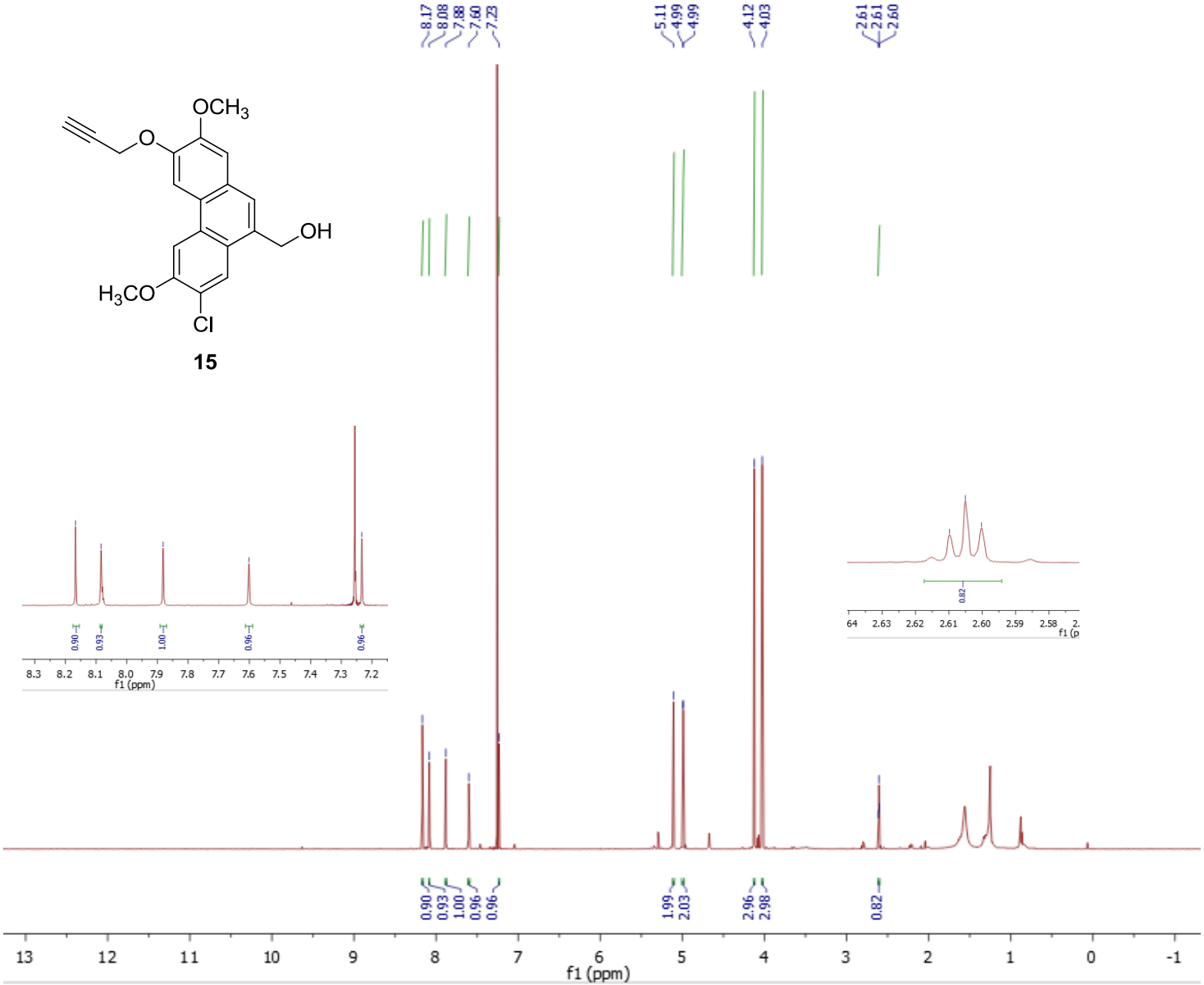

^{1}H NMR spectrum (500 MHz, $CDCl_3$) of (7-chloro-2,6-dimethoxy-3-(prop-2-yn-1-yloxy)phenanthren-9-yl)methanol (**15**).

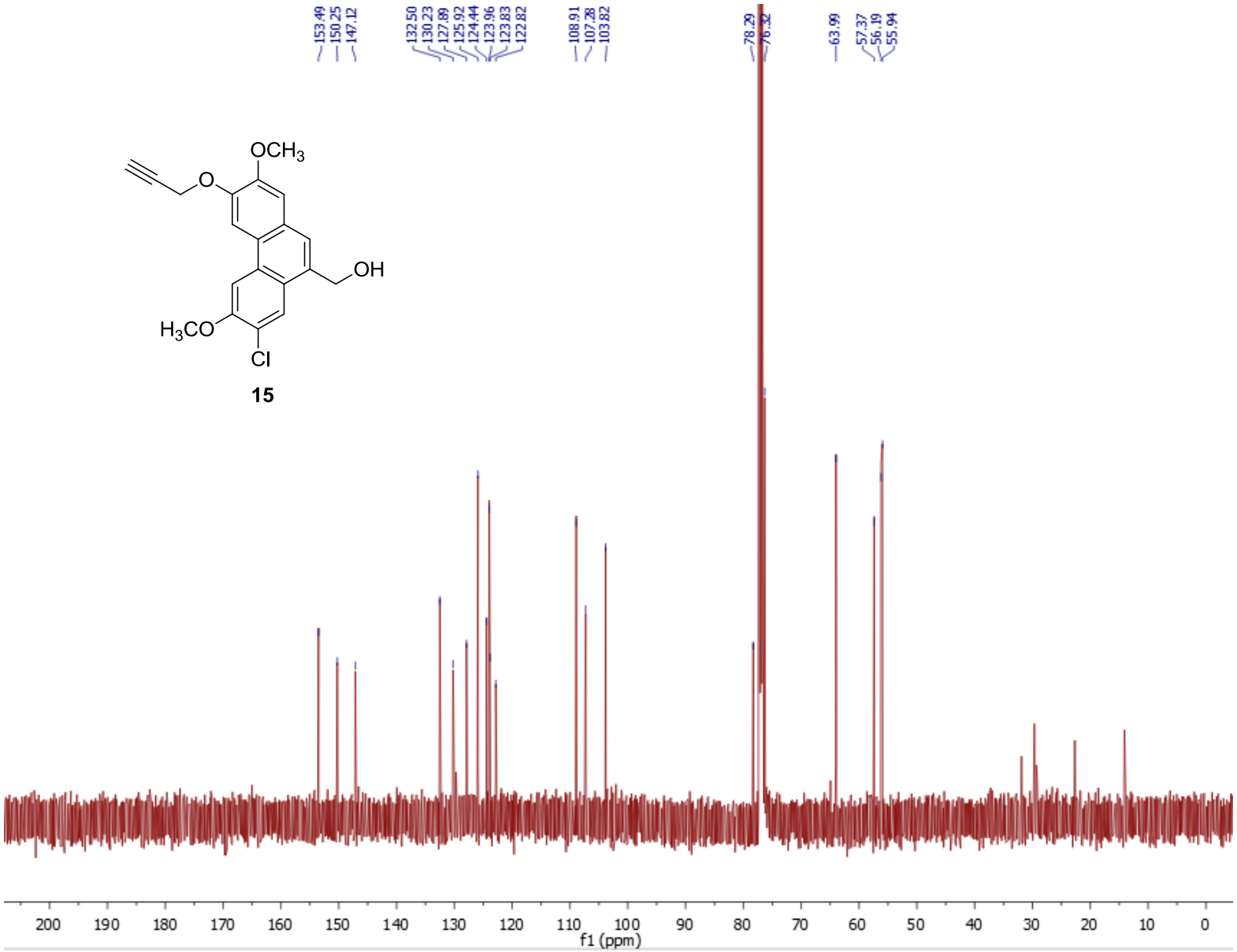

^{13}C NMR spectrum (125 MHz, $CDCl_3$) of (7-chloro-2,6-dimethoxy-3-(prop-2-yn-1-yloxy)phenanthren-9-yl)methanol (**15**).

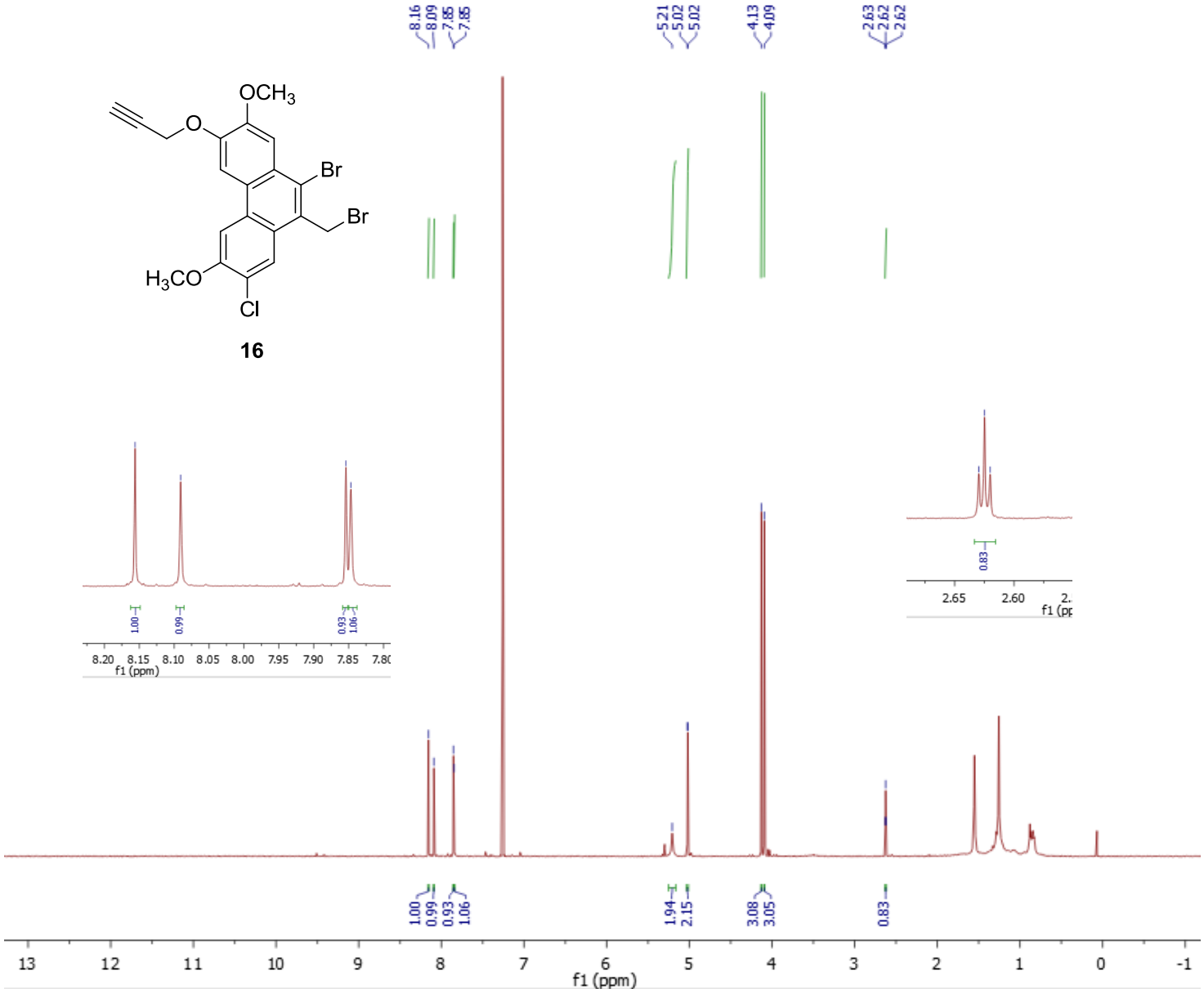

^{1}H NMR spectrum (500 MHz, $CDCl_3$) of 9-bromo-10-(bromomethyl)-2-chloro-3,7-dimethoxy-6-(prop-2-yn-1-yloxy)phenanthrene (**16**).

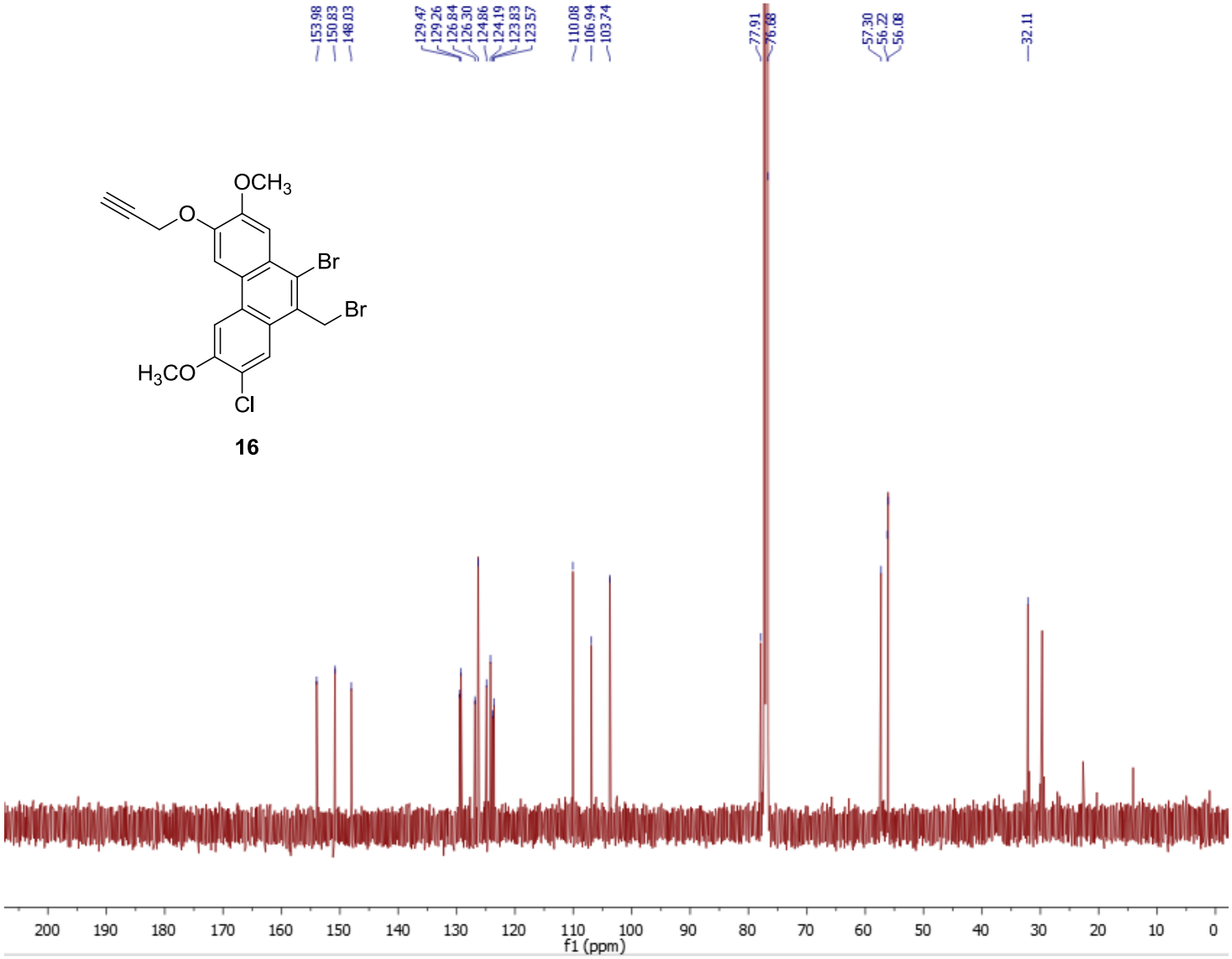

^{13}C NMR spectrum (125 MHz, $CDCl_3$) of 9-bromo-10-(bromomethyl)-2-chloro-3,7-dimethoxy-6-(prop-2-yn-1-yloxy)phenanthrene (**16**).

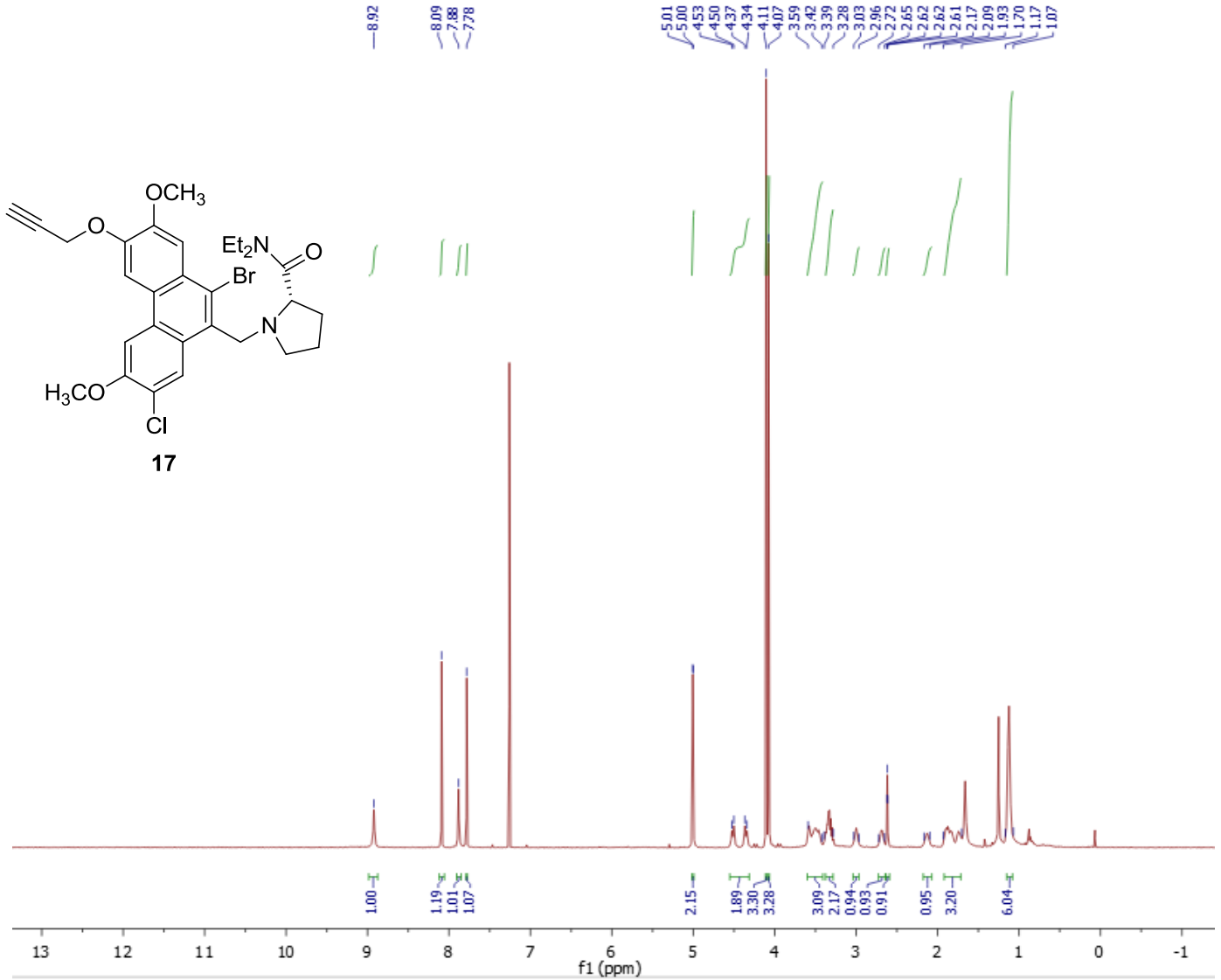

^{1}H NMR spectrum (500 MHz, $CDCl_3$) of (*S*)-1-((10-bromo-7-chloro-2,6-dimethoxy-3-(prop-2-yn-1-yloxy)phenanthren-9-yl)methyl)-*N*,*N*-diethylpyrrolidine-2-carboxamide (**17**).

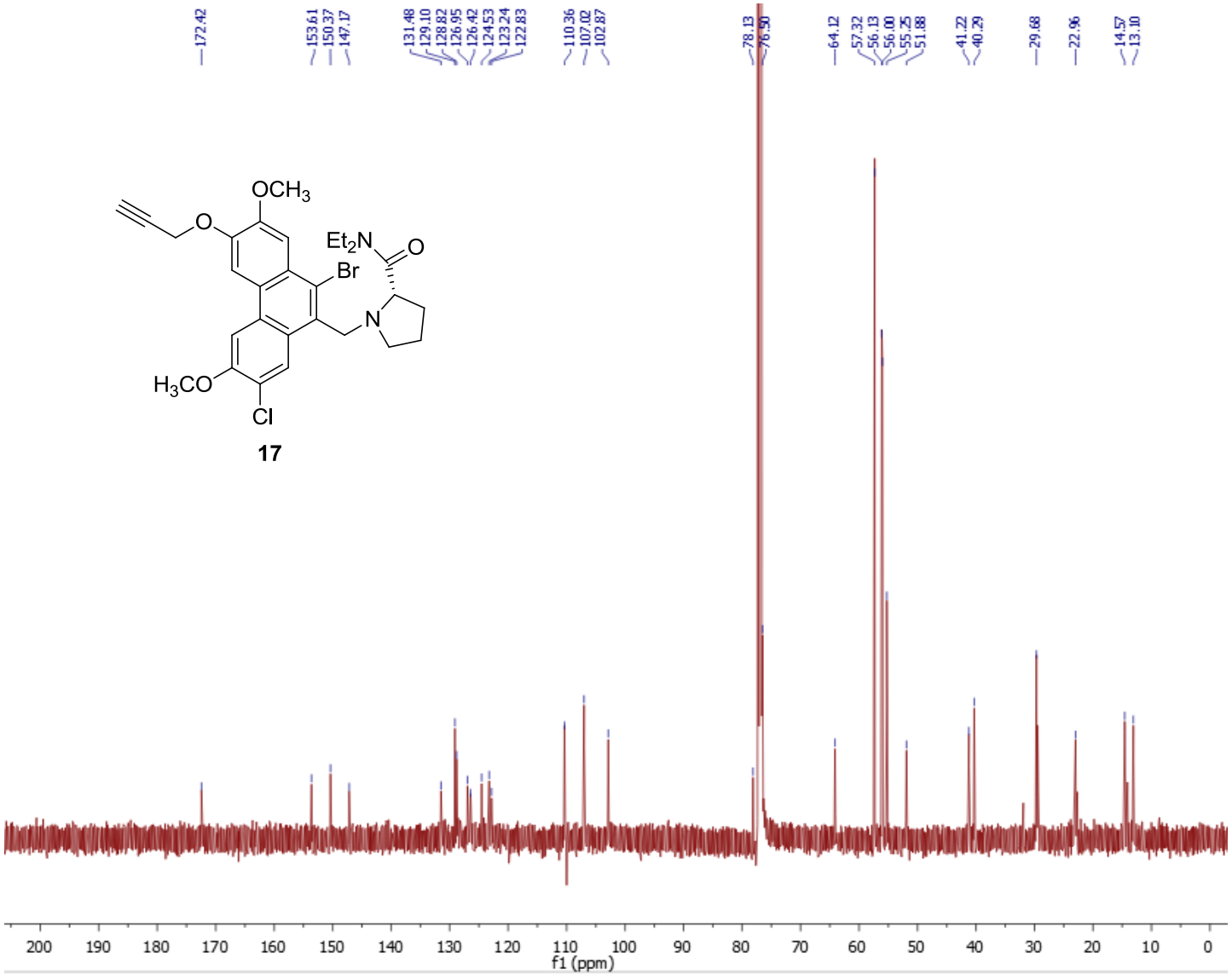

^{13}C NMR spectrum (125 MHz, $CDCl_3$) of (*S*)-1-((10-bromo-7-chloro-2,6-dimethoxy-3-(prop-2-yn-1-yloxy)phenanthren-9-yl)methyl)-*N*,*N*-diethylpyrrolidine-2-carboxamide (**17**).

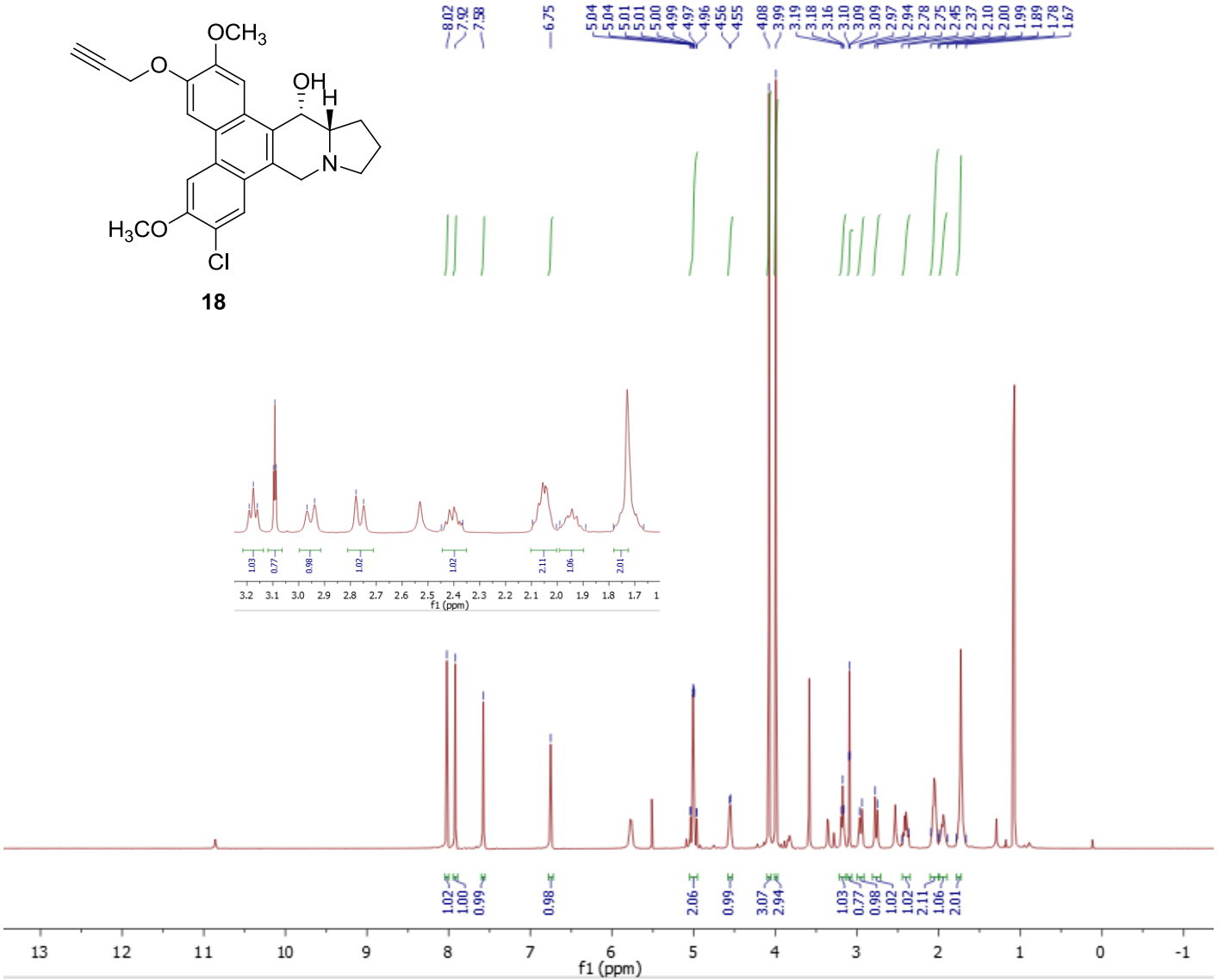

^{1}H NMR spectrum (500 MHz, THF-d_8) of (13a*S*,14*S*)-7-chloro-2,6-dimethoxy-3-(prop-2-yn-1-yloxy)-9,11,12,13,13a,14-hexahydrodibenzo[*f*,*h*]pyrrolo[1,2-*b*]isoquinolin-14-ol (**18**).

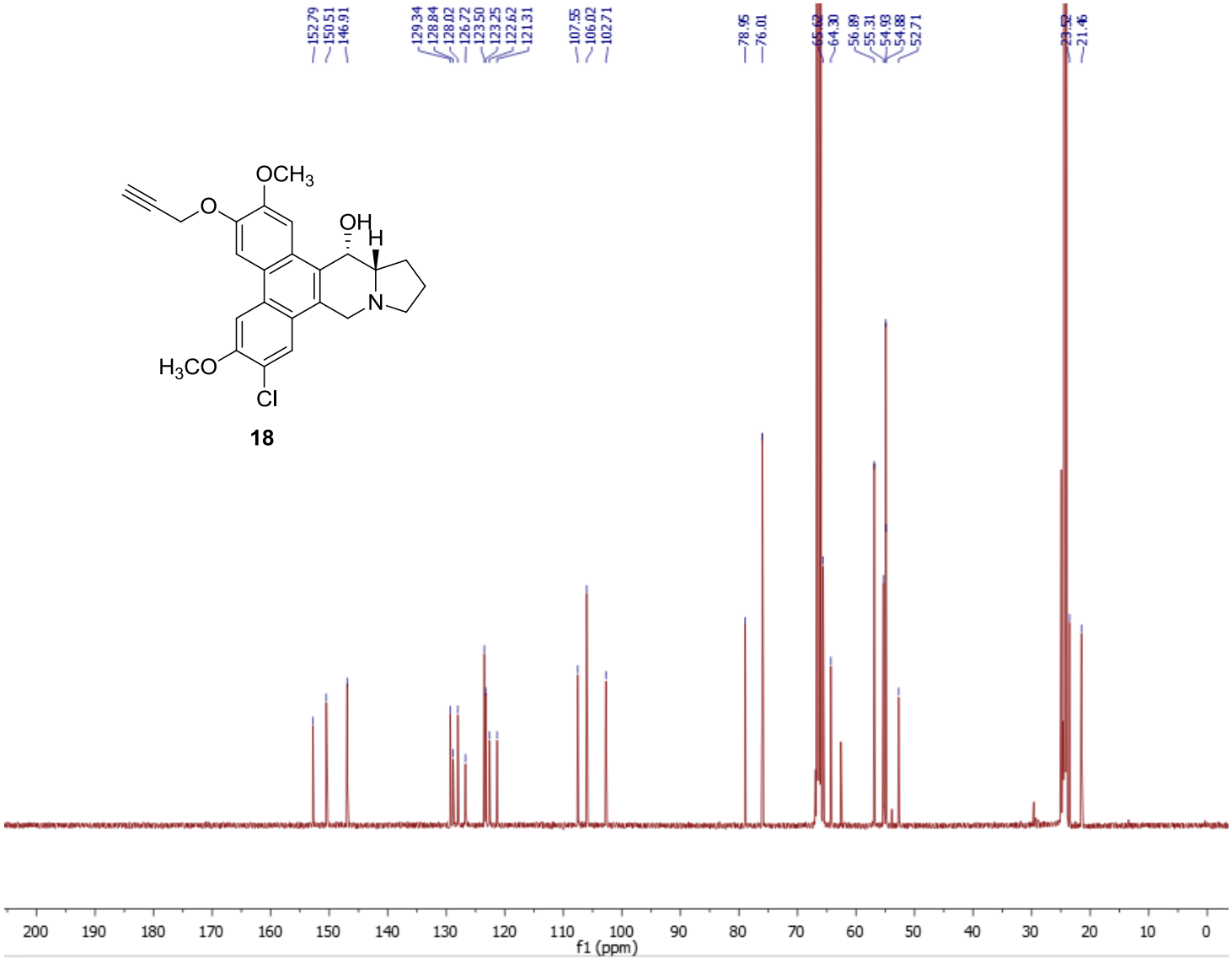

^{13}C NMR spectrum (125 MHz, THF-d_8) of (13a*S*,14*S*)-7-chloro-2,6-dimethoxy-3-(prop-2-yn-1-yloxy)-9,11,12,13,13a,14-hexahydrodibenzo[*f*,*h*]pyrrolo[1,2-*b*]isoquinolin-14-ol (**18**).

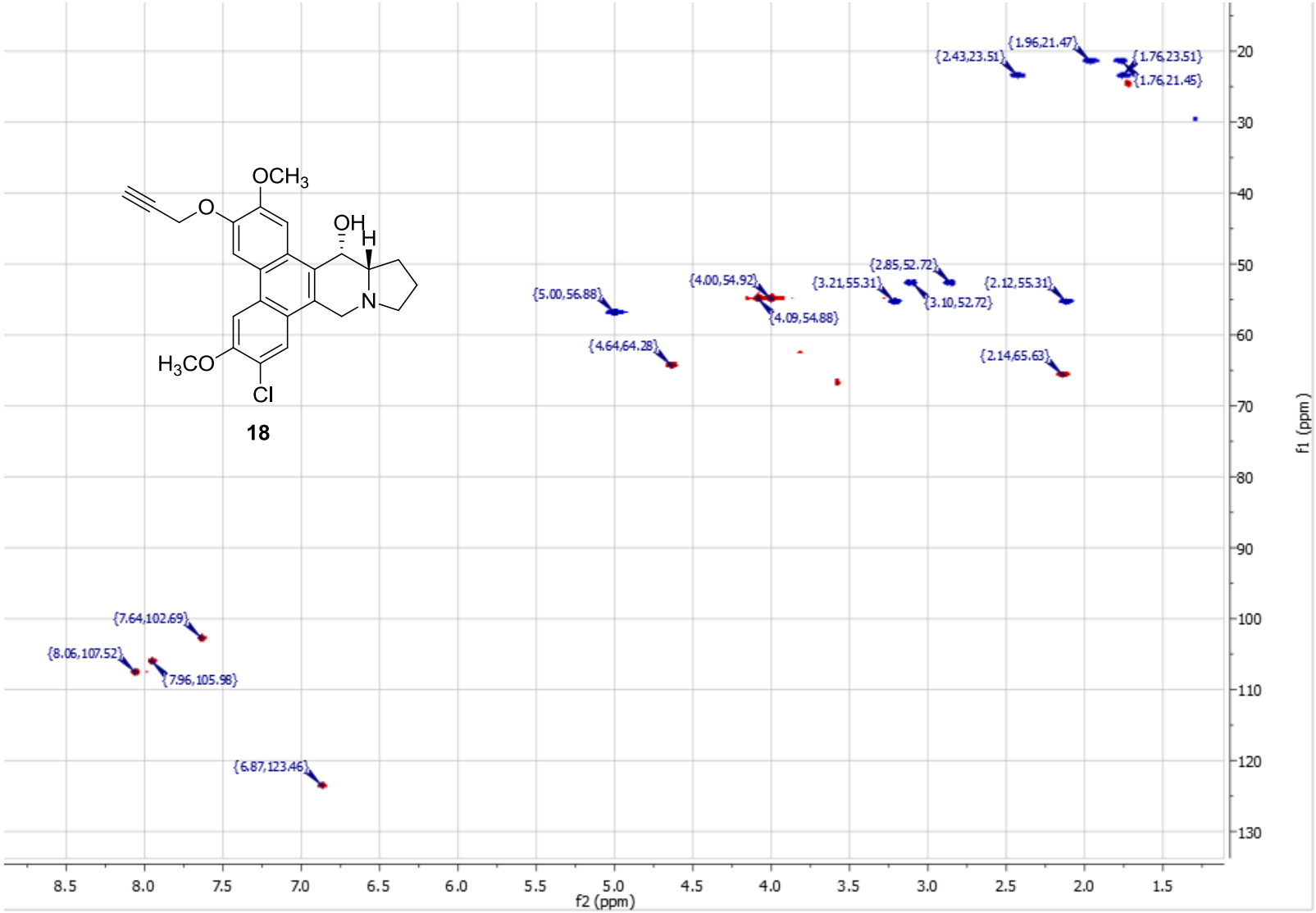

^{1}H-^{13}C HSQC NMR spectrum (500 MHz, THF-d_8) of (13a*S*,14*S*)-7-chloro-2,6-dimethoxy-3-(prop-2-yn-1-yloxy)-9,11,12,13,13a,14-hexahydrodibenzo[*f*,*h*]pyrrolo[1,2-*b*]isoquinolin-14-ol (**18**).

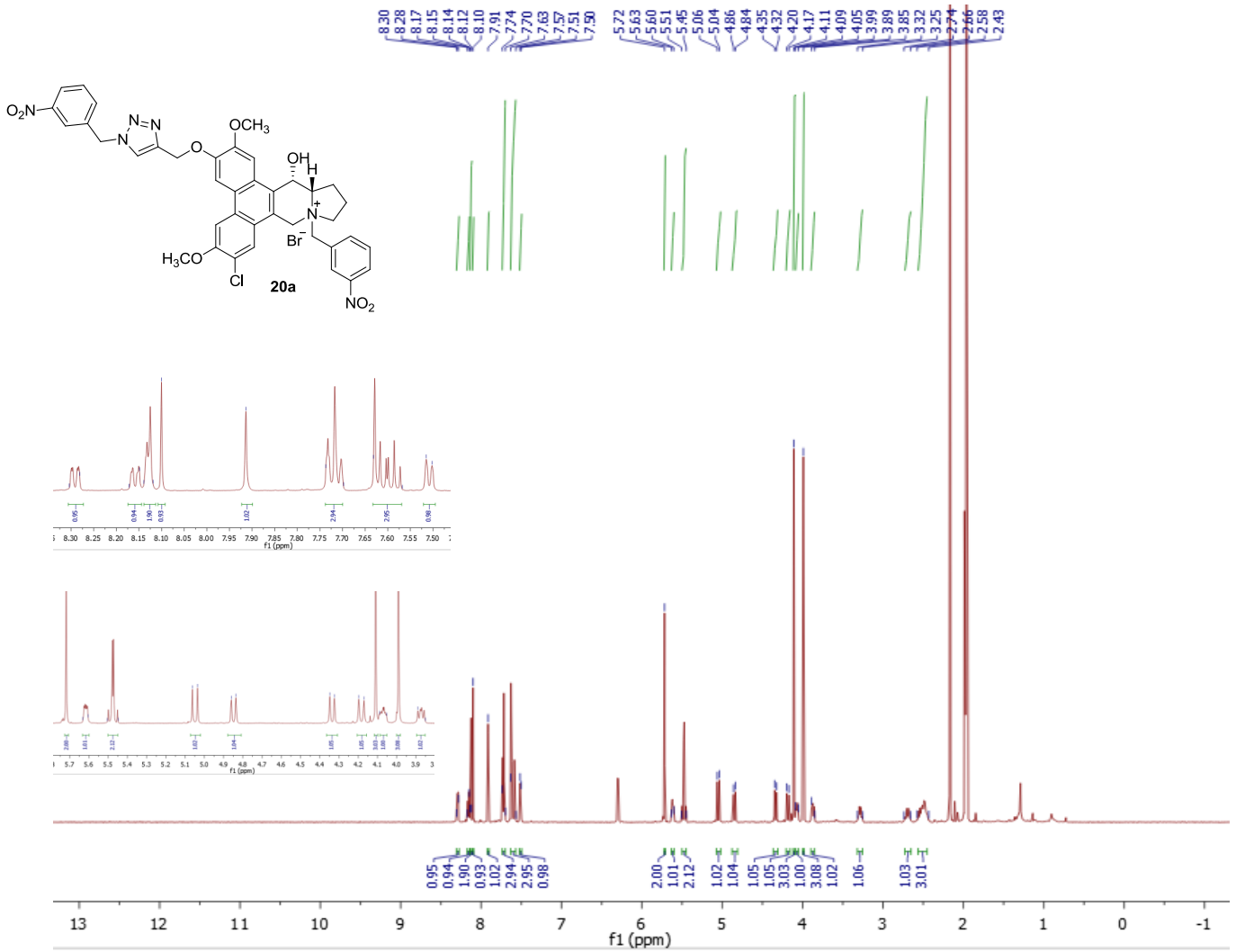

^{1}H NMR spectrum (600 MHz, CD_3CN) of (13a*S*,14*S*)-7-chloro-14-hydroxy-2,6-dimethoxy-10-(2-nitrobenzyl)-3-((1-(3-nitrobenzyl)-1H-1,2,3-triazol-4-yl)methoxy)-10,11,12,13,13a,14-hexahydro-9H-dibenzo[*f*,*h*]pyrrolo[1,2-*b*]isoquinolin-10-ium bromide (**20a**).

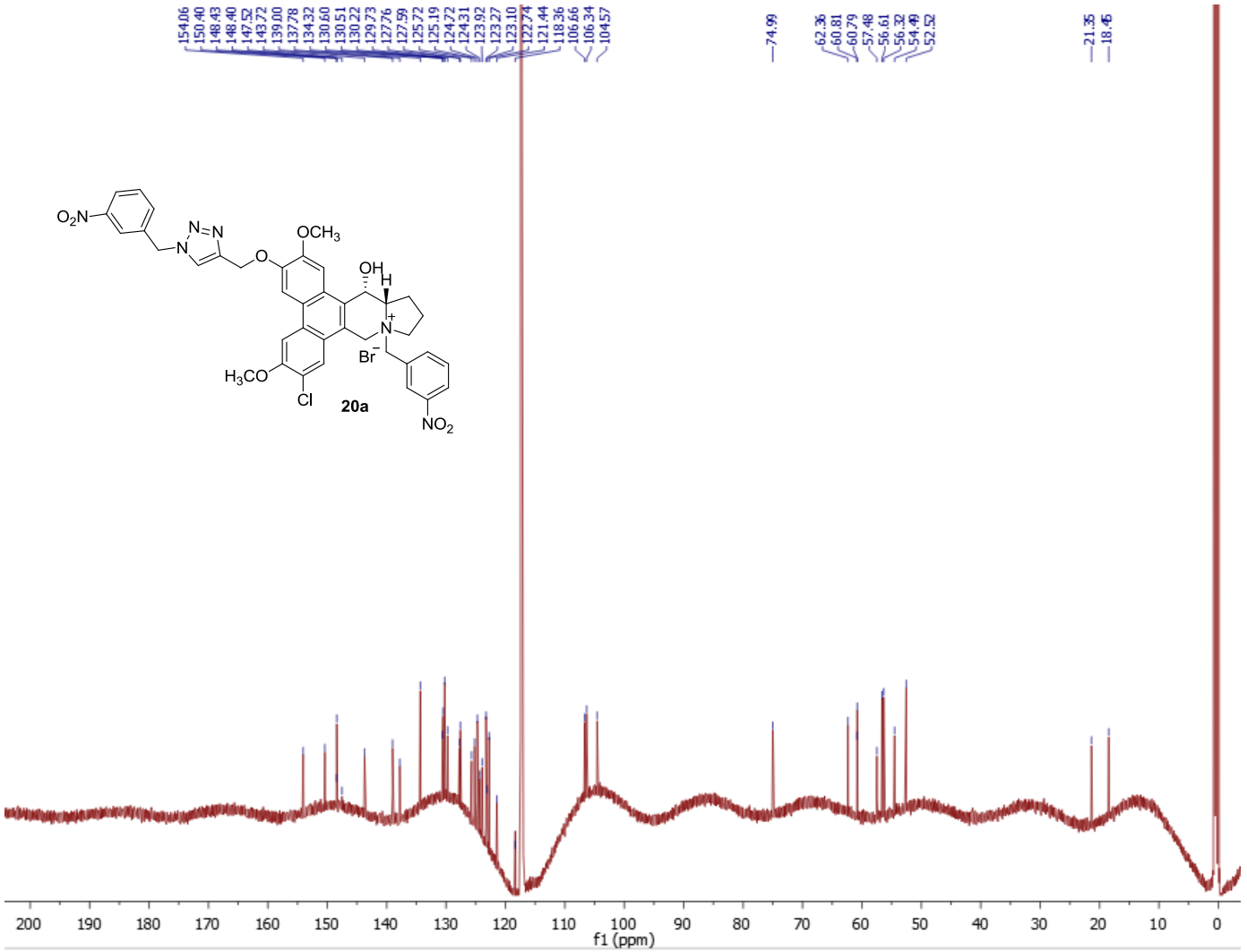

^{13}C NMR spectrum (150 MHz, CD_3CN) of (13a*S*,14*S*)-7-chloro-14-hydroxy-2,6-dimethoxy-10-(2-nitrobenzyl)-3-((1-(3-nitrobenzyl)-1H-1,2,3-triazol-4-yl)methoxy)-10,11,12,13,13a,14-hexahydro-9H-dibenzo[*f*,*h*]pyrrolo[1,2-*b*]isoquinolin-10-ium bromide (**20a**).

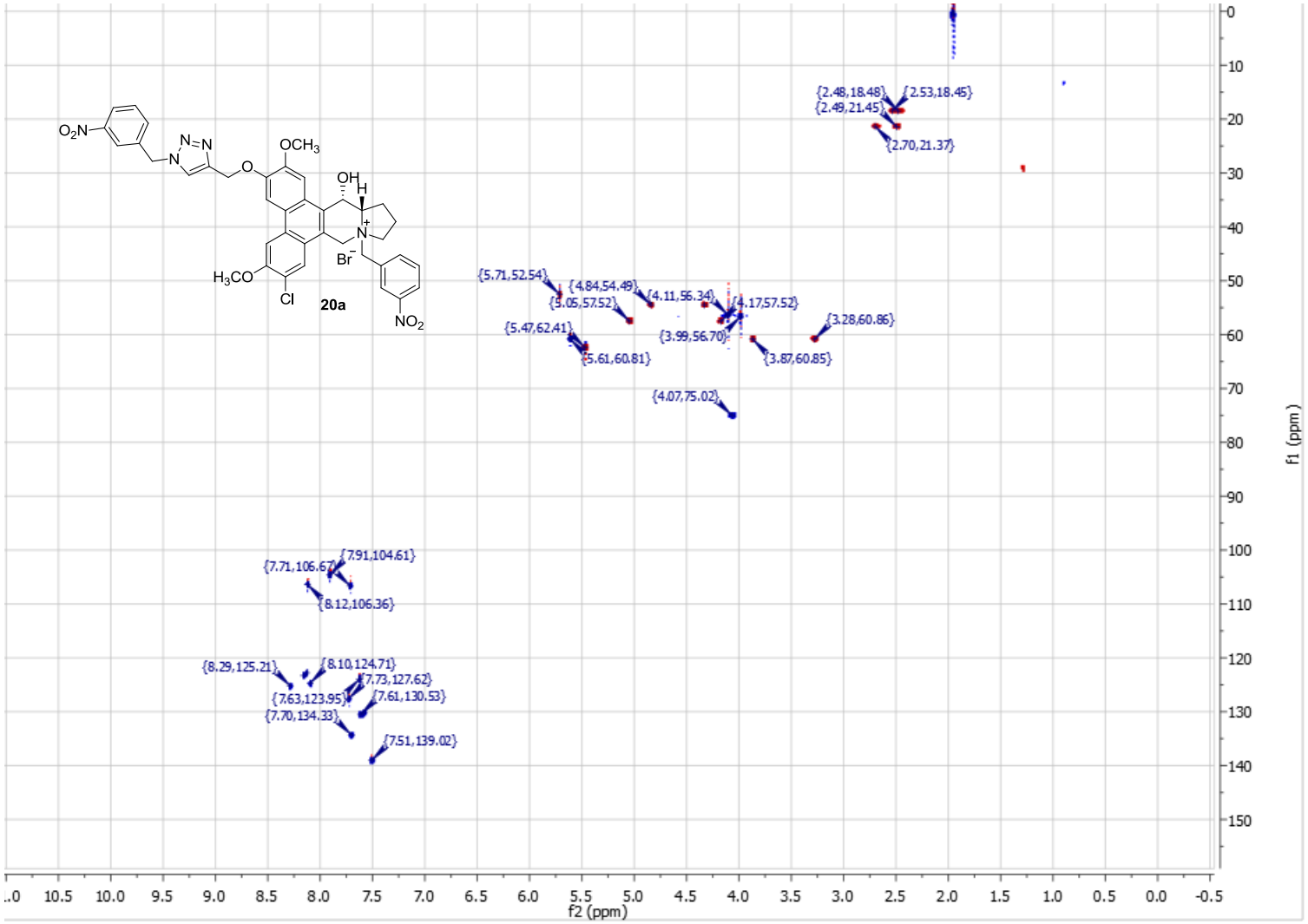

^{1}H-^{13}C HSQC NMR spectrum (600 MHz, CD_3CN) of (13a*S*,14*S*)-7-chloro-14-hydroxy-2,6-dimethoxy-10-(2-nitrobenzyl)-3-((1-(3-nitrobenzyl)-1H-1,2,3-triazol-4-yl)methoxy)-10,11,12,13,13a,14-hexahydro-9H-dibenzo[*f*,*h*]pyrrolo[1,2-*b*]isoquinolin-10-ium bromide (**20a**).

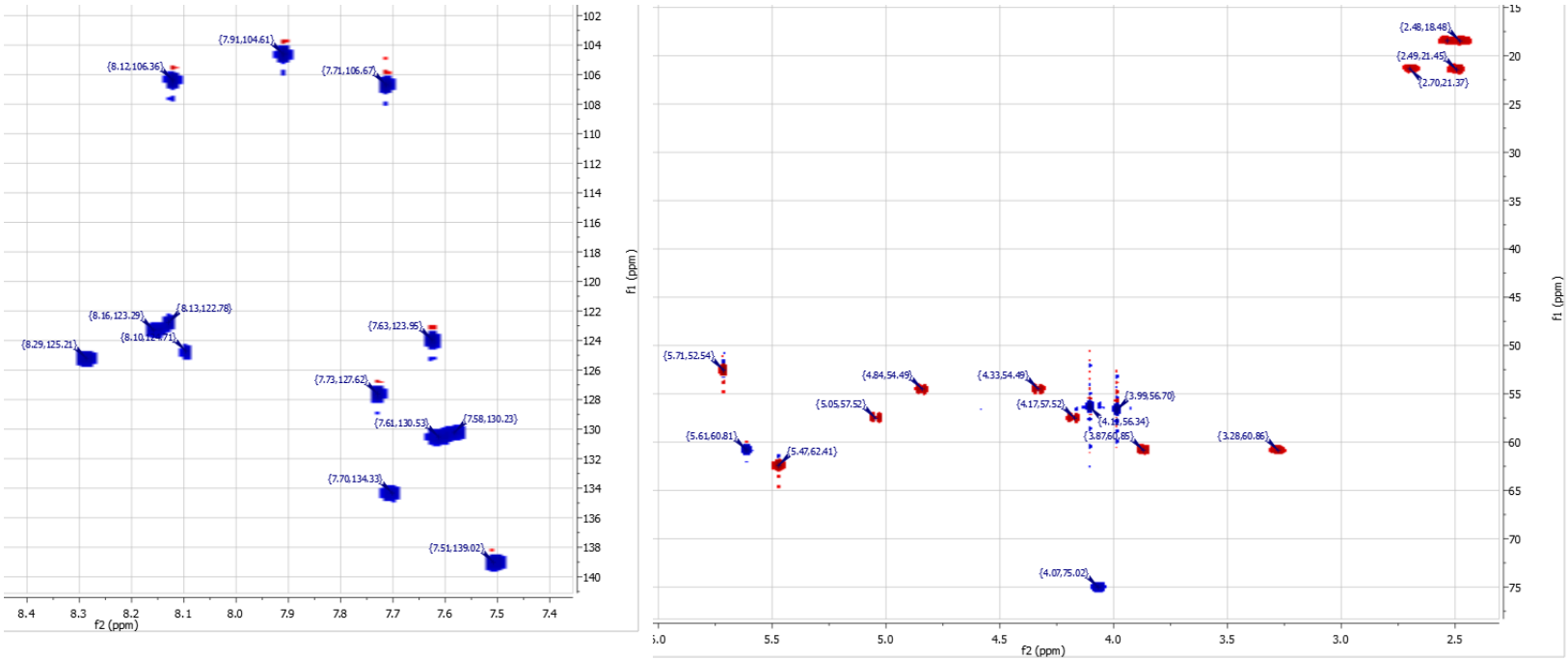

Detailed view of ^{1}H-^{13}C HSQC NMR spectrum (600 MHz, CD_3CN) of (13a*S*,14*S*)-7-chloro-14-hydroxy-2,6-dimethoxy-10-(2-nitrobenzyl)-3-((1-(3-nitrobenzyl)-1H-1,2,3-triazol-4-yl)methoxy)-10,11,12,13,13a,14-hexahydro-9H-dibenzo[*f*,*h*]pyrrolo[1,2-*b*]isoquinolin-10-ium bromide (**20a**).

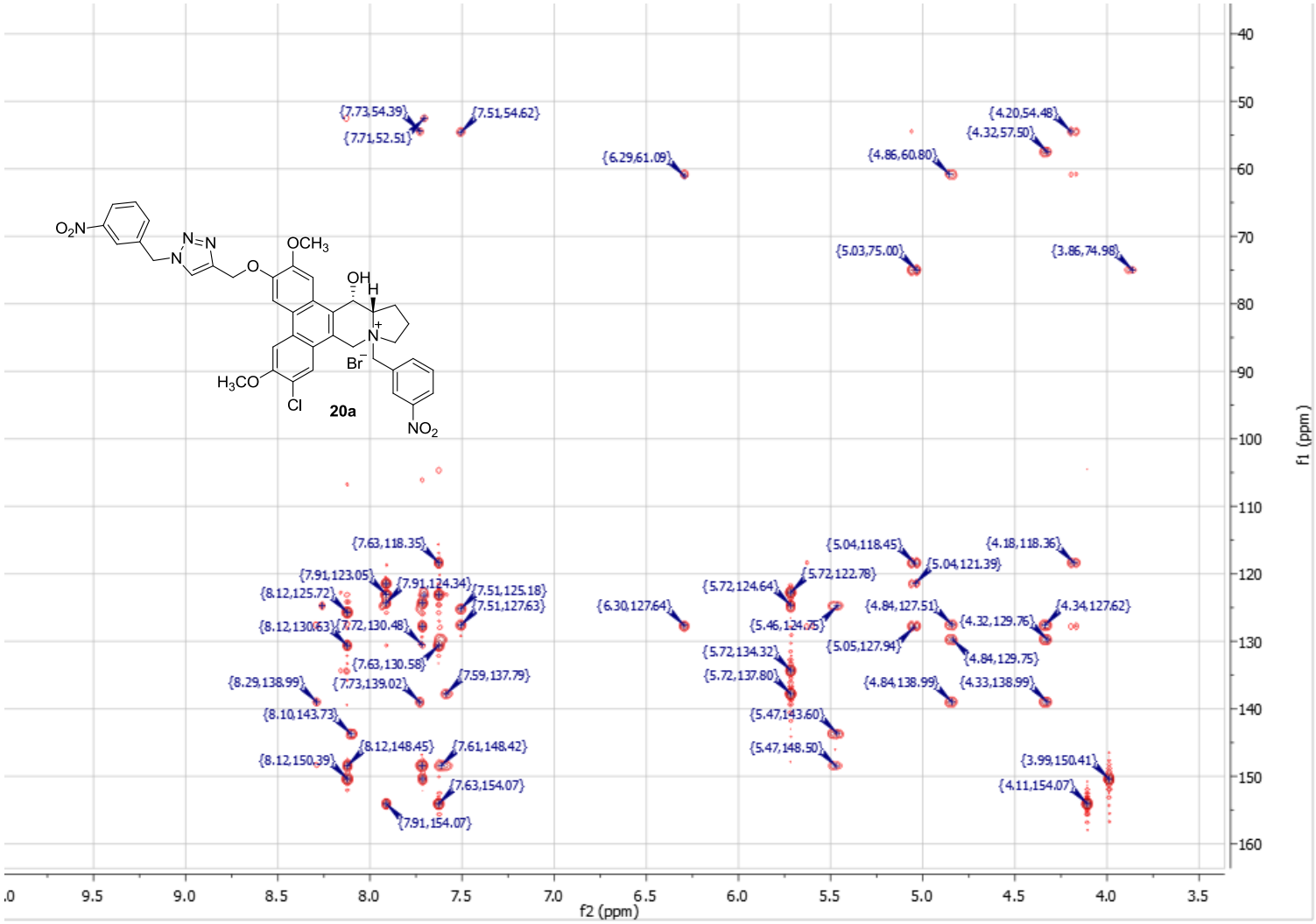

^{1}H-^{13}C HMBC NMR spectrum (600 MHz, CD_3CN) of (13a*S*,14*S*)-7-chloro-14-hydroxy-2,6-dimethoxy-10-(2-nitrobenzyl)-3-((1-(3-nitrobenzyl)-1H-1,2,3-triazol-4-yl)methoxy)-10,11,12,13,13a,14-hexahydro-9H-dibenzo[*f*,*h*]pyrrolo[1,2-*b*]isoquinolin-10-ium bromide (**20a**).

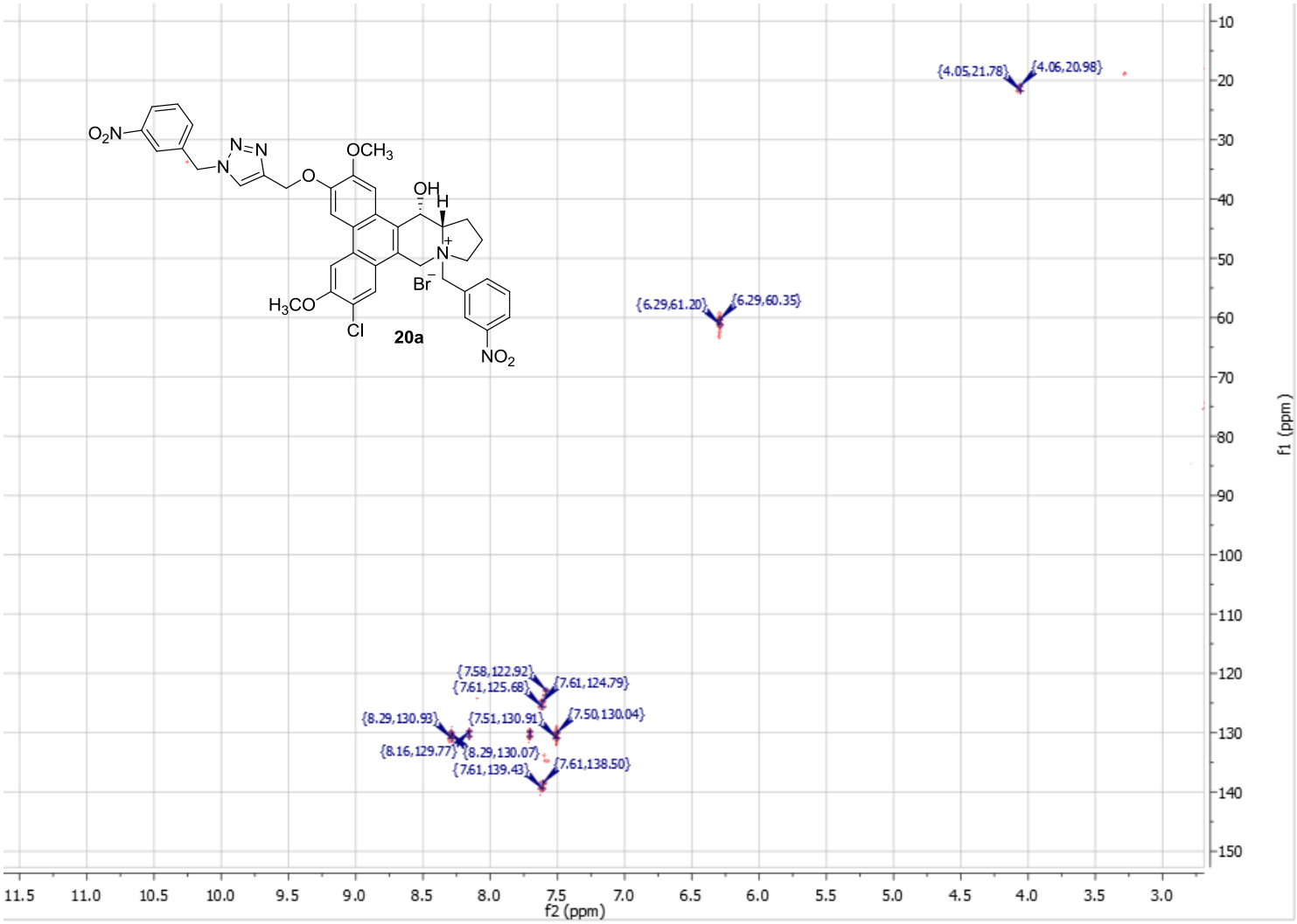

^{1}H-^{13}C H2BC NMR spectrum (600 MHz, CD_3CN) of (13a*S*,14*S*)-7-chloro-14-hydroxy-2,6-dimethoxy-10-(2-nitrobenzyl)-3-((1-(3-nitrobenzyl)-1H-1,2,3-triazol-4-yl)methoxy)-10,11,12,13,13a,14-hexahydro-9H-dibenzo[*f*,*h*]pyrrolo[1,2-*b*]isoquinolin-10-ium bromide (**20a**).

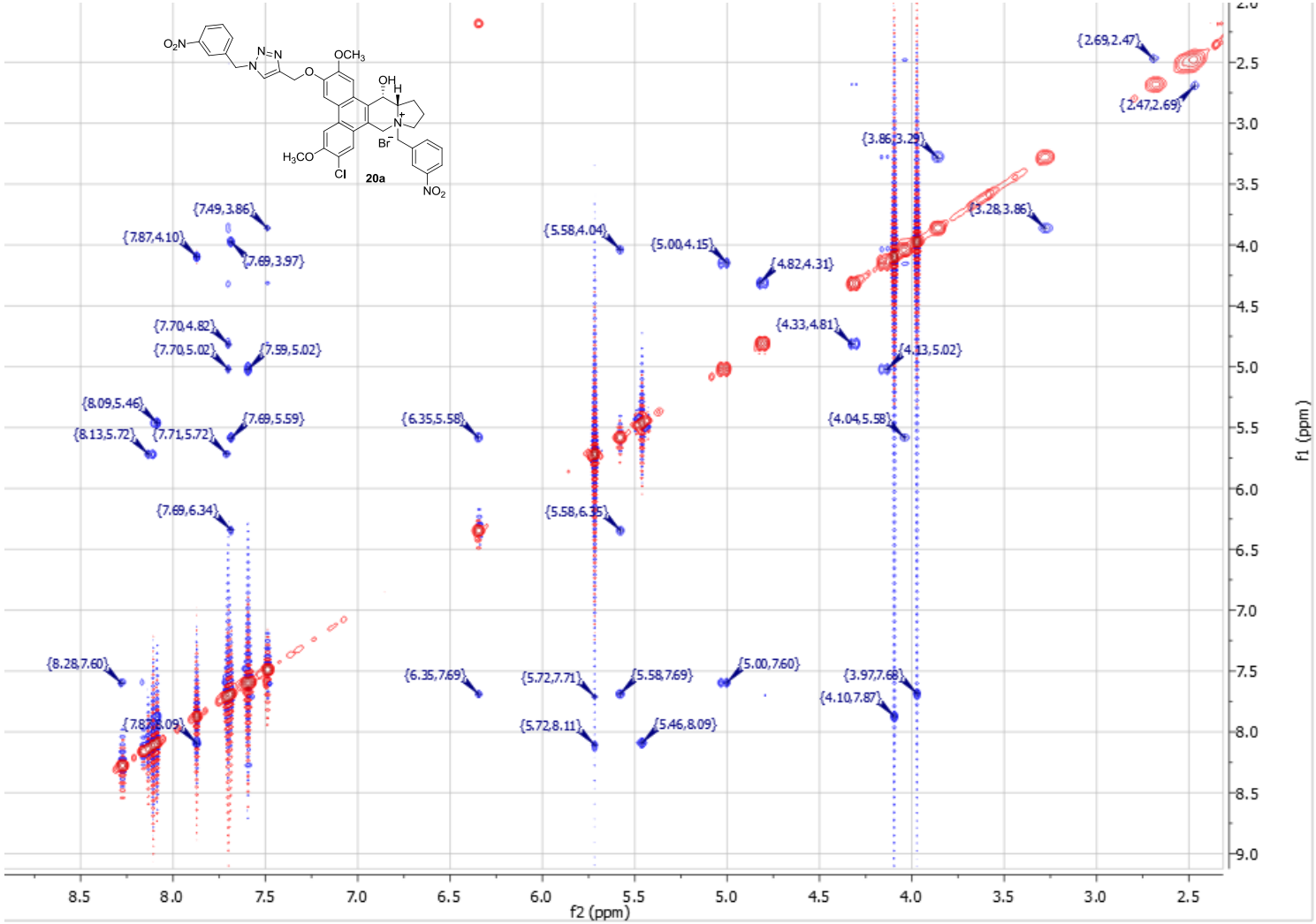

NOESY NMR spectrum (500 MHz, CD_3CN) of (13a*S*,14*S*)-7-chloro-14-hydroxy-2,6-dimethoxy-10-(2-nitrobenzyl)-3-((1-(3-nitrobenzyl)-1H-1,2,3-triazol-4-yl)methoxy)-10,11,12,13,13a,14-hexahydro-9H-dibenzo[*f*,*h*]pyrrolo[1,2-*b*]isoquinolin-10-ium bromide (**20a**).

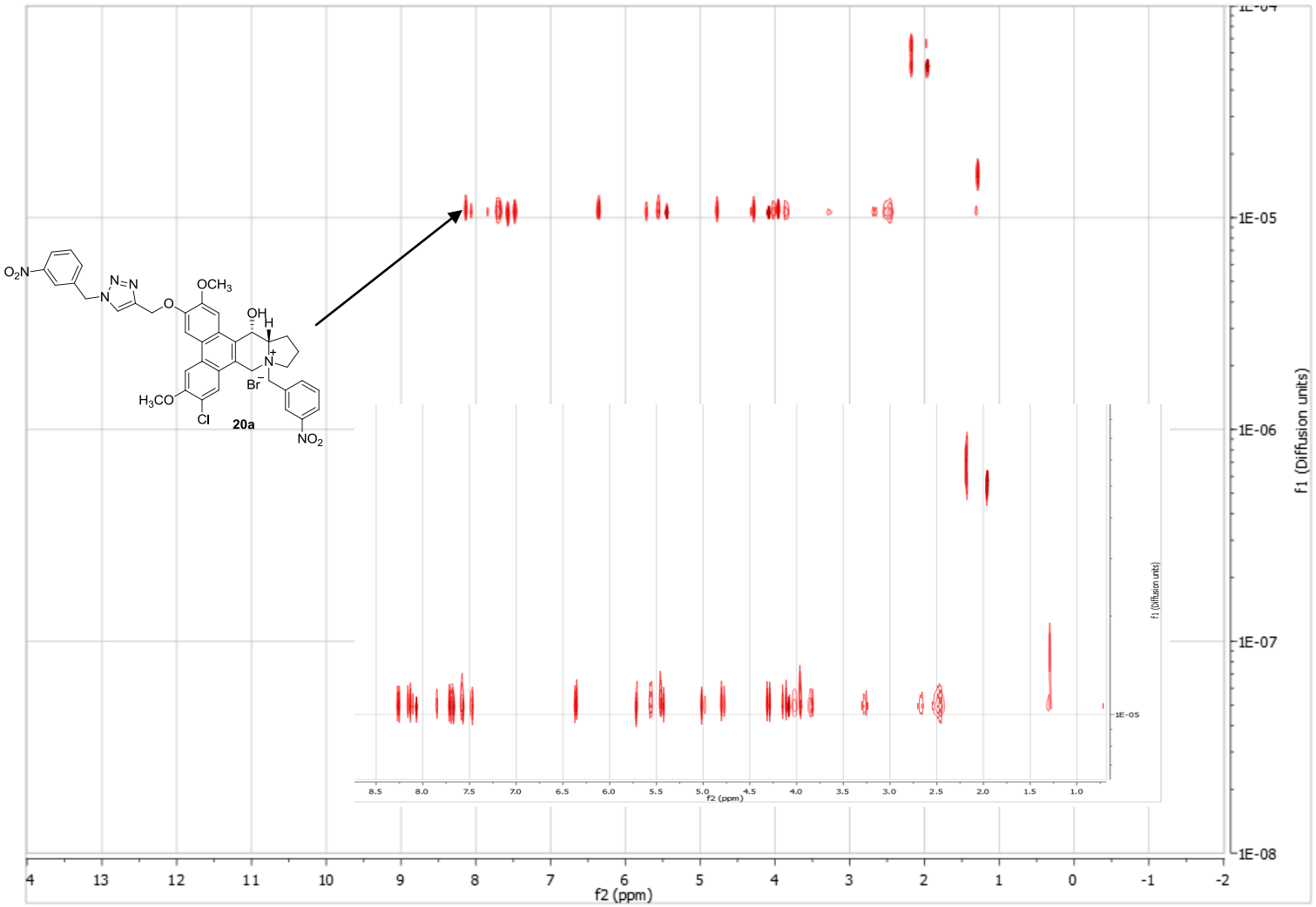

DOSY NMR spectrum (500 MHz, CD_3CN) of (13a*S*,14*S*)-7-chloro-14-hydroxy-2,6-dimethoxy-10-(2-nitrobenzyl)-3-((1-(3-nitrobenzyl)-1H-1,2,3-triazol-4-yl)methoxy)-10,11,12,13,13a,14-hexahydro-9H-dibenzo[*f*,*h*]pyrrolo[1,2-*b*]isoquinolin-10-ium bromide (**20a**).

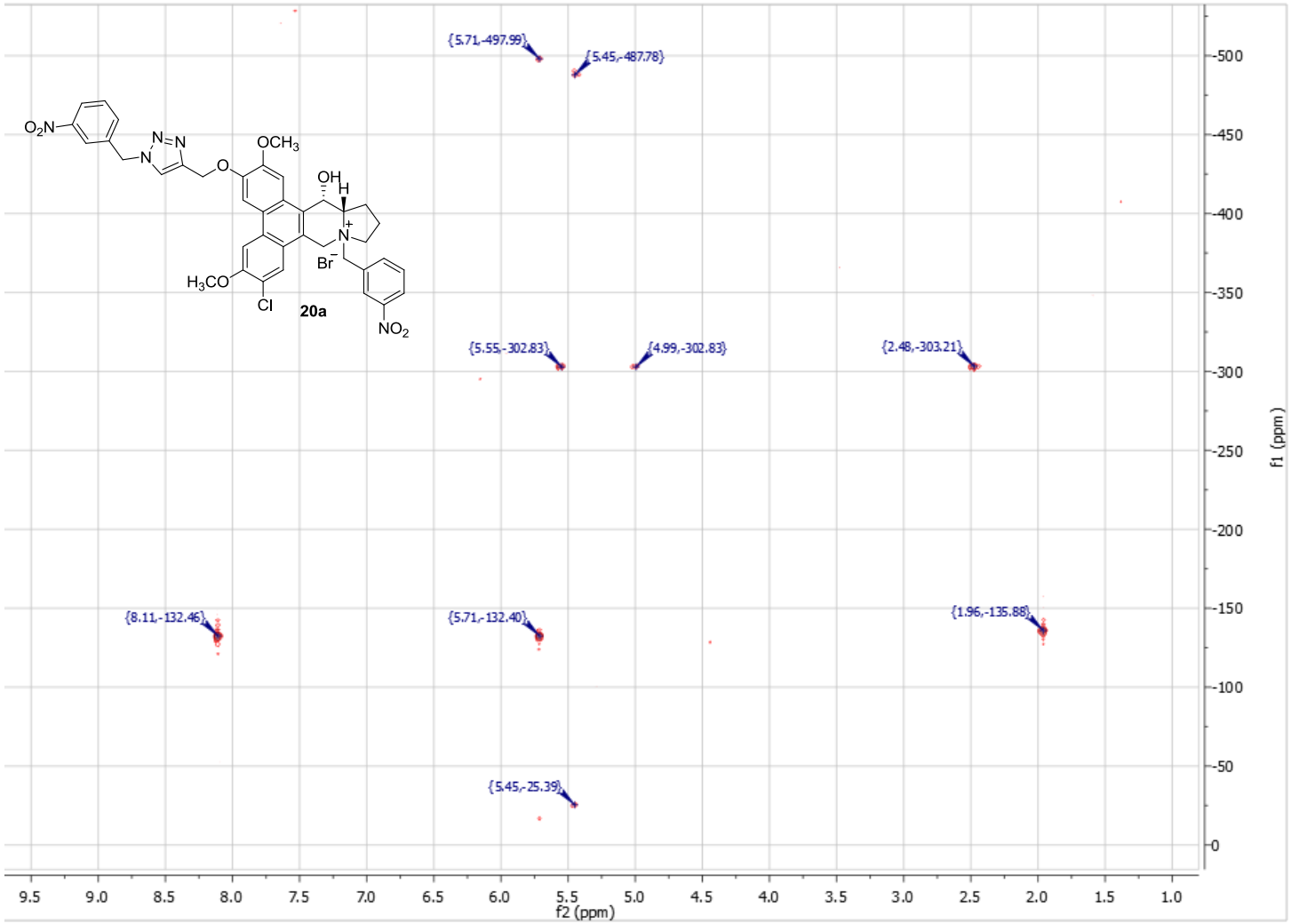

^{1}H-^{15}N HMBC NMR spectrum (600 MHz, CD_3CN) of (13a*S*,14*S*)-7-chloro-14-hydroxy-2,6-dimethoxy-10-(2-nitrobenzyl)-3-((1-(3-nitrobenzyl)-1H-1,2,3-triazol-4-yl)methoxy)-10,11,12,13,13a,14-hexahydro-9H-dibenzo[*f*,*h*]pyrrolo[1,2-*b*]isoquinolin-10-ium bromide (**20a**).

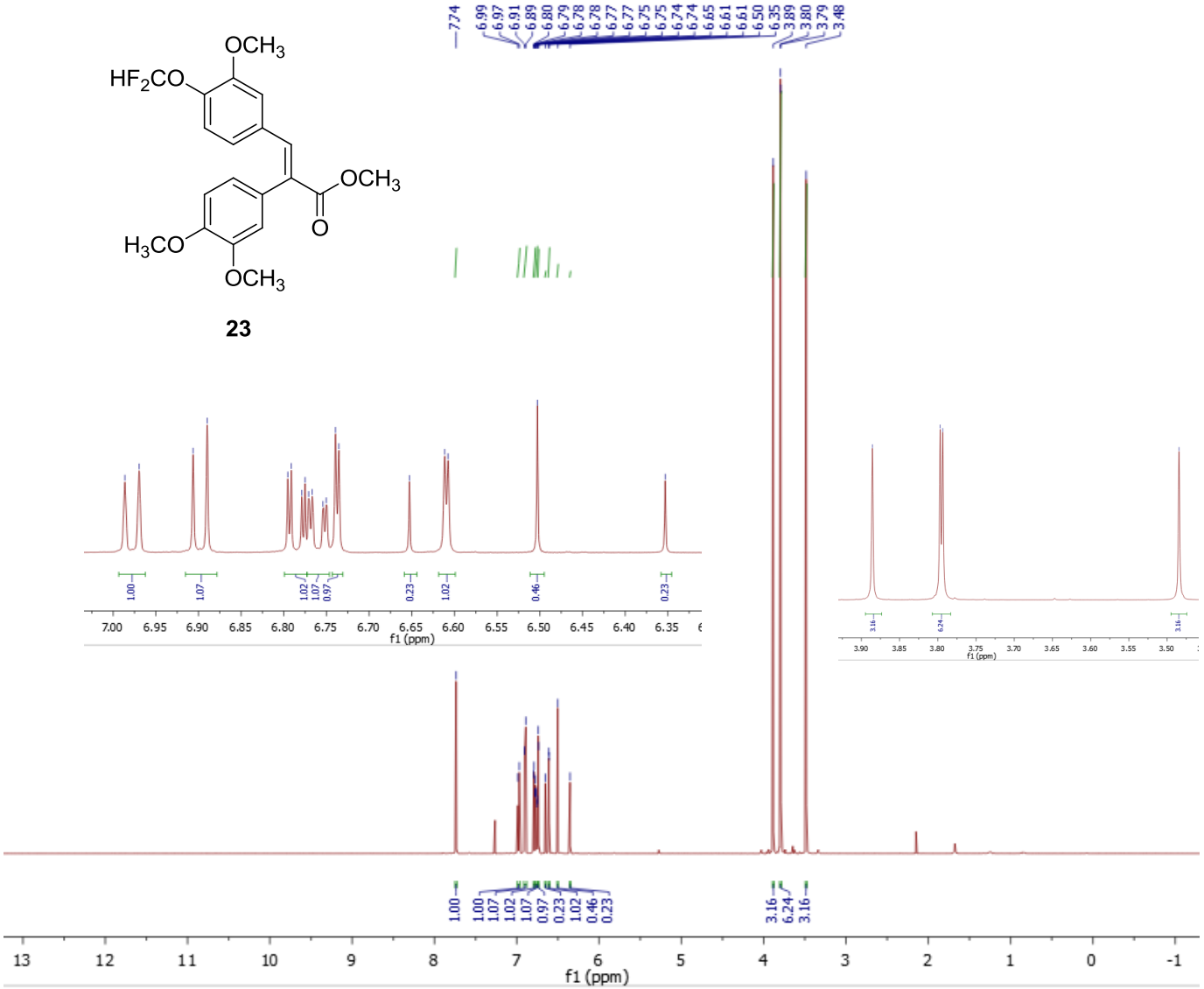

^{1}H NMR spectrum (500 MHz, $CDCl_3$) of (*E*)-methyl 3-(4-(difluoromethoxy)-3-methoxyphenyl)-2-(3,4-dimethoxyphenyl)acrylate (**23**).

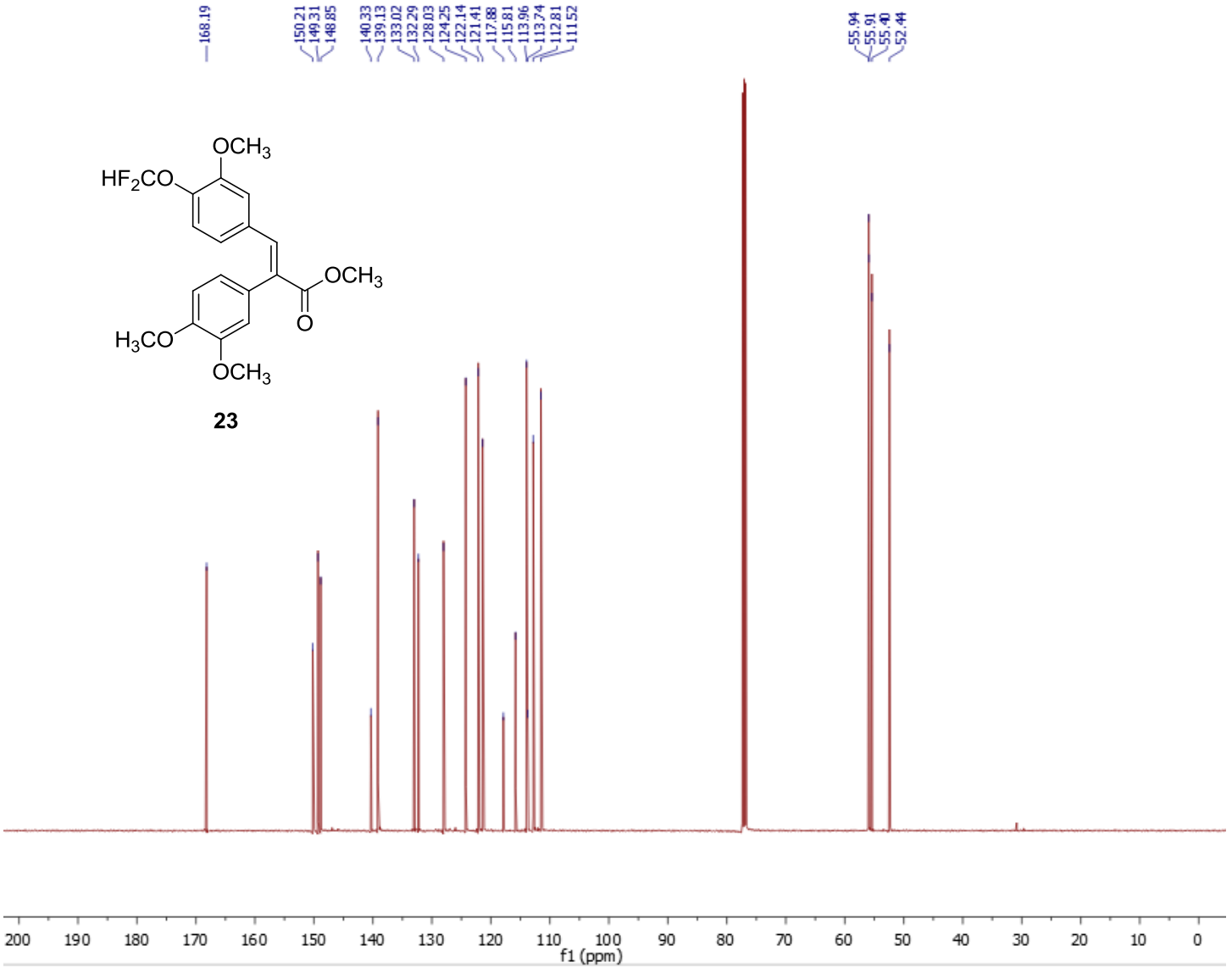

^{13}C NMR spectrum (125 MHz, $CDCl_3$) of (*E*)-methyl 3-(4-(difluoromethoxy)-3-methoxyphenyl)-2-(3,4-dimethoxyphenyl)acrylate (**23**).

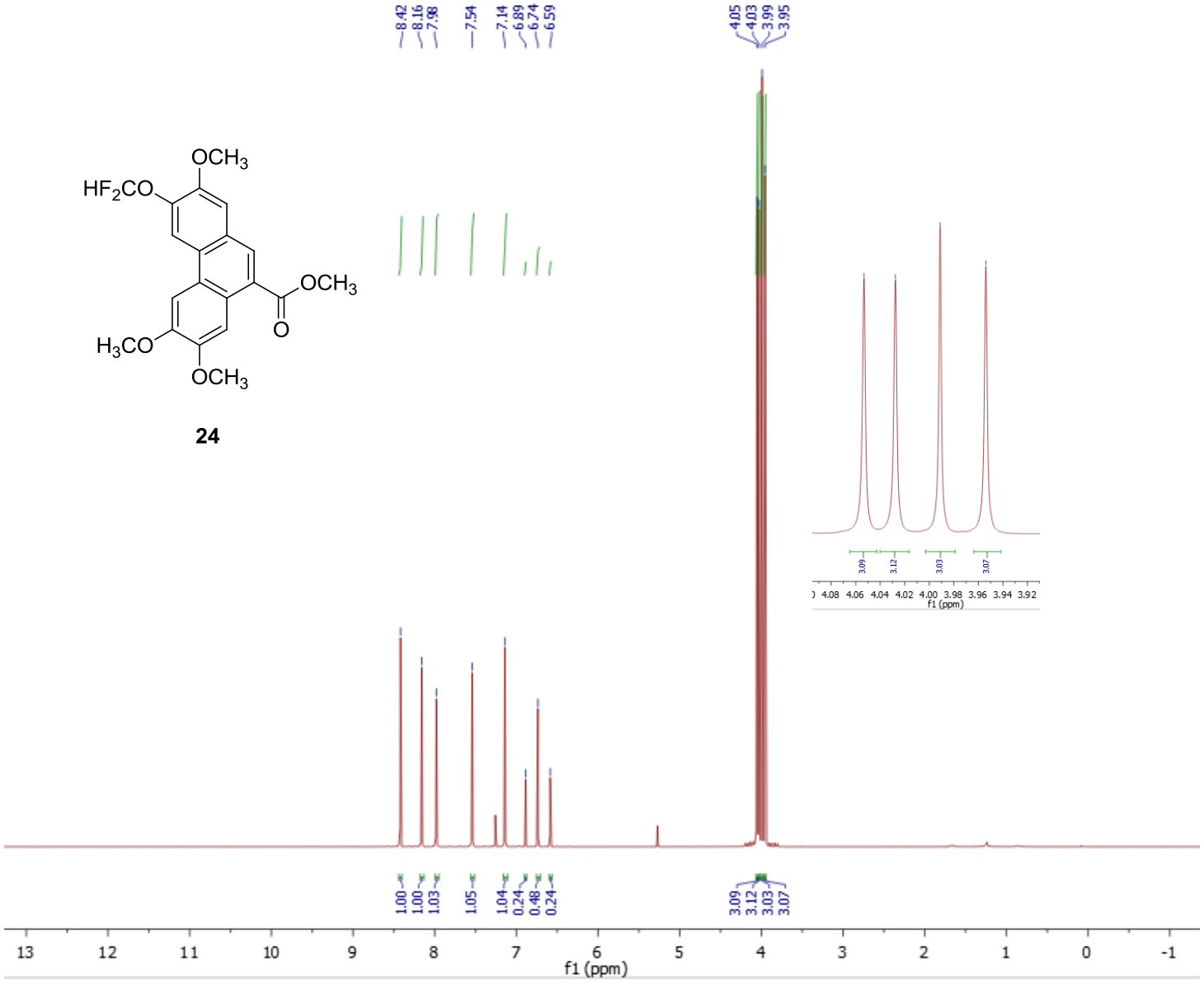

^{1}H NMR spectrum (500 MHz, $CDCl_3$) of methyl 3-(difluoromethoxy)-2,6,7-trimethoxyphenanthrene-9-carboxylate (**24**).

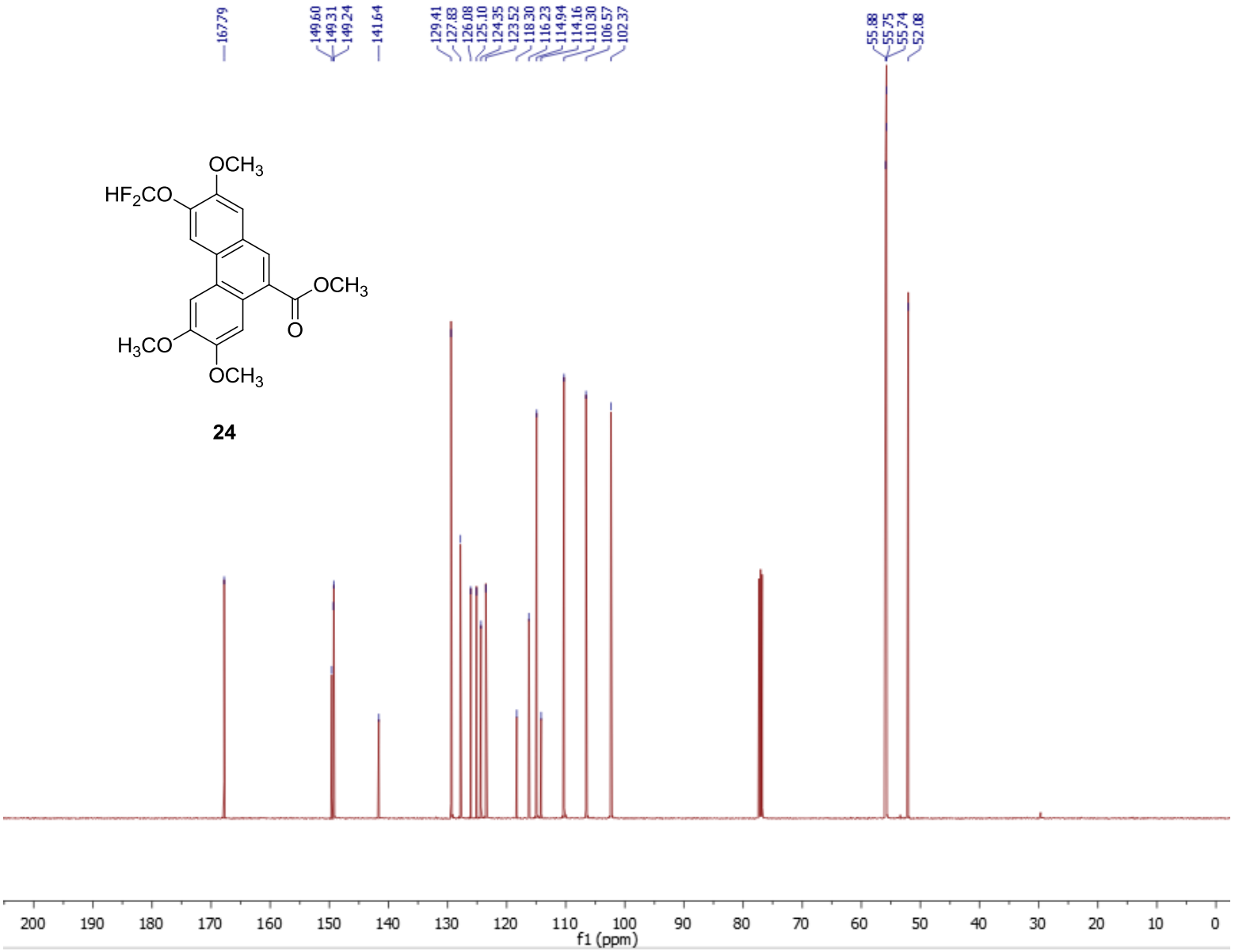

^{13}C NMR spectrum (125 MHz, $CDCl_3$) of methyl 3-(difluoromethoxy)-2,6,7-trimethoxyphenanthrene-9-carboxylate (**24**).

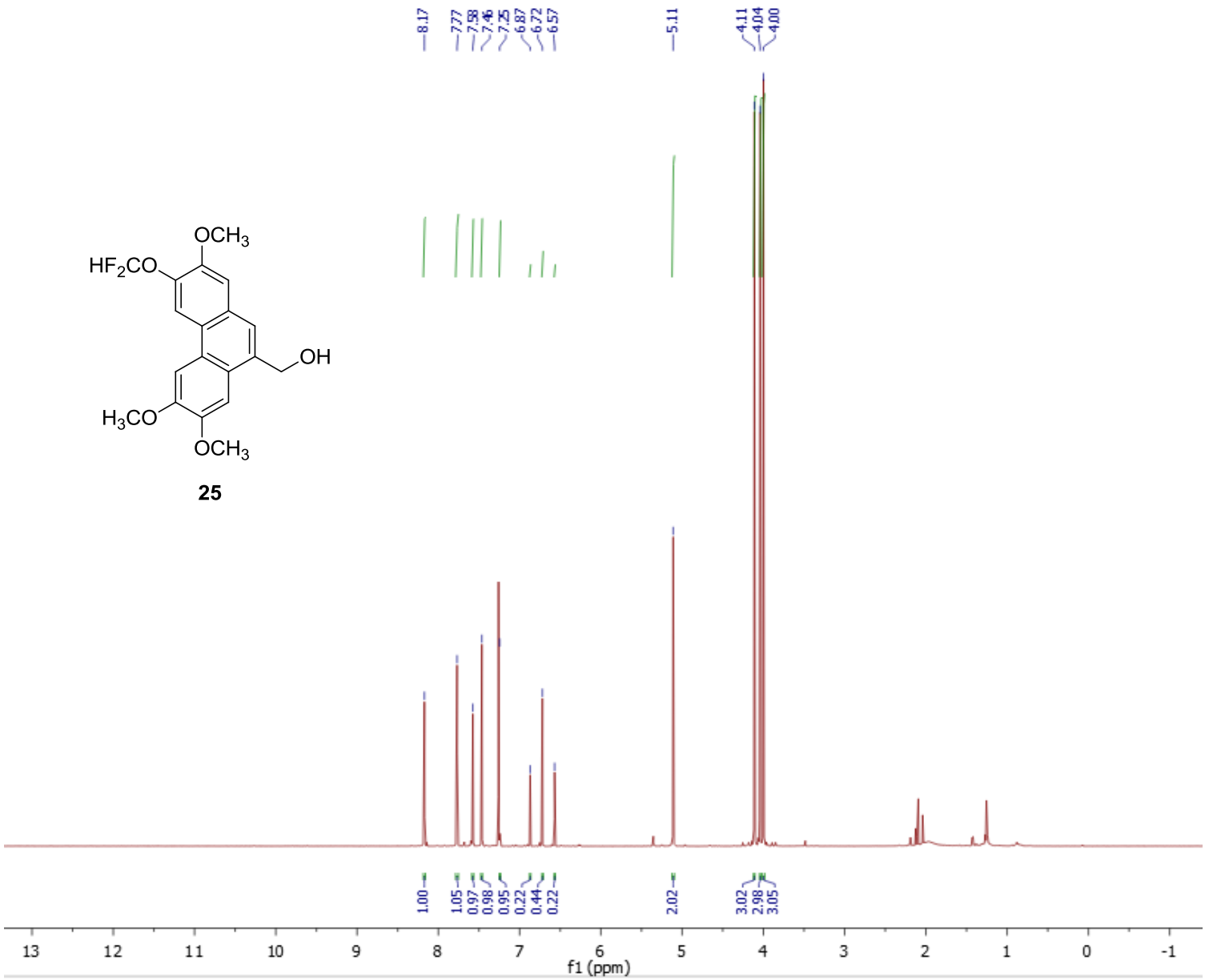

^{1}H NMR spectrum (500 MHz, $CDCl_3$) of (3-(difluoromethoxy)-2,6,7-trimethoxyphenanthren-9-yl)methanol (**25**).

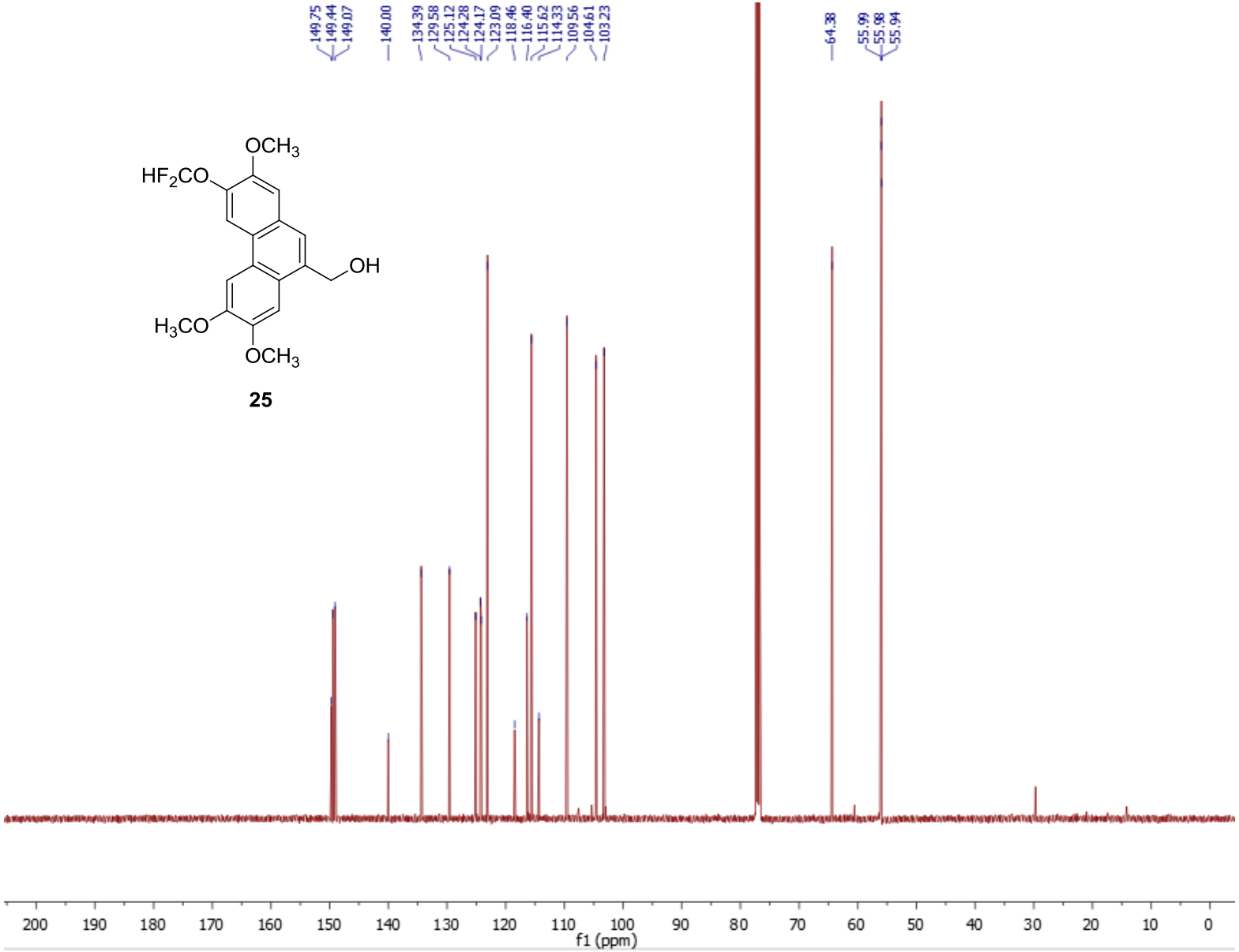

^{13}C NMR spectrum (125 MHz, $CDCl_3$) of (3-(difluoromethoxy)-2,6,7-trimethoxyphenanthren-9-yl)methanol (**25**).

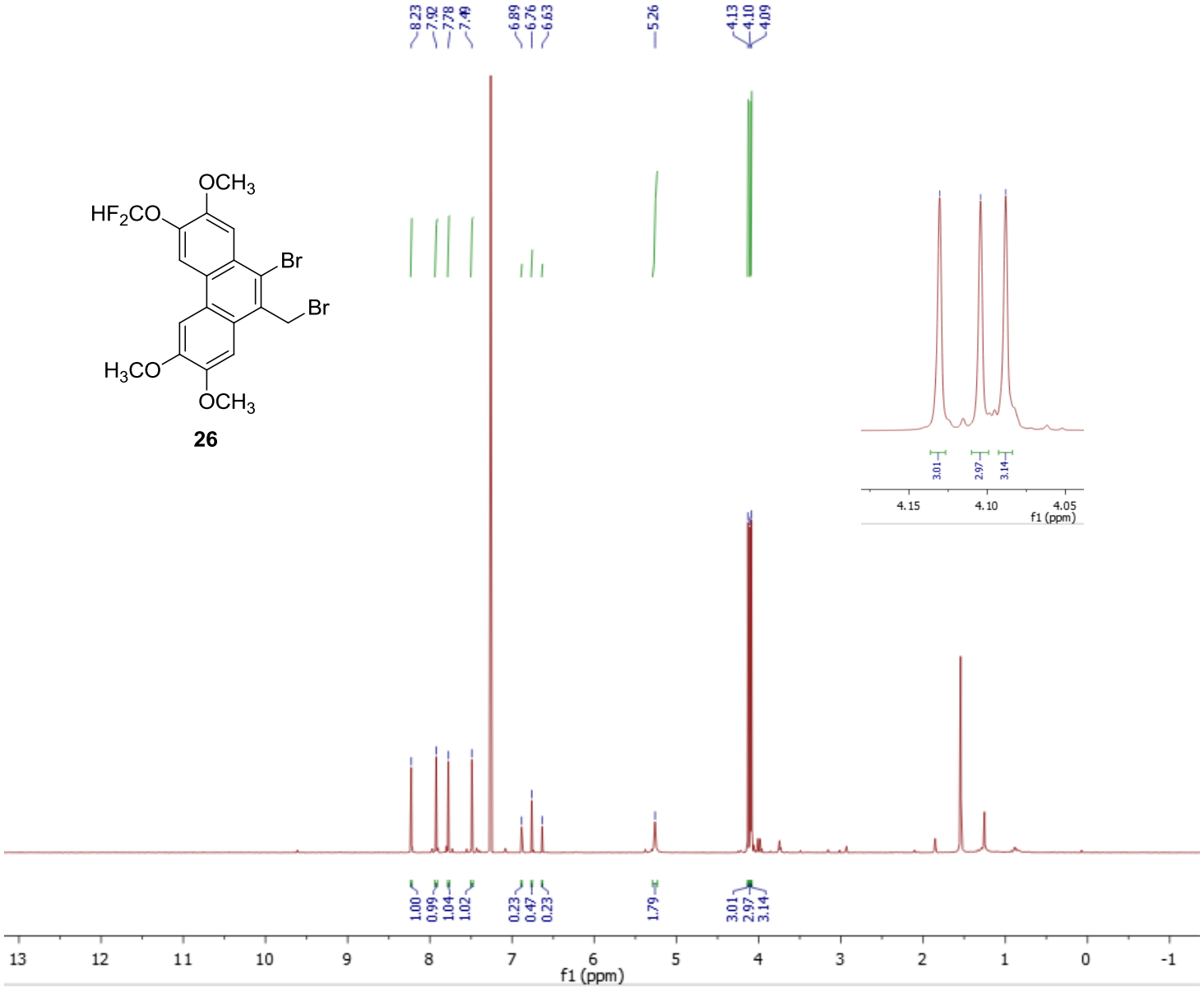

^{1}H NMR spectrum (600 MHz, $CDCl_3$) of 9-bromo-10-(bromomethyl)-6-(difluoromethoxy)-2,3,7-trimethoxyphenanthrene (**26**).

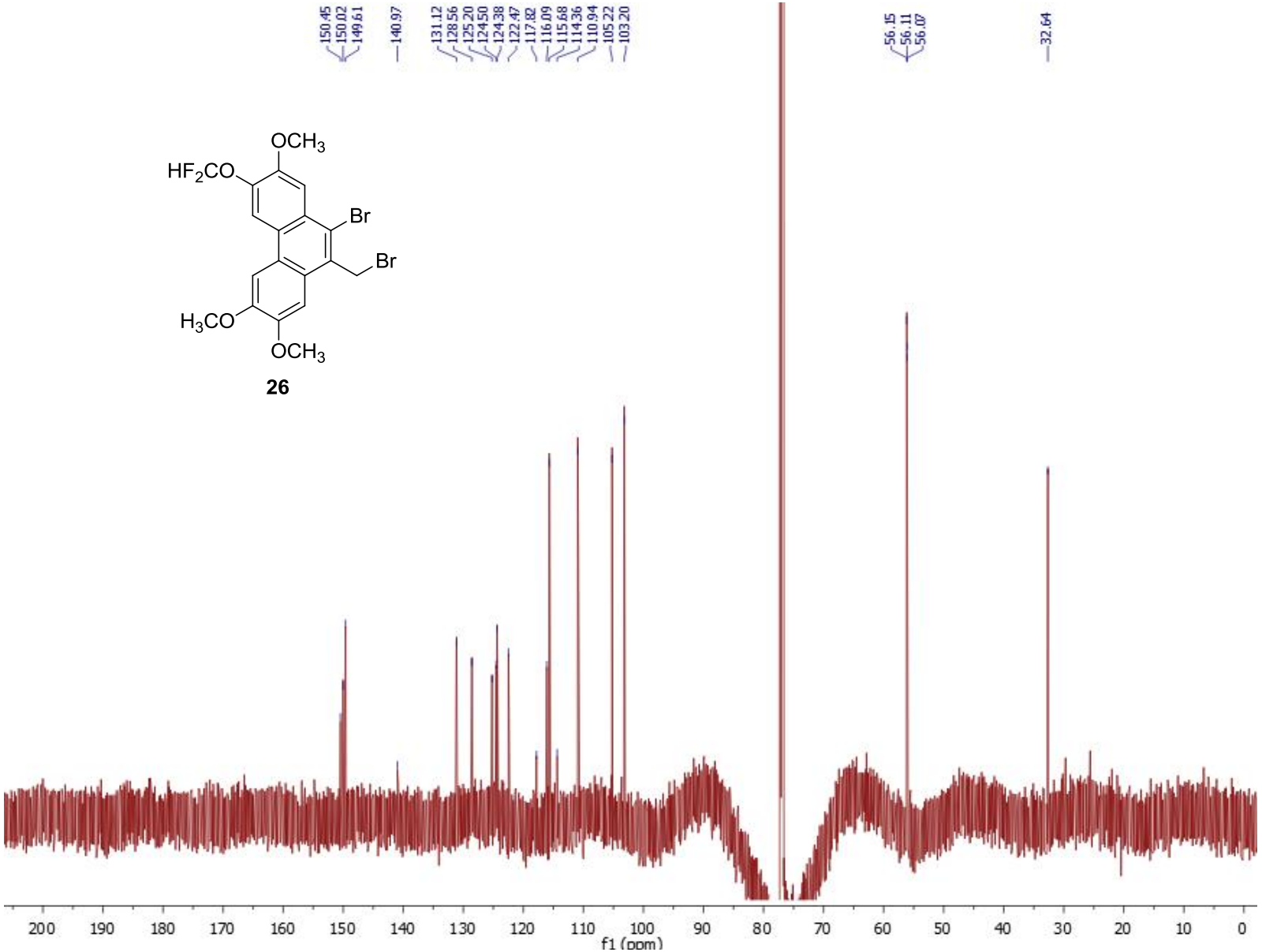

^{13}C NMR spectrum (150 MHz, $CDCl_3$) of 9-bromo-10-(bromomethyl)-6-(difluoromethoxy)-2,3,7-trimethoxyphenanthrene (**26**).

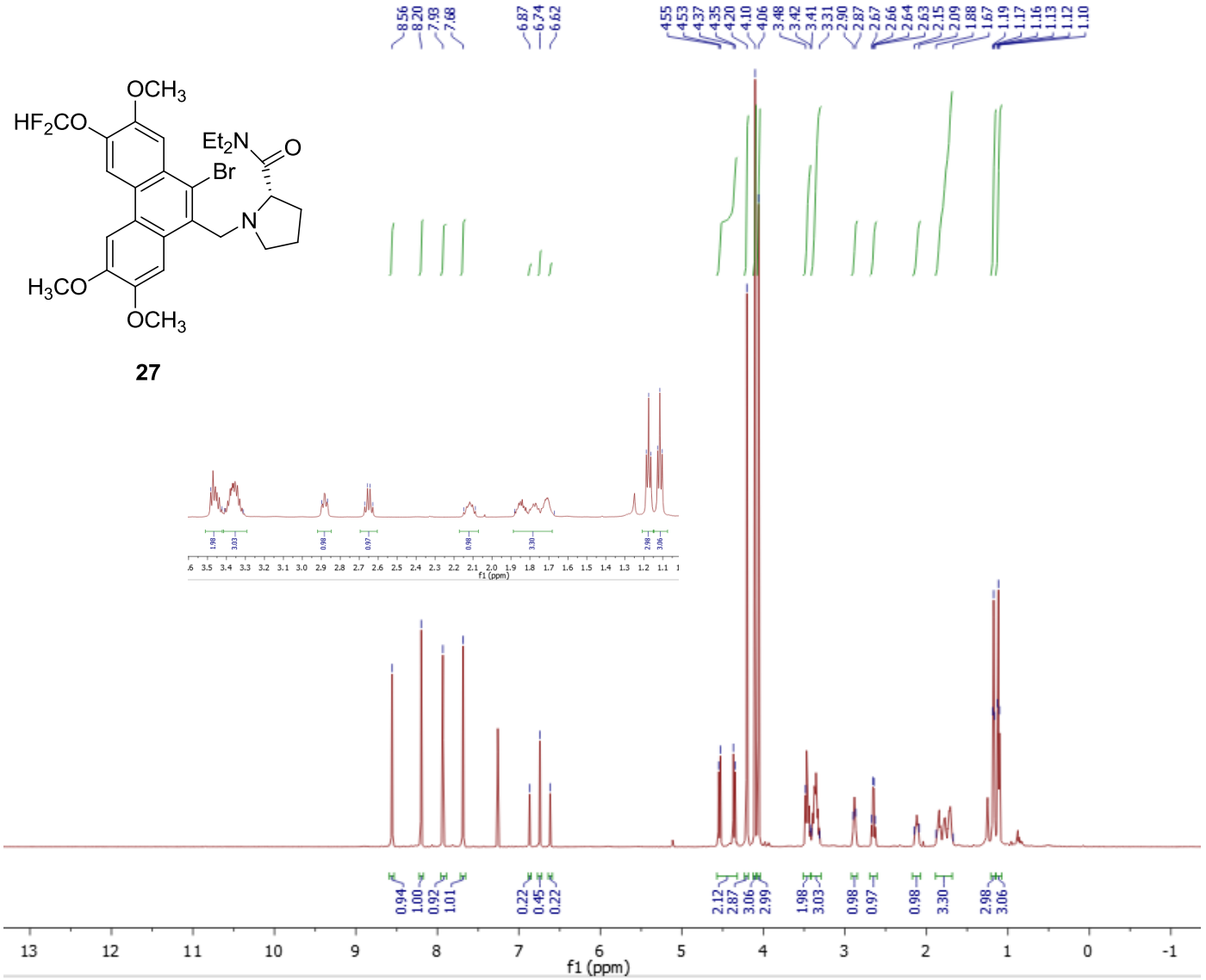

^{1}H NMR spectrum (600 MHz, $CDCl_3$) of (*S*)-1-((10-bromo-3-(difluoromethoxy)-2,6,7-trimethoxyphenanthren-9-yl)methyl)-*N*,*N*-diethylpyrrolidine-2-carboxamide (**27**).

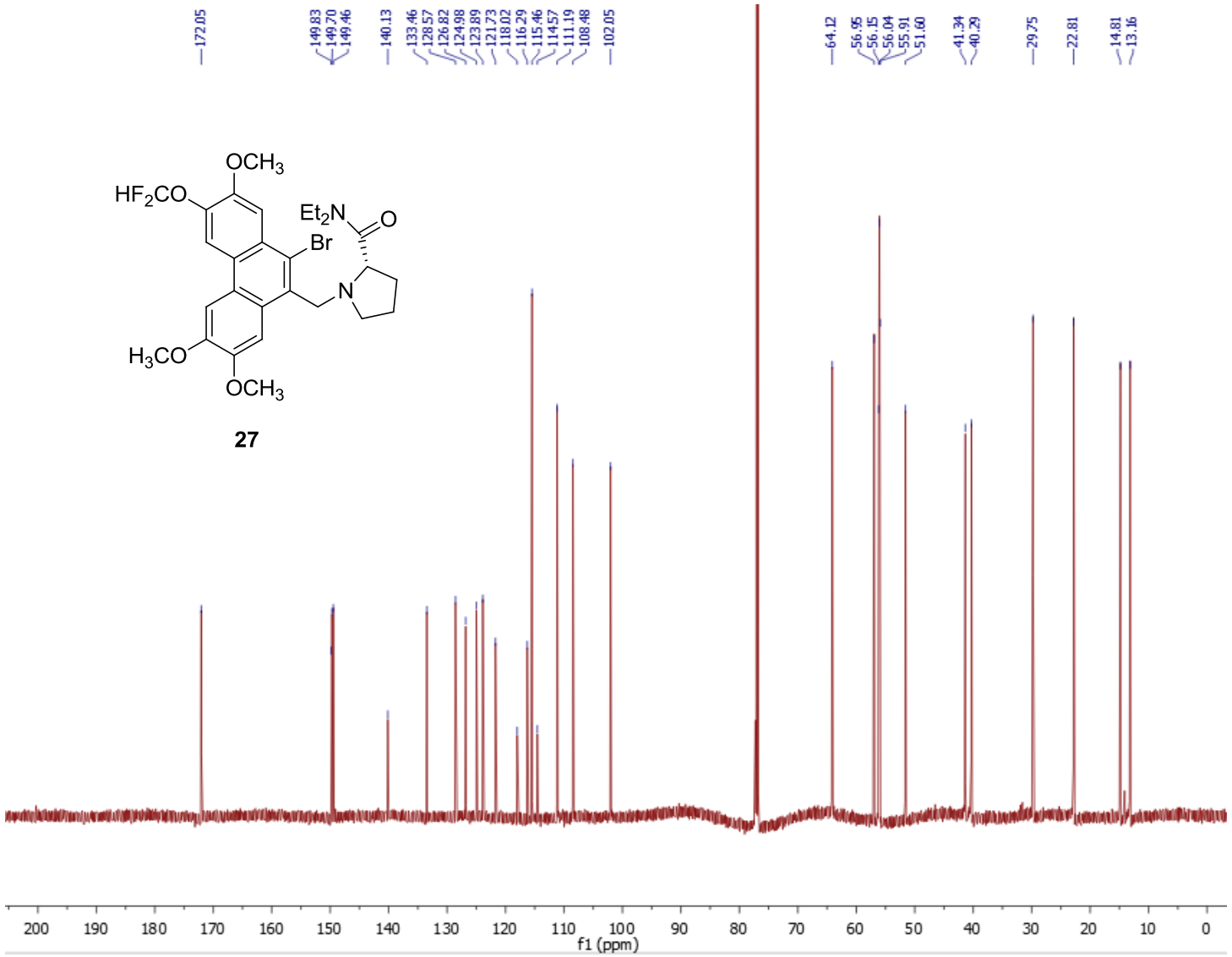

^{13}C NMR spectrum (150 MHz, $CDCl_3$) of (*S*)-1-((10-bromo-3-(difluoromethoxy)-2,6,7-trimethoxyphenanthren-9-yl)methyl)-*N*,*N*-diethylpyrrolidine-2-carboxamide (**27**).

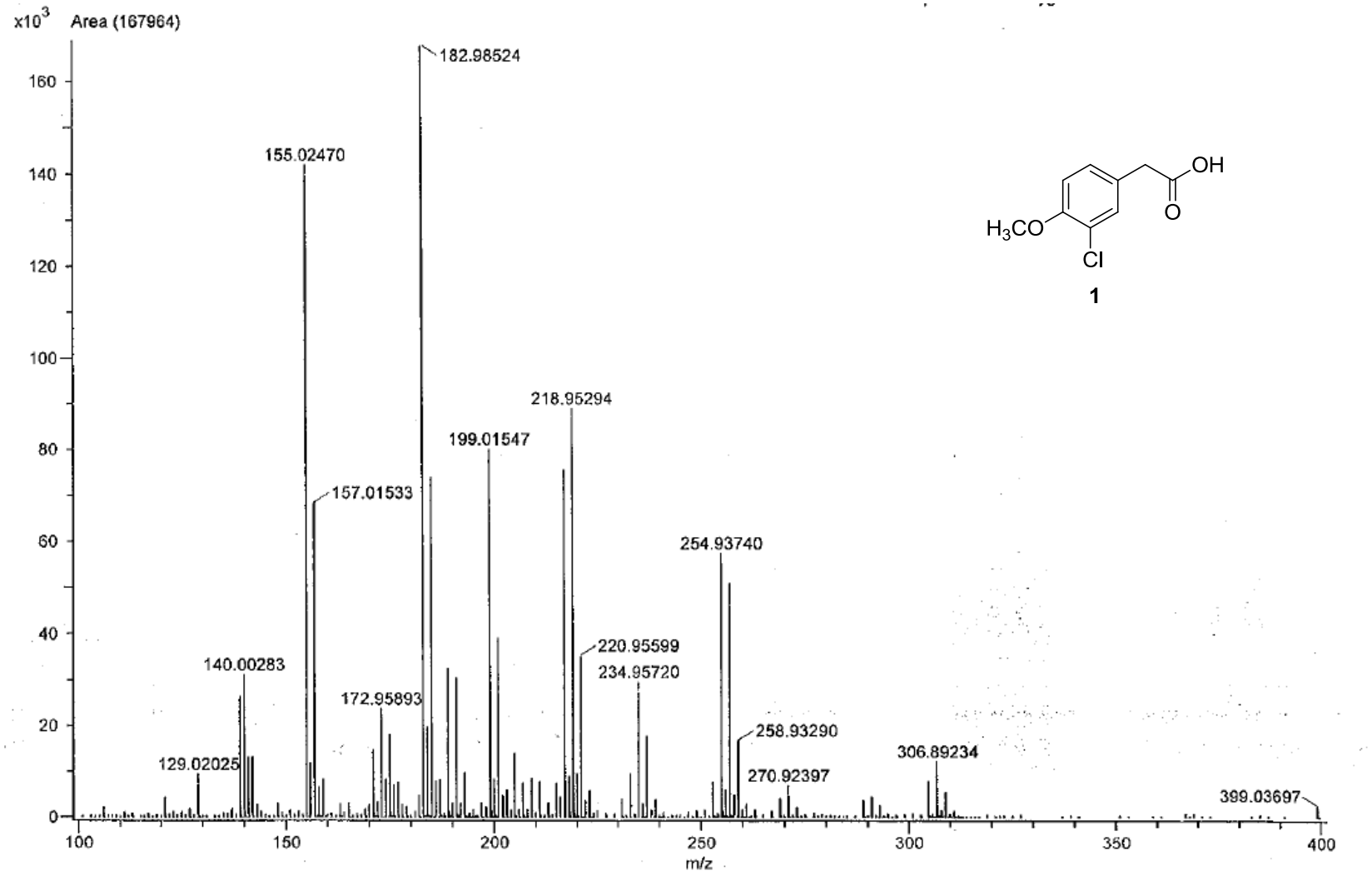

Mass spectrum of 2-(3-chloro-4-methoxyphenyl)acetic acid (**1**).

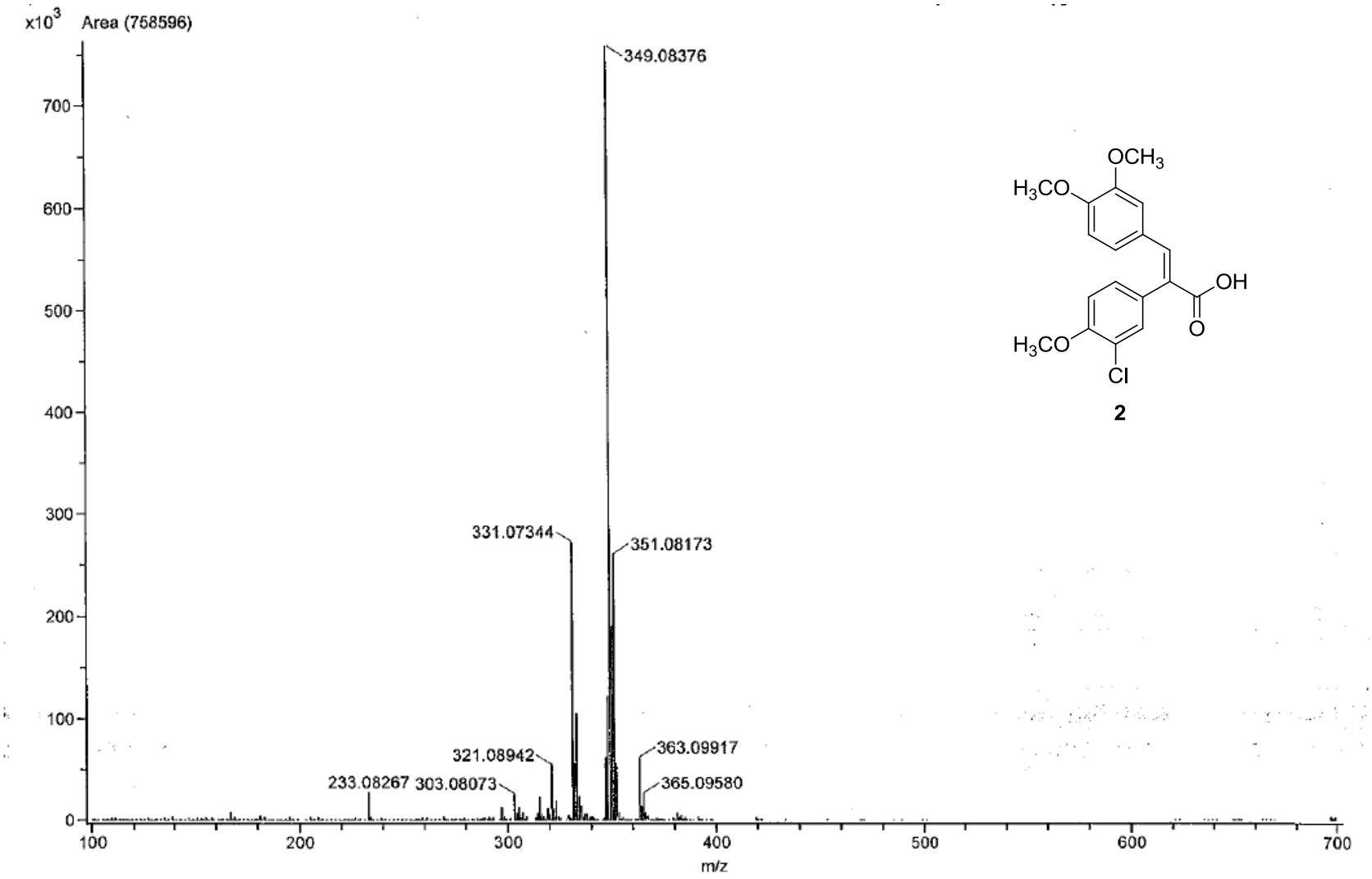

Mass spectrum of (*E*)-2-(3-chloro-4-methoxyphenyl)-3-(3,4-dimethoxyphenyl)acrylic acid (**2**).

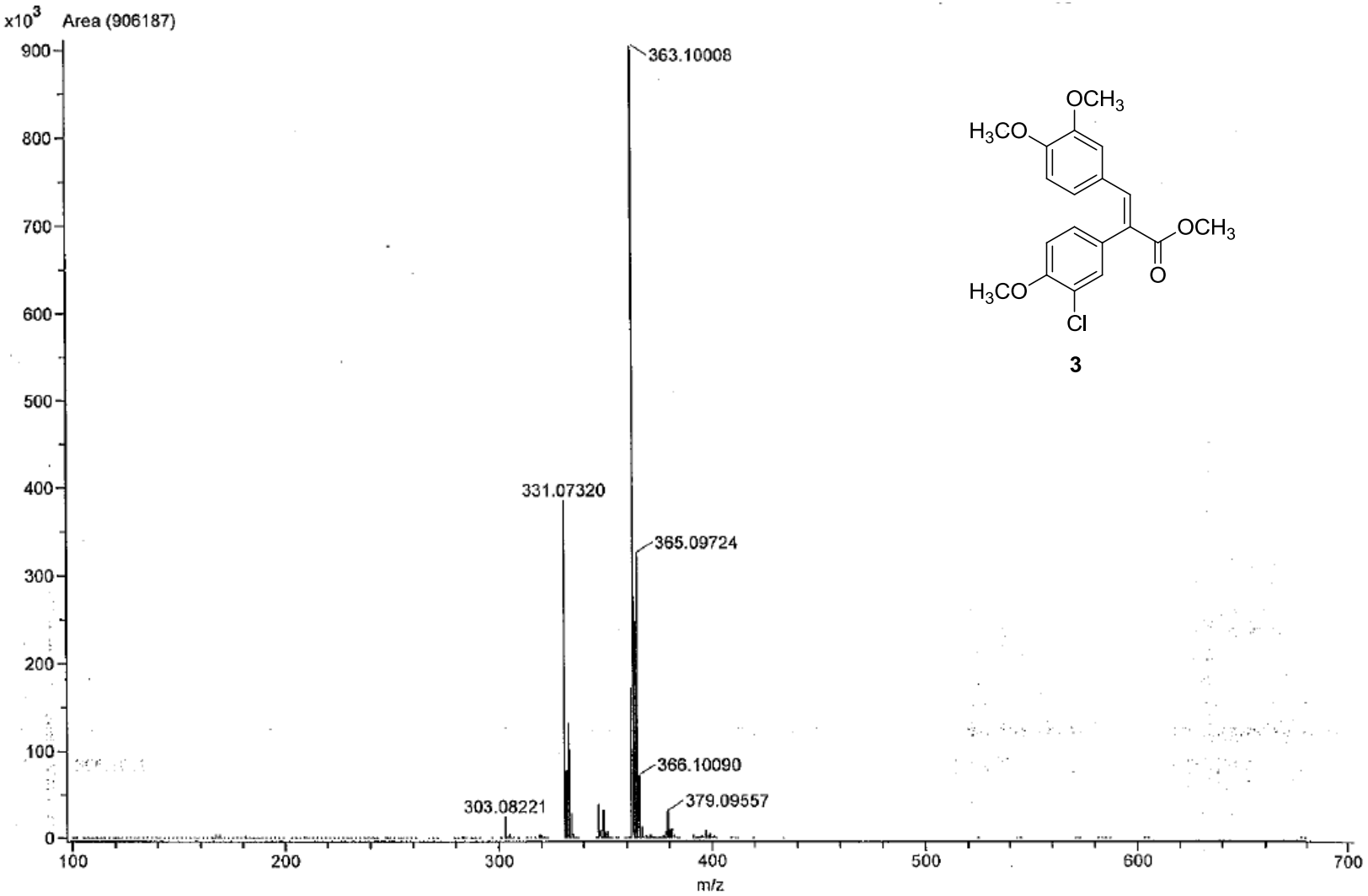

Mass spectrum of (*E*)-methyl 2-(3-chloro-4-methoxyphenyl)-3-(3,4-dimethoxyphenyl)acrylate (**3**).

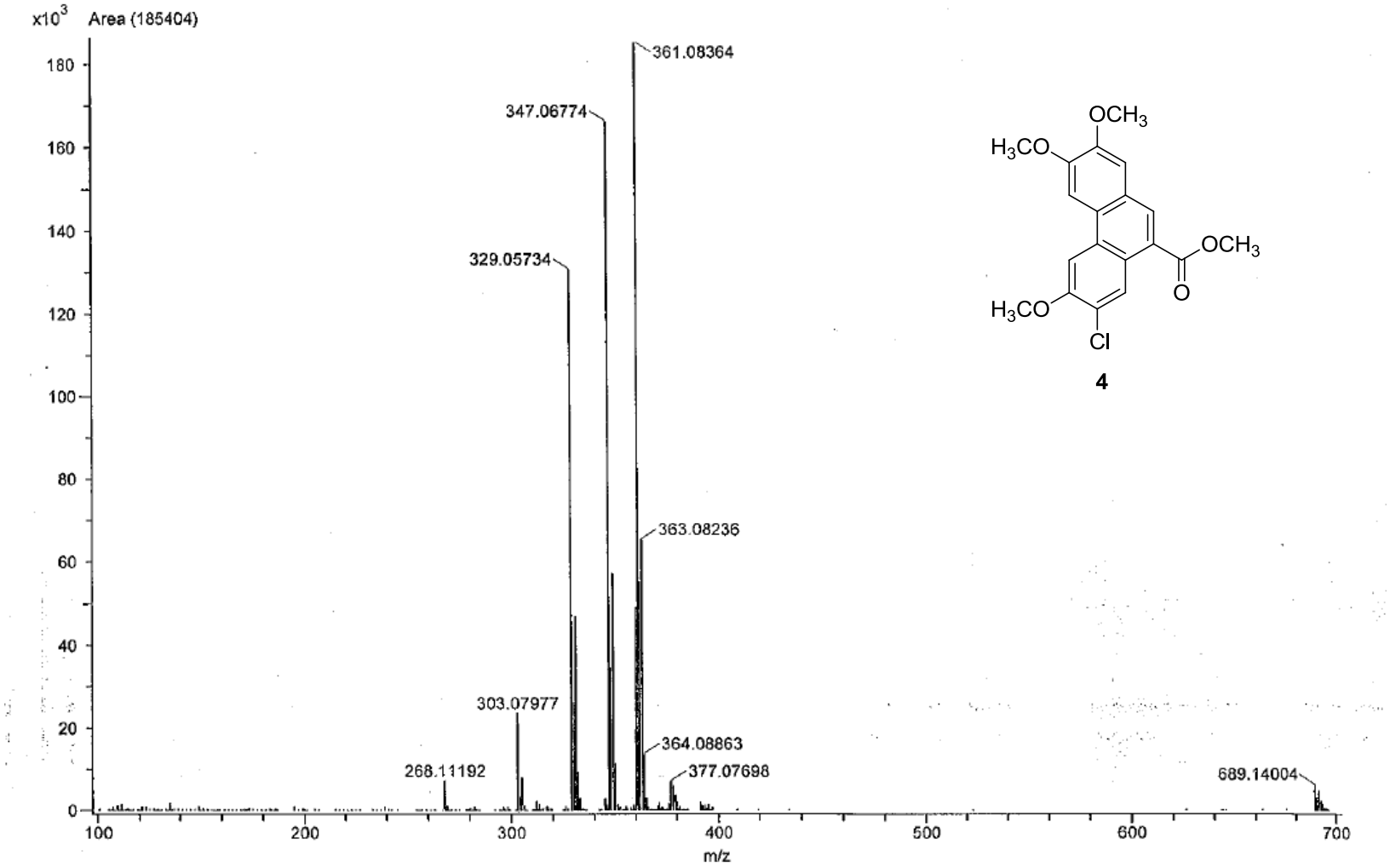

Mass spectrum of methyl 7-chloro-2,3,6-trimethoxyphenanthrene-9-carboxylate (**4**).

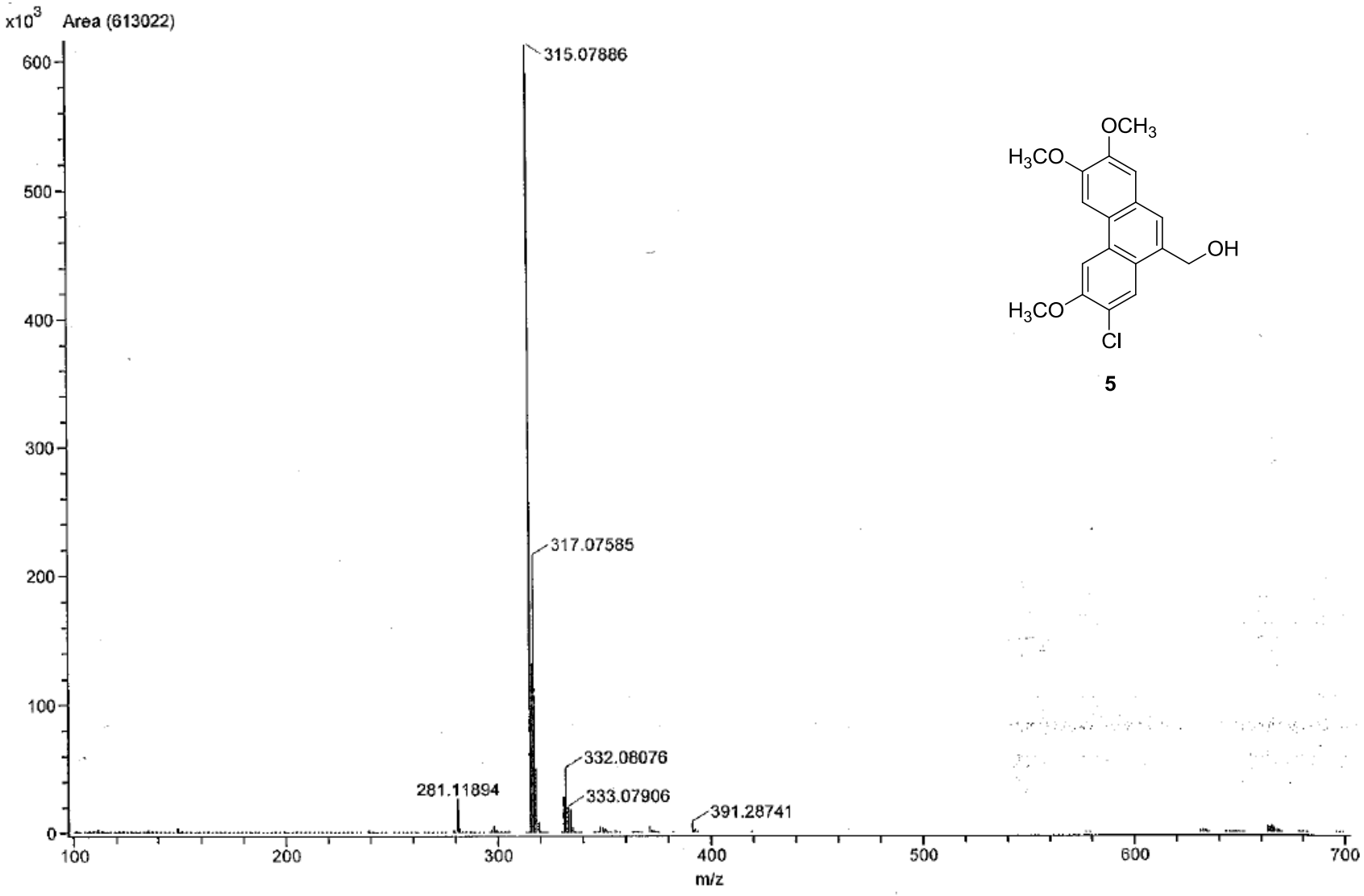

Mass spectrum of (7-chloro-2,3,6-trimethoxyphenanthren-9-yl)methanol (**5**).

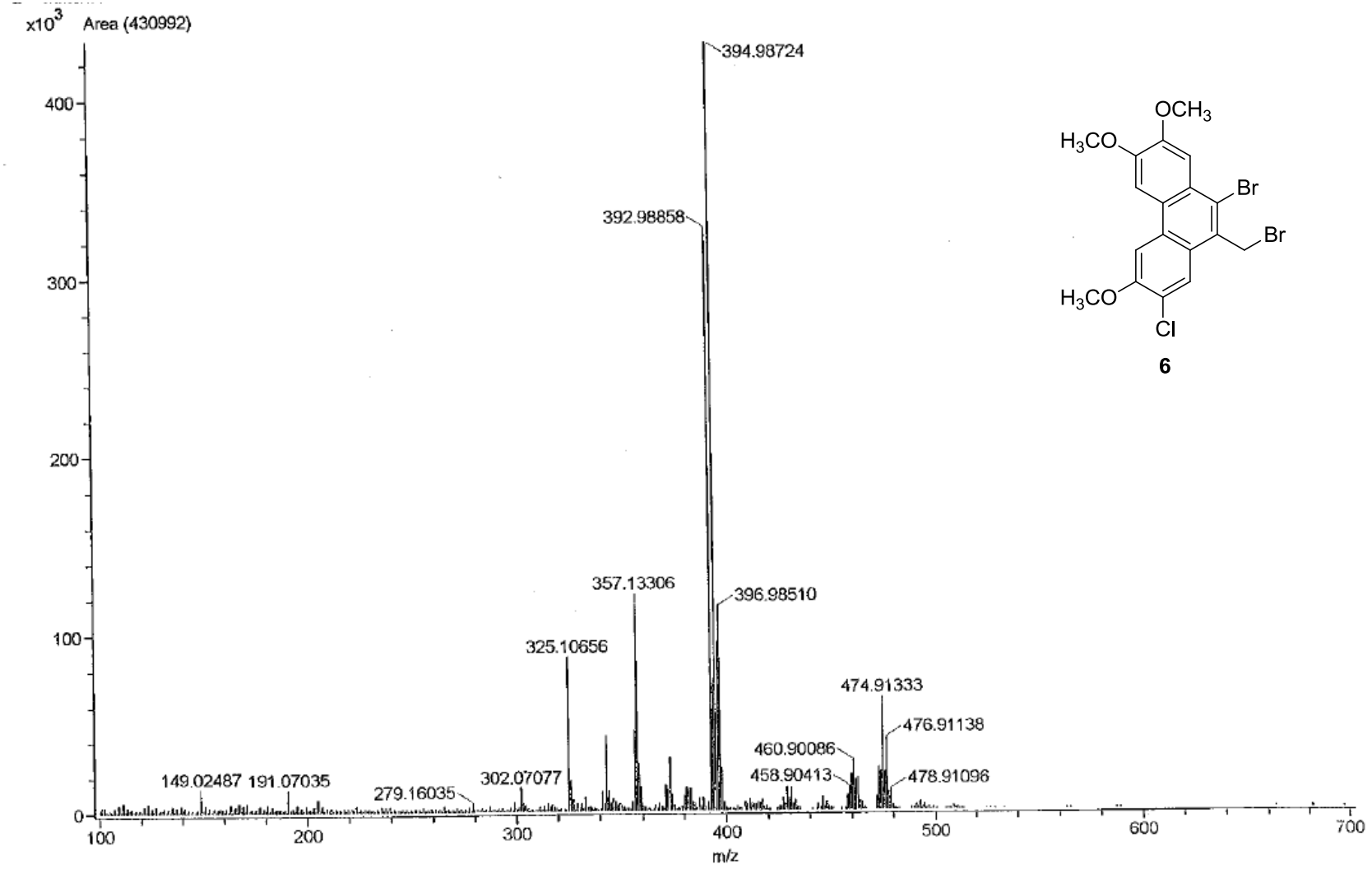

Mass spectrum of 9-bromo-10-(bromomethyl)-2-chloro-3,6,7-trimethoxyphenanthrene (**6**).

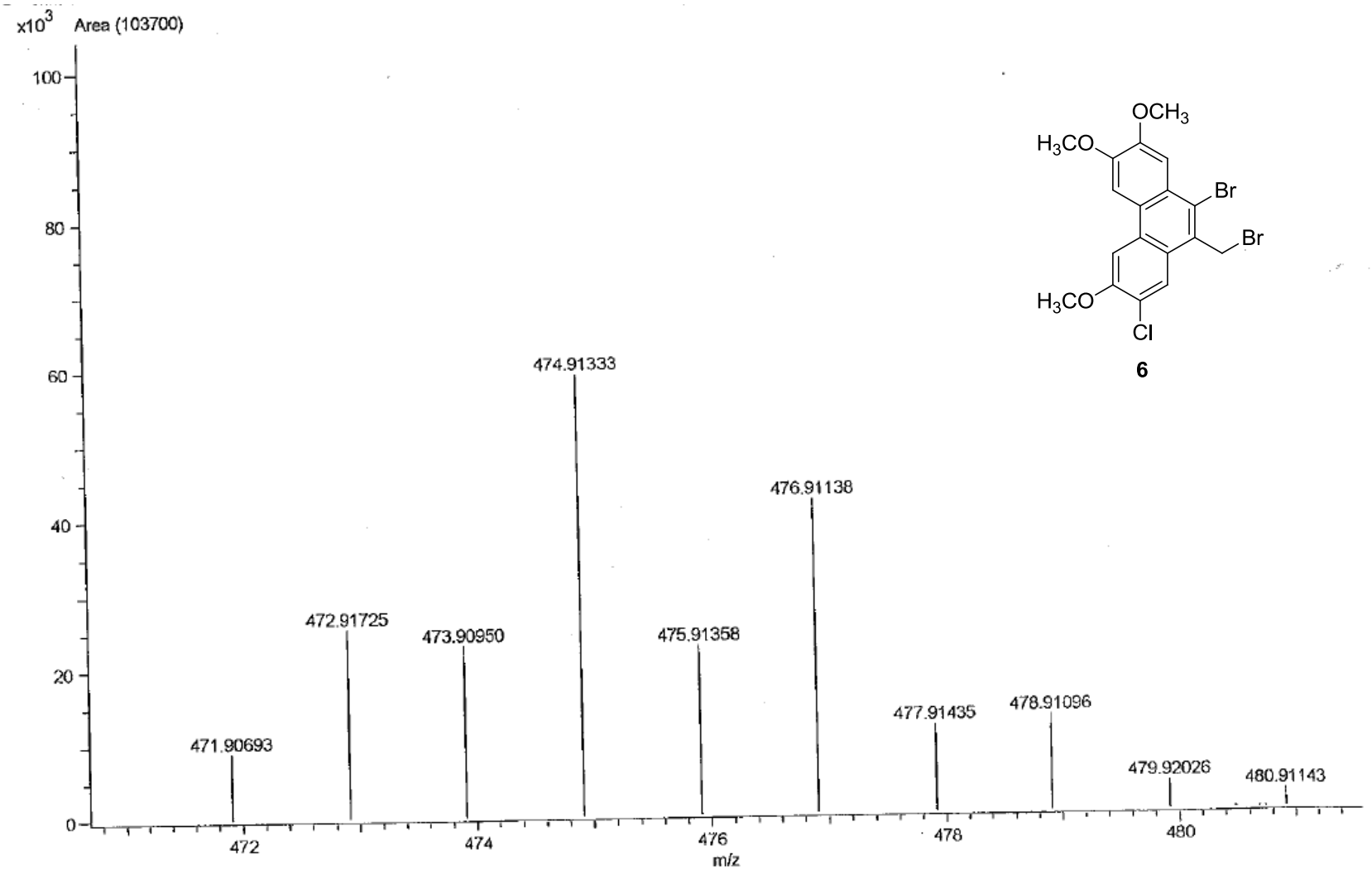

Detailed view of mass spectrum of 9-bromo-10-(bromomethyl)-2-chloro-3,6,7-trimethoxyphenanthrene (**6**).

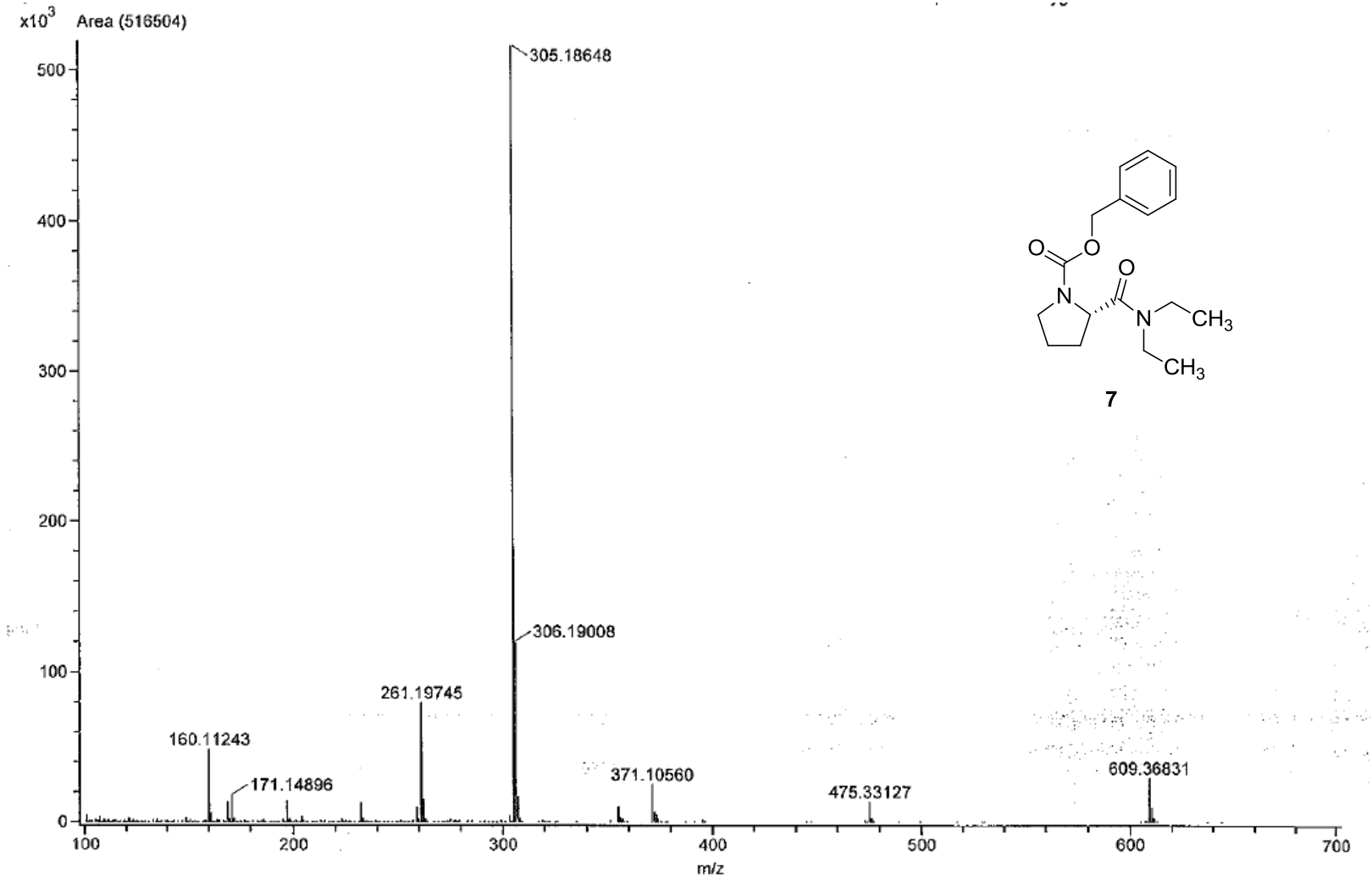

Mass spectrum of (*S*)-benzyl 2-(diethylcarbamoyl)pyrrolidine-1-carboxylate (**7**).

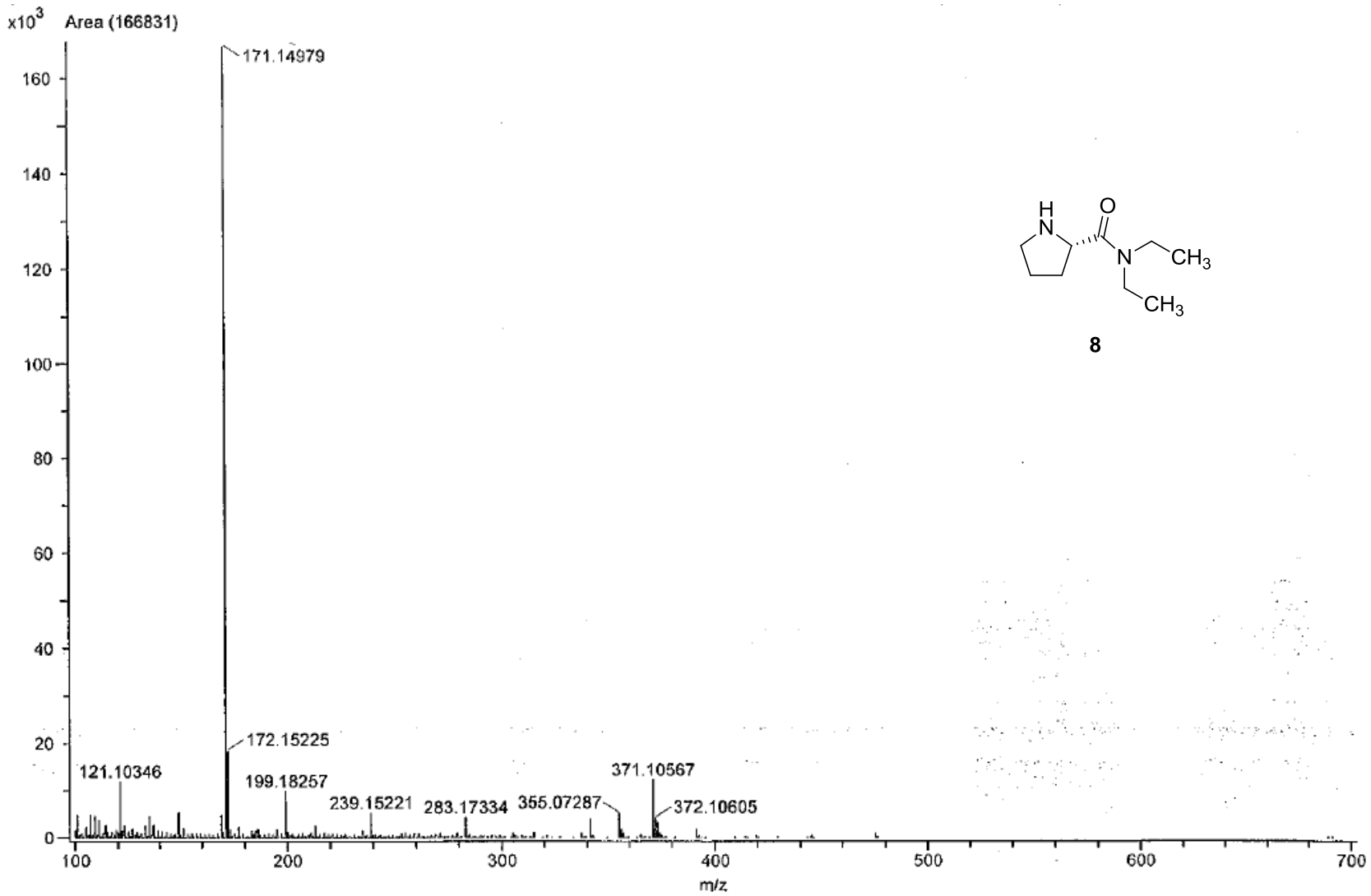

Mass spectrum of (*S*)-*N*,*N*-diethylpyrrolidine-2-carboxamide (**8**).

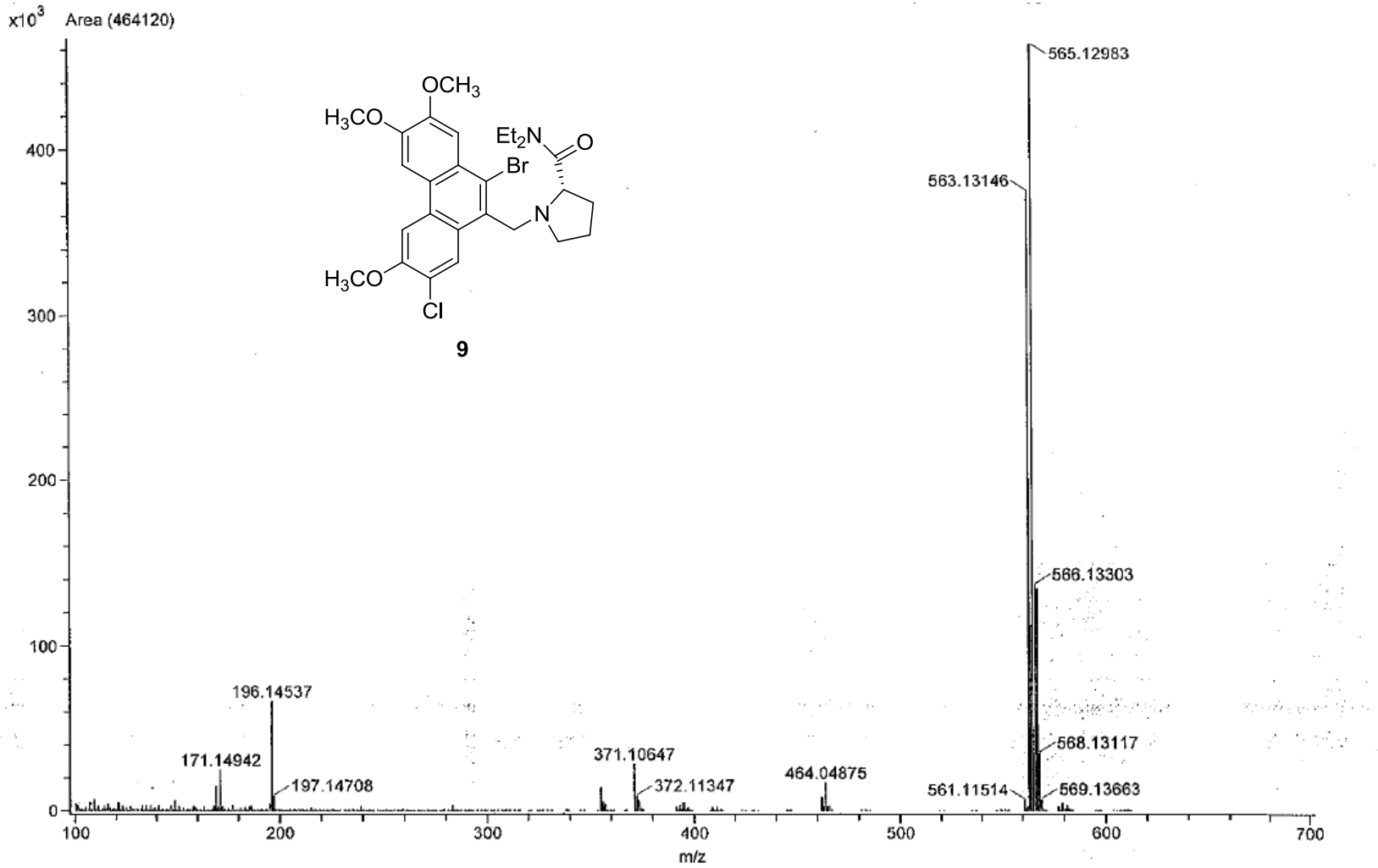

Mass spectrum of (*S*)-1-((10-bromo-7-chloro-2,3,6-trimethoxyphenanthren-9-yl)methyl)-*N*,*N*-diethylpyrrolidine-2-carboxamide (**9**).

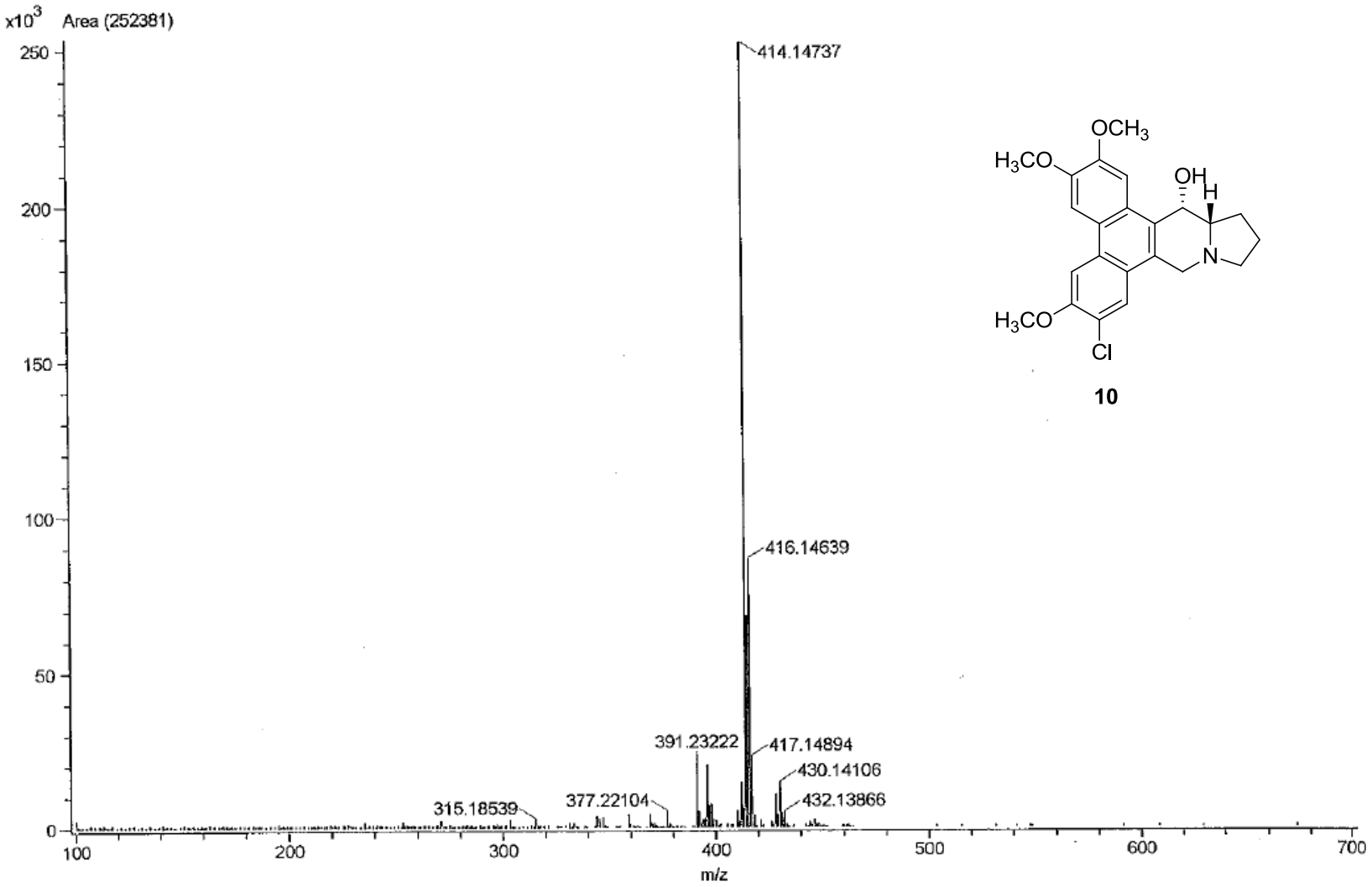

Mass spectrum of (13a*S*,14*S*)-7-chloro-2,3,6-trimethoxy-9,11,12,13,13a,14-hexahydrodibenzo[*f*,*h*]pyrrolo[1,2-*b*]isoquinolin-14-ol (**10**).

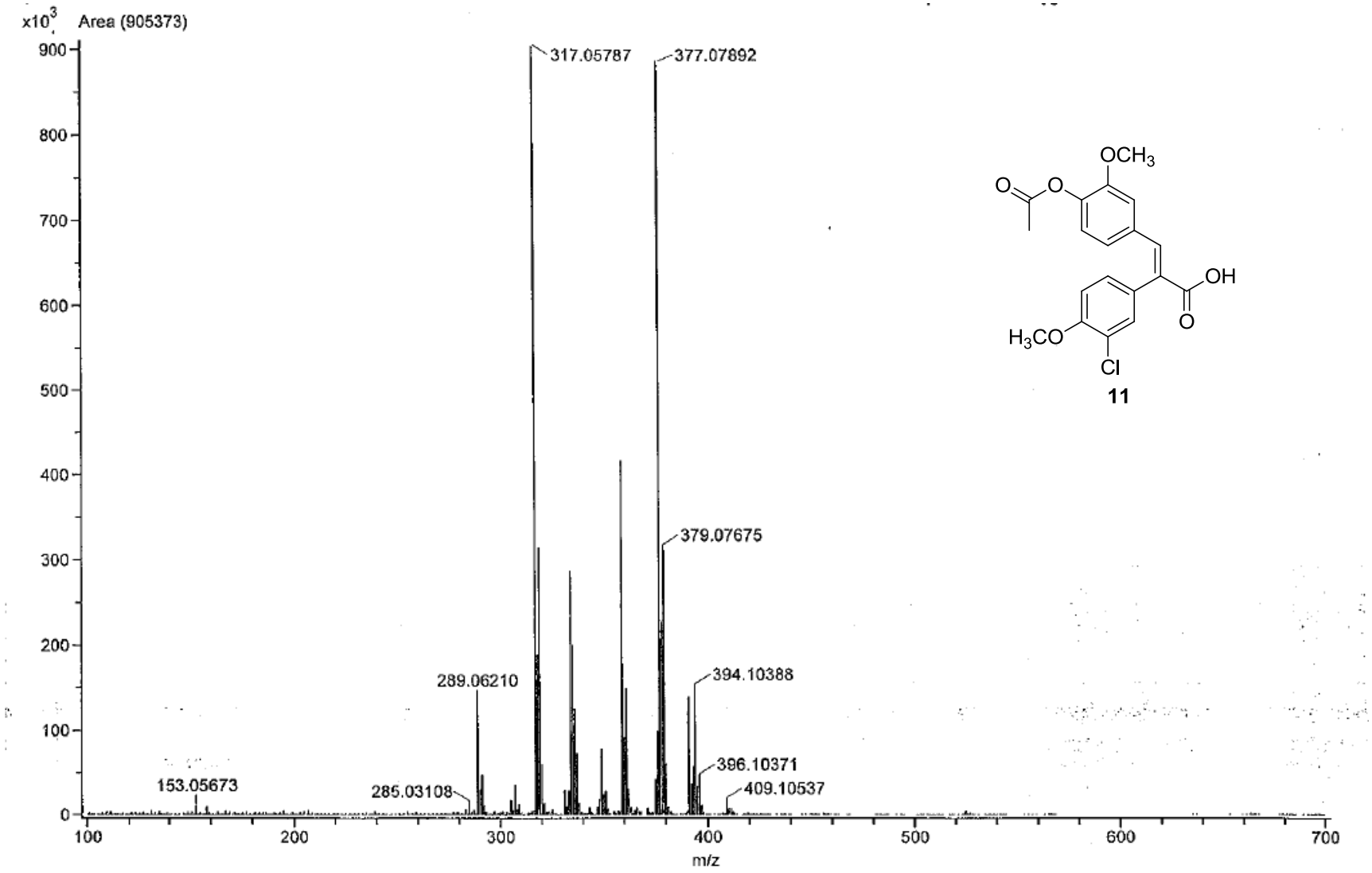

Mass spectrum of (*E*)-3-(4-acetoxy-3-methoxyphenyl)-2-(3-chloro-4-methoxyphenyl)acrylic acid (**11**).

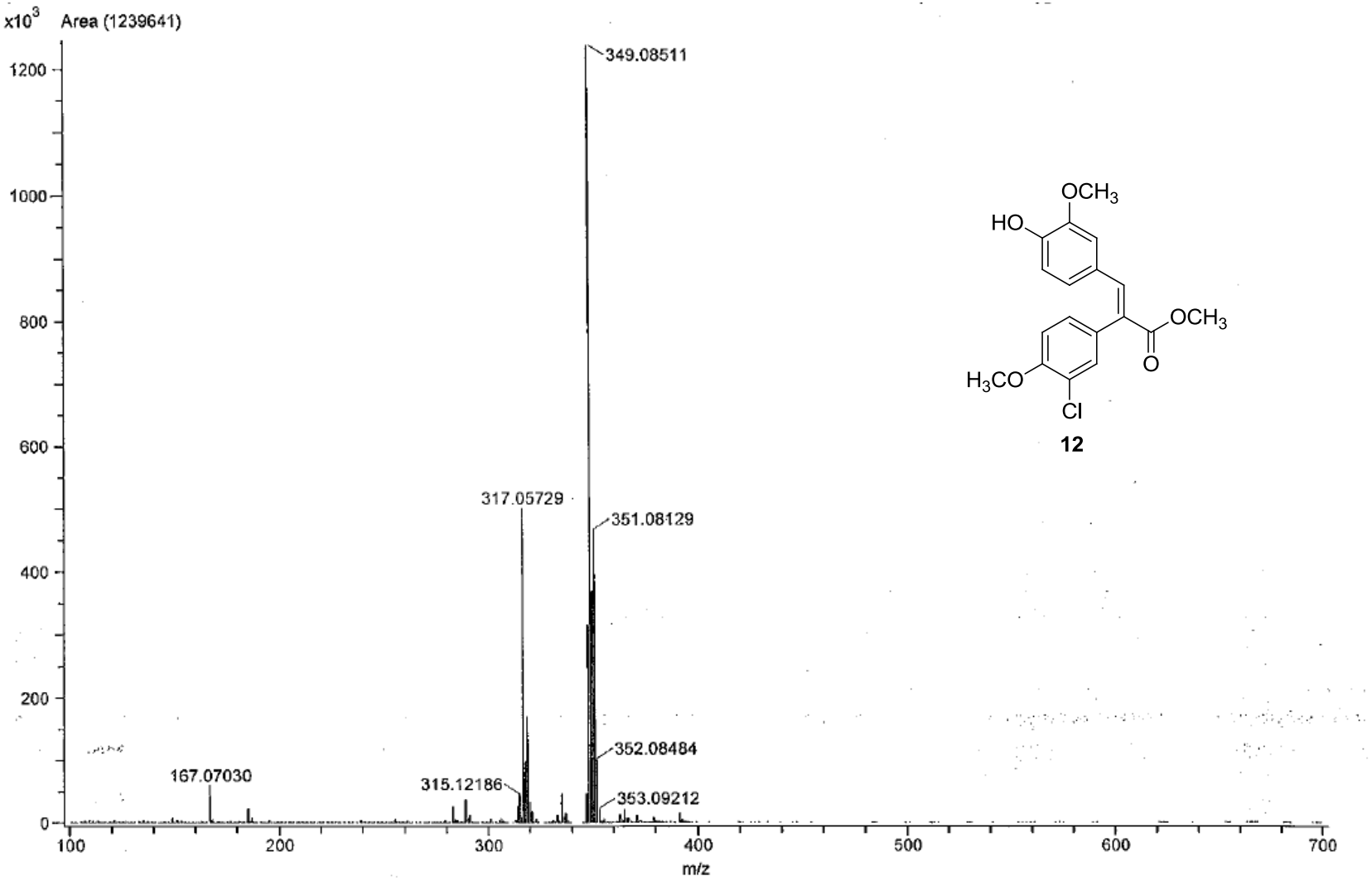

Mass spectrum of (*E*)-methyl 2-(3-chloro-4-methoxyphenyl)-3-(4-hydroxy-3-methoxyphenyl)acrylate (**12**).

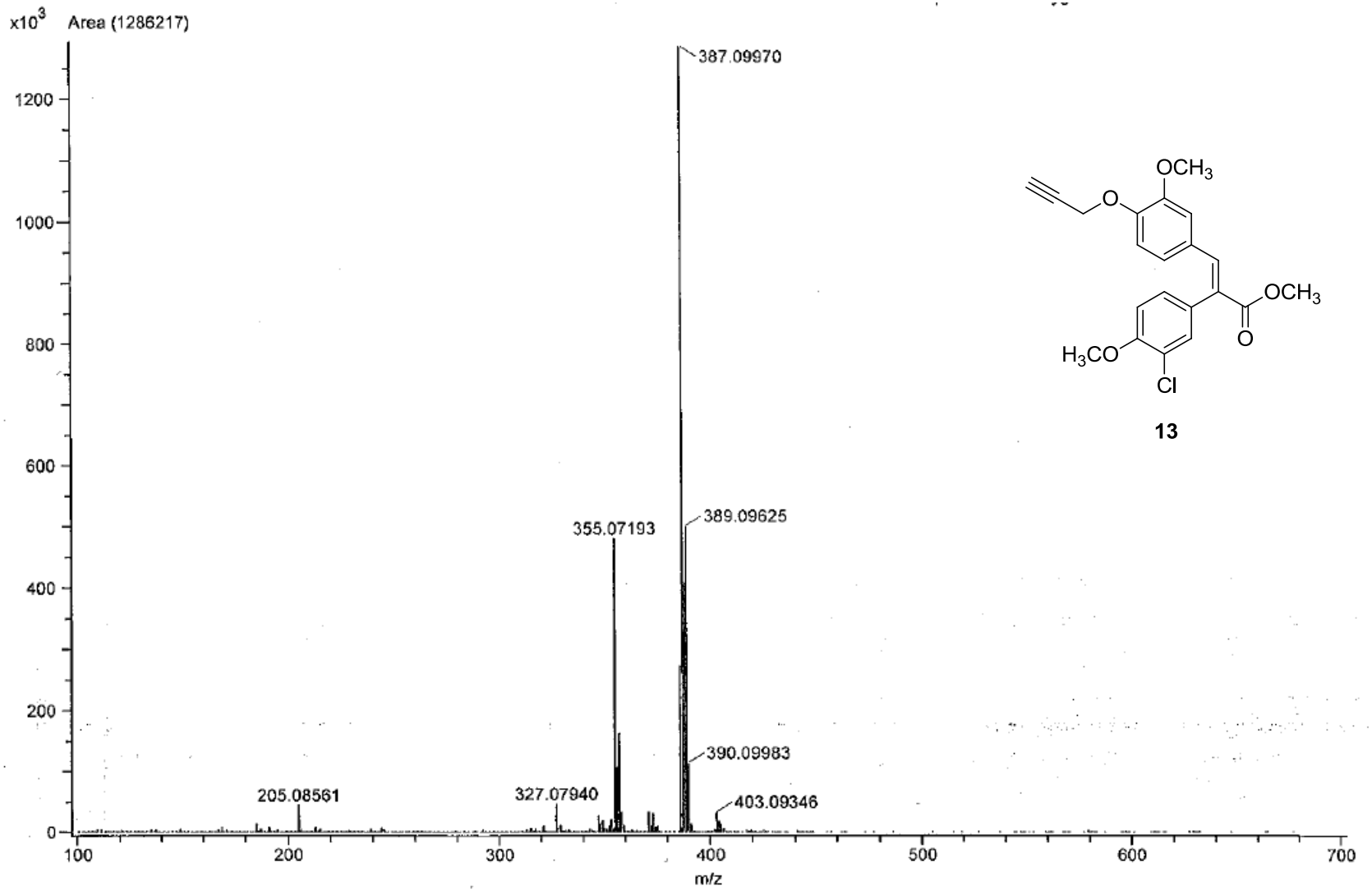

Mass spectrum of (*E*)-methyl 2-(3-chloro-4-methoxyphenyl)-3-(3-methoxy-4-(prop-2-yn-1-yloxy)phenyl)acrylate (**13**).

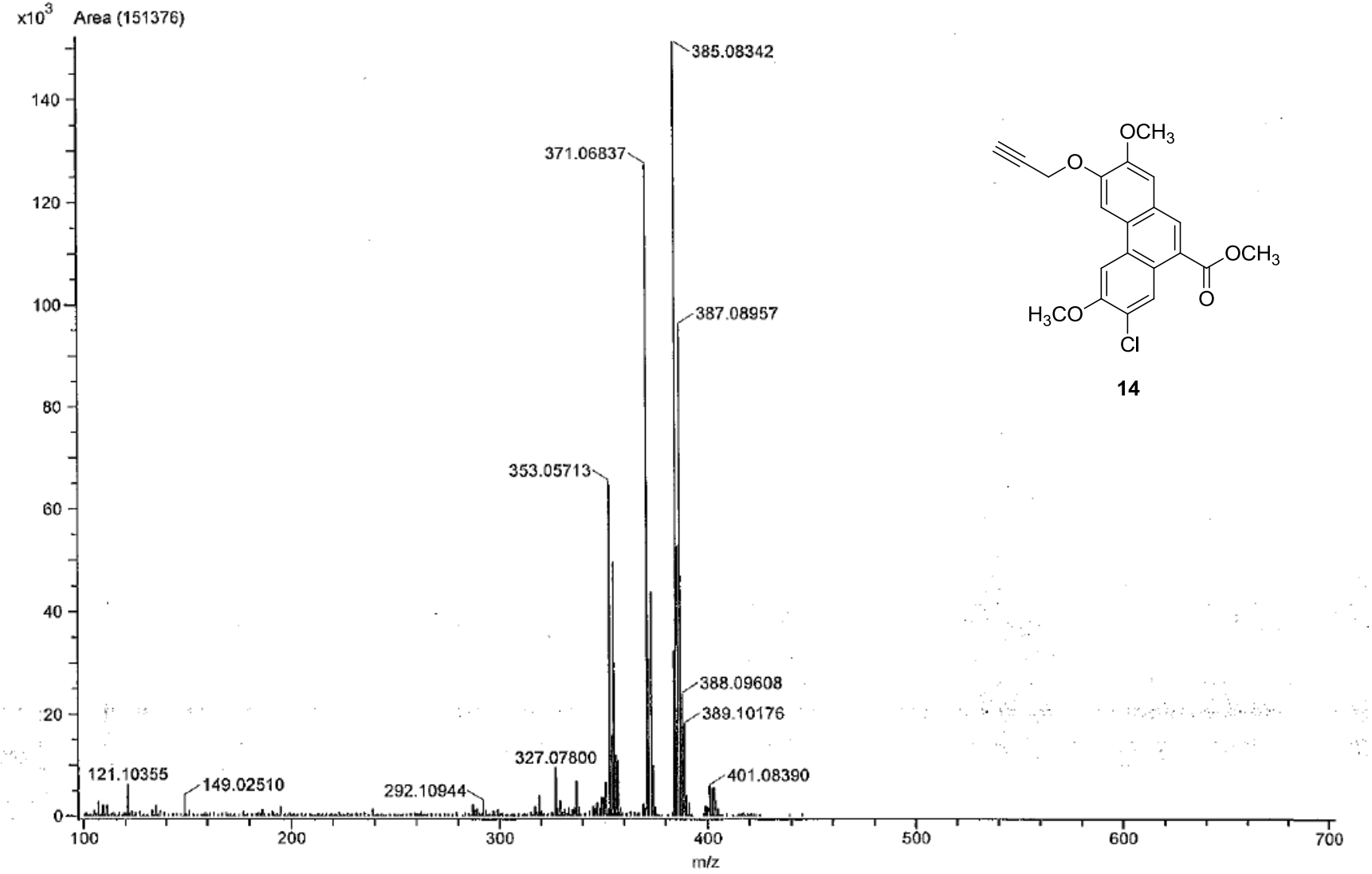

Mass spectrum of methyl 7-chloro-2,6-dimethoxy-3-(prop-2-yn-1-yloxy)phenanthrene-9-carboxylate (**14**).

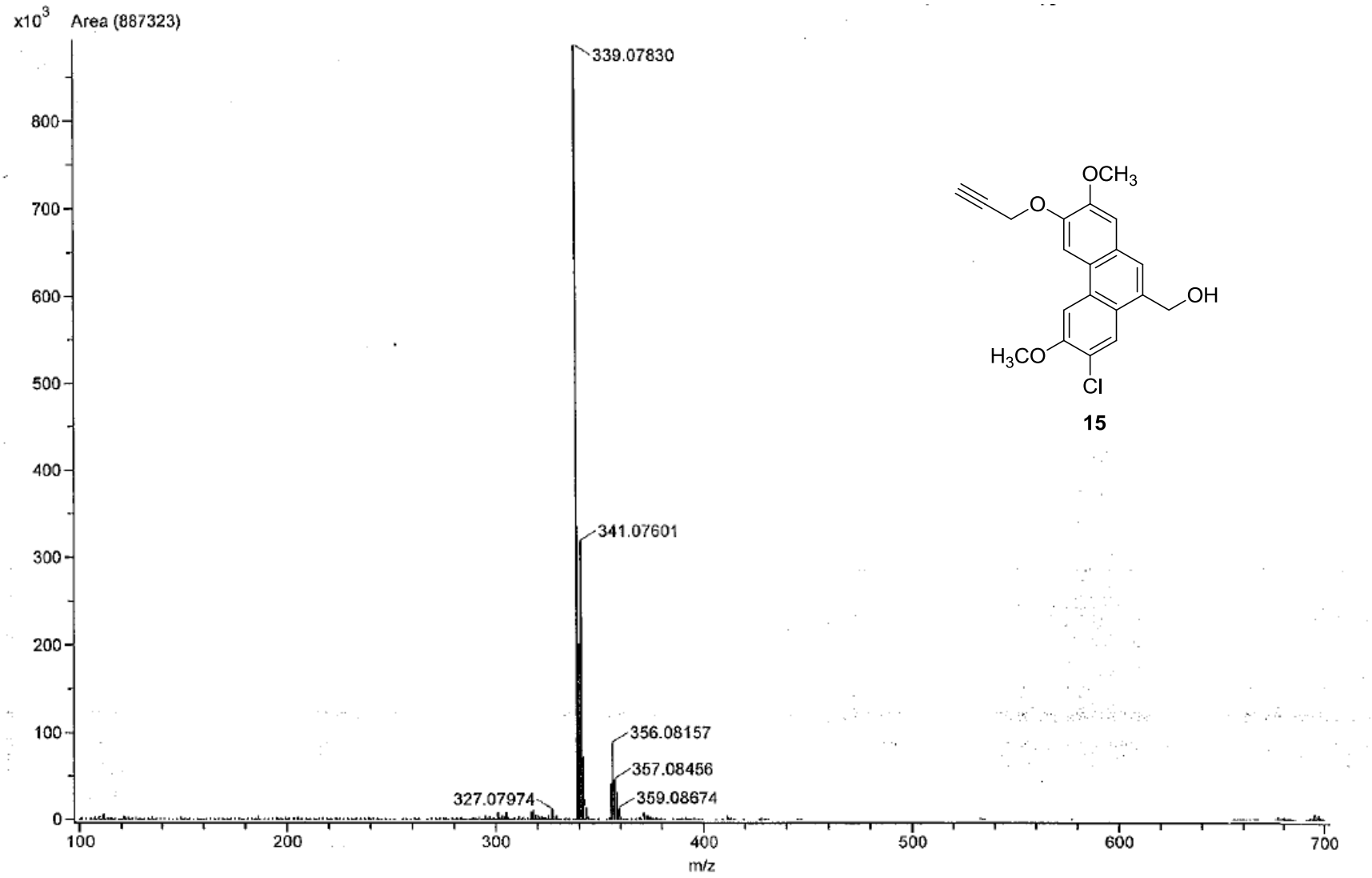

Mass spectrum of (7-chloro-2,6-dimethoxy-3-(prop-2-yn-1-yloxy)phenanthren-9-yl)methanol (**15**).

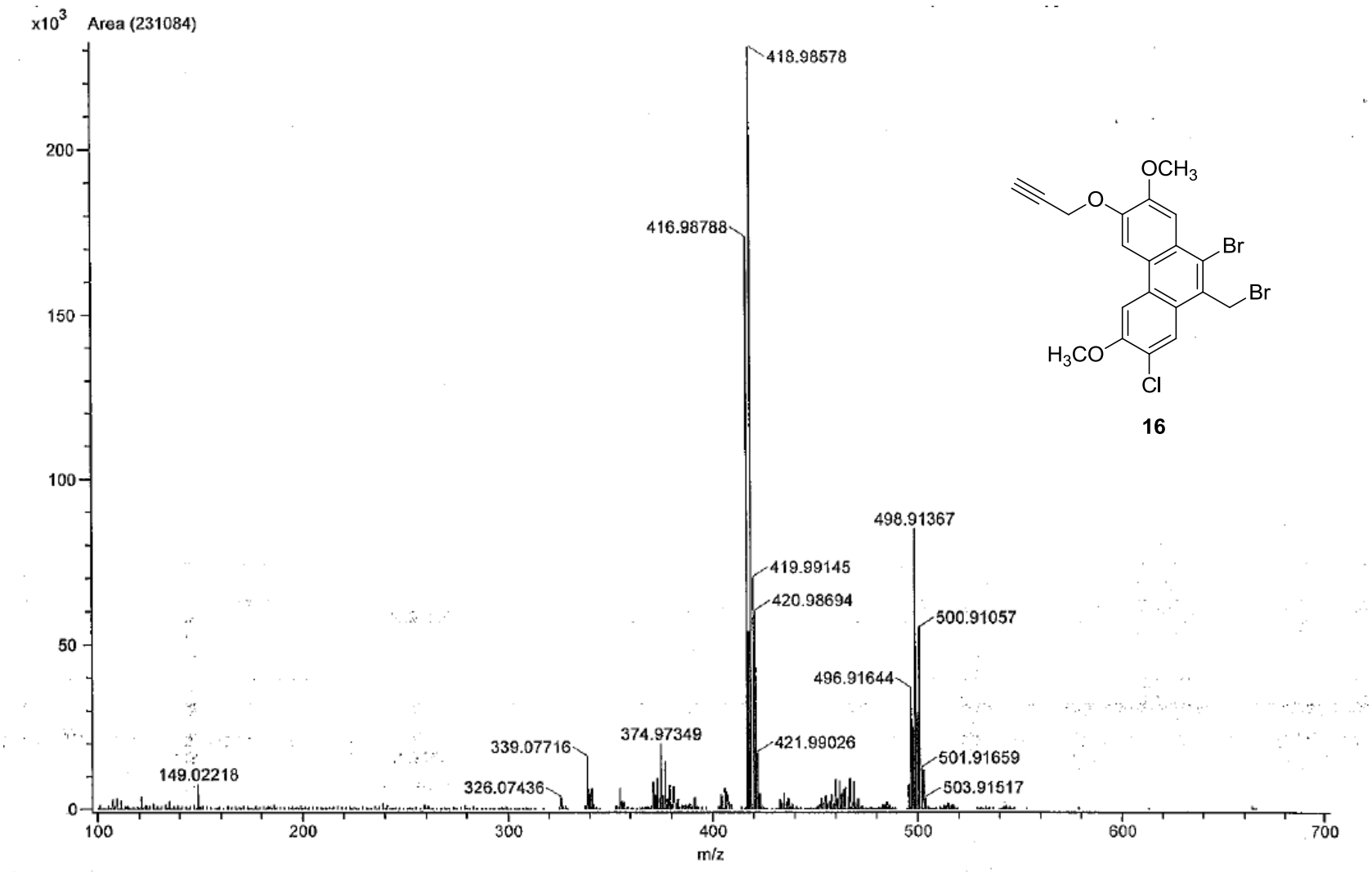

Mass spectrum of 9-bromo-10-(bromomethyl)-2-chloro-3,7-dimethoxy-6-(prop-2-yn-1-yloxy)phenanthrene (**16**).

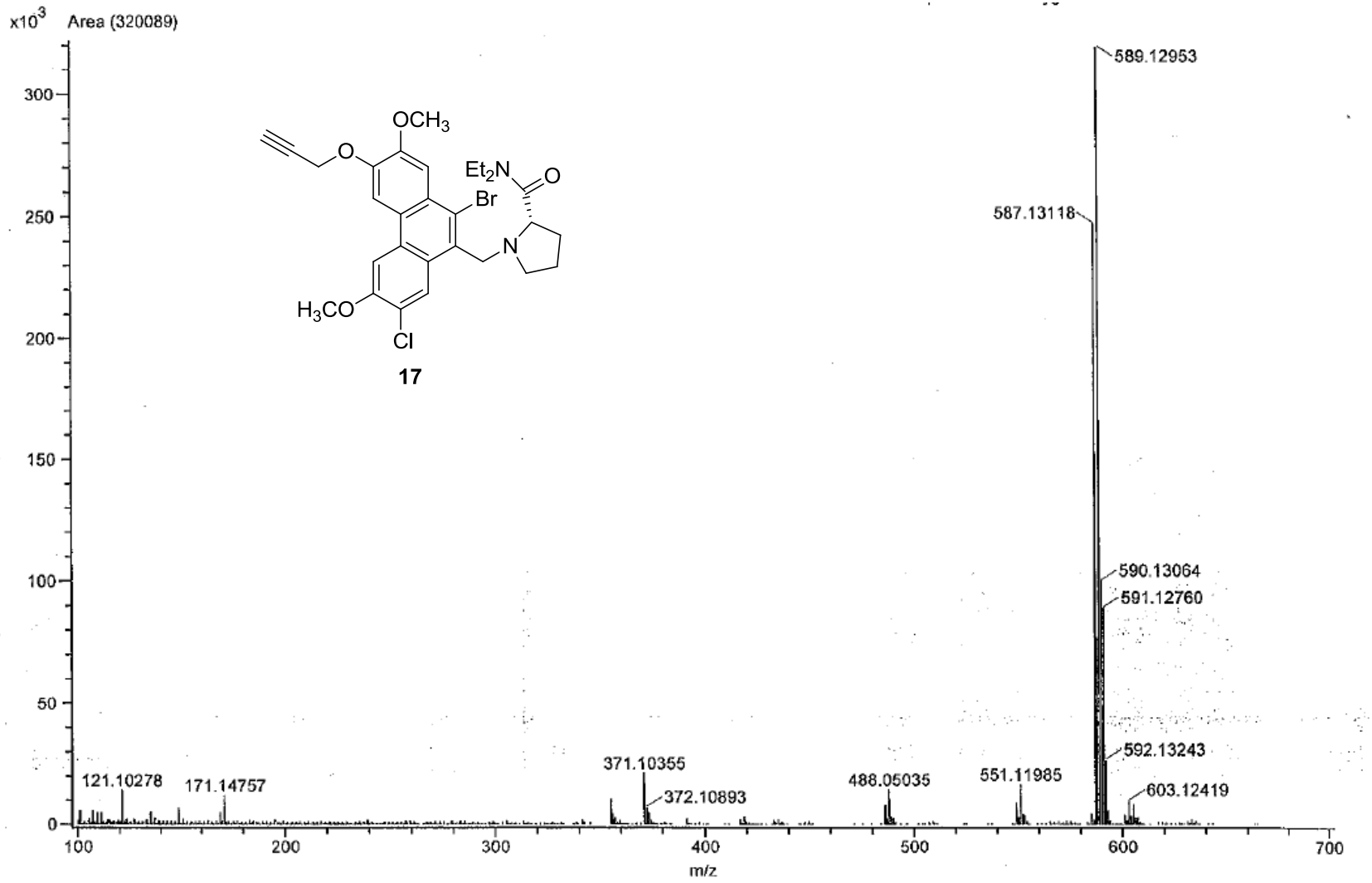

Mass spectrum of (*S*)-1-((10-bromo-7-chloro-2,6-dimethoxy-3-(prop-2-yn-1-yloxy)phenanthren-9-yl)methyl)-*N*,*N*-diethylpyrrolidine-2-carboxamide (**17**).

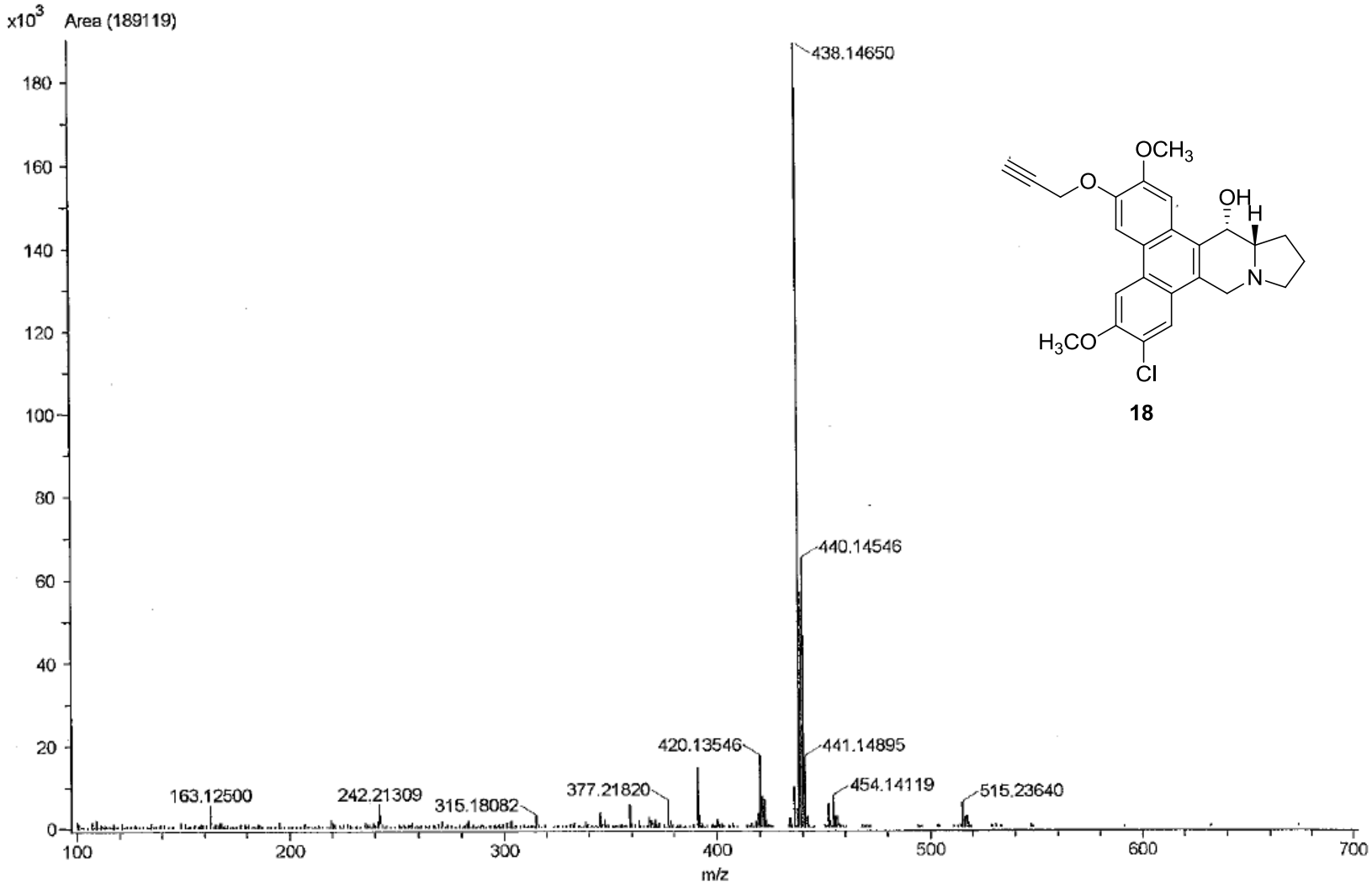

Mass spectrum of (13a*S*,14*S*)-7-chloro-2,6-dimethoxy-3-(prop-2-yn-1-yloxy)-9,11,12,13,13a,14-hexahydrodibenzo[*f*,*h*]pyrrolo[1,2-*b*]isoquinolin-14-ol (**18**).

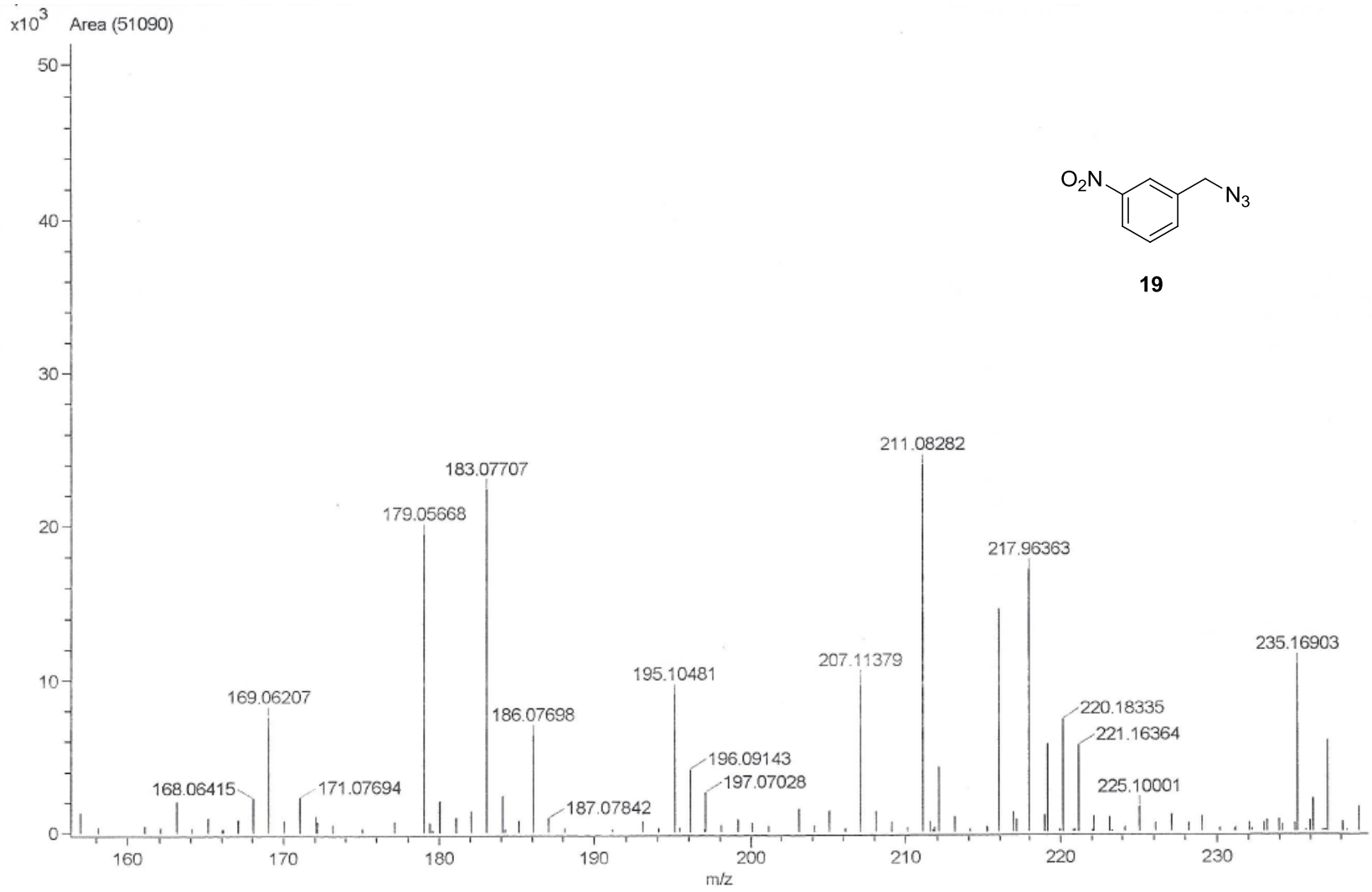

Mass spectrum of 1-(azidomethyl)-3-nitrobenzene (**19**).

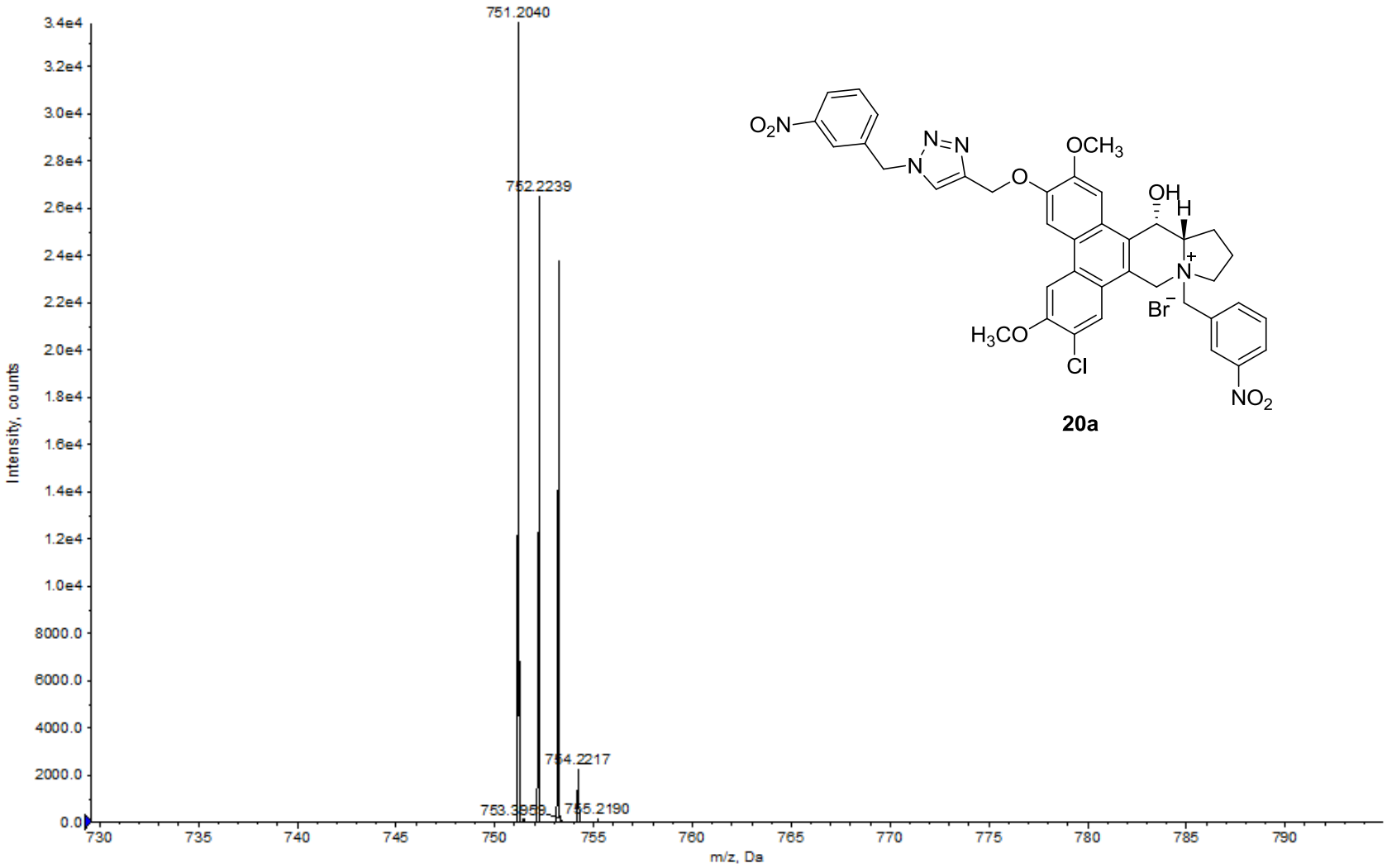

Mass spectrum of the positive ion of (13a*S*,14*S*)-7-chloro-14-hydroxy-2,6-dimethoxy-10-(2-nitrobenzyl)-3-((1-(3-nitrobenzyl)-1H-1,2,3-triazol-4-yl)methoxy)-10,11,12,13,13a,14-hexahydro-9H-dibenzo[*f*,*h*]pyrrolo[1,2-*b*]isoquinolin-10-ium bromide (**20a**).

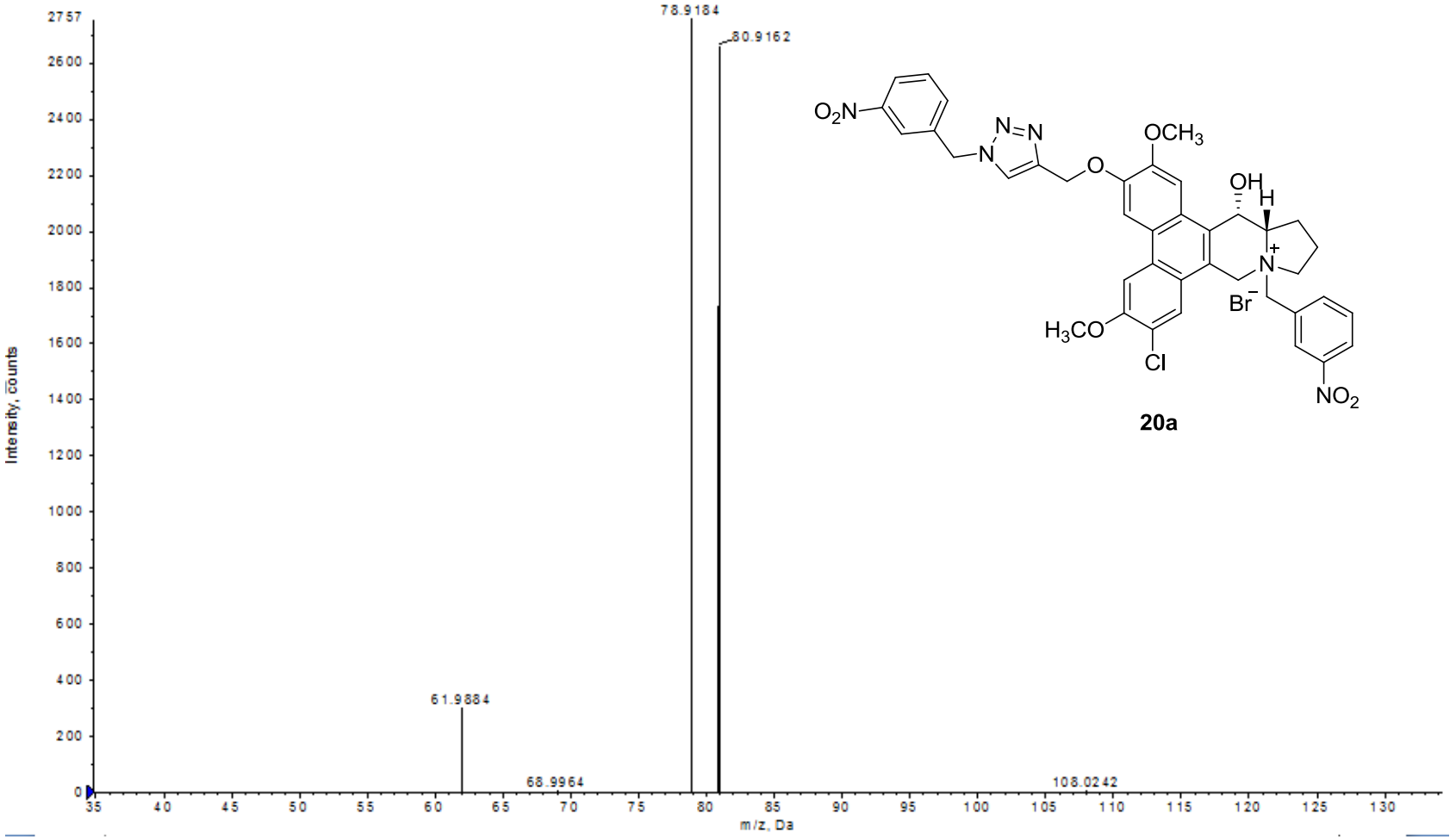

Mass spectrum of the negative ion of (13a*S*,14*S*)-7-chloro-14-hydroxy-2,6-dimethoxy-10-(2-nitrobenzyl)-3-((1-(3-nitrobenzyl)-1H-1,2,3-triazol-4-yl)methoxy)-10,11,12,13,13a,14-hexahydro-9H-dibenzo[*f*,*h*]pyrrolo[1,2-*b*]isoquinolin-10-ium bromide (**20a**).

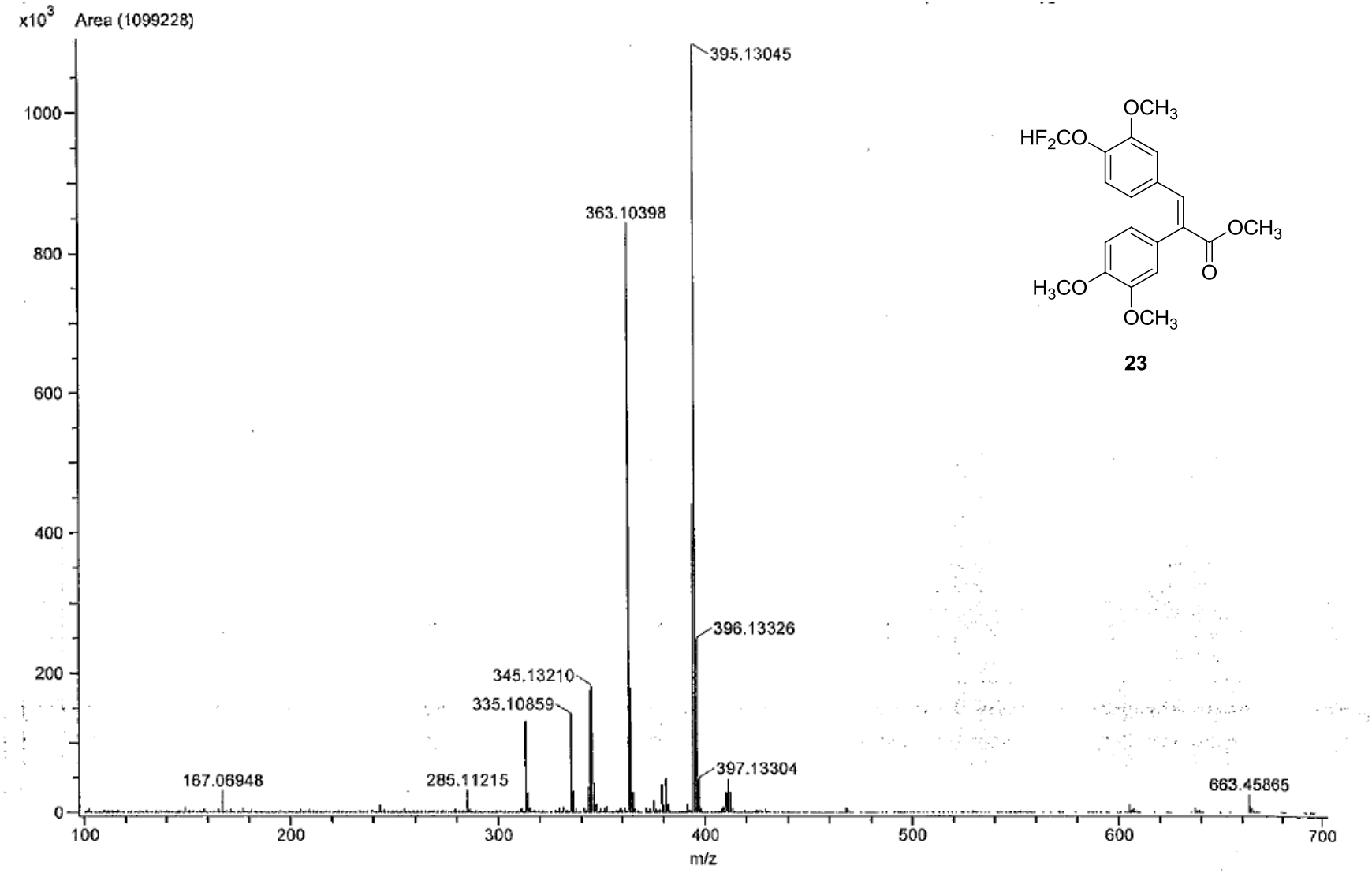

Mass spectrum of (*E*)-methyl 3-(4-(difluoromethoxy)-3-methoxyphenyl)-2-(3,4-dimethoxyphenyl)acrylate (**23**).

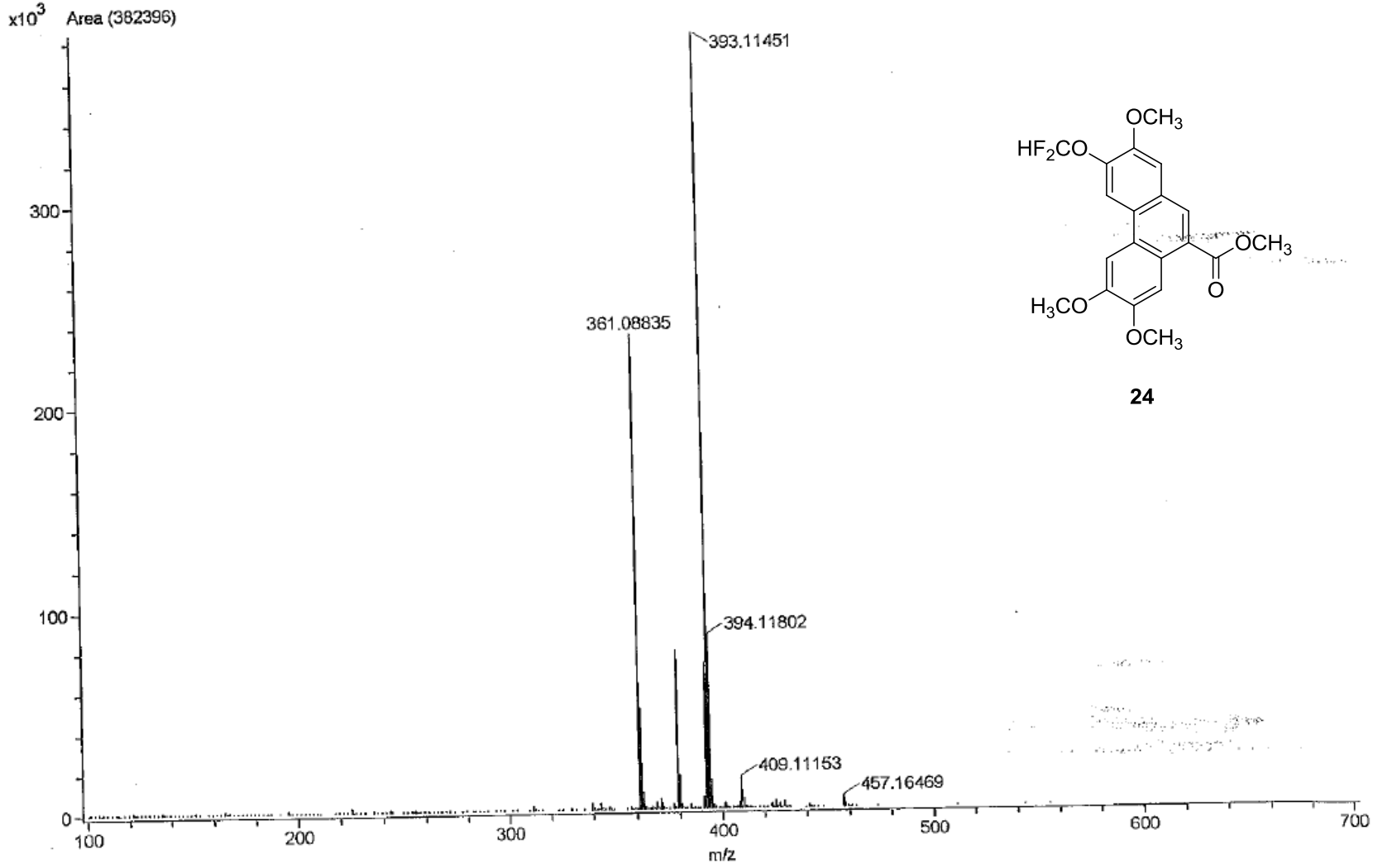

Mass spectrum of methyl 3-(difluoromethoxy)-2,6,7-trimethoxyphenanthrene-9-carboxylate (**24**).

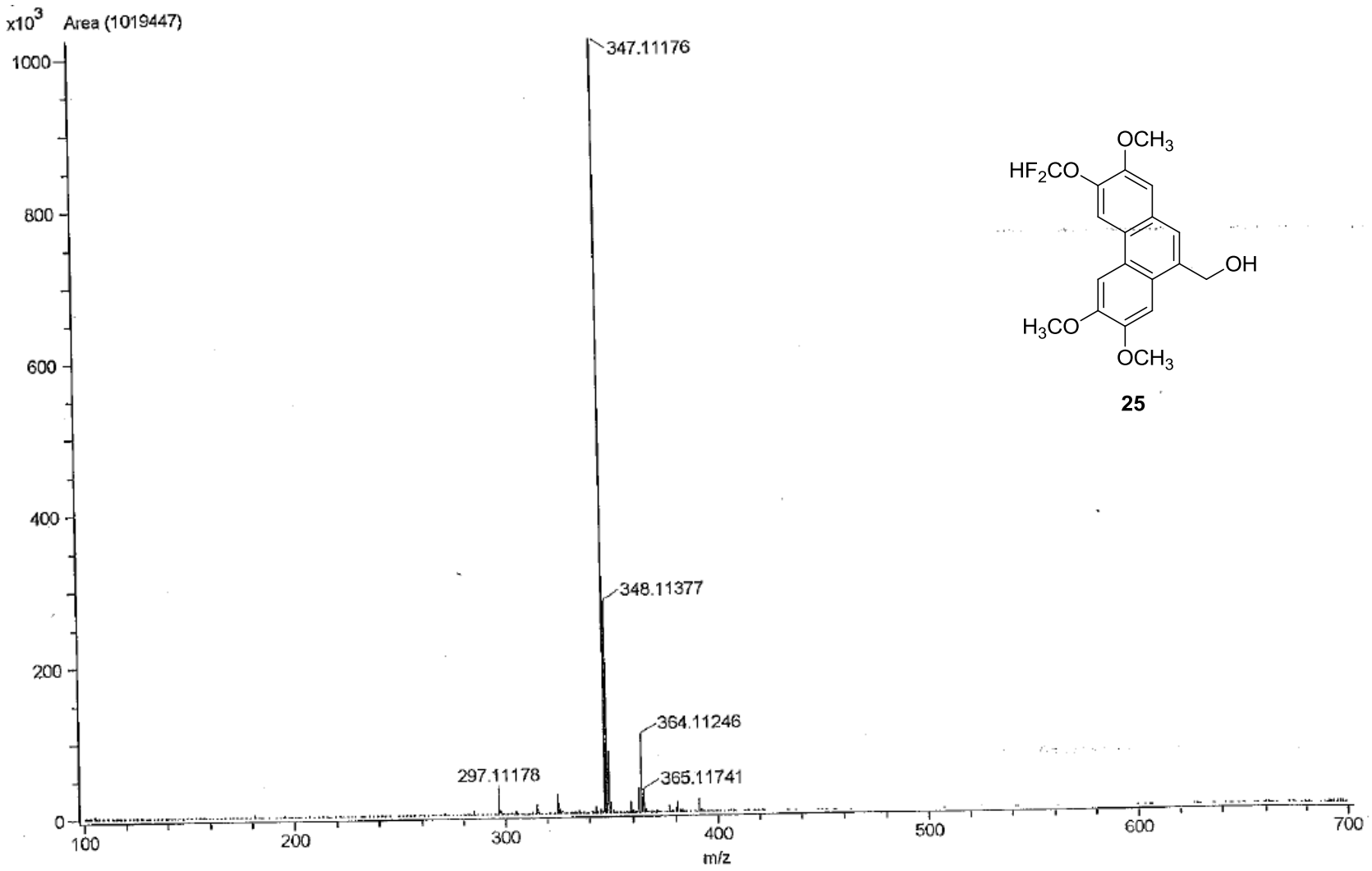

Mass spectrum of (3-(difluoromethoxy)-2,6,7-trimethoxyphenanthren-9-yl)methanol (**25**).

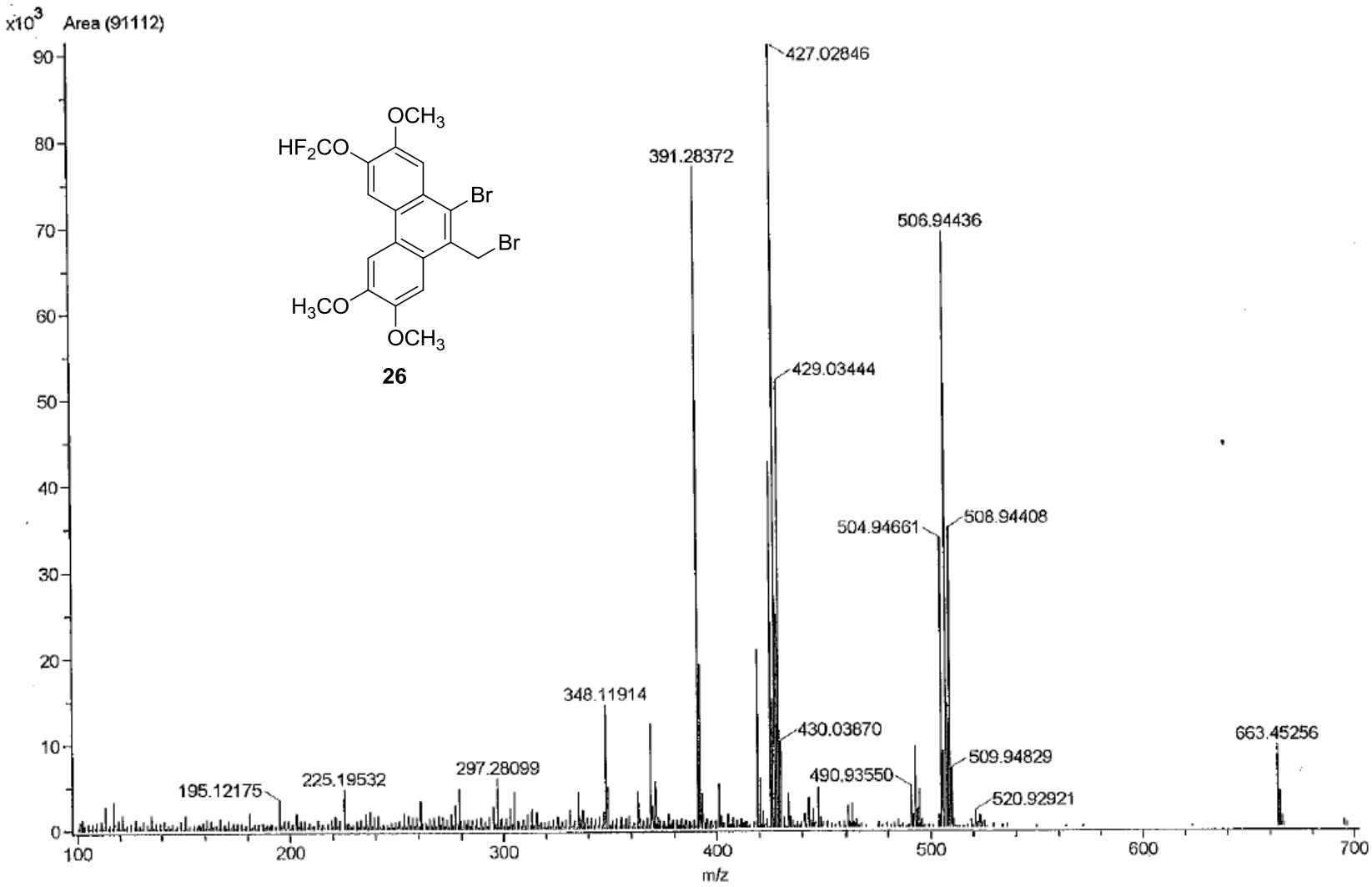

Mass spectrum of 9-bromo-10-(bromomethyl)-6-(difluoromethoxy)-2,3,7-trimethoxyphenanthrene (**26**).

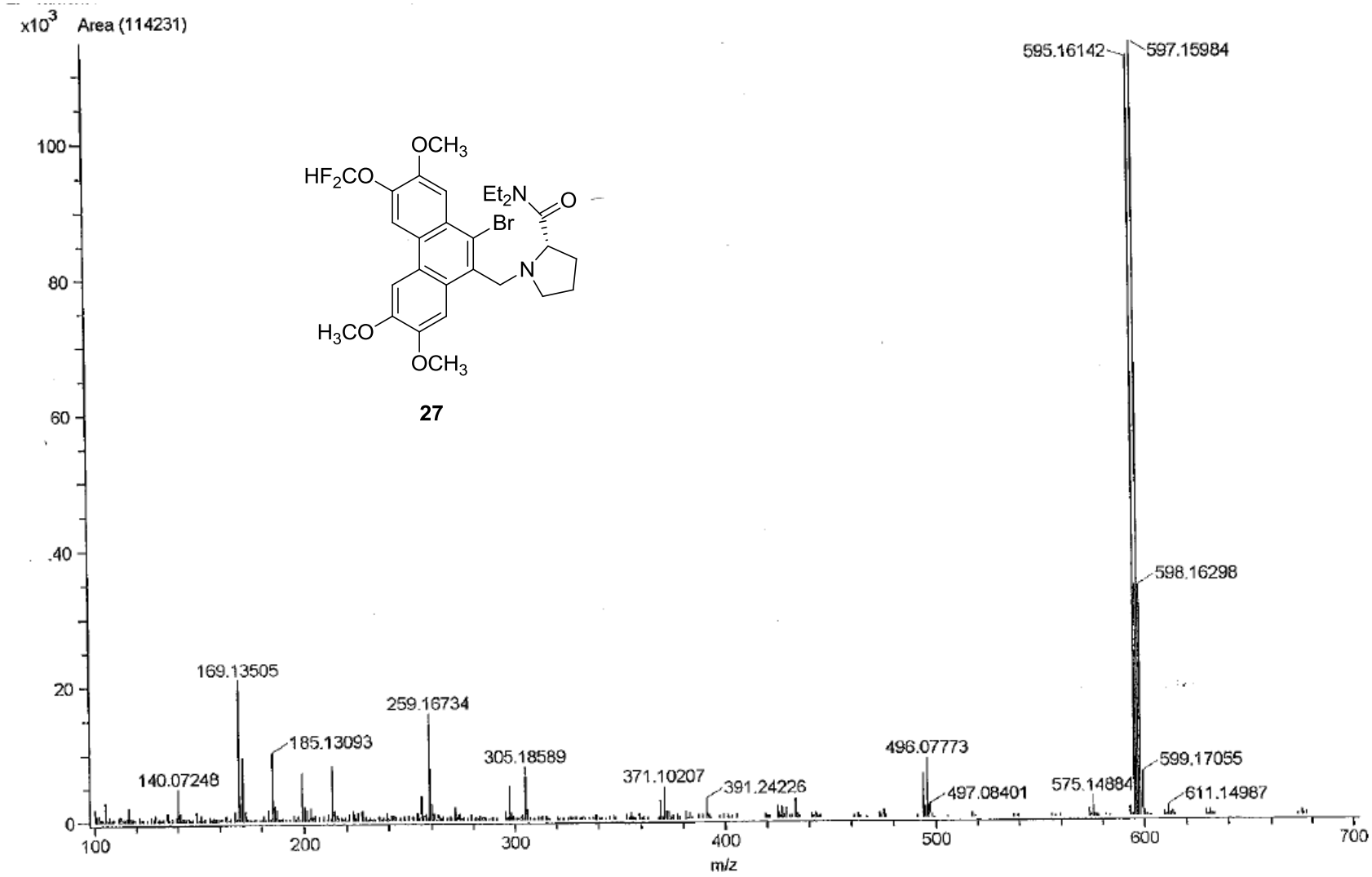

Mass spectrum of (*S*)-1-((10-bromo-3-(difluoromethoxy)-2,6,7-trimethoxyphenanthren-9-yl)methyl)-*N*,*N*-diethylpyrrolidine-2-carboxamide (**27**).

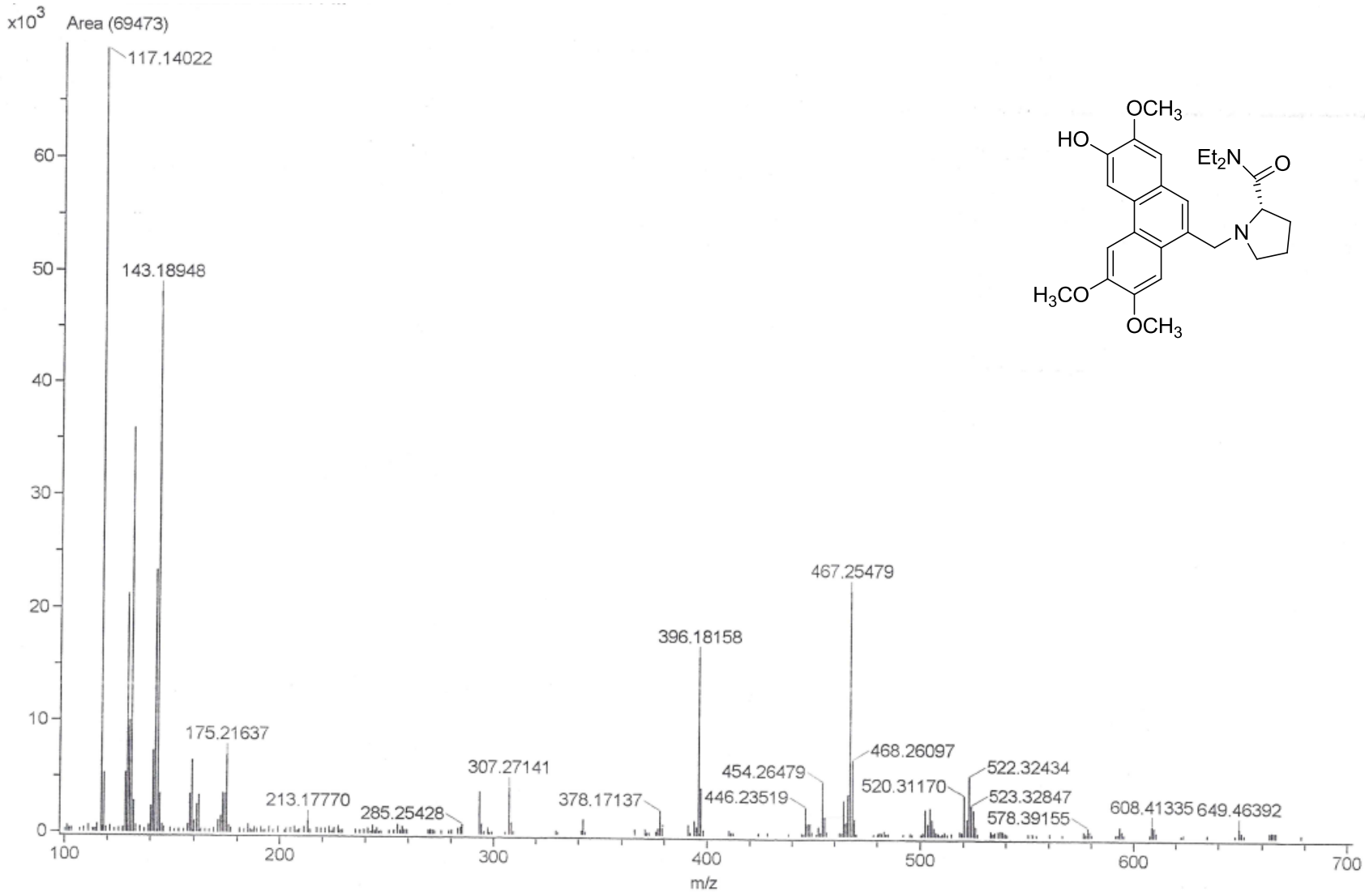

Mass spectrum of (*S*)-*N*,*N*-diethyl-1-((3-hydroxy-2,6,7-trimethoxyphenanthren-9-yl)methyl)pyrrolidine-2-carboxamide as an unexpected product in the synthesis of compound **28**.

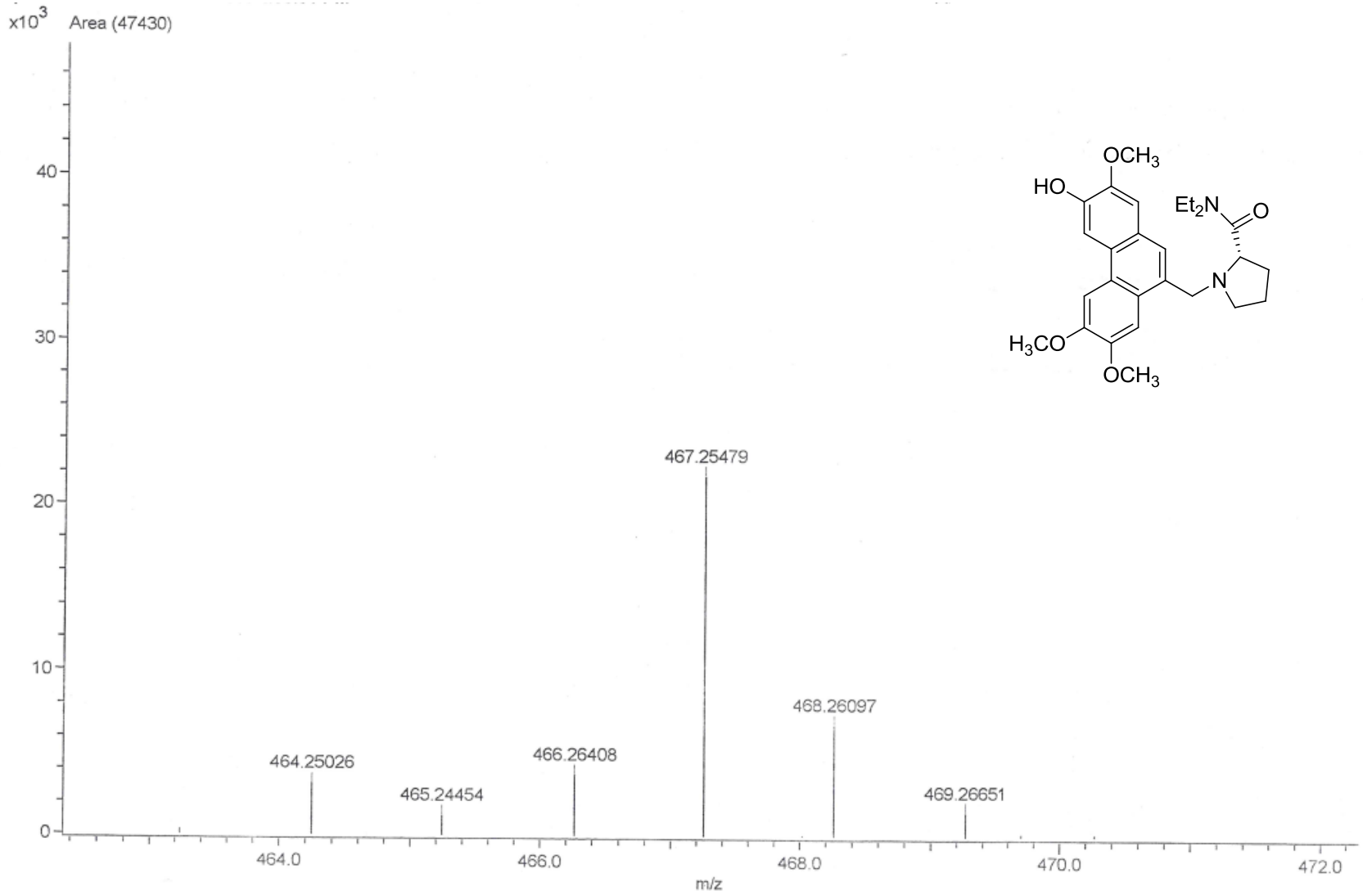

The detailed view of mass spectrum of (*S*)-*N*,*N*-diethyl-1-((3-hydroxy-2,6,7-trimethoxyphenanthren-9-yl)methyl)pyrrolidine-2-carboxamide as an unexpected product in the synthesis of compound **28**.

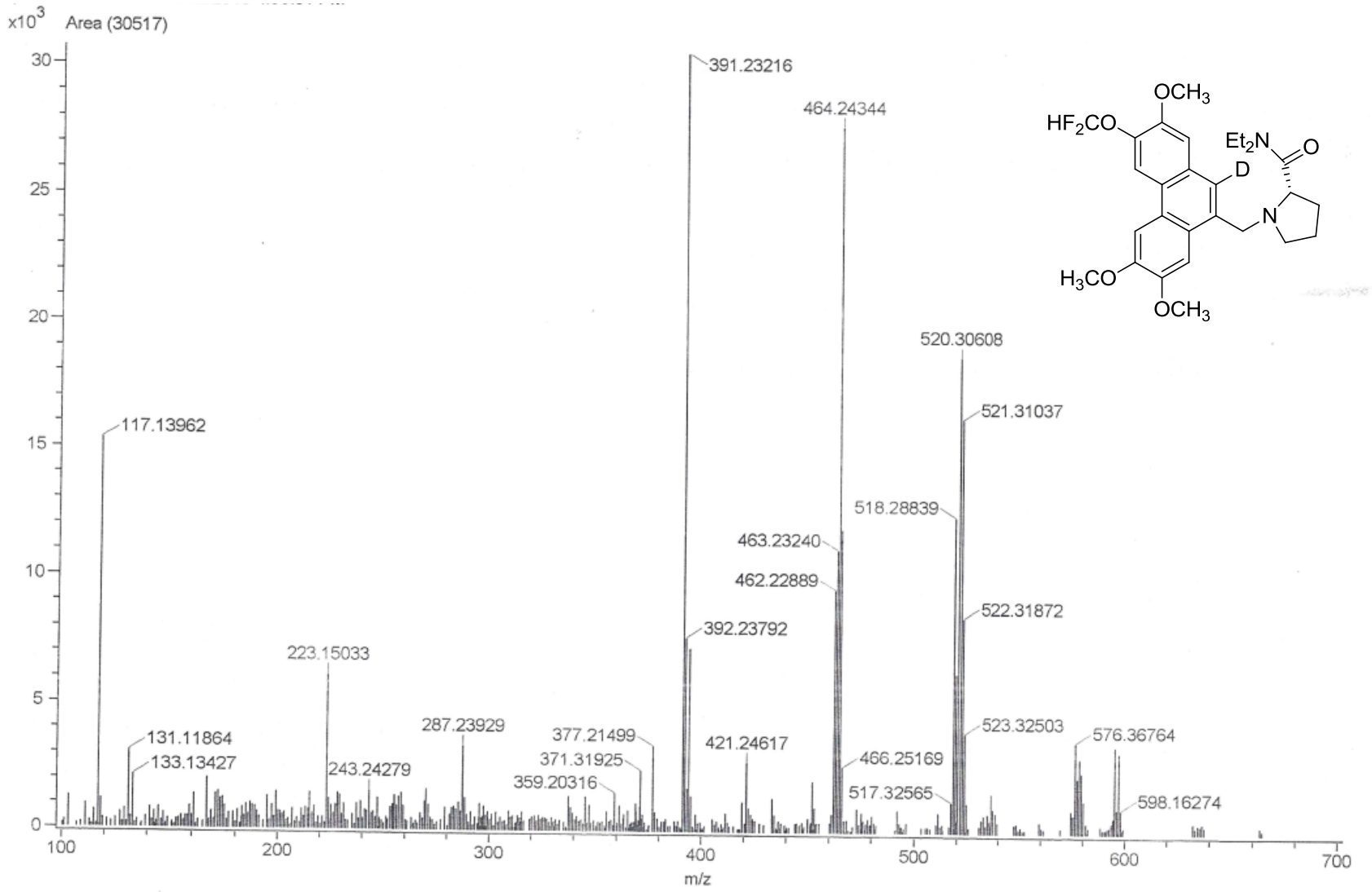

Mass spectrum of the deuterated (*S*)-1-((3-(difluoromethoxy)-2,6,7-trimethoxyphenanthren-9-yl)methyl)-*N*,*N*-diethylpyrrolidine-2-carboxamide as the intermediate towards the synthesis of compound **28**.

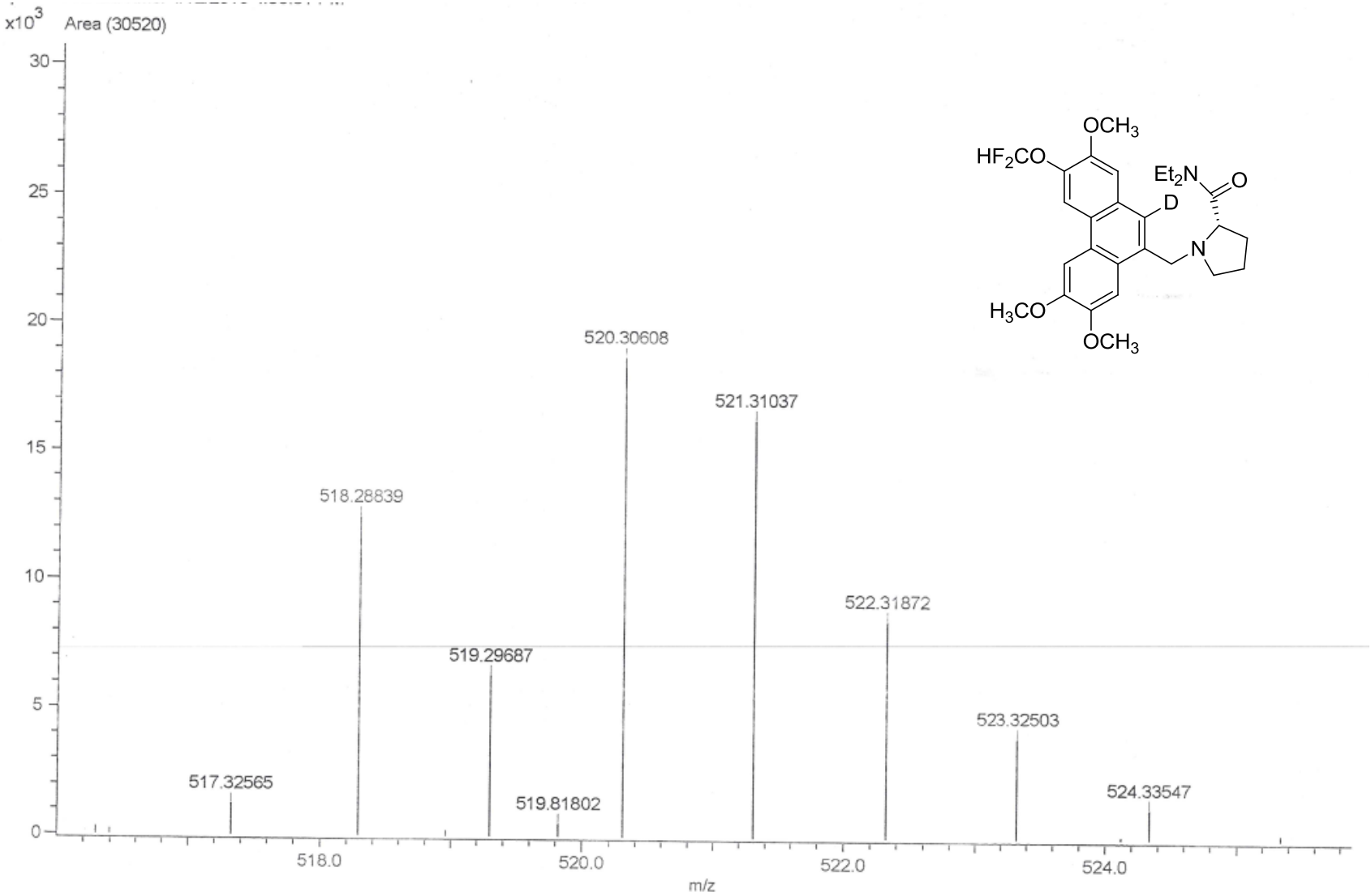

The detailed view of mass spectrum of the deuterated (*S*)-1-((3-(difluoromethoxy)-2,6,7-trimethoxyphenanthren-9-yl)methyl)-*N*,*N*-diethylpyrrolidine-2-carboxamide as the intermediate towards the synthesis of compound **28**.

VITA

Yundi Gan was born on June 10th, 1987 in Kaifeng, China, where he attended the High School Affiliated to Henan University. He was then admitted to the College of Chemistry and Chemical Engineering of Henan University located in the same city to complete the study for his Bachelor of Science in chemistry in 2010. Afterwards he moved to the United States of America to continue his career in the University of Tennessee, Knoxville, where he joined Dr. David C. Baker's lab focusing on organic chemistry. He obtained his Doctor of Philosophy from Department of Chemistry at the University of Tennessee, Knoxville in 2015.